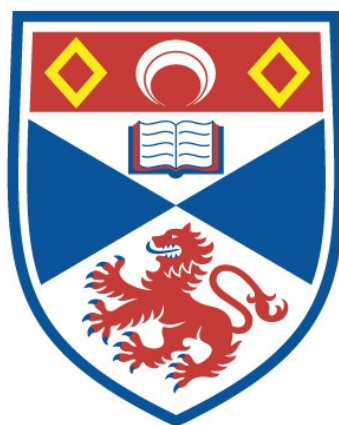


SYNTHESIS OF NEW MICROPOROUS SOLIDS BY  
TEMPLATE DESIGN

Graham William Noble

A Thesis Submitted for the Degree of PhD  
at the  
University of St Andrews



1999

Full metadata for this item is available in  
St Andrews Research Repository  
at:

<http://research-repository.st-andrews.ac.uk/>

Please use this identifier to cite or link to this item:

<http://hdl.handle.net/10023/15108>

This item is protected by original copyright



**Synthesis of  
New Microporous Solids  
by Template Design**



A thesis submitted to the University of St. Andrews as part fulfilment for the degree of  
Doctor of Philosophy.

By

Graham William Noble

August 1998

ProQuest Number: 10166811

All rights reserved

INFORMATION TO ALL USERS

The quality of this reproduction is dependent upon the quality of the copy submitted.

In the unlikely event that the author did not send a complete manuscript and there are missing pages, these will be noted. Also, if material had to be removed, a note will indicate the deletion.



ProQuest 10166811

Published by ProQuest LLC (2017). Copyright of the Dissertation is held by the Author.

All rights reserved.

This work is protected against unauthorized copying under Title 17, United States Code  
Microform Edition © ProQuest LLC.

ProQuest LLC.  
789 East Eisenhower Parkway  
P.O. Box 1346  
Ann Arbor, MI 48106 – 1346



TR D 210

## Declarations

I, Graham William Noble, hereby certify that this thesis, which is approximately 53,000 words in length, has been written by me, that it is a record of the work carried out by me and that it has not been submitted in any previous application for a higher degree.

Date 21. 8 . 98

Signature of candidate

I was admitted as a research student in October 1994 and as a candidate for the degree of Ph.D. in September 1995; the higher for which this is a record was carried out at the University of St. Andrews between 1994 and 1998.

Date 21. 8 . 98

Signature of candidate

I hereby certify that the candidate has fulfilled the conditions of the Resolution and Regulations appropriate for the degree of Ph.D. in the University of St. Andrews and that the candidate is qualified to submit this thesis in application for that degree.

Date 21. 8 . 98

Signature of supervisor

In submitting this thesis to the University of St. Andrews I understand that I am giving permission for it to be made available for use in accordance with the regulations of the University Library for the time being in force, subject to any copyright vested in the work not being affected thereby. I also understand that the title and abstract will be published, and that a copy of the work may be made and supplied to any bona fide library or research worker.

Date 21. 8 . 98

Signature of candidate

## Acknowledgements

I have become indebted to many people during my time at St. Andrews, too many to mention by name, however, there are several people who deserve a special thankyou.

Firstly, I would like to thank my supervisor, Dr. Paul A. Wright for giving me the opportunity to study for a Ph.D. and for his endless patience, advice, encouragement and above all his boundless enthusiasm throughout my studies. I also wish to acknowledge the help of many former (and present) Ph.D. students and the technical staff of the St. Andrews chemistry department.

Again there are a few in particular who deserve special mention; Mr. Jim Rennie and Mr. Robert Cathcart for their technical assistance over the years and soon to be doctors Vinton Carter and David Woodcock for their encouragement and computer expertise. I would also like to thank Drs. Philip Lightfoot, Russell Morris, Susan Blake and Graham Turner for all their help and advice. I would also like to thank Dr. Diane Stirling (University of Glasgow) for allowing me the time to finish this thesis.

On a more personal note, I thank Drs. Leslie Sawers, Elizabeth-Ann Williams, Joanne Rankin and soon to be doctors Lewis Murray, Graham Kiddle and Louise Buchanan for keeping me sane outwith chemistry here at St. Andrews.

Finally, I would to thank my family and Miss Margaret Opsahl, whose support and encouragement has helped me greatly, especially over the writing of this thesis.

For providing financial assistance, The University of St. Andrews is also gratefully acknowledged for awarding me a studentship.

## Abstract

The rational design and synthesis of organic templates for the synthesis of new microporous materials has resulted in the production of five new materials, three of which are known to be microporous, the other two being better described as being open framework materials. The first three microporous materials are named STA-1, -2 and -3 (for St. Andrews) and have structural compositions of the form  $Mg_xAl_{1-x}PO_4 \cdot x/n R^{n+} \cdot yH_2O$  ( $Mg_{0.18}Al_{0.82}PO_4 \cdot R_{0.094} \cdot 0.22H_2O$ , as determined by EDX for STA-1). The fourth novel microporous solid is a boron aluminophosphate (BAIPO) and the fifth an aluminophosphate solid containing its organic template intact. All of the new materials were synthesised following a systematic study over a wide range of templates including 5 homologous series designed specifically to be used as templates in the production of aluminosilicates and -phosphates.

The structure of the first two magnesium aluminophosphates (STA-1, STA-2) to be solved by single microcrystal diffraction at the ESRF at Grenoble on crystals approximately  $30 \times 30 \times 30 \mu m$  in size is described. The *in situ* location of the template was determined directly from x-ray diffraction in the second of these materials and has formed part of a combined experimental and computational study into template location within novel frameworks. The study shows how the encapsulation of the template is directly responsible for the similarity in pore architecture between MAPO-56 and STA-2 (which co-crystallise) since the template adopts the same orientation in both materials.

Polymeric / oligomeric templates have also formed part of this study. These templates are shown to influence the phase, crystallinity, particle size and catalytic performance of the product magnesio-aluminophosphate MAPO-31. Computer modelling has also been utilised to interpret the experimental data obtained from the systematic study on the use of polymeric templates.

The *in situ* synthesis and subsequent encapsulation of two coordination complexes inside the supercage of zeolite-Y, including the 3-methyl-1,3,5,8,12-pentaazacyclotetradecane macrocycle is also described.

## Publications

The Structure of the Microporous Magnesium Aluminophosphate STA-1, prepared using a Rationally-Designed Template and Solved by Microcrystal Diffraction

G.W.Noble, P.A.Wright, P.Lightfoot, R.E.Morris, K.J.Hudson, Å.Kvick, H.Graafsma, *Angew. Chem. Int. Ed. Engl.*, 1997, **36**, 81

The Templated Synthesis and Structure Determination by Synchrotron Microcrystal Diffraction of the Novel Small Pore Magnesium Aluminophosphate STA-2

G.W. Noble, P.A. Wright and Å. Kvick, *J. Chem. Soc. Dalton Trans.*, 1997, **9**, 976

Experimental and Computational Studies of Magnesiumaluminophosphates synthesised using Polymeric and Oligomeric Templates.

P.A. Wright, P.A. Cox, G.W. Noble and V. Patinec, To appear in "*Proceedings of the 12<sup>th</sup> International Zeolite Conference, Baltimore*", 1998

Synthesis and Structure of Novel Aluminophosphates and Aluminophosphonates

P.A. Wright, G.W. Noble and V.J. Carter, Chapter in, "*Responsive Inorganic Materials*". Proceedings of the 3<sup>rd</sup> Royal Society-Unilever Indo-UK Forum on Materials Science and Engineering, Bangalore, 1996 (submitted)

Experimental and Computational Studies of the Templating of Magnesiumaluminophosphates

P.A. Wright, P.A. Cox, G.W. Noble, V. Patinec, P. Lightfoot and R.E. Morris, *in preparation*

Multi-Quantum Magic Angle Spinning NMR of a Series of Aluminophosphates and Aluminophosphonates

D. Tunstall, V.J. Carter, P.A. Wright and G.W. Noble, *in preparation*

## **Chapter Summary**

- Chapter 1: Introduction
- Chapter 2: Characterisation Techniques
- Chapter 3: Synthesis of Organic Templates
- Chapter 4: Template Study on Microporous Solids
- Chapter 5: Structure Solution of STA-1
- Chapter 6: The Structural Chemistry of STA-2
- Chapter 7: Experimental and Computational Study on Polymeric Templates
- Chapter 8: Encapsulation of Coordination Complexes
- Chapter 9: Conclusions and Further Work
- Appendix 1: Abbreviations
- Appendix 2: Common Structures
- Appendix 3: Additional Information on STA-2
- Appendix 4: Coordinates for MAPO-31 / DABCOC6 Docking Experiment

# Contents

## Chapter One

### Introduction

1.1.0	Introduction	Page	1
	1.1.1 Zeolites vs. Aluminophosphates	Page	2
	1.1.2 Zeolite Synthesis	Page	5
	1.1.3 Factors Affecting Zeolite Synthesis	Page	7
1.2.0	Historical Progress in Zeolite Synthesis, The Use of Organic Templates	Page	8
	1.2.1 Cation Templates	Page	11
	1.2.2 Templating Theories	Page	14
1.3.0	Designer Templates	Page	17
1.4.0	Structure Characterisation	Page	20
1.5.0	The Need for New Materials	Page	22
1.6.0	Zeolite Applications	Page	22
1.7.0	Catalysis	Page	24
1.8.0	References	Page	27

# Contents

## Chapter Two Characterisation Techniques

2.1.0	Introduction	Page 30
2.1.1	X-ray Diffraction	Page 30
2.1.2	Introduction to Crystallography	Page 31
2.1.3	Introduction to X-ray Crystallography	Page 34
2.1.4	Theory of X-ray Diffraction	Page 37
2.1.5	Solving a Crystal Structure	Page 39
2.1.5a	Direct Methods	Page 39
2.1.6	Structure Refinement	Page 41
2.1.7	The Single Crystal Experiment	Page 43
2.1.8	X-ray Powder Diffraction	Page 44
2.1.9	Synchrotron Radiation	Page 47
2.2.0	Nuclear Magnetic Resonance Spectroscopy	Page 49
2.2.1	Introduction to Nuclear Magnetic Resonance Spectroscopy	Page 49
2.2.2	The Theory of NMR	Page 50
2.2.3	The NMR Experiment	Page 52
2.2.4	FT NMR Spectroscopy	Page 54
2.2.5	Solid State NMR Spectroscopy	Page 55
2.2.6	Magic Angle Spinning NMR	Page 57
2.3.0	Computer Modelling	Page 59
2.3.1	Introduction	Page 59
2.3.2	Simulated Annealing	Page 60
2.3.3	Structure Docking	Page 62
2.4.0	Other Techniques	Page 64
2.4.1	Introduction	Page 64
2.4.2	Thermal Analysis	Page 65
2.4.3	Microanalysis	Page 65

## Contents

2.4.4 Density	Page 65
2.4.5 Scanning Electron Microscopy	Page 66
2.5.0 References	Page 67

## Chapter Three Synthesis of Organic Templates

3.1.0 Introduction	Page 69
3.2.0 Experimental	Page 69
3.3.0 Results and Discussion	Page 72
3.3.1 Commercial Templates	Page 74
3.3.2 Systematic Templates	Page 76
3.3.3 The Triethylammonium Series	Page 78
3.3.4 The Tripropylammonium Series	Page 81
3.3.5 The Quinuclidine Series	Page 82
3.3.6 The 1,4-diazabicyclo[2.2.2]octane (DABCO) Series	Page 85
3.3.7 The 3,5-dimethylpiperidine Series	Page 87
3.3.8 Further Novel Templates	Page 89
3.4.0 References	Page 93

## Contents

### Chapter Four Template Study on Microporous Solids

4.1.0	Introduction	Page 94
4.2.0	Experimental	Page 95
4.3.0	Results and Discussion	Page 96
	4.3.1 Commercial Templates	Page 97
	4.3.2 Developing Optimum Zeolite Synthesis Conditions	Page 99
	4.3.3 Synthesis of Aluminophosphates	Page 102
	4.3.4 New Synthesis Methods	Page 102
	4.3.5 Characterisation of a New Phase	Page 105
	4.3.6 Systematic Template Variation	Page 111
	4.3.7 Novel Templates	Page 130
4.4.0	Conclusions	Page 135
4.5.0	References	Page 136

## Contents

### Chapter Five The Structure Solution of STA-1

5.1.0	Introduction	Page 138
5.2.0	Experimental	Page 138
5.3.0	Results and Discussion	Page 139
	5.3.1 Establishing Framework Density	Page 142
	5.3.2 MASNMR Spectroscopy	Page 142
	5.3.3 Thermal Analysis	Page 145
	5.3.4 Simulated Annealing	Page 146
	5.3.5 Single Microcrystal Diffraction	Page 147
	5.3.6 Template Docking into STA-1	Page 155
5.4.0	Conclusions	Page 157
5.5.0	References	Page 159

## Contents

### Chapter Six The Structural Chemistry of STA-2

6.1.0	Abstract	Page 161
6.2.0	Experimental	Page 161
6.3.0	Results and Discussion	Page 163
6.3.1	Thermal Analysis and Nitrogen Adsorption	Page 165
6.3.2	Solid State MASNMR	Page 167
6.3.3	Synthesis of Single Crystals	Page 171
6.3.4	Structure Solution	Page 174
6.3.5	Rietveld Refinement based on Structure Derived from Single Crystal Diffraction	Page 188
6.3.6	Computer Modelling	Page 189
6.4.0	Conclusions	Page 189
6.5.0	References	Page 190

## Contents

### Chapter Seven

#### Experimental and Computational Studies on Polymeric Templates

7.1.0	Introduction	Page 192
7.2.0	Experimental	Page 193
7.3.0	Results and Discussion	Page 196
	7.3.1 Scanning Electron Microscopy	Page 199
	7.3.2 Solid State MASNMR	Page 201
	7.3.3 Thermal Analysis	Page 202
	7.3.4 Computer Modelling	Page 205
	7.3.5 Structure Blocking	Page 209
	7.3.6 Catalysis	Page 213
	7.3.7 Synthesis of STA-3 using DABCOC2	Page 213
7.4.0	Conclusions	Page 216
7.5.0	References	Page 217

## Contents

### Chapter Eight

#### Encapsulation of Coordination Complexes

8.1.0	Introduction	Page 218
	8.1.1 Coordination Complexes	Page 220
	8.1.2 Encapsulation of Complexes	Page 222
8.2.0	Experimental	Page 223
	8.2.1 The Synthesis of 1,9-diamino-3,7-diazanonane (2,3,2-tet)	Page 223
	8.2.2 Synthesis of 3-methyl-1,3,5,8,12-pentaazacyclotetradecane	Page 224
	8.2.3 Ion Exchange Between $\text{Na}^+$ and $\text{M}^{2+}$ in Zeolite-Y	Page 227
	8.2.4 The Encapsulation of 3-methyl-1,3,5,8,12-pentaazacyclotetradecane	Page 227
	8.2.5 Encapsulation of Cobalt Phthalocyanine	Page 227
8.3.0	Results and Discussion	Page 229
8.4.0	Conclusions	Page 234
8.5.0	References	Page 234

## **Contents**

### **Chapter Nine Conclusions and Further Work**

9.1.0	Introduction	Page 236
9.2.0	Conclusions	Page 236
9.3.0	Further Work	Page 239
9.4.0	References	Page 242

### **Appendices**

Appendix I :	Abbreviations	Page 243
Appendix II:	Reference Structures	Page 245
Appendix III:	Additional Information on STA-2	Page 253
Appendix IV:	Coordinates for the MAPO-31 / DABCOC6 Docking Experiment	Page 254

## Chapter One

### Introduction

#### 1.1.0 Introduction

Long winded writers I abhor,  
And glib, prolific chatters:  
Give me the ones who tear and gnaw  
their hair and pens to tatters:  
who find their writing such a chore  
they write what only matters.

- From "Crooks", by Piet Hein

The aim of the Ph.D. project described in this thesis was to synthesise new microporous solids to be used as heterogeneous catalysts by the systematic design of organic templates. A secondary aim of the project has been to encapsulate inorganic complexes inside microporous solids so as to combine the high selectivity of homogeneous catalysts with the ease of separation of heterogeneous catalysts.

In the writing of this thesis, I have tried to adhere to the principle outlined above and attempted to write the results obtained from this research as concisely as possible. It is appropriate however, to outline some of the work which is available in the scientific literature relevant to this research and to explain the theory behind many of the techniques that have been used throughout this project. Chapters one and two address these issues. Chapters three to seven describe the new research aimed at synthesising new microporous materials. Chapter eight focuses on the synthesis of encapsulated complexes inside zeolite-Y. The overall conclusions derived from this thesis and suggestions as to possible future work which may be used to expand this research are presented in chapter nine.

A full list of the abbreviations used throughout this thesis is given in appendix 1. Appendices 2 and 3 give details of commonly synthesised known structures produced throughout this research and additional details on STA-2 respectively. Appendix 4 contains the atomic coordinates of MAPO-31 and DABCOC6 which were used in a computer docking experiment explained in chapter 7.

### 1.1.1 Zeolites vs. Aluminophosphates

The aim of this project is to synthesise new microporous solids, but much of the work contained in this thesis is only concerned with zeolites and aluminophosphates. It is important therefore to explain the relationship between these different classes of material.

Microporous solids (also known as molecular sieves) are found widely in nature (mainly as aluminosilicates) and may also be synthesised (in a variety of compositions) in the laboratory. The name, 'molecular sieve' was first proposed by McBain in 1932<sup>[1]</sup> to describe materials that had specific adsorptive properties. He stated that a material must be able to separate a mixture of compounds solely on the basis of their molecular size or shape to be classified as a molecular sieve. At this time only zeolites and a few microporous charcoals were known and consequently the terms, microporous solid, molecular sieve and zeolite became interchangeable.

However, today there are at least thirteen different subclasses of microporous solid known and the classification between the different groups has become more important. Figure 1.1 shows the different classes of materials known, and their relationship to each other under the generic title, "Molecular sieve".

The work contained in this thesis has only been concerned with the zeolites, SAPOs (silicon aluminophosphates) and the EIAPOs (elemental aluminophosphates, e.g. magnesium). The other subclasses of microporous solids are included in the figure purely for reference and to stress the importance of defining which type of materials have been synthesised during this project.

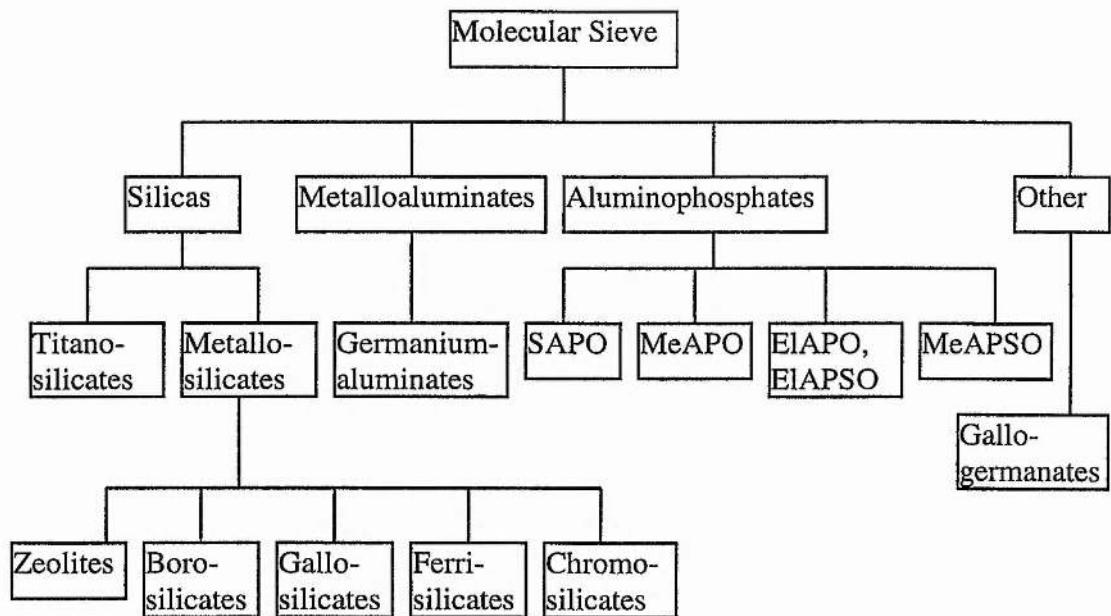
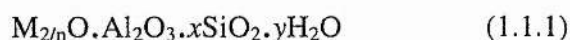


Figure 1.1 Classification of Molecular Sieve materials. This project has only been concerned with the zeolites, SAPOs and the elemental aluminophosphates, ElAPOs.

Zeolites are arguably the most important of all of the molecular sieves as they are currently the most extensively used materials due to their unique structures and their thermal and mechanical stability. Strictly speaking zeolites are tectatoaluminosilicates<sup>[2]</sup>. That is microporous solids, whose framework contains only aluminium, silicon and oxygen. Both the aluminium and the silicon are tetrahedrally coordinated to oxygen and observe strict alternation. Failure of the aluminium and silicon to alternate in this manner is in violation of Lowenstein's rule<sup>[3]</sup> which states that aluminium ions can not occupy adjacent positions, i.e. Al-O-Al bonds are unlikely to form. This is the reason why aluminium can not substitute for more than 50% of the silicon in the zeolite framework.

Zeolites have an empirical formula of;



where M represents the exchangeable cations (generally from Group I or II ions although organic cations may be used to balance the framework charge) and n represents the cation valence.  $x$  is greater than or equal to 2, since  $Al^{3+}$  can not occupy adjacent tetrahedral sites in the zeolite framework. The framework structure contains uniformly sized and shaped pores or channels around the same size as many small organic molecules. These well defined microporous structures are responsible for microporous solids possessing their unique properties and also for differentiating them from the microporous charcoals, which tend to be amorphous<sup>[1]</sup>.

Zeolites tend to be categorised as being large, medium or small according to the size of their pore or channel openings. Table 1.1 demonstrates this classification system and is based on an ideal planar configuration for rings, with an oxygen van der Waals radius of 1.35 Å.

Classification	Number of T-atoms in ring	Approximate pore size (Å)
Ultra-large	14	9
Large	12	7.5
Medium	10	6
Small	8	4.5

Table 1.1 Classification of zeolites according to their pore size. (Adapted from *Molecular Sieves Principles of synthesis and identification*, by R. Szostak<sup>[1]</sup>.)

The above classification method does not take into account the shape of the pores or channels, nor does it take into account whether the porosity consists largely as pores or as channels but it does describe the adsorptive properties of these materials.

Microporous solids may generally be classified in the same way as the zeolites. The major differences between the different subclasses as outlined in figure 1.1 are largely due to differences in framework composition. For example zeolites possess a net negative framework charge due to  $\text{AlO}_4^-$  species in the framework, whereas other microporous solids may have neutral frameworks like the  $\text{AlPO}_4$ 's and silicas.

### 1.1.2 Zeolite Synthesis<sup>[1,4-6]</sup>

Hydrothermal synthesis is the most common method for synthesising aluminosilicates. This method involves a few rudimentary steps to react a mixture of silicon and aluminium species, metal cations, organic templating molecules and water to synthesise a crystalline aluminosilicate zeolite.

The source of both the silica and the alumina are important in determining the final outcome of the synthesis. Typical silica sources include:- colloidal silica, soda glass, fumed silica (Cabosil) and silicon alkoxides such as tetraethylorthosilicate. The synthesis of zeolites in the course of this project has involved all of these sources but has concentrated on the use of colloidal silica as the main silica source for the zeolites described within this thesis. There are several sources of aluminium for zeolite synthesis also and these include:- gibbsite, pseudoboehmite, aluminate and metallic aluminium powder. The zeolites described in this project have used pseudoboehmite ( $\text{Al}_2\text{O}_3 \cdot 3\text{H}_2\text{O}$ ) as their aluminium source.

The four steps possible to synthesise an aluminosilicate are:-

- 1) Ageing
- 2) Supersaturation
- 3) Nucleation
- 4) Crystal growth

Ageing occurs when before synthesis the gel is kept below the crystallising temperature for a certain period of time. The ageing time is often crucial for obtaining a desired

product. For example zeolite-Y (described in chapter eight) requires an ageing time of 48 hours before being placed into the oven at 100°C to allow crystallisation to occur.

During ageing (partial) dissolution of the silica sol occurs and is promoted by the basic conditions required for zeolite formation (usually pH 8-14). This process increases the silicon concentration in the gel, and usually the rate increases with temperature. Silicon-29 and aluminium-27 NMR performed on the gels show that the silica reacts with aluminium species, which are almost exclusively  $\text{Al}(\text{OH})_4^-$  under these basic conditions, combining to form aluminosilicate species<sup>[5]</sup>. Amongst these aluminosilicate species, secondary building units, SBUs have been identified. Dent-Glasser and Lachowski also reported the presence of SBUs in the zeolite synthesis gels although they used trimethylsilylation to isolate the aluminosilicate species rather than NMR<sup>[7,8]</sup>.

It is interesting to see the presence of these SBUs in the synthesis gels of zeolites because they were first proposed in 1959 by R.M. Barrer *et al*<sup>[9]</sup> as an explanation as to how complicated three dimensional network structures could be formed from aluminosilicate gels.

The SBU concept was later developed by Meier in 1968, as a means of classifying the growing number of zeolite structure types that were being identified at that time. With the recent advances in the use of templates to synthesise new materials it is not surprising that Barrer's theory of SBUs being responsible for the nucleation and growth of zeolite structures has been superseded<sup>[10]</sup>. Indeed Barrer himself later acknowledged that there could be a variety of ways in which zeolites could form and that SBUs need not necessarily indicate the actual mode of growth.

During ageing and especially at elevated temperatures during the initial part of crystallisation of the zeolite, supersaturation occurs. This is when the silica and aluminium dissolve into the gel to create the aluminosilicate species described above.

Nucleation can then occur in one of two ways, either by the presence of impurities or foreign bodies in the gel, or by spontaneous nucleation. The nucleation caused by impurities or foreign particles can to an extent be suppressed by filtering the gel before being placed into the reaction vessel (autoclave). Secondary nucleation is induced by crystals and is connected to the phenomenon of seeding. The seed particles (crystals) increase in size as crystalline material is deposited on them. Since they have a larger surface area than that provided by fresh nuclei, crystal growth readily occurs here to produce high crystal yields in a short space of time. This is one of the reasons why autoclaves must be washed thoroughly after use to ensure that there are no seed crystals left behind. Failure to do this may result in the same material being synthesised repeatedly despite changes in the synthesis conditions (including the template used).

Finally crystal growth is achieved after nucleation by the addition or condensation of aluminosilicate precursor species. It is believed that crystal growth occurs at the crystal face - solution interface by the addition of aluminosilicate precursors onto the growing crystal surfaces.

### 1.1.3 Factors Affecting Zeolite Synthesis<sup>[1,2,5,11]</sup>

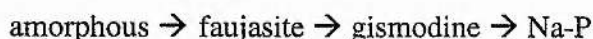
The mechanism of synthesis for zeolites, and indeed all microporous solids, is still not fully understood and there are many variables that can have significant effects on the nature of the crystalline product. Some of the factors that are known to be important in the synthesis of zeolites are described below. It should be stated that although this and the preceding section have been centred on the synthesis of zeolites, appropriate variation of the chemistry also makes these descriptions applicable to the other microporous materials.

The chemical composition of the synthesis gel, specifically the relative ratios of Si : Al and  $\text{OH}^-$  : Si is one of the most important factors in determining the outcome of crystallisation. This can influence the level of nucleation in solution, the speed at which the gel crystallises, the nature of the crystalline material as well as the crystal size,

morphology and the framework aluminium content. These can all affect the properties of the material produced.

Alkalinity is also an important factor when synthesising zeolites. The typical pH range for zeolite synthesis is 8-14 and this is important as hydroxide ions are required to help create the aluminium and silicon species needed to form the aluminosilicate precursors needed for zeolite formation. Generally an increased pH will increase reactant concentrations and accelerate crystal growth. pH can alter the nature of the ionic species present in the synthesis gel influencing the Si : Al ratio in the final crystallised product.

Usually increased temperatures and reaction times have a favourable affect on zeolite synthesis. Increased temperatures lead to shorter crystallisation times and the crystallinity of a sample usually increases with time. However, zeolites are governed by Ostwald's rule of successive phase transformations and consequently the thermodynamically least favourable phase forms first and is replaced in time by more stable phases. For example crystallising zeolite-Y can follow the sequence<sup>[12]</sup>:



The temperature can also affect the nature of the final crystallised phase, generally increasing temperatures lead to smaller pored or even dense phases being produced.

Organic additives or templates as they are frequently called can also have a highly significant effect on the synthesis of zeolites. This will be discussed further in chapter three.

### **1.2.0 Historical Progress in Zeolite Synthesis, The Use of Organic 'Templates'**

Deville was the first to report on one such attempt when in 1862 he reported the synthesis of levynite. Deville claimed that levynite was produced after he had heated potassium silicate and sodium aluminate together in a sealed glass ampoule<sup>[6]</sup>. Unfortunately this and other similar early claims that were made before the use of x-ray

diffraction techniques must be regarded with caution as characterisation was carried out primarily using mineralogical techniques based mainly on chemical and optical properties of what is likely to have been microcrystalline materials. It is interesting to note however, that Deville and others of that time were trying to synthesise zeolites under geological conditions.

The first reliably characterised zeolites were synthesised around the 1940s by Barrer and co-workers. Their work utilised inorganic cations such as sodium and potassium to successfully synthesise known natural zeolite materials. They also produced several new materials including ZK-5 which is not found in nature but was not fully characterised until later. Zeolite-A, reported in 1956, two hundred years after the initial discovery of zeolites by Cronsted<sup>[13]</sup>, is generally regarded as being the first fully characterised novel zeolite not found in nature. It was formed again using inorganic cations but significantly under much milder conditions to those used by Deville. In fact zeolite-A's synthesis at atmospheric pressure, high water concentrations and temperatures not exceeding 100°C replicated the natural sedimentary conditions under which zeolites form in nature. These reaction conditions are often referred to as the hydrothermal synthesis method and this method, the most widely used method for the synthesis of zeolites.

Shortly after the development of the hydrothermal synthesis technique, there was another major advance in zeolite technology. Two independent zeolite groups, Barrer and Denny<sup>[14]</sup> and Kerr and Kokotailo<sup>[15]</sup> began to investigate the use of organic cations instead of inorganic cations in the synthesis of zeolites. In 1961, Barrer and Denny reported the use of tetramethylammonium hydroxide and alkylammonium cations in the synthesis of a zeolite. These ions are able to organise water molecule networks around them into clusters, which is most likely a consequence of the hydrophobic character of the alkyl groups.

The mechanism by which organic or inorganic cations contribute to the synthesis of zeolites is still not fully understood but their influence on the synthesis of new materials has been dramatic over the last thirty years. This effect is perhaps best illustrated by

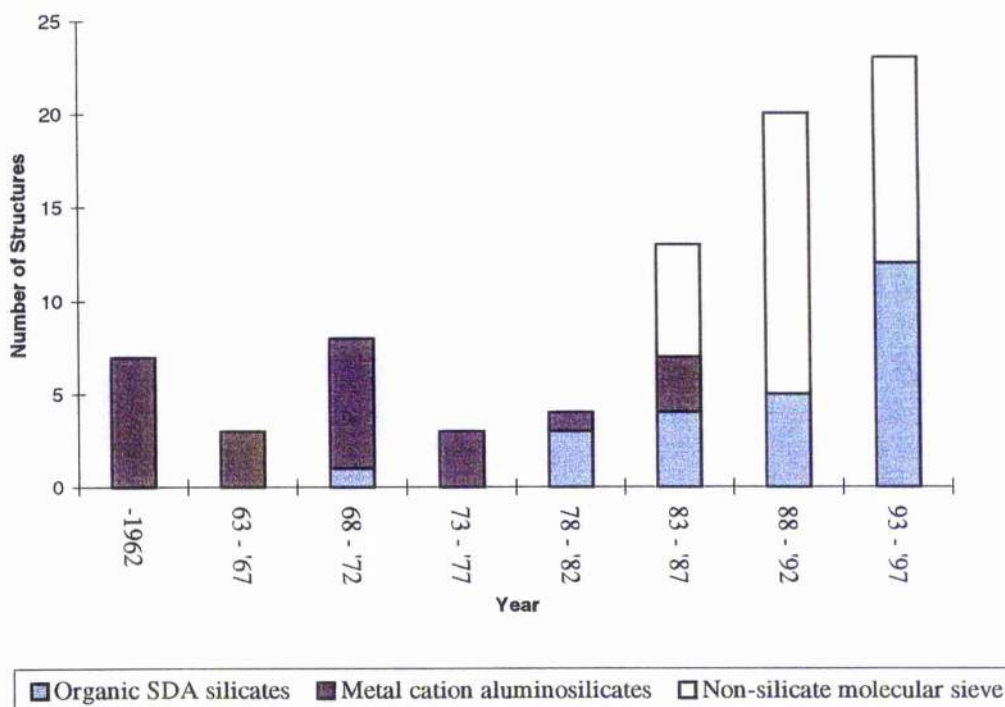


Figure 1.2 New tetrahedrally coordinated structures (diagram courtesy of P.A.Wright<sup>[16]</sup>).

Figure 1.2 above shows the number of new tetrahedrally coordinated materials reported since 1962. Both the blue and yellow colours indicate the use of templates as described by the key shown in the figure. It is obvious therefore that the use of organic templates has had and continues to have a dramatic impact on the synthesis of new tetrahedrally coordinated materials.

The sudden increase in number of microporous solids discovered after 1982 is due to both the pioneering work of Flanigen *et al*<sup>[17]</sup>, who were the first to develop the aluminophosphates at Union Carbide in 1982, and the recent advances in the use of 'designer' templates in silicate-based microporous solids, especially by Zones.

Organic additives are often called templates due to the close relationship found between the size and shape of the organic molecules and the size and shape of the pores and channels of the microporous materials that they synthesise<sup>[18,19]</sup>. It is for this reason that

Organic additives are often called templates due to the close relationship found between the size and shape of the organic molecules and the size and shape of the pores and channels of the microporous materials that they synthesise<sup>[18,19]</sup>. It is for this reason that the term organic template will be used throughout the remainder of the thesis. It should be stated however, that these molecules are not true templates in the strictest sense of the word as several different framework topologies may form from a single organic species depending upon other reaction variables. Similarly the same framework topology may form even when using a variety of different template molecules, for example ZSM-5 or MAPO-5 (see chapter four).

### 1.2.1 Cation Templates

The mechanisms of zeolite formation are extremely complex due to the number of different variables that can influence the final product of framework that forms. Several of these variables have already been discussed (section 1.2.1). This section is concerned with arguably the most important variable - that is the influence than an organic or inorganic cation may have on the crystallisation of zeolites. Whilst it is noted that aluminophosphates and zeolites form under different reaction conditions (e.g. pH) their methods of crystallisation are analogous and so the discussion that follows is applicable to both types of material. It is perhaps also interesting to note that tetrahedrally coordinated microporous aluminophosphates have not been reported as being synthesised in the absence of an organic based template molecule<sup>[1]</sup>, indicating that the templates behave in a complex manner and are involved with more than simply directing possible framework topologies.

The ways in which organic and inorganic cations may affect the synthesis of zeolites are summarised below in table 1.2.

Nature of Cation	Possible Affect	
Inorganic	Balancing charge  Morphology  Crystal Purity  Yield  Structure Direction	since $AlO_2^-$ species are present in the framework, this is less important for aluminophosphates.  presence of specific cations e.g. $Na^+$ and $K^+$ can have a dramatic influence on the morphology of crystals (see chapter six).
Organic	Gel Modifier  Chemical interactions  Physical interactions  Void filler (perhaps)  Structure direction or templating	which could result in the formation of structures with higher $SiO_2 / Al_2O_3$ than could be achieved in the absence of the organic cations. TMA for example has been used to extend the Si/Al of the known synthetic analogues of the natural zeolites.  With other components in the gel, altering the character of the gel. Organic bases for example could alter the pH of the crystallising gel.  with other components in the gel, altering the solubility of various species, ageing characteristics, transport and thermal properties and crystallisation time of the gel.  since much of the water present in the higher Si/Al zeolites is probably adsorbed into the structure during crystal formation.

Table 1.2 Summary of Cation Affects on Zeolites Synthesis (Adapted from Szostak<sup>[11]</sup>)

Both the inorganic and the organic cations can act as structure directors since cations are known to influence the ordering of water molecules in aqueous solution. The extent to which cations can do this determines if they exhibit “structure making” or “structure breaking” characteristics<sup>[5,19]</sup>.

Structure making cations are usually small highly charged cations such as  $\text{Na}^+$  and  $\text{Li}^+$  which interact strongly with the water molecules, breaking the water hydrogen bonds before rearranging the molecules into an organised cluster, as illustrated in figure 1.3.

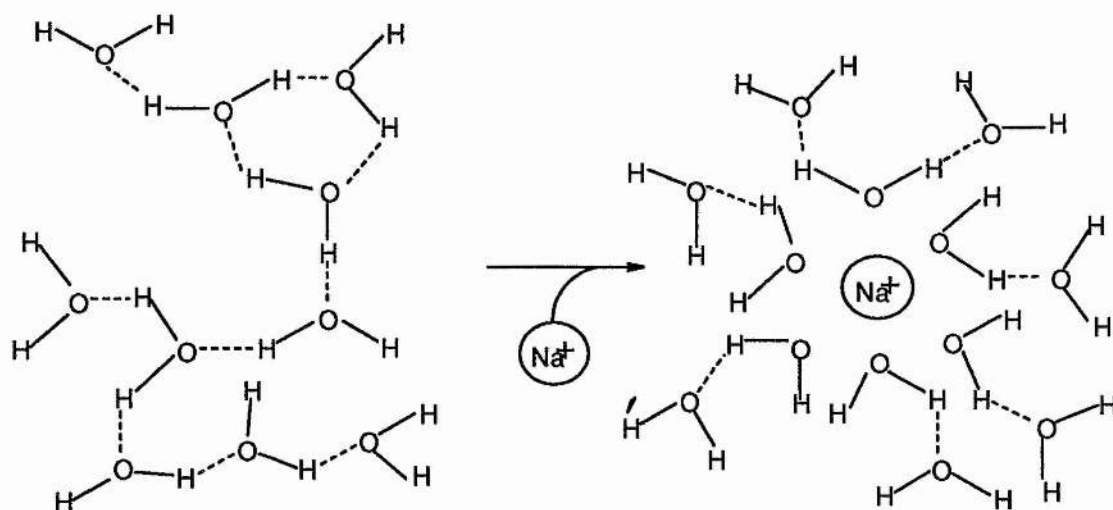


Figure 1.3 Schematic representation of the structure making interactions between a sodium cation and water molecules in an aqueous solution. (Figure taken from P.A. Jacobs *et al*<sup>[51]</sup>.)

Structure breaking cations are by comparison to structure making cations usually larger for example  $\text{NH}_4^+$  and  $\text{K}^+$ . These cations also interact with water molecules, breaking the hydrogen bonds but are less able due to their smaller charge density to arrange the water molecules around them. However, not all large cations exhibit structure breaking characteristics. Alkyl ammonium cations for example are able to arrange water molecules around them into clusters, probably as a consequence of their hydrophobic character at the alkyl group.

The ability to form organised water molecule clusters around a cation has an important consequence in zeolite synthesis. Silicate and aluminate  $\text{TO}_4$  units can partially replace the water molecules (oxygen on silicon replaces the oxygen of water) and in this way contribute to the formation of cage-like structures<sup>[51]</sup>.

This crude micro-order to macro-order description can be demonstrated by the incorporation of tetramethyl ammonium (TMA) inside sodalite cages. The large TMA cation can not enter into or diffuse out of a sodalite cage once formed for steric reasons. However, sodalite formed in the presence of TMA<sup>[14]</sup> has been shown to contain approximately one TMA cation per sodalite cage. It is obvious therefore that the water molecules surrounding the TMA ion must have been replaced by aluminosilicate  $\text{TO}_4$  units as previously described.

### 1.2.2 Templating Theories

Rationalising the exact role of templates in zeolite synthesis is made particularly difficult as the overall mechanism by which zeolites crystallise is not well understood. Many factors, such as the synthesis gel composition or reaction conditions can have a dramatic effect on the outcome of the synthesis. Furthermore direct observation of an organic template *in situ* within a zeolite framework is often not possible. Consequently several theories have emerged in an attempt to explain the exact role of organic templates in zeolite formation.

Lok and co-workers proposed a template theory based on the micro-order to macro-order model described above<sup>[20]</sup>, after conducting a large literature review. They conceded that other factors such as synthesis gel composition or reaction conditions were significant but still decided that the templates contributed greatly to the frameworks that formed. Obvious criticisms of this theory include the fact that an organic template may facilitate the formation of several different frameworks depending upon other reaction variables. Similarly a single framework may be produced by using a variety of different templates.

Despite these concerns however, this model is still the basis of many theories into the synthesis of specific templates for the rational design of new tetrahedrally coordinated frameworks. This is also the theory upon which this research project is based namely that organic template molecules influence the arrangement of oxide tetrahedra around themselves in a specific way dependent upon their structural shapes and electrostatic

distributions. Attempts to circumvent the problems outlined above have been made by maintaining consistent “standard” aluminophosphate and zeolite gel compositions and reaction conditions throughout the project, differing only on the nature of the template present. The actual experimental conditions are explained in detail in chapter four.

Vaughan’s Extended Structure Approach (ESA)<sup>[19]</sup> has also been an attempt at rationalising the template role. This theory which was also based on the findings of an extensive literature review is a little more relevant to zeolites than to aluminophosphates although it stills follows the basic theory outlined by Lok. The most significant modification of the ESA theory is that it attributes the formation of a zeolite topology not solely to the organic cation present but also with consideration of the inorganic ions present. Thus the ESA theory is based on the structure directing properties of two cations which it defines as primary and secondary. Micro-ordering of the synthesis gel into extended structures or framework sheets is achieved by the primary cations. These are usually small, highly charged cations such as Na<sup>+</sup>. Macro-ordering of the synthesis gel into zeolite crystallites is then achieved by the secondary cations which are typically the larger, less densely charged organic cations.

Jacobs *et al* utilised this approach when attempting to elucidate the role of crown ethers in the synthesis of zeolite-Y (FAU) and hexagonal zeolite-Y (EMT)<sup>[21]</sup>. Both materials are members of the same zeolite family consisting of common faujasite sheets (sodalite cages linked via hexagonal prisms or 6T-atom rings) which can join at three inequivalent positions denoted by A, B and C. In FAU (cubic) the stacking sequence can be described as being ABCABC...whilst EMT (hexagonal) has an ABABAB.... Stacking sequence. This system was studied because the zeolites were synthesised using two similar templates, namely 15-crown-5 and 18-crown-6 respectively.

It was observed that controlling the ratio of the amount of each ether present in solution could control the extent to which each zeolite phase was present in an intergrowth composition. After careful analysis using a variety of techniques it was revealed that two types of surface hole were present, the hypo-hole and the relatively larger hyper-hole which were preferentially occupied by the 15-crown-5 and 18-crown-6 ethers

respectively. The ESA was used to rationalise these results. A full explanation of these results are presented in reference [21] but to summarise the 18-crown-6 ether, acting as a secondary cation is able to act as a structure blocking molecule such that successive faujasite layers can only add in an ABABAB.. fashion and hence promote the formation of EMT.

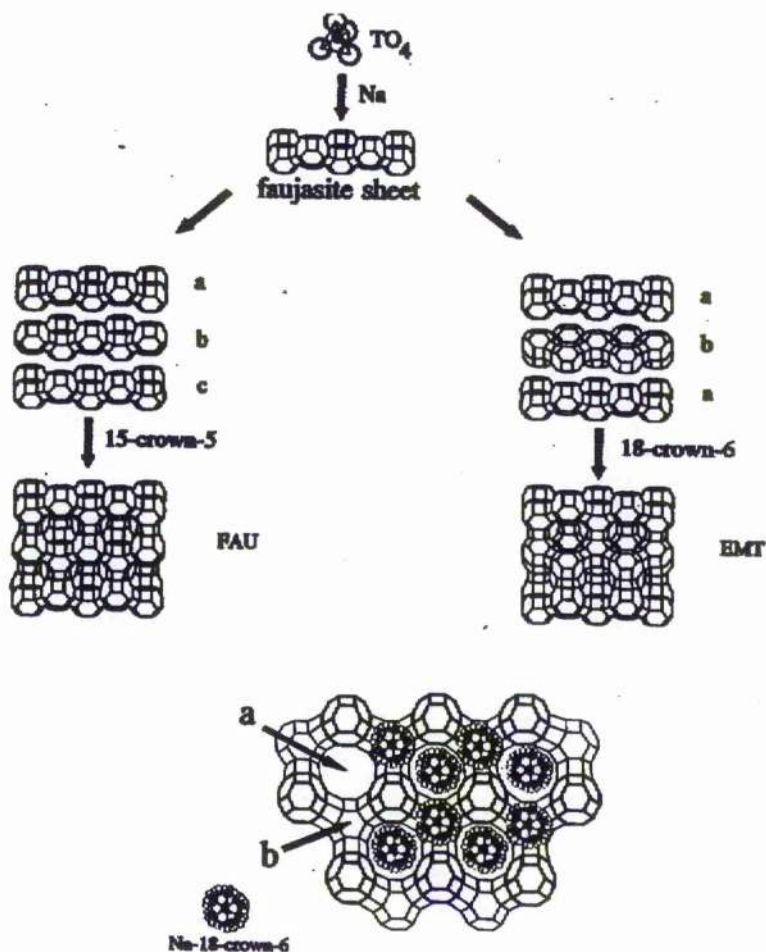


Figure 1.4 Representation of the formation of the end-members, FAU and EMT, along with an illustration of the faujasite sheet showing the surface holes containing the 18-crown-6 ethers. The arrows indicate the hyper- (a) and the hypo- (b)-holes. The 18-crown-6 ethers in the hypo-holes blocks the formation of FAU. (Figure reproduced from P.A. Jacobs *et al*<sup>[51]</sup>.)

### 1.3.0 Designer Templates

The desire to synthesise and develop new zeolite topologies which have large pores or channels to be used for catalysis has led to the development of 'designer templates'. These are molecules that have been specifically designed so as to promote the formation of the desired framework. Because these templates often fall out with the range of commercially available templates owing to their specific sizes and shapes it is often necessary to synthesise the template molecules before synthesising the zeolite.

Important considerations for template design include:-

- (1) the size and shape of the molecule as this will determine to a large extent the size and shape of the pores / channels present in the zeolite.
- (2) the stability of the molecule, since the template must remain intact throughout the zeolite synthesis, often at high temperatures and under highly basic conditions.
- (3) ease of preparation and characterisation. Zeolites are only useful catalysts when the template has been removed from the framework structure, normally by calcination. It is important therefore that the templates can be synthesised in high yields at low cost (as they can not be reused and are only required for the initial preparation of the zeolite) to be commercially viable.
- (4) charge balance potential. Zeolites form with a negatively charged framework and it is important to balance this charge, possibly by using a positively charged template.
- (5) solubility, because the organic template is to be used in aqueous conditions it is vital to control its hydrophobic nature. This can be achieved by controlling the carbon to nitrogen ratio of the template since the nitrogen atom is positively charged in tetra alkylammonium ions and helps the template to become miscible in water.

The use of designer templates has been one of the major factors involved in the sudden increase in new tetrahedrally coordinated framework structures reported since the 1980's (see figure 1.2 and reference [16]). The synthesis of the small pore aluminosilicate, SSZ-16 by Lobo *et al*<sup>[22]</sup> is an excellent example of the use of designer templates to synthesise a new framework topology. The SSZ-16 framework is isostructural to

isostructural to MAPO-56, and interestingly the same 1,4-diquinuclidinium cation can be used in the production of both materials. Although the template position was not determined for SSZ-16 which was solved using synchrotron powder diffraction data, the template has been located inside MAPO-56 by single crystal diffraction in the course of the research described in this thesis.

Other large pore silicate based materials recently synthesised using designer templates include CIT-1<sup>[23]</sup> and CIT-5<sup>[24]</sup>. CIT-1 (California Institute of Technology-1) was the first synthetic zeolite to have intersecting 10- and 12- ring pores that was not an intergrowth of different polymorphs. It is related to SSZ-26 and SSZ-33 but both of these materials are faulted<sup>[5]</sup>, hindering their catalytic potentials unlike CIT-1 which is an active catalyst for the cracking of n-butane when aluminium is substituted into its framework. The templates required to produce both CIT-1 and CIT-5 which is an ultra-large pore zeolite containing 14T-atom pores are shown in figure 1.5.

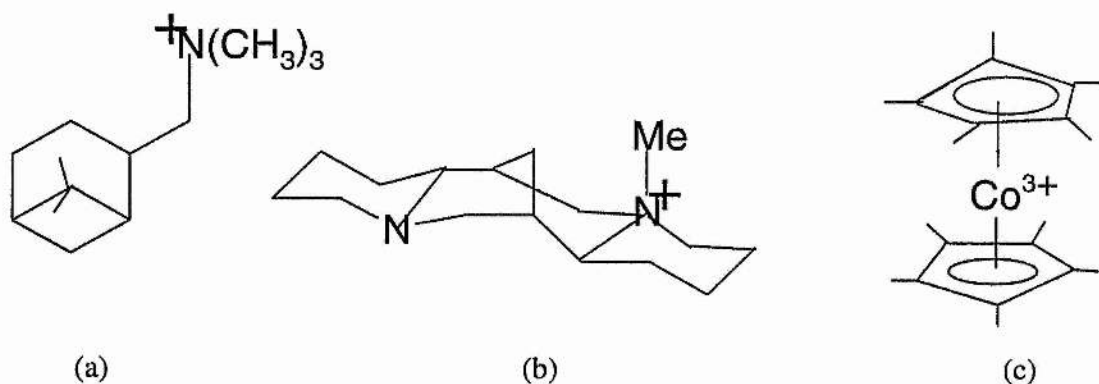


Figure 1.5 Designer templates recently used to produce (a) CIT-1, (b) CIT-5 and (c) UTD-1.

It is interesting to note that in most of the work described above by Davis, Lobo and Zones, the carbon to nitrogen ratio was around 13 : 1 so as to maintain the solubility of the template in the aqueous conditions used to prepare the zeolites. Other approaches to achieve template solubility can be used however, as was demonstrated by the production of the first 14T-atom pore zeolite, UTD-1<sup>[26]</sup> (University of Texas-1) which used

bis-(pentamethyl-cyclo-pentadienyl)-cobalt (III) hydroxide as the template (also shown in figure 1.5 above).

With the obvious advances in the use of the designer templates to synthesise aluminosilicates it is perhaps surprising that this method has not been more widely adopted in the production of new aluminophosphates. The designer template approach has however been adopted in the work described in this thesis.

Other researchers have also used the approach and DAF-1 and DAF-5 are notable examples. DAF-1 was synthesised from the systematic study of alkylammonium cations<sup>[27]</sup> and forms the basis upon which the work contained in this thesis is based. The production of DAF-1 highlights the value in adopting an empirical approach to the synthesis of new materials.

An alternative approach is however taken by Lewis *et al* who have developed a computer program to predict the possible frameworks synthesised by different organic templates. The technique known as ZEBEDEE<sup>[28]</sup> (zeolites by evolutionary de novo design) was designed to predict the size and shape of template topologies and was able to predict the choice of 4-piperidinopiperidine as the choice of template employed to synthesise DAF-5<sup>[29]</sup>.

The use of computer modelling techniques to design new templates (and / or new frameworks) are important as was demonstrated by the synthesis of DAF-5, however, there are too many reaction variables in the synthesis of microporous solids to be overcome by computational techniques alone.

The recently determined cobalt gallium phosphate structures denoted by the IZA codes: SBE<sup>[30]</sup>, SBS<sup>[30]</sup>, CGS<sup>[30]</sup> and CGF<sup>[30]</sup> prepared from 1,9-diaminononane, 1,7-diaminoheptane, quinuclidine and DABCO respectively further underlines the efficacy of the empirical approach used in this project.

#### 1.4.0 Structure Characterisation

Many of the important physicochemical properties of zeolites, for example catalysis and adsorption, are defined by their unique tetrahedral frameworks. In order to optimise these properties, a detailed knowledge of the framework structures is vital to understand these structure/property relationships. An understanding of the framework as well as the occluded location and conformation of the organic species is vital in trying to rationalise the role of organic templates in zeolite synthesis. A complete listing of all known tetrahedrally coordinated frameworks can be found in the “*Atlas of Zeolite Structure Types*”<sup>[31]</sup> and the associated Web page<sup>[30]</sup>.

The study and characterisation of zeolite frameworks has traditionally been a complex and non-trivial problem due to many crystallographic problems inherent to this class of material. Not least of these problems is that zeolites tend to form as microcrystallites (usually of the order 0.001 to 10  $\mu\text{m}$ ) and as such are unsuitable for conventional single crystal analysis. Powder diffraction is also made difficult by structural faulting (zeolite-beta being an extreme example<sup>[32]</sup>), crystal twinning, lattice intergrowths, multiple phases and impurities which are all common in zeolite chemistry. Consequently a variety of techniques are often required to fully characterise a zeolite structure.

X-ray powder diffraction is the currently the most widely used method for investigating zeolite framework structures. X-ray powder diffraction (XRD) overcomes many of the particle size problems by irradiating a sample of microcrystals which are assumed to be in all possible crystallographic orientations. Unfortunately there is a considerable loss of information obtained by powder diffraction over single crystal methods but it is still possible to determine the size and shape of the unit cell and often to determine the space group. The amount of information obtained from x-ray powder diffraction can be improved by using more intense radiation such as synchrotron radiation. Not only can this often yield better resolved powder diffraction patterns but it can also allow single crystal studies on micron sized samples. The use of single microcrystal diffraction has been used in this project and the results of these studies are presented in chapters five and six.

Even with synchrotron radiation there are finite limits to the amount of information that may be obtained from powder diffraction methods. The determination of the location of the organic template within zeolite frameworks for example is particularly difficult. This is because the diffractograms are dominated by contributions by the heavier framework atoms. Template disorder also makes the template less “visible” to x-ray diffraction.

The most commonly used technique to complement the information obtained from x-ray diffraction is solid state magic angle spinning nuclear magnetic resonance (MASNMR) spectroscopy. This is essentially a “short range” technique sensitive to atomic or environmental changes over a few bond lengths. Carbon-13 MASNMR can rapidly identify the nature of the organic species present within the zeolite framework and can often prove that a template molecule has been incorporated intact. Information on zeolite frameworks not offered by diffraction techniques can be obtained using MASNMR. Silicon-29 MASNMR for example can reveal the structural environments of the silicon atoms revealing the number of neighbouring aluminium atoms and the proportions of each present in the sample. MASNMR performed on the  $^{27}\text{Al}$  nucleus can also reveal framework information such as the relative amounts of the tetrahedrally and octahedrally coordinated atoms present within a sample. This is an important consideration for both computational investigations and for determining the catalytic potential of a zeolite.

Other commonly used techniques employed in the characterisation of zeolites include scanning electron microscopy (SEM) and high resolution transmission electron microscopy (HRTEM). Both of these techniques are capable of offering information on crystallite size and shape. HREM in particular is proving an ideal tool for investigating phase purity, the extent and frequency of crystal twinning in a sample and stacking disorders. HREM was used by Newsam *et al* in the characterisation of zeolite beta<sup>[32]</sup>. Computer modelling is also being used to predict the location of the templates within zeolite frameworks and as a means of predicting which frameworks could be directed using possible organic templates<sup>[28]</sup>.

### 1.5.0 The Need for New Materials<sup>[2,16]</sup>

With over one hundred tetrahedrally coordinated microporous solid framework topologies known, and innumerable framework compositions, the question arises, “Is there still a need for more new structures”? The answer is simply, “Yes”.

Different framework topologies bring with them new pore architectures that differ in both size and shape from existing materials. This results in each new microporous material having its own unique chemical and physical properties. For example, frameworks with higher void volumes could be useful for a variety of catalytic and adsorption applications, currently materials are restricted to only about 50% void volume. Chiral frameworks may be useful for asymmetric synthesis or the separation of enantiomers, both properties would be much sought after by the pharmaceutical industries. There is also a need for large pore structures that will permit catalytic transformations of larger molecules.

There are many synthetic targets that are still to be accomplished in the synthesis of microporous solids. Traditionally the synthesis of new microporous solids has been by Edisonian methods (i.e. trial and error) due to the complexity of the zeolite systems which makes them difficult to understand or control. The work contained in this thesis adopts a more rational approach to the synthesis of new materials.

### 1.6.0 Zeolite Applications<sup>[33]</sup>

Microporous solids are one of the most widely used class of chemicals in industrial chemistry today. Their uses easily span the fine chemicals and bulk chemicals divisions as they are used for such diverse things as livestock food to catalytic cracking in petrol refineries. This section is intended to illustrate several of the more common uses of zeolites only and should not be considered as a comprehensive list of zeolite applications.

zeolites only and should not be considered as a comprehensive list of zeolite applications.

The unique properties of zeolites and microporous solids in general arise from their uniform and periodic pore or channel distribution. Zeolite pores are typically around the same size as small molecules. These properties allow molecular sieves (as they are frequently called) to recognise, discriminate and organise molecules with precisions that can be less than  $1\text{\AA}$ <sup>[3]</sup>. This “sieving” capability is often exploited by organic chemists during the synthesis of organic compounds.

Composition, as well as architecture, is also an important consideration for the application of a microporous solid. It is the presence of extra-framework cations that can move freely throughout the zeolite structure that is exploited when the zeolite is used for dehydrating or ion-exchange purposes. Crystalline zeolites often contain water molecules that are coordinated to the exchangeable cations. If these water molecules are removed by heating the zeolite (possibly under vacuum) then the zeolite will actively adsorb water when available to allow the cations to return to their preferred high coordination state. This plus the fact that zeolites can have up to 50% internal void space makes dehydrated zeolites very effective desiccants.

The mobility of the extra-framework cations within the zeolite are also used for ion-exchange purposes, that is when the internal cations are replaced by cations from the surrounding solution. The largest scale industrial production of zeolites is that devoted to the production of the sodium form of zeolite-A for use by the detergent industry. Zeolite-A is added to detergents to act as a water softener, where it readily exchanges  $\text{Na}^+$  for  $\text{Ca}^{2+}$  and  $\text{Mg}^{2+}$  ions present in “hard” water, thereby preventing the precipitation of the surfactants. The use of zeolite-A as a water softener has the additional advantage in that it removes the need for ecologically damaging polyphosphates to be used in washing powders.

Other ion-exchange applications for zeolites include radioisotope scavenging, waste water treatment and agricultural uses. Clinoptilolite has the ability to ion-exchange  $\text{Cs}^+$

radioisotopes from aqueous nuclear wastes and is currently being used by British Nuclear Fuels for cleaning purposes at Sellafield. Clinoptilolite, chabazite and zeolite-A have all been used to facilitate the clean up after the nuclear accidents at Chernobyl and Three Mile Island. As well as  $\text{Cs}^+$ , clinoptilolite is also able to exchange  $\text{NH}_4^+$  cations which makes it ideal for waste water treatment plants. Japan, Hungary and the USA use zeolites to help purify waste water. Once absorbed the  $\text{NH}_4^+$  cations can be released again if added to soil and in this way can act as a controlled release fertiliser. The academic literature describes how the quality of soil may be improved by adding up to 10% zeolite to it, resulting in increased crop yield.

### 1.7.0 Catalysis

Zeolites are excellent solid acid catalysts and are widely used throughout industry. The acidity arises from the zeolites readily available source of protons (Brønsted acidity) or unsaturated cations (Lewis acidity) and it is largely the strength of the zeolites acidity and coupled with their unique shape selective properties that make them ideal catalysts.

Zeolites are ideal because of their qualities outlined above to be used in the petrochemicals industry where important reactions include cracking, isomerisation and alkylations. Important side reactions include the formation of coke. The size and shape of the zeolite pores can minimise the range of possible compounds formed and hence impose a degree of selectivity but it can not prevent the formation of coke. Coke is a catalyst poison which rapidly deactivates the catalyst and so must be removed i.e. the catalyst must be regenerated to remove the coke blocking its pores and covering up the catalysts active sites.

In the cracking reactor itself the catalyst is passed quickly through a tubular reactor and into a disengaging unit where a gas-solid separation occurs. The solid particles (zeolite) flows continuously to a fluidized regenerator, where the coke is burned off in air before flowing back into the reactor to be mixed with gas oil (and steam to disperse and rehydroxylate the zeolite). The combustion of the coke carried by the zeolite provides sufficient power to run the system continuously. Fresh catalyst particles have to be continuously added and the old ones removed as the catalyst structure becomes damaged

slowly over a period of time. A schematic diagram of this process is shown below in figure 1.6.

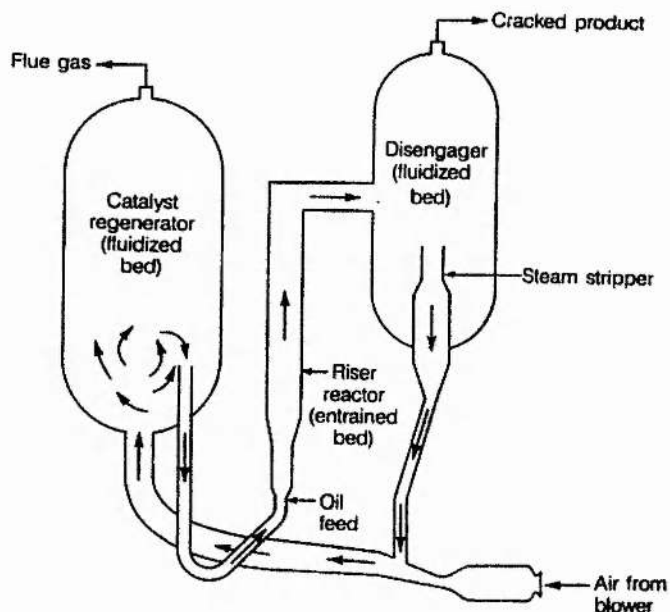


Figure 1.6 Schematic diagram of catalytic cracking. The flow pattern of the catalyst particles is illustrated by the arrows. (Taken from B.C. Gates, Catalytic Chemistry<sup>[3]</sup>.)

The zeolites' acidity which is associated with the framework charge (see figure 1.4) is one of the main features that make zeolites interesting for catalysis. Other important attributes include<sup>[34]</sup>:

- 1) well defined pore-size distribution;
- 2) high surface area;
- 3) good thermal and hydrothermal stability;
- 4) high resistance to hetero-atom (e.g. sulphur, nitrogen) poisoning;
- 5) low coke forming tendency ( for ZSM-5 for example );
- 6) strong tuneable acidity; and
- 7) molecular shape selective control of reactions.

The acidity provides the catalytic activity, the well defined size and shape of pores provide the shape selectivity<sup>[35]</sup>, see figure 1.8.

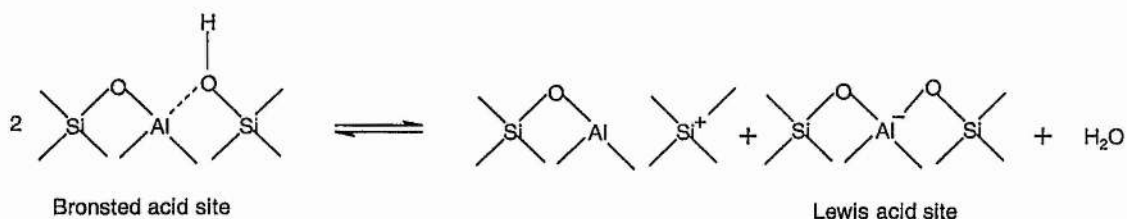


Figure 1.7 The source of zeolite framework acidity. The acid strength can be varied by changing the Si / Al ratio.

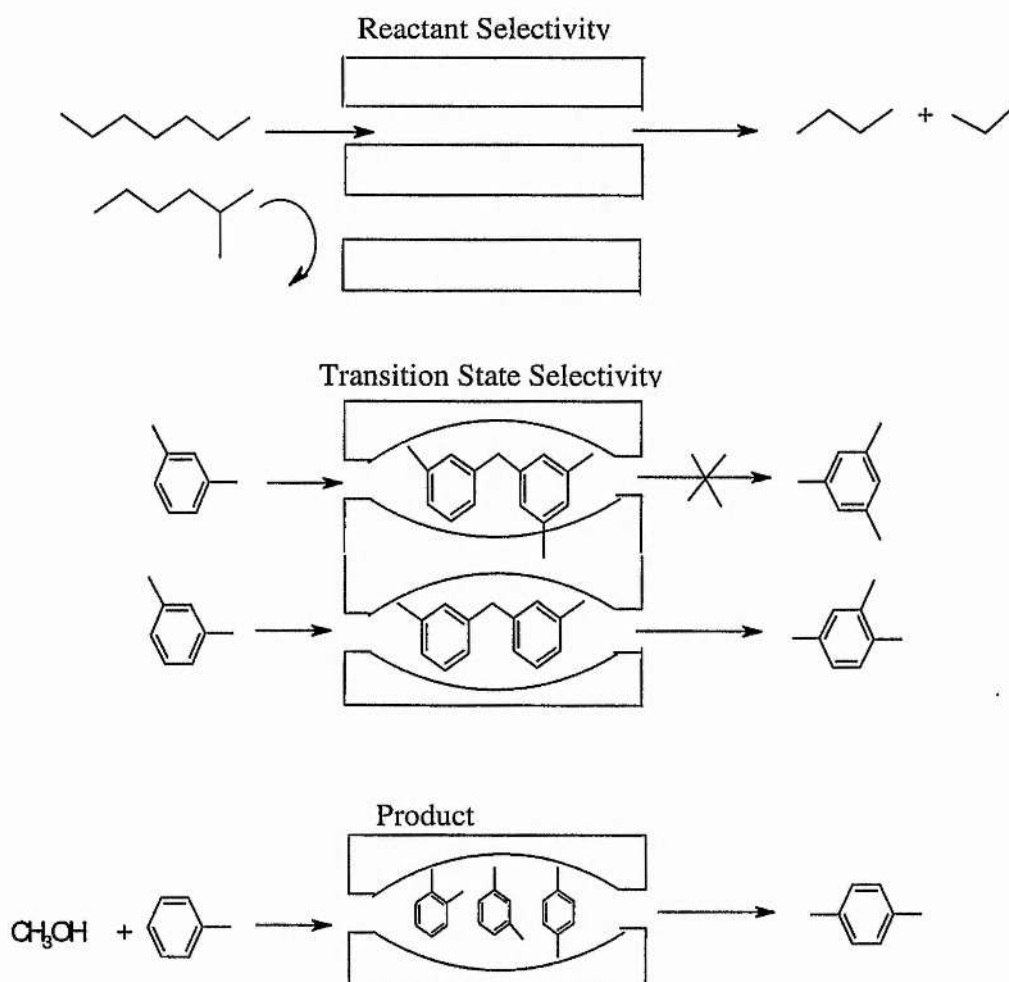


Figure 1.8 Shape selectivity in zeolites. From the top, reactant selectivity (rejection of branched hydrocarbons), transition state shape selectivity and product selectivity.

The use of zeolites as catalysts was first announced in 1960 by Wiesz and Frillete<sup>[36]</sup>. They noticed the shape selective properties of the "molecular sieve", whilst studying paraffin isomerisation and cracking reactions. Since then the use of zeolites and microporous solids as catalysts has developed dramatically<sup>[37]</sup> such that they are now used in both the bulk and fine chemical industries.

### 1.8.0 References

- 1 R. Szostak, *Molecular Sieves Principles of Synthesis and Identification*, Van Norstrand Reinhold, 1989
- 2 M.E. Davis and R.F. Lobo, *Chem. Mater.*, 1992, **4**, 756
- 3 B.C. Gates, *Catalytic Chemistry*, John Wiley & Sons, 1992
- 4 R. Szostak, *Handbook of Molecular Sieves*, Van Norstrand Reinhold, 1992
- 5 E.J.P. Feijen, J.A. Martens and P.A. Jacobs, *Zeolites and Microporous Materials: State of the Art (1994)*, *Studies in Surface Science and Catalysis*, **84**, 3
- 6 Alan Dyer, *An Introduction to Zeolite Molecular Sieves*, John Wiley & Sons, 1988
- 7 L.S. Dent Glasser and E.E. Lachowski, *J. Chem. Soc., Dalton Trans.*, 1980, 393
- 8 L.S. Dent Glasser and E.E. Lachowski, *J. Chem. Soc., Dalton Trans.*, 1980, 399
- 9 R.M. Barrer, J.W. Baynham, F.W. Bultitude and W.M. Meier, *J. Chem. Soc.*, 1959, 195
- 10 C.T.G. Knight, *Zeolites*, 1990, **10**, 140
- 11 S.I. Zones, R.A. Van Norstrand, D.S. Santilli, D.M. Wilson, L. Yuen and L.D. Scampavia, *Zeolites: Facts, Figures, Future*, Elsevier Science Publishers, 1989, 299
- 12 D.W. Lewis, C.M. Freeman and C.R.A. Catlow, *J. Phys. Chem.*, 1995, **99**, 11194
- 13 A.F. Cronsted, *Akad. Handl.*, Stockholm, 1756, **17**, 20 (cited from reference [5])

- 14 R.M. Barrer and P.J. Denny, *J. Chem. Soc.*, 1961, 971
- 15 G.T. Kerr and G. Kokotailo, *J. Am. Chem. Soc.*, 1961, **83**, 4675
- 16 R.E. Morris and P.A. Wright, *Chemistry and Industry*, 1998, 256
- 17 S.T. Wilson, B.M. Lok, C.A. Messina, T.R. Cannon and E.M. Flanigen, *J. Am. Chem. Soc.*, 1982, **104**, 1146
- 18 R.E. Boyett, A.P. Stevens, M.G. Ford and P.A. Cox, *Zeolites*, 1996, **17**, 3
- 19 A.P. Stevens, Ph.D. Thesis, University of Portsmouth, 1996
- 20 Ch. Baerlocher and W.M. Meier, *Helv. Chim. Acta.*, 1970, **53**, 1295
- 21 E.J. Feijen, K.D. Vadder, M.H. Bosschaerts, J.L. Lievens, J.A. Martens, P.J. Grobet and P.A. Jacobs, *J. Am. Chem. Soc.*, 1994, **116**, 2950
- 22 R.F. Lobo, S.I. Jones and R.C. Medrud, *Chem. Mater.*, 1996, **8**, 2409
- 23 R.F. Lobo and M.E. Davis, *J. Am. Chem. Soc.*, 1995, **117**, 3766
- 24 P. Wagner, M. Yoshikawa, M. Lovallo, K. Tsuji, M. Tsapatsis and M.E. Davis, *Chem. Commun.*, 1997, 2179
- 25 R.F. Lobo, M. Pan, I. Chan, H.X. Li, R.C. Medrud, S.I. Zones, P.A. Crozier and M.E. Davis, *Science*, 1993, **262**, 1543
- 26 C.C. Freyhardt, M. Tsapatsis, R.F. Lobo, K.J. Balkus Jr. and M.E. Davis, *Nature*, 1996, **381**, 295
- 27 P.A. Wright, C. Sayag, F. Rey, D.W. Lewis, J.D. Gale, S. Natajarai and J.M. Thomas, *J. Chem. Soc. Faraday Trans.*, 1995, **91(19)**, 3537
- 28 D.W. Lewis, D.J. Willock, C.R.A. Catlow, J.M. Thomas and G.J. Hutchings, *Nature*, 1996, **382**, 604

- 29 G. Sankar, J.W. Wyles, R.H. Jones, J.M. Thomas, C.R.A. Catlow, D.W. Lewis, W. Clegg, S.J. Coles and S.J. Teat, *Chem. Commun.*, 1998, 117
- 30 IZA web page, <http://www.iza-sc.ethz.ch/IZA-SC/AtlasHome.html>
- 31 W.M. Meier, D.H. Olson and Ch. Baerlocher, *Atlas of Zeolite Structure Types*, 4<sup>th</sup> Edition (revised), Elsevier, 1996
- 32 J.M. Newsam, M.M.J. Treacy, W.T. Koetsier and C.B. de Gruyter, *Proc. Roy. Soc. Lond.*, 1988, **A420**, 375
- 33 A. Dyer, *Encyclopaedia of Inorganic Chemistry*, Vol.8 T-Z, R.B. King (Editor in Chief), J. Wiley and Sons, 1994
- 34 Shell report based on a presentation for the Royal Society, Science into Industry Exhibition and soiree, May 1992
- 35 S.M. Ceisy, *Chemistry in Britain*, 1995 (May), 473
- 36 P.B. Weisz and Frilett, *J. Phys. Chem.*, 1960, **64**, 382
- 37 W.O. Hagg, *Zeolites and Microporous Materials; State of the Art (1994)*, *Studies in Surface Science and Catalysis*, **84**, 1375

## Chapter Two

### Characterisation Techniques

#### 2.1.0 Introduction

The aim of this chapter is to introduce and describe the theory and application of the main characterisation techniques used throughout this project. X-ray diffraction and nuclear magnetic resonance spectroscopy (NMR) have been the most widely used although the project has required the utilisation of many different experimental and computational methods.

X-ray diffraction and nuclear magnetic resonance spectroscopy are complementary techniques, ideal for the detailed characterisation of microporous materials. X-ray diffraction provides long range structural information whilst NMR provides more detailed chemical information on the local environment of selected atoms including coordination. NMR is therefore particularly useful in this context, determining the nature and structure of organic template molecules within the framework structures as they often exhibit disorder within the frameworks (rendering them unsuitable for characterisation by diffraction techniques). This will become more obvious later as the theory behind the NMR and x-ray diffraction experiments are explained.

Computational modelling has also been undertaken to predict the location of templates inside the known framework structures as templates are often not found experimentally. Further information about the content and location of templates has been obtained from thermogravimetric and microanalysis as well as scanning electron microscopy.

Due to the strong synthetic bias of the project a “working knowledge” of many characterisation techniques has proven to be more essential than specialist knowledge of any one individual technique. Consequently the following discussions on theory and applications of the techniques used throughout this project are descriptive rather than detailed. Specialist knowledge when required has been obtained from departmental

experts (e.g. crystallographers) and this is clearly indicated throughout the text at the appropriate time.

### 2.1.1 X-ray Diffraction

### 2.1.2 Introduction to Crystallography

Crystallography, the study of crystals, has long been a source of interest and fascination for scientists. In 1665 Robert Hooke wrote whilst studying crystal morphologies<sup>[1]</sup>:-

So I think, had I time and opportunity, I could make probable that all these regular Figures that are so conspicuously various and curious, and so adorn and beautify such multitudes of bodies....arise only from three or four several positions or postures of Globular particles.....

Four years later in 1669 Neil Stenston, Professor of Anatomy at Copenhagen and Victor Aposolic of the North, concluded that the corresponding angles of different quartz crystals were always the same. This was later extended to other substances after the invention of the contact goniometer in 1780. This again implied that the external appearance of crystals was due to an internal source of symmetry.

Haüy too concluded that the external appearance of crystals were the consequence of some smaller internal structural sub-unit after studying calcite crystals<sup>[2]</sup>. Today we now know that there are essentially seven distinct structural sub-units giving rise to seven crystal systems as shown below in table 2.1. Haüy's structural sub-unit, the parallelepiped that when repeated in a close packed array in three dimensions fills the whole crystal in what is now called the unit cell. The unit cell itself can be constructed from an even smaller arrangement of atoms called the asymmetric unit <sup>[3]</sup>. For example zeolite-A has approximately 480 atoms in its unit cell but these can be generated from only 9 atoms, the asymmetric unit atoms and the symmetry operators associated with the zeolite-A unit cell.

Crystal System	Number of Lattices and Symbols	Conventional Axis and Angles	Essential Symmetries
Triclinic	1 P	a, b, c $\alpha, \beta, \gamma$	none
Monoclinic	2 P, C	a, b, c $\alpha = \gamma = 90^\circ, \beta$	diad axis mirror plane (or inverse diad axis)
Orthorhombic	4 P, I, C, F	a, b, c $\alpha = \beta = \gamma = 90^\circ$	three orthogonal diad or inverse diad axis.
Tetragonal	2 P, I	a = b, c $\alpha = \beta = \gamma = 90^\circ$	one tetrad or inverse tetrad axis
Rhombohedral	1 R	a = b = c $\alpha = \beta = \gamma$	one triad or inverse triad axis
Hexagonal	1 P	a = b, c $\alpha = \gamma, \beta = 120^\circ$	one hexad or inverse hexad axis
Cubic	3 P, I, F	a = b = c $\alpha = \beta = \gamma = 90^\circ$	four triad axes

Table 2.1 The Seven Crystal Systems of modern crystallography. The axis and angles can be used to create all the different unit cells as shown in figure 2.1.

It should be noted from the above table that only rotational symmetries of 2, 3, 4 and 6 are allowed as these are the only symmetrical objects i.e. rectangles, triangles, hexagons that are able to completely fill all space in two dimensions. Consequently there are only 32 allowed crystallographic point groups.

In three dimensions if translational symmetry is also allowed over an infinite area of space, then there are fourteen different types of unit cell. These are more commonly known as the fourteen Bravais lattices after A. Bravais the mathematician who first proposed that all crystal structures could be described by one of these fourteen lattices.

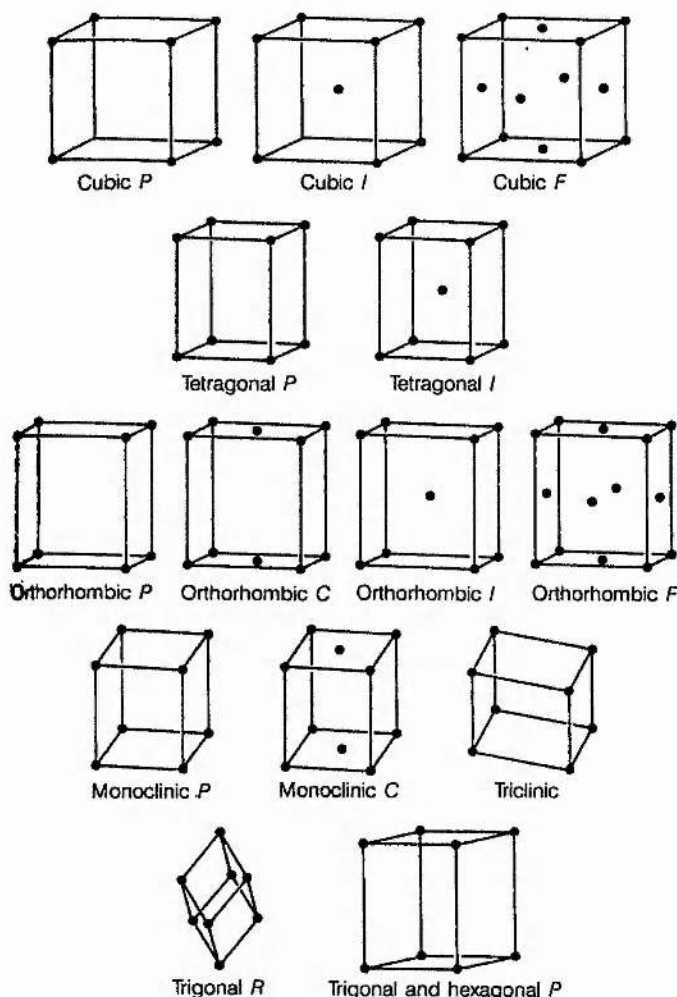


Figure 2.1 The Fourteen Bravais Lattices. Here *P*, *I* and *C* refer to primitive, body-centred and *C*, face centred (could also be *A* or *B*) which denotes points in the *ab* plane.

A lattice is an infinite array of points in space, each of which is surrounded in an identical way by its neighbours. As a consequence of allowing translational symmetry, point groups must be replaced by space groups. Space groups are able to describe the symmetry of crystals in the same way that point groups are able to describe the symmetry of isolated molecules. There are 230 space groups in nature<sup>[4]</sup> which describe all of the possible permutations of symmetry that are available to crystals and these can be generated from the 32 allowed point groups by introducing the possibility of the translation elements. It is sometimes possible to assign more than one possible unit cell or space group to a material

or space group to a material in which case the unit cell or space group with the highest symmetry is always chosen as this better represents the symmetry of the crystal <sup>[2]</sup>.

The use of reciprocal intercepts (hkl) as a means to specifying individual lattice planes or crystal faces within a crystal was proposed by W. H. Miller in 1839 <sup>[1]</sup>. For example a plane parallel to an axes would intercept at 1/ infinity and hence has an index of 0. It should be noted however, that Miller indices are related to a particular unit cell and are not uniquely defined for a given crystal face.

Thus by the end of the nineteenth century, scientists had already been able to deduce much of the chemistry associated with crystals and indeed had laid the foundations built on by modern crystallographers. Abbé had also shown in the nineteenth century that optical microscopy to study materials at the micron level was intrinsically wavelength limited and that a form of electromagnetic radiation with a much shorter wavelength would be required to further investigate materials with improved resolution. That electromagnetic radiation was soon discovered by Roëntgen when he discovered x-rays in 1895. It is, however, unlikely that Roëntgen or anyone else realised at first how powerful x-rays were to become throughout the twentieth century as a tool of unparalleled power for probing at the atomic structure of crystals.

### 2.1.3 Introduction to X-ray Crystallography<sup>[2,5,6]</sup>

In 1912 Max von Laue, a theoretical physicist at the University of Munich, suggested that if x-rays were indeed wavelike in nature and had wavelengths comparable in magnitude with the atomic distances within crystals, then they should diffract x-rays. Soon afterwards W. Friedrich and P. Knipping performed an experiment, passing x-rays through a crystal of copper sulphate and observed a definite diffraction pattern. This experiment not only established the wave properties of x-rays but also gave birth to the new science of x-ray crystallography.

On hearing of this work, William Bragg and his son Lawrence, in England, also became interested in x-ray crystallography. Lawrence using Laue patterns was able to solve the

structures of NaCl, KCl (1912) and ZnS (1913) whilst his father devised a spectrometer that could measure the intensity of x-rays<sup>[7]</sup>. The spectrometer showed that the target element produced its own characteristic x-ray line spectrum and this could be used in crystallographic work. Using this the Braggs developed an alternative and simpler method to x-ray crystallography than that of Laue and were awarded the 1915 Nobel Prize for physics.

The Bragg method still forms the basis of modern x-ray crystallography and is based on the use of monochromatic x-rays. The Braggs demonstrated that the diffraction of x-rays could be represented as “reflections” from parallel planes of atoms within a crystal. This model made it easy to calculate the angle the crystal must make to the incoming x-rays for constructive interference to occur. The Bragg equation is derived by considering that the path difference between waves scattered from adjacent parallel lattice planes must be an integral number of wavelengths. The equation is satisfied showing diffraction maxima when the glancing angle,  $\theta$ , satisfies Bragg's Law:

$$n \lambda = 2d \sin \theta \quad (2.1.1)$$

where,  $n = 1, 2, 3, \dots$  are reflections of the 1<sup>st</sup>, 2<sup>nd</sup>, 3<sup>rd</sup>.. order corresponding to the path differences of 1, 2, 3, ...wavelengths.  $\lambda$  represents the wavelength of the x-rays,  $d$  is the inter-planar distance and  $\theta$ , the angle of incidence between the x-rays and crystal.

Braggs law can be extended to show that there is a lower limit for any given x-ray wavelength to the inter-planar spacings that can give observable resolution between diffraction maxima. Since the maximum value of  $\sin \theta = 1$ , the limit is given by  $d_{\min} = n \lambda / \sin \theta_{\max} = \lambda / 2$ .

$$d_{\min} = \lambda / 2 \quad (2.1.2)$$

where,  $d_{\min}$  is the minimum observable inter-planar spacing

Using Bragg's law the interatomic distances and unit cell dimensions can be determined after "indexing the reflections" i.e. assigning each reflection to a specific plane for example the 110 or the 211 plane etc.. Although indexing the pattern can after be done by hand (See Woolfston<sup>[2]</sup>, Atkins<sup>[3]</sup>, Cheetham and Day<sup>[5]</sup> for detailed discussion) more commonly this is now performed by specially designed computer programs such as VISSER<sup>[9]</sup>. Indexing patterns invariably leads to the discovery of systematic absences in the collected data caused by the internal symmetry of the unit cell of a crystal.

Systematic absences occur because some atoms in one motif will scatter x-rays exactly out of phase with atoms of another resulting in destructive interference being produced and hence no observable peak in the diffraction pattern. A full description of systematic absences associated with each space group can be obtained in the International Tables of Crystallography, volume B<sup>[4]</sup>. Systematic absences are important as they define the symmetry of the unit cell and an understanding of them often reveals the identity of the crystals space group. Systematic absences arise solely from the translation symmetry elements within the unit cell for example screw axis and glide planes.

A screw axis relates one part of a unit cell to another by rotation plus a translation. For example a three fold screw axis,  $3_1$ , represents a 3 fold rotation plus a translation of  $1/3$  unit cells. Glide planes relate two parts of the unit cell by reflection across a plane plus a translation. A *c*-glide for example might involve a reflection across a plane perpendicular to *b* plus a translation of  $c/2$  along *c*.

Indexing the reflections obtained from Bragg's law can describe much of the size and symmetry of the unit cell but we must also consider how x-rays are scattered by individual atoms if we are to locate the atomic positions within a unit cell. The following discussion (as with the previous ones on Bragg's law and systematic absences) is necessarily brief, however, further details may be obtained from Woolfson<sup>[2]</sup> and the details therein.

### 2.1.4 Theory of X-ray Diffraction <sup>[1-3, 5,6]</sup>

X-rays are scattered by their interaction with atomic electrons, and interference occurs from x-rays scattered between different parts of the atom. Consequently the atomic scattering factor  $f_x$  of an atom,  $x$ , decreases with increasing scattering angle,  $2\theta$ . To a good approximation  $f_x$  is wavelength independent but is proportional to the atomic number and is therefore very small for light atoms such as hydrogen.

For a unit cell containing several atoms it is important to consider interference between waves scattered from different atoms such that:

$$\text{Total scattering amplitude} = \sum (f_n \cdot \text{phase factor}) \quad (2.1.3)$$

Where  $f_n$  is the atomic scattering factor for  $n$  atoms. This is the structure factor,  $F$ , and can be expressed mathematically as:-

$$F_{hkl} = \sum_{j=1}^N f_j \exp\{2\pi i(hx_j + ky_j + lz_j)\} \quad (2.1.4)$$

Where  $F_{hkl}$  is the structure factor for reflection  $hkl$  and  $f_j$  is the atomic scattering factor for an atom  $j$  having the atomic coordinates  $x$ ,  $y$ ,  $z$ . The total number of atoms present in the unit cell is represented by,  $N$ .

Equation (2.1.4) can be simplified into real and imaginary parts such that:-

$$F_{hkl} = A_{hkl} + iB_{hkl} \quad (2.1.5)$$

$$A = \sum_{j=1}^N f_j \cos 2\pi(hx_j + ky_j + lz_j) \quad (2.1.5a)$$

$$B = \sum_{j=1}^N f_j \sin 2\pi(hx_j + ky_j + lz_j) \quad (2.1.5b)$$

Where  $A$  is the real component and  $iB$  the imaginary one.

From equations (2.1.5a) and (2.1.5b),  $\phi_{hkl}$ , the phase angle can be determined as:-

$$\tan \phi_{hkl} = \frac{B_{hkl}}{A_{hkl}} \quad (2.1.6)$$

Because the x-rays interact with the atomic electrons it is possible knowing  $F$  to calculate the electron density,  $\rho$ , and hence locate the atomic positions within the unit cell via the equation:-

$$\rho(xyz) = \frac{1}{v} \sum_{h=-\infty}^{\infty} \sum_{k=-\infty}^{\infty} \sum_{l=-\infty}^{\infty} F_{hkl} \exp\{-2\pi i(hx + ky + lz)\} \quad (2.1.7)$$

Where  $\rho(xyz)$  is the electron density at point  $(x,y,z)$  and  $v$  is the volume of the unit cell.

This equation can be rewritten to slightly separate the phase from the magnitude of the structure factor, just as in equation (2.1.3) as:-

$$\rho(xyz) = \frac{1}{v} \sum_{h=-\infty}^{\infty} \sum_{k=-\infty}^{\infty} \sum_{l=-\infty}^{\infty} |F_{hkl}| \cos\{2\pi(hx + Ky + lz) - \phi_{hkl}\} \quad (2.1.8)$$

It is not possible to calculate  $F_{hkl}$  directly from experiment although it is known to be related to the observed intensity of a reflection,  $I$ , which can be measured from experiments. The nature of the relationship is described by equation (2.1.9) below

$$I_{hkl} = sLpF_{hkl}^2 \quad (2.1.9)$$

$S$  is a scale factor,  $L$  is a Lorentz correction for the peak shape (usually  $L = (\sin 2\theta)^{-1}$  for single crystal data) and  $p$  is a polarisation correction,  $p = \frac{(1 + \cos^2 2\theta)}{2}$  Equation 2.1.9 can essentially be simplified to:-

$$I_{hkl} \propto F_{hkl}^2 \quad (2.1.10)$$

This means that the magnitude of the structure factor,  $|F_{hkl}|$ , can be determined directly from experiment but not the phase i.e. the sign of  $F_{hkl}$ , subsequently equation (2.1.8) can not be used directly to locate the atom positions within the unit cell. This dilemma, determining the sign of the structure factor, is termed the “phase problem” in x-ray crystallography and arises because since the phase angle,  $\phi_{hkl}$  can not be measured experimentally.

### 2.1.5 Solving a Crystal Structure <sup>[1-3, 5,6,8]</sup>

Although the phase problem can not be overcome directly from experiment to locate the atomic positions within a given unit cell in order to solve the crystal structure it can be circumvented. In practice there are in essence two main techniques used, the Patterson method and direct methods. The Patterson method requires at least one atom significantly heavier than the others in the unit cell and is widely used for inorganic materials (such as organometallic compounds) but it is not widely used for microporous materials and consequently will not be discussed here. Direct methods alternatively utilise statistical relationships associated with invariant points in the unit cell. Invariant points are points that do not change depending upon the choice of origin for the unit cell. Both methods exploit knowledge of crystal symmetry to simplify the phase problem and make it possible to solve crystal structures. For example zeolite A has approximately 480 atoms within the unit cell but it is only necessary to locate 9 atoms in order to place all the others by symmetry. The structure solution of STA-1 and STA-2 described later in this thesis (chapters five and six respectively) used the direct methods approach to resolve the magnesium aluminophosphate structures.

#### 2.1.5a Direct Methods <sup>[5,6, 8-10]</sup>

Direct methods for structure solution is the method of choice when there are very few heavy atoms per unit cell i.e. when all the atoms present have approximately the same atomic number. Direct methods is a statistical method for predicting phases and ideally requires:-

- (1) That all atoms have the same x-ray scattering power,
- (2) that the distribution of the atoms within a unit cell is quasi-random.

A more detailed description of the direct methods technique for solving crystal structures can be obtained from Cheetham and Day<sup>[5]</sup>, Woolfston<sup>[9]</sup> and Giacocazzo<sup>[6]</sup> but basically the method relies on the formation of normalised structure factors,  $E_{hkl}$ .

$$|E_{hkl}|^2 = \frac{|F_{hkl}|^2}{\epsilon \sum_n f_n^2} \quad (2.1.11)$$

Where,  $\epsilon$  is usually 1 although this can change for certain classes of reflection.

The summation is over all  $n$  atoms in the unit cell and for Fourier calculations  $E_{hkl}$  has the same phase as  $F_{hkl}$ . The prediction of these phases are based on the Sayre probability relationship<sup>[10]</sup>:-

$$s(hkl) \approx s(h'k'l') \cdot s(h-h', k-k', l-l') \quad (2.1.12)$$

For centrosymmetric structures  $s(hkl)$  indicates the phase of  $E_{hkl}$  and  $\approx$  means probably equal to. The probability that this relationship holds depends upon  $|E_{hkl}|$  such that:

$$P = \frac{1}{2} + \frac{1}{2} \tanh \left\{ \frac{1}{N} |E_{hkl} \cdot E_{h'k'l'} \cdot E_{h-h', k-k', l-l'}| \right\} \quad (2.1.13)$$

Where,  $N$  is the number of atoms in the unit cell and

$$\tanh = \frac{(e^x - e^{-x})}{(e^x + e^{-x})} \quad (2.1.14)$$

The probability,  $P$ , is then worked out as a function of  $n$  as described in Cheetham and Day<sup>[5]</sup>. All of these calculations are performed by computer such that an E-map, which is

equivalent to an electron density map may be produced and the atomic coordinates located.

### 2.1.6 Structure Refinement<sup>[5-7]</sup>

Both the Patterson method and the direct method described above only provide approximate atomic coordinates. To obtain absolute atomic coordinates, it is often necessary to refine the crystal structure. The initial coordinates can be optimised using a least squares refinement to minimise the equation:

$$D = \sum_{hkl} W_{hkl} \left( |F_{hkl}^{obs}| - |F_{hkl}^{calc}| \right)^2 \quad (2.1.15)$$

$W_{hkl}$  is a weight factor given to the observation  $|F_{hkl}|$  and the superscripts obs and calc represent observed and calculated structure factors respectively.

At this stage it is important to account for the thermal motion of atoms too. This can be calculated via the equation:

$$F_{hkl}^{calc} = \sum_n f_n \cos 2\pi(hx + ky + lz) e^{-B_n \sin^2 \theta / \lambda^2} \quad (2.1.16)$$

Where,  $B_n = 8\pi^2 \overline{\mu_n^2}$  which is the isotropic temperature factor. The mean square amplitude of vibration for an atom, n, is represented by  $\overline{\mu_n^2}$ .

Once the refinement is complete the accuracy of the structure solution may be tested using a reliability factor, R, or a weighted reliability factor, R<sub>w</sub>, where:-

$$R = \frac{\sum_{hkl} |F_{hkl}^{obs} - F_{hkl}^{calc}|}{\sum_{hkl} F_{hkl}^{obs}} \times 100 \quad (2.1.17)$$

$$\text{and } R_w = \frac{\sum_{hkl} w_{hkl}^{\frac{1}{2}} |F_{hkl}^{obs} - F_{hkl}^{calc}|}{\sum_{hkl} w_{hkl}^{\frac{1}{2}} F_{hkl}^{obs}} \quad (2.1.18)$$

Usually  $R_w$  factors are more reliable gauges as to the accuracy of a structure solution as they rely both upon the observed  $F$  values and the errors associated with those  $F$  values. A typical weighting scheme could be:-

$$w = \sigma^2(F) + g F^2 \quad (2.1.19)$$

Where  $\sigma$ , is the standard deviation on  $F$  and  $g$  is a small numerical scale factor usually of the order 0.01 to 0.001.

Finally the “solved structure” can be tested for any omissions by calculating a difference Fourier map:

$$\Delta(xyz) = \frac{1}{V} \sum_h \sum_k \sum_l (F_{hkl}^{obs} - F_{hkl}^{calc}) \cos 2\pi(hx + ky + lz) \quad (2.1.20)$$

This should reveal not only errors in the structure solution but also the location of hydrogen atoms, although it may not be possible to further refine their atomic coordinates.

### 2.1.7 The Single Crystal Experiment <sup>[1-3, 5,6]</sup>

Single crystal x-ray analysis is probably the most widely used, definitive method for determining a crystal structure. The experiment usually involves mounting a crystal on a fine glass capillary and placing the sample into an automated four circle diffractometer as shown schematically below in figure 2.2.

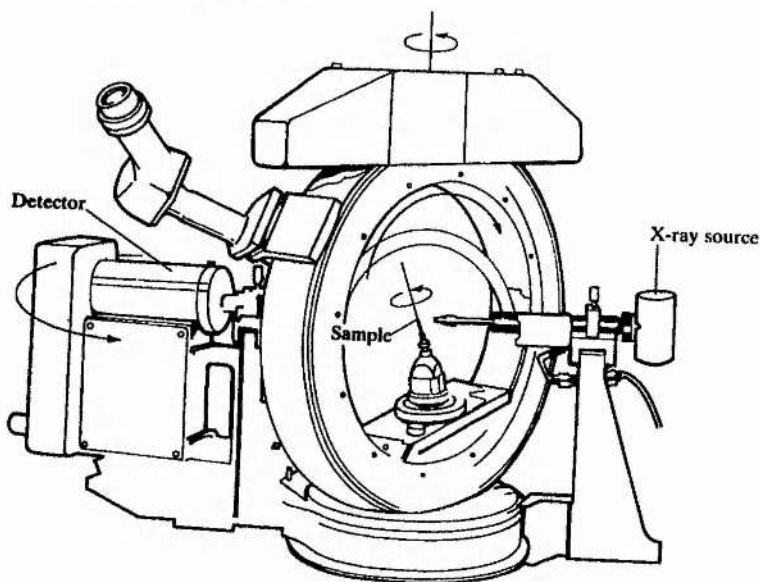


Figure 2.2 A schematic representation of an automated four circle diffractometer. Any possible  $hkl$ -reflection may be obtained by this computer controlled system. Picture taken from Atkins<sup>[3]</sup>.

The crystal is initially set at a random orientation. The unit cell is usually determined by randomly rotating the crystal in the x-ray beam until a minimum of twenty reflections are observed. These are indexed to obtain the unit cell dimensions and space group of the crystal. The settings of the four circle diffractometer angles to observe any particular (hkl)-reflections are computed. The intensity of each reflection is then measured in turn and background intensities are obtained by measurements at slightly different angles, this process is fully automated and computer controlled.

Once collected the data can be analysed and refined by use of modern specially designed computer software packages such as the teXsan suite of programs<sup>[11]</sup> in order to solve

the crystal structure. These types of programs are based on the theory as described above and normally use direct methods to surmount the phase problem.

One of the major limitations of the laboratory single crystal method is that it requires a sufficiently large, good quality single crystal. The minimum crystal size for most laboratory based single crystal diffractometers is approximately 1.0 x 0.5 x 0.5 mm. Crystals of this size are not always available for materials such as peptides, polymers, ceramics or as is relevant to this project, microporous solids. Consequently the laboratory single crystal experiment is unable to solve the structure of many important or interesting materials and other techniques must be employed. For solid crystalline materials powder x-ray diffraction is often the second choice for solving crystal structures not amenable to single crystal analysis.

### 2.1.8 X-ray Powder Diffraction <sup>[2,3,5,6,12]</sup>

Powders often consist of crystallites too small for single crystal experiments. This has one important consequence in terms of diffraction theory. A single crystal can be orientated in an x-ray beam so that only one reflection at a time can be obtained and have its own individual intensity measured so as to facilitate the construction of a three dimensional electron density map from structure factors. Powders consist (ideally) of an infinite number of crystallites arranged in all possible orientations. Since all possible orientations of crystallite should be present, all lattice planes will scatter at the appropriate  $2\theta$  angle as governed by Bragg's equation. A series of cones of scattered x-rays is then formed as opposed to an individual reflection. The resulting cone of reflections essentially condense the diffraction information to one dimension as opposed to the single crystal experiment's three dimensions. This reduction in data makes structure solution a very difficult non routine process. The cones of scattered x-rays produced by passing x-rays through a powder sample contained in a glass capillary are represented in figure 2.3.

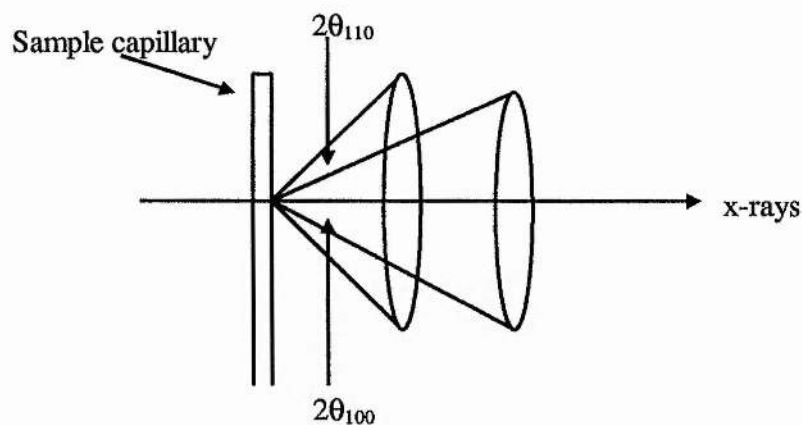


Figure 2.3 Scattering x-rays into cones by a powder sample.

There is a significant loss of information as very often the intensity due to individual reflections can not be determined because of peak overlap (see figure 2.4). This is the main reason why the solving of crystal structures by x-ray powder diffraction is not a routine operation, unlike single crystals. At present direct methods are the most widely used and best established tool for the solution of structures using powder data and new and improved computer software is still being developed around these principles.

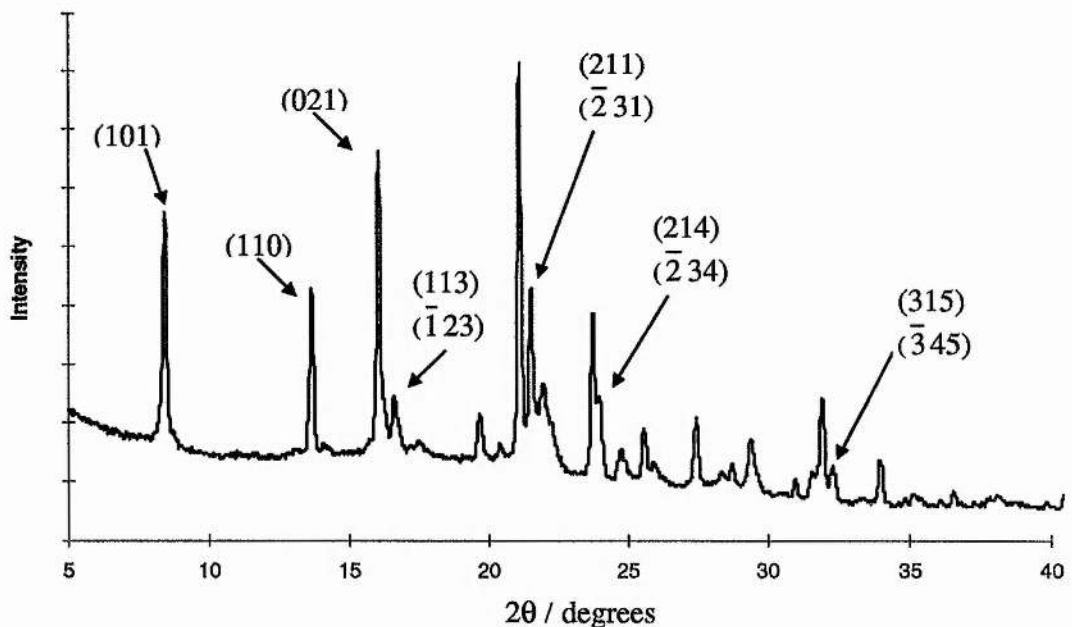


Figure 2.4 Powder x-ray diffractogram of STA-2 showing peak indices, notice that increasing  $2\theta$  values result in more unambiguously indexed peaks. (For clarity only selected peaks are indexed).

Powder diffraction has traditionally been mainly used for:-

(1) Phase Identification<sup>[13]</sup>

The x-ray powder diffraction pattern of a compound provides a characteristic pattern similar to a finger print. This can be used to identify a compound by comparison to known compounds listed in the JCPDS files which contain in excess of 44000 materials.

(2) Quantitative analysis of mixtures<sup>[5]</sup>

Powder XRD can be used to identify the phases present in a mixture of compounds and to determine the relative amounts of each phase within the mixture. This process compares the relative intensities of characteristic lines from each phase and normally requires the use of standards, e.g. quartz.

### (3) Precise determination of lattice parameters<sup>[5]</sup>

The lattice parameters are readily obtained for high symmetry compounds but the indexing of low symmetry patterns may be more difficult. Once properly indexed using one of the computer programs designed for this e.g. VISSER<sup>[9]</sup>, the structure may become obvious from comparison to a known compound which may be isostructural.

### (4) Determination of particle size<sup>[5]</sup>

The approximate particle size of the crystallites present in the powder sample may be determined using the Scherrer equation.

The powder x-ray diffraction data presented later in this thesis were collected in transmission mode on a STADI / P high resolution diffractometer, using Ge monochromised Cu K<sub>α1</sub> radiation at 0.02° increment of 2θ using a small position sensitive detector (PSD) covering 6° in 2θ. The powder samples were prepared by sandwiching them between two sheets of x-ray transparent Mylar film in a flat plate sample holder. The sample was spun to reduce the effects of preferred orientation. Most of the data presented in this thesis were collected over the range 5-50° (2θ) although this was extended to 5-80° (2θ) for new phases or specific phases of interest. Trace amounts of vaseline was usually required in order to secure the sample in the x-ray beam during data collection. Vaseline has two distinctive peaks at 21.44° and 23.21° (2θ) and these are clearly indicated at the appropriate times.

## 2.1.9 Synchrotron Radiation<sup>[6]</sup>

A synchrotron is a particle accelerator where an electron beam is passed around a circle up to 800 meters in circumference using powerful electromagnets. The electrons emit radiation as they are accelerated around the synchrotron. The radiation that is produced covers a wide range of frequencies and wavelengths including those of x-rays. Insertion devices are used to change the wavelength maximum. It is possible to select radiation of a desired wavelength using monochromators such that wavelengths far shorter than those of conventional laboratory x-ray generators can be used for diffraction experiments.

Synchrotrons can provide better resolution of data as explained by equation 2.1.2, and hence less peak overlap problems for powder diffraction.

Synchrotron x-ray powder data can therefore aid in the indexing, refinement and even structure solution of microcrystalline solids. Powder x-ray diffraction data were collected on STA-2 (see chapter 6) at the European Synchrotron Radiation Facility (ESRF) in Grenoble, France on BM16. The station is maintained by Drs. Andrew Finch and Gavin Vaughan whose help is gratefully acknowledged.

Because they are more brilliant than laboratory sources, synchrotron x-rays can be used to obtain statistically significant reflection intensities from smaller crystals than can be studied using laboratory diffractometers. Synchrotrons therefore provide more intense, better resolved data points for structure solution for both powders and single crystals. Because of the increased intensity of the radiation and the high degree to which this can be collimated or focused, smaller crystals can now be used than was previously possible. Conventional x-ray diffractometers require crystals to be at least 0.1 x 0.1 x 0.5 mm in size, to obtain sufficiently good data; synchrotrons do not. Rotating anode diffractometers, which are also available in conventional laboratories can often make use of smaller crystals owing to the increased intensity of the x-rays obtained when using these machines (typically around 10x that of a normal x-ray generator). The wavelength however, is fixed as with all conventional x-ray generators which is another advantage of using synchrotron radiation. The ability to select a desired wavelength and the use of single crystals, as small as 10 x 10 x 10  $\mu\text{m}$  has led to the new but quickly developing area of single microcrystal diffraction.

Single microcrystal diffraction has wide spread implications for inorganic chemistry <sup>[14-16]</sup>, biological chemistry and material sciences. With the advent of single microcrystal diffraction it may become possible to routinely solve the structures of many more as yet unknown materials that can not be formed as sufficiently large crystals for conventional x-ray diffractometers.

Single microcrystal diffraction data were used to solve the structures of both STA-1 and STA-2. Data were collected at the ESRF using beamline BL-16 ID11<sup>[17,18]</sup> maintained by Professor Åke Kvick, his assistance is also gratefully acknowledged.

Limitations of the use of synchrotrons stem mainly from the availability of synchrotron facilities themselves. The immense cost involved in both constructing and maintaining a synchrotron require them to be central international facilities.

## **2.2.0 Nuclear Magnetic Resonance Spectroscopy** <sup>[3, 5, 19-22]</sup>

### **2.2.1 Introduction to Nuclear Magnetic Resonance Spectroscopy**

The nuclear magnetic resonance (NMR) phenomenon was first observed by two independent research groups led by Purcell at Harvard and Bloch at Stanford in 1946<sup>[1]</sup>. Since that time NMR has rapidly become the single most important technique for structure identification and elucidation in molecular chemistry due to its versatility.

NMR is the study of the properties of molecules containing magnetic nuclei by applying a magnetic field and observing the frequency at which they come into resonance with an electromagnetic field. The technique is becoming increasingly more applicable to solids as well to liquids. NMR provides excellent detailed short order information about atoms environment. This detailed short range information, usually over two or three bond lengths, makes NMR a very good complementary technique to X-ray diffraction and consequently these techniques are often used in conjunction to characterise novel materials exhibiting disorder. For example MASNMR can offer environmental information for selected atoms in the unit cell revealing not only which atoms are adjacent to the selected atom but the abundance of each neighbour too. This information can not be determined from x-ray diffraction.

Throughout this project NMR spectroscopy has been used for the characterisation of relatively simple organic template molecules in the liquid state using a Varian 300MHz spectrometer. Solid state NMR has also been performed on a Bruker 400 MSL

spectrometer with the help of Barbara Gore at UMIST to investigate several new microporous materials synthesised during the research described in this thesis. As these novel crystalline materials were studied mainly by x-ray diffraction and the organic molecules characterised were relatively simple, the NMR spectroscopy undertaken has been both limited and on a basic level compared to the potential capability of the technique. Similarly the following description on the theory of NMR is likewise limited and basic, however, further details are available from references [19-22].

### 2.2.2 The Theory of NMR<sup>[1, 3, 19-22]</sup>

Some nuclei possess intrinsic spins and thus act as magnets with magnetic dipole moments. The nuclear spin is identified by the quantum number  $I$ . Generally it is found that atoms in the periodic table having nuclei with:-

- 1) odd mass numbers have half integral spin,
- 2) even mass numbers but odd atomic number have integral spin, and
- 3) even mass and atomic numbers have zero spin.

Subsequently atoms such as  $^{12}\text{C}$  and  $^{16}\text{O}$  have no spin and are in effect invisible to NMR spectroscopy. For the remainder of this discussion only nuclei with  $I = \frac{1}{2}$  will be considered e.g.  $^1\text{H}$ ,  $^{13}\text{C}$ ,  $^{31}\text{P}$ .

A proton with  $I = \frac{1}{2}$  may adopt two possible orientations according to the quantum number  $m_I$  where  $m_I = I, I-1, \dots, -I$ . The two states are  $m_I = +\frac{1}{2}$  ( $\uparrow$ ) denoted  $\alpha$ , and  $m_I = -\frac{1}{2}$  ( $\downarrow$ ) denoted  $\beta$ . In a magnetic field,  $B$ , the two states have different energies determined by;

$$E_{m_I} = -\mu_z B = -\gamma \frac{h}{2\pi} B_{m_I} \quad (2.2.1)$$

Where,  $E_{m_I}$  is the energy of the  $m_I$  orientation,  $\mu_z$  is the  $z$  direction component of the nuclear magnetic moment such that  $\mu_z = -\gamma \frac{h}{2\pi} m_I$ ,  $h$  is Planck's constant and  $\gamma$  is the magnetogyric ratio of the nucleus.

The energy separations of the two states of spin  $-\frac{1}{2}$  nuclei is equal to:  $\gamma \frac{h}{2\pi} B$ .

For most nuclei  $\gamma$  is positive and hence the  $\beta$  state is above the  $\alpha$  state but has fewer spins according to the Boltzmann distribution function (Equation 2.2.2).

$$\frac{N_{\beta}}{N_{\alpha}} = e^{-\Delta E/kT} \quad (2.2.2)$$

The  $\alpha$  and  $\beta$  spin states can be shown schematically as in figure 2.4 below.

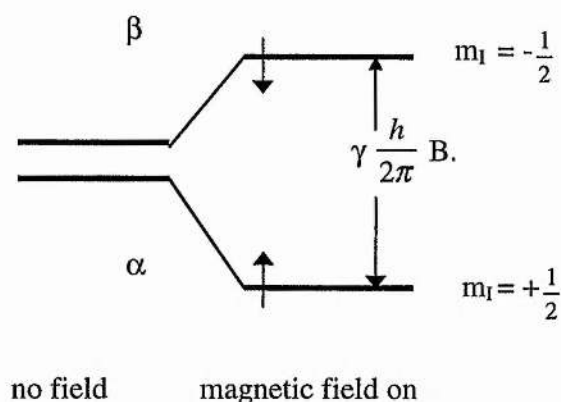


Figure 2.5 The nuclear spin energy levels of spin  $-\frac{1}{2}$  nucleus in a magnetic field. Resonance occurs when the separation in energy between levels equals the energy of applied radio frequency (RF) causing an absorption of photons and  $\beta \leftarrow \alpha$ .

If electromagnetic radiation of frequency,  $\nu$ , is passed over the sample, the energy separations come into resonance with the radiation when the frequency satisfies the resonance condition:

$$h \nu = \gamma \frac{h}{2\pi} B \quad (2.2.3)$$

The higher the magnetic field strength, the greater the energy difference between the  $\alpha$  and  $\beta$  state, hence greater net absorption is obtained. This means that smaller samples

can be used. The high magnetic field also simplifies the appearance of many spectra as there are no unambiguous absorptions.

In order to reach higher magnetic fields, superconducting magnets of the homogeneity and stability necessary for high resolution NMR were developed. A description of the new Nb/Zr superconducting magnet and its potential was published in *Science* in October 1964<sup>[26]</sup>. This has since been superseded by Nb/Ti which is more stable than the Nb/Zr magnet.

### 2.2.3 The NMR Experiment<sup>[20, 21]</sup>

There are in essence two types of NMR experiment: continuous wave (CW) and pulsed Fourier transform (FT). Continuous wave was the technique originally pioneered by both Purcell and Bloch.

In CW NMR spectroscopy, a small proportion of the applied (RF) signal is absorbed in promoting some of the  $\alpha$  nuclei to the higher energy state, this response is picked up in a receiving coil. The frequency range being studied is varied steadily from one extreme to the other either by changing the magnetic field or by altering the frequency. The spectrum obtained can be plotted directly as absorbance (intensity) against frequency. This spectrum is said to be in the frequency domain.

The CW technique has limited sensitivity even at high magnetic fields and consequently is useful for a relatively small number of nuclei.  $^1\text{H}$  is probably the best nuclei to be studied in this way due to its relatively large magnetogyric ratio and short relaxation times. The problem arises because measuring the spectrum depends on scanning a large range of frequencies even though NMR absorption only takes place at a few frequencies. The detector, therefore, detects no signal for most of the experiment leading to problems with maximising the signal to noise ratio necessary for clear unambiguous spectra. If the signals detected are also weak, for example  $^{13}\text{C}$  nuclei have an isotope abundance of approximately 1% and an intrinsically less sensitive nuclei than  $^1\text{H}$ , then the time

to make repeated scans to obtain a good spectrum, with good signal to noise ratios, becomes too long in practice.

In 1966 R.R. Ernst and W.A. Anderson addressed the problems associated with CW NMR spectroscopy by developing a new technique called Fourier transform (FT) NMR. The essential difference between FT and CW NMR is that FT NMR excites all possible resonances simultaneously rather than sequentially by means of a pulse of RF. The data obtained directly in this way is referred to as a free induction decay (FID) which is in the time domain but is processed by an online computer using a Fourier transform to obtain an intensity versus frequency spectrum as before. A schematic diagram showing a FT spectrometer is shown in figure 2.6.

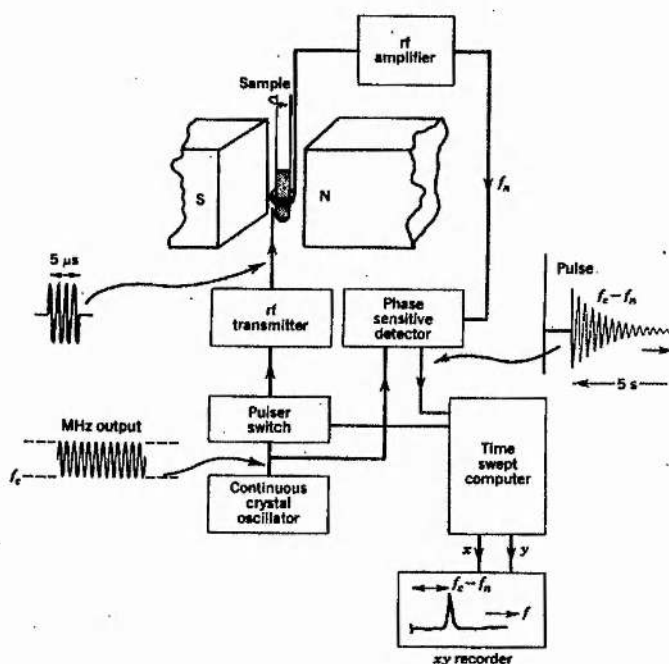


Figure 2.6 A Fourier transform NMR spectrometer with online computer needed to convert data from the time domain to the frequency domain.  $F_c$  is the carrier frequency and  $f_n$ , the Larmor frequency. Taken from Alberty and Silbey<sup>[21]</sup>.

### 2.2.4 FT NMR Spectroscopy<sup>[19-21]</sup>

The improvement both in sensitivity and efficiency in NMR spectroscopy since the development of the FT technique is such that almost all nuclei can now be investigated by NMR spectroscopy. Sample sizes too have decreased due to the increased sensitivity such that a  $^1\text{H}$  FT NMR spectrum can now be obtained routinely in solution from a 0.1 mg sample of a typical organic compound within a few seconds.

In FT NMR the sample is flooded by a wide range of frequencies by means of a short burst or pulse of RF energy. This pulse is the equivalent of a band of frequencies centred around the oscillator frequency or carrier frequency ( $f_c$ ). The band width depends on the duration of the pulse, e.g. a 10  $\mu\text{s}$  pulse could cover a frequency range of around  $10^5$  Hz. The nuclei continue to emit signals at their characteristic Larmor frequencies ( $F_n$ ) as they relax back to their ground states after being excited by the RF pulse. This process is detected by a probe coil and is called the free induction decay (FID). Each FID contains the information of one complete spectrum collected between pulses. These data can be stored and averaged after many pulses by computer, greatly improving the signal-to-noise ratio compared with CW experiments.

The FID of a single resonance takes the form of an exponentially decaying cosine wave with frequency  $f = f_c - f_n$ . With more than one resonance the FID patterns become more complicated. The FID data are converted from the time domain to the frequency domain using a mathematical Fourier transform like:-

$$F(\omega) = \int_{-\infty}^{\infty} f(t)e^{-i\omega t} \quad (2.2.4)$$

Where,  $F(\omega)$  represents the CW experiment and  $f(t)$  the FT experiment.

The effect of the Fourier transform is more graphically illustrated in figure 2.7 which shows the form of the FID before and after the Fourier transformation.

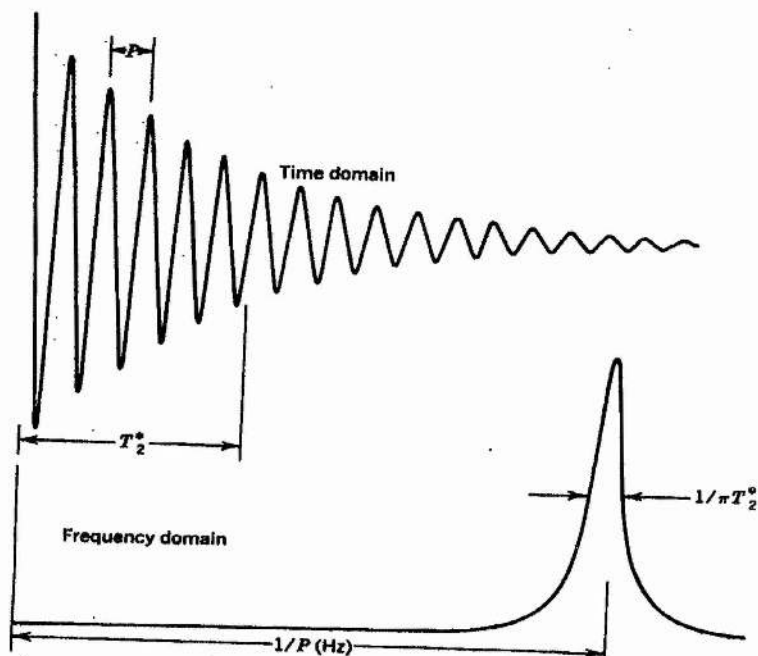


Figure 2.7 FID pattern (upper) before being converted to the frequency domain. Taken from Alberty and Silbey<sup>[21]</sup>.

### 2.2.5 Solid State NMR Spectroscopy<sup>[5,8]</sup>

In solution the fast motions of the molecules average out interactions between nuclei and nuclei and any electric field gradients present. For dipolar and quadrupolar coupling interactions the average values are exactly zero, the net effect of which are discrete values for chemical shifts, coupling constants and narrow line widths.

By comparison, there are broad line widths in the solid state because the nuclei are trapped in a solid matrix which prevents the anisotropic interactions described above averaging to zero. The main interactions that can occur in the solid state between a nucleus and a magnetic field are:-

## (1) the Zeeman interaction

The Zeeman effect is the modification of an atomic spectrum by the application of a strong magnetic field.

## (2) the dipolar interaction

Dipolar interactions are the same as those observed between two small bar magnets. The dipolar Hamiltonian,  $H_{dd}$ , can be expressed as:-

$$H_{dd} = R[A + B + C + D + E + F] \quad (2.2.5)$$

Where, each of the terms A to F contain both a spin factor and a geometric factor. In liquids all of these terms are reduced to zero by isotropic tumbling.

## (3) Chemical shift interaction

Nuclear magnetic moments interact with the local magnetic field. The local magnetic field often differs from the applied magnetic field because the latter can induce electronic orbital angular momentum which in turn gives rise to a small additional magnetic field  $\delta B$ . This additional field may increase or decrease the actual magnetic field felt by the nucleus and is proportional to the applied field. The chemical shift can therefore be either positive or negative and either the RF frequency or the magnetic field will have to change to bring the shielded nucleus back into resonance. In most instruments this is accomplished via an adjustment of the magnetic field by passing a direct current through an auxiliary winding. The chemical shift of a nucleus,  $\delta$ , is the difference between its resonance frequency and that of a reference standard and is defined by:-

$$\delta = \frac{\nu_{sample} - \nu_{ref}}{\nu_{ref}} \quad (2.2.6)$$

Usually the chemical shift, which is a unitless quantity is expressed in ppm. There is no absolute standard with which to compare chemical shifts although normally for  $^1\text{H}$  and  $^{13}\text{C}$  NMR a small amount of tetramethylsilane (TMS) is added to the sample as an internal standard. The position of the TMS peak is arbitrarily assigned the value zero.

(4) spin - spin coupling interaction

As in solution, an indirect electron - coupled interaction can take place between two nuclear spins. In most cases this term will be smaller than those described above but could be important for the determination of chemical structures.

(5) quadrupolar interactions

This occurs only for nuclei with  $I > \frac{1}{2}$  and arises from the interaction of the nuclear electric quadrupolar moment with a non-homogeneous electric field.

### 2.2.6 Magic Angle Spinning NMR<sup>[5, 8, 21]</sup>

The terms in the dipolar Hamiltonian that cause NMR line broadening in solids involve geometric factors of the type  $(3 \cos^2 \theta - 1)$  where  $\theta$ , is the angle between the internuclear vector and the magnetic field. If these terms were averaged to zero, i.e.  $(3 \cos^2 \theta - 1) = 0$  then anisotropic dipolar line broadening would be eliminated as in the solution case. This occurs when  $\theta = 54.44^\circ$  and this angle is called the "magic angle". In the magic angle spinning (MAS) NMR experiment the sample is spun around an axis at  $54.44^\circ$  to the applied magnetic field at a frequency comparable to the frequency spread of the shift anisotropy. Spinning below this frequency can result in the introduction of unwanted spinning side bands. These satellite resonances appear symmetrically on either side of the genuine resonance separated by the spinning rate in Hz.

A schematic diagram representing the axis of rotation for a solid sample at the magic angle is shown below in figure 2.8. Figure 2.9 shows the  $^{13}\text{C}$  solution and MASNMR spectra of 1,4-diquinuclidinium bromide (the hydroxide form was used in the solid sample which was used as a template in the formation of STA-2), to demonstrate the differences in peak width between solution and solid state NMR.

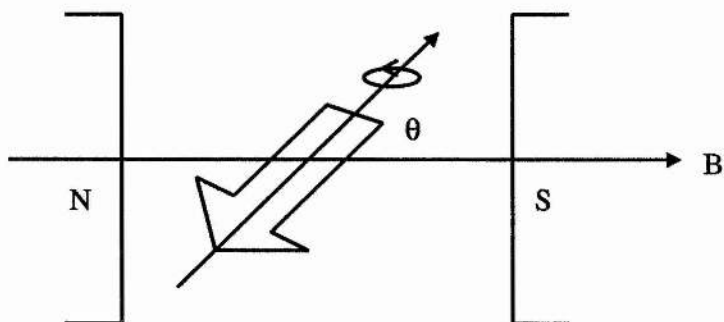


Figure 2.8 Schematic representation of the experimental arrangement for sample spinning. In MAS NMR  $\theta = 54.44^\circ$ .

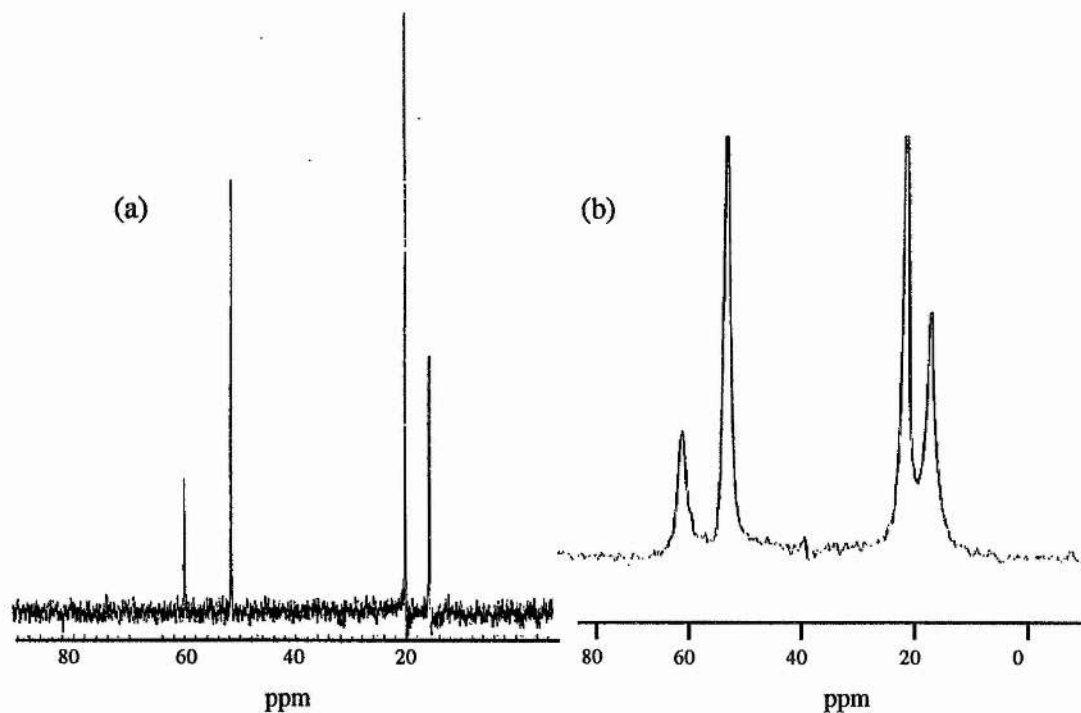


Figure 2.9 Carbon-13 of (a) solution and (b) MAS- NMR spectra of 1,4-diquinuclidinium bromide / hydroxide respectively to demonstrate the difference in peak width between the two techniques.

MAS NMR can also average the chemical shifts and the spin - spin couplings as well as the dipolar interactions to their isotropic values. The chemical shifts of molecules in the solid state are usually similar to those found in solution.

### 2.3.0 Computer Modelling<sup>[24 - 27]</sup>

#### 2.3.1 Introduction

Microporous solids, and zeolites in particular, are commercially important materials as described in chapter 1. It is important therefore to understand and control their synthesis in order to further exploit them. There are many different factors that can have a significant impact on the synthesis of a zeolite, one of the most important of these being the inclusion of organic templates. At present, however, the exact role of these templates is poorly understood. Direct observation of incorporated templates within zeolites is difficult by either diffraction or spectroscopic techniques, partly because zeolites crystallise predominately as powders. Consequently synchrotron radiation is often required to collect diffraction data with sufficiently high resolution in order to be useful. The structure solution of STA-1 and STA-2 provide examples of both the strength of this technique but also its limitations. STA-2 encapsulates the template molecules within the cages of its highly symmetric framework, thereby imposing a form of order on the template as the templates motion is restricted. Consequently single microcrystal analysis was able to determine the template position since templates had a periodic arrangement within the framework. The template location could not have been determined directly using any other technique and as such demonstrates the power of this technique. STA-1 by comparison has a more open three dimensional framework within which the template location was not found by single microcrystal diffraction. It is likely that template disorder within the magnesium aluminophosphate structure is responsible for this since a disordered template would not have the regular atomic periodicity required for accurate diffraction studies. In the case of materials like STA-1, the elucidation of template location by experimental techniques often fail and an alternative approach must be adopted.

Computer modelling and graphics techniques offer a viable alternative to many of these experimental problems and are becoming increasingly sophisticated to give a unique method of studying the template / zeolite relationship at the atomic level. These computer aided investigations offer an insight into the physical and chemical properties responsible for their structure directing activities thus increasing our understanding of how zeolites form. Currently computer modelling has been used to explain the formation of crystallographic stacking faults<sup>[28]</sup>, locate templates and predict the effect of using specific templates for the formation of new structures<sup>[29]</sup>.

During the course of this research, two computer modelling programs have been used, simulated annealing (SA) and Structure Docking. SA was used in an attempt to predict the structure of STA-1. Structure docking has been used in collaboration with Dr. Paul Cox of the University of Portsmouth, to locate organic templates in STA-1 and to help understand the role of the polymeric templates that control the formation of AFI and ATO (see chapter 7)<sup>[30]</sup>. Both programs are run using Insight software from Biosym/MSI and are contained within the Catalysis module.

### 2.3.2 Simulated Annealing<sup>[24]</sup>

There are two distinctive steps in solving a crystal structure. The first step involves the solution or circumvention of the phase problem to give an approximate crystal structure. Structure refinement, step two, is the refinement of step one to give an accurate structure solution. SA is one possible way of obtaining an approximate structure as in step one above.

SA is used to adjust an initially random arrangement of each type of atom within the unit cell so as to minimise the value of a figure of merit or energy function. The energy function is designed so as to produce solutions that are both chemically and physically feasible and concurrent with known experimental data.

The SA program requires the chemical composition, dimensions and symmetry of the crystallographic unit cell as input. These include:-

- (1) the unit cell dimensions. These are obtained by successful indexing of x-ray diffractograms using programs such as VISSER<sup>[31]</sup>.
- (2) the space group of the material. This is again obtained by successful indexing of the XRD pattern by considering the systematic absences present. Usually there are several possible space groups identified from laboratory powder XRD patterns as the resolution is not sufficient to identify only one possibility.
- (3) the total number of tetrahedrally coordinated framework atoms (T) in the unit cell. This can be determined from thermogravimetric analysis (TGA) and density measurements.
- (4) the number of unique T-atoms, that is the crystallographically unique T-atoms within the unit cell. This can not be determined directly from experiment but can be estimated from structures with similarly sized unit cells and densities.

Once the input requirements have been submitted a figure of merit is created that represents the reasonableness of a given arrangement of T-atoms within the unit cell. The figure of merit is used as a guide for adjusting the given T-atom arrangement towards one that agrees with experimental data. Minimising this figure of merit or energy function is not the same as minimising a thermodynamic energy function as there are no oxygen atoms included in the calculations.

SA is the process by which the T-atoms are adjusted within the unit cell in order to minimise the figure of merit. An initial conformation is given and energy value  $E_{old}$ . The system is then heated to a high temperature to allow the atoms to move. A new conformation is accepted if its energy,  $E_{new}$  is less than or equal to  $E_{old}$ . At first most moves are accepted but as the temperature is slowly decreased fewer and fewer new T-atom conformations are accepted. Usually the final conformation will be near to a global "energy" minimum for the system.

The SA process can of course generate many possible zeolite framework structures. The correct one is identified by comparison of the known and calculated diffraction pattern for each possible framework once oxygen atoms have been included. As each framework

will produce its own distinctive XRD pattern this provides a convenient method of identification.

### 2.3.3 Structure Docking <sup>[25-27]</sup>

Structure docking has been used to locate possible template locations within known microporous solids. The process utilises a combined Monte Carlo - Simulated Annealing (MC-SA) technique to generate low energy template locations.

Once a suitable framework (host) and template (guest) have been identified, the guest can either be manually docked (placed at a reasonable (or known) region inside the host) or docked under computer control using a Monte Carlo (MC) technique. The advantage of using MC docking is that this technique makes no assumptions about likely guest locations or conformations within the host. MC begins using a high temperature molecular dynamics calculation on the guest molecule to sample conformational possibilities. The conformations with the lowest energies are used in the docking process. The docking process itself is based on random selection of molecular orientations within the host followed by calculation of a trial interaction energy for the host guest system. A docked conformation is accepted and saved for further investigation if the interaction energy falls below a predetermined threshold value.

The interaction energy,  $E_{interaction}$ , is calculated as being a combination of the Van der Waals potential and coulombic interactions between each atom of the guest and host structure. The objective of docking is to calculate the energies of one molecule relative to another to identify the lowest energy orientations. The interaction energy between two atoms,  $i$  and  $j$  can be expressed by:-

$$E_{interaction} = \sum_i \sum_j \left( \frac{A_{ij}}{r_{ij}^{12}} - \frac{B_{ij}}{r_{ij}^6} + \frac{q_i q_j}{\epsilon r_{ij}} \right) \quad 2.3.1$$

Where, the Van der Waals potential is,  $\frac{A_{ij}}{r_{ij}^{12}} - \frac{B_{ij}}{r_{ij}^6}$  and the coulombic interaction is equal to  $\frac{q_i q_j}{\epsilon r_{ij}}$ .  $q$  is the atomic point charge,  $r_{ij}$  is the interatomic distance between  $i$  and  $j$ ,  $\epsilon$  is the dielectric constant.

Each MC structure is energy minimised and then further refined using SA to produce final docked conformations. The docking methodology can be summarised by the flow diagram shown in figure 2.10.

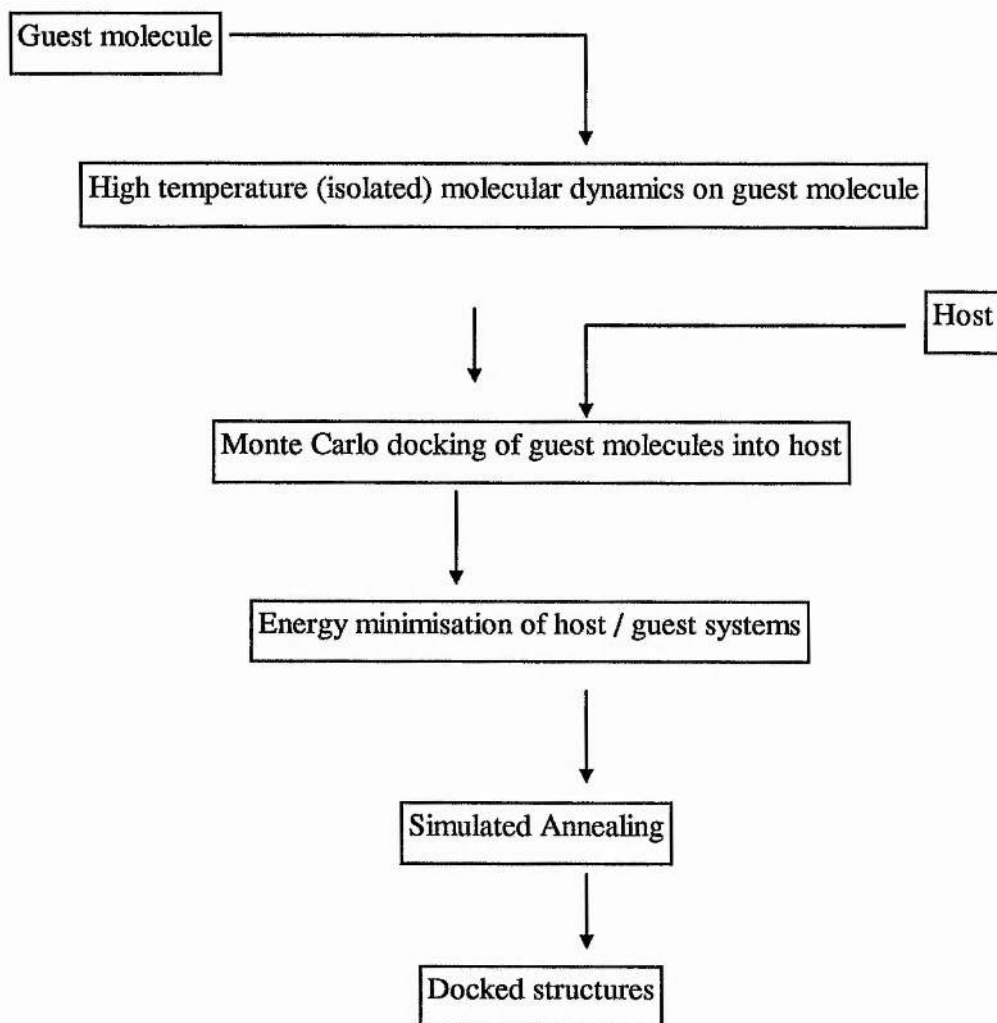


Figure 2.10 Flow diagram showing the Docking Process. Reproduced from Biosym User Manual, 1996, page 236.

## 2.4.0 Other Techniques

### 2.4.1 Introduction

X-ray powder diffraction and NMR spectroscopy have been the most extensively used characterisation techniques throughout this project. Due to the strong synthetic bias of this project, however, several other techniques have been used (not least computer modelling) and these are briefly described here. The aim of this section is to indicate the range of characterisation techniques used rather than explain the theory behind them.

### 2.4.2 Thermal Analysis<sup>[32]</sup>

Thermal analysis is widely used in a variety of ways throughout solid state chemistry. Two methods of thermal analysis, thermogravimetric and differential thermal analysis have been used in this project. Thermogravimetric analysis (TGA) is a technique for measuring a change in weight of a substance as a function of temperature or time. Typically a few milligrams of sample are accurately weighed out and placed onto a balance pan in an alumina or platinum crucible. A similar amount of a reference material e.g.  $\alpha\text{-Al}_2\text{O}_3$  is also accurately weighed and placed onto a balance. The two materials are then tared relative to each other sealed into the thermal analyser. The temperature is then increased for example by  $5^\circ\text{C} / \text{minute}$  between  $30$  and  $800^\circ\text{C}$  in oxygen (as for the work in this thesis). The change in weight of the sample is then monitored. Differential thermal analysis (DTA) is performed simultaneously with the TGA on the same instrument. DTA measures the difference in temperature between the sample and the reference material. DTA can therefore indicate if the change in weight (normally a decrease) with temperature is endothermic or exothermic. TGA / DTA was performed on a TA Instruments SDT 2960 Thermoanalyser.

### 2.4.3 Microanalysis

Microanalysis is used to determine the composition of an organic molecule. The technique can measure the relative percentages of carbon, nitrogen and hydrogen atoms in a molecule. This can provide a good method to confirm the composition and hence formation of a particular organic molecule.

### 2.4.4 Density

The density of a material can be determined by using a mixture of diiodomethane (having a density of  $3.325 \text{ gcm}^{-3}$ ) and 1-bromobutane (having a density of  $1.276 \text{ gcm}^{-3}$ ) provided that its density is between these two. If it is then the material will sink when it is added to pure 1-bromobutane as it will have a greater density. It will float however, if placed in pure diiodomethane. By adding diiodomethane to the material in 1-bromobutane it is

possible to obtain the density of the material as it has the same density as the resultant liquid just as it begins to float. By measuring the mass of  $1 \text{ cm}^3$  of the liquid the density of the liquid and hence the solid can easily be obtained from the equation:

$$\text{density} = \text{mass} / \text{volume} \quad (2.4.1)$$

#### 2.4.5 Scanning electron Microscopy (SEM)

SEM has been performed with the aid of Mr. Irvine Davidson at the Gatty Marine laboratory, The University of St. Andrews SEM was used to identify characteristic crystal morphologies of both known and novel materials and for chemical analysis of selected areas. SEM has two distinct advantages over conventional microscopes. Firstly the shorter wavelength of electrons compared to light allows far greater resolution and hence can be used to study smaller samples in more detail. Secondly selected area analysis can be performed (EDX). X-rays are produced by electron transitions within the sample caused by the electron beam of the microscope. The electron transitions are specific to each type of atom in the periodic table. By monitoring the x-rays it is possible to obtain both a qualitative and quantitative composition of the sample. SEM coupled with EDX therefore provides a powerful way of examining the morphology and composition of the sample.

### 2.5.0 References

1. W.J. Moore, *Basic Physical Chemistry*, Prentice - Hall International Editions, 1983
2. M.M. Woolfson, *An Introduction to X-ray Crystallography*, Cambridge University Press, 1978
3. P.W. Atkins, *Physical Chemistry*, 4<sup>th</sup> Edition, Oxford University Press, 1992
4. The International Union of Crystallography, *International Tables for X-ray Crystallography*, Kluwer Academic Publishers, 1995
5. A.K. Cheetham and P. Day, *Solid State Chemistry Techniques*, Clarendon Press Oxford, 1983
6. C. Giacovazzo (Editor), *Fundamentals of Crystallography*, Oxford University Press, 1995
7. R.S. Drago, *Physical Methods For Chemists (2<sup>nd</sup> Edition)*, Saunders College Publishing, 1992
8. L.J.M. Sawers, *Ph.D. Thesis*, The University of St. Andrews, 1997
9. M.M. Woolfson, *Direct Methods in Crystallography*, Oxford University Press, 1961
10. D. Sayre, *Acta Cryst.*, 1952, **5**, 60
11. TeXan, *Single Crystal Analysis Software*, Version 1.6, Molecular Structure Corporation, The Woodlands, Houston TX, 1993
12. G.H. Stout and L.H. Jensen, *X-ray Structure Determination*, Wiley Interscience, U.S.A., 1989
13. Powder Diffraction File - Inorganic Compounds, JCDPS International Centre for Diffraction Data, Philadelphia, 1984
14. M. Helliwell, V. Kancic, G.M.T. Cheetham, M.M. Harding, B.M. Kariuki and P.J. Rizkalla, *Acta Cryst.*, 1993, **B49**, 49
15. G.M.T. Cheetham and M.M. Harding, *Zeolites*, 1996, **16**, 245
16. M.J. Gray, J.D. Jasper, A.P. Wilkinson and J.C. Hansen, *Chem. Mater.*, 1997, **9**, 976
17. Å. Kvick and M. Wulff, *Rev. Sci. Instrum.*, 1992, **62**, 1073
18. M. Krumrey, Å. Kvick and W. Schwegle, *Rev. Sci. Instrum.*, 1994, **66**, 976
19. R.K. Harris, *Nuclear Magnetic Resonance Spectroscopy*, Pitman Publishing INC., 1983

20. D.H. Williams and I. Fleming, *Spectroscopic Methods in Organic Chemistry*, 4<sup>th</sup> Edition (Revised), McGraw - Hill Book Company, 1989
21. R.A. Alberty and R.J. Silbey, *Physical Chemistry*, John Wiley & Sons, 1992
22. G.K. Vemulapalli, *Physical Chemistry*, Prentice - Hall International Editions, 1993
23. F.A. Nelson and H.E. Weaver, *Science*, 1964, **146**, 223
24. Biosym Inc., Insight II, Version 2.0.0, *User Manual*, 1993
25. Biosym / MSI Inc., Insight II, Version 3.0.0, *User Manual*, 1995
26. Biosym / MSI Inc., Catalysis, Version 4.0.0, *User Manual*, 1996
27. A.P. Stevens, *Ph.D. Thesis*, University of Portsmouth, 1996
28. A.P. Stevens and P.A. Cox, *J. Chem. Soc., Chem. Commun.*, 1995, **3**, 343
29. D.W. Lewis, D.J. Willock, C.R.A. Catlow, J.M. Thomas and G.J. Hutchings, *Nature*, 1996, **382**, 604
30. W.H. Meier, D.H. Olson and Ch. Baerlocher, *Atlas of Zeolite Structure types (Zeolites, 17, 1996)*, Elsevier, London, 4<sup>th</sup> Edition, 1996
31. J.W. Visser, *J. Appl. Cryst.*, 1969, **2**, 89
32. A. R. West, *Basic Solid State Chemistry*, John Wiley & Sons, 1991

## Chapter Three

### Synthesis of Organic Templates

#### 3.1.0 Introduction

The aim of this chapter is to introduce the organic template molecules that have been synthesised and used in the course of this project. The nature of organic bases and the rôle that they have on the synthesis of microporous solids has already been discussed in chapter one. The results of hydrothermal synthesis employing the template molecules described in this chapter will be discussed fully in chapter four.

For simplicity the names of the organic molecules synthesised in this project have been abbreviated as their full IUPAC names are very long. Appendix I contains a full list of the abbreviations used throughout this project.

#### 3.2.0 Experimental

Commercial templates and all other chemicals used in the synthesis of novel templates were purchased from reputable suppliers (Aldrich, Avocado, Johnston Mathey, etc.) and used without further purification. Similarly all of the equipment used for the synthesis of organic templates are standard pieces of laboratory equipment.

The synthesis of almost all of the organic templates described in this thesis have been prepared essentially from the same process using the Menshutkin reaction<sup>[1]</sup>. The Menshutkin reaction is an example of a  $S_N2$  reaction pathway as described in most organic chemistry textbooks, for example Morrison and Boyd<sup>[2]</sup>. The  $S_N2$  reaction or substitution nucleophilic bimolecular reaction, as it is more formally called, follows second order kinetics where the concentrations of both reagents are important to the overall rate of the reaction. The general case between an organic bromide and hydroxide ions to form an alcohol is shown below to demonstrate the reaction

mechanism.

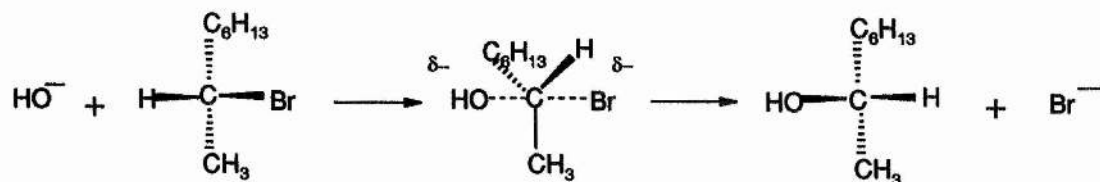
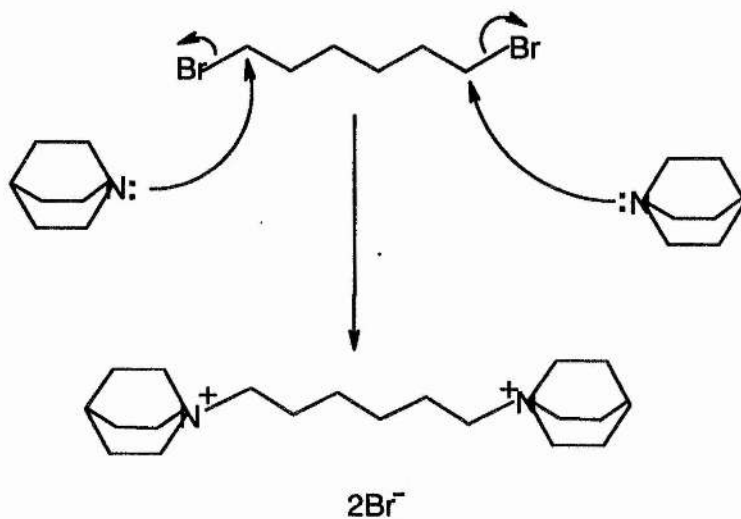


Figure 3.1 The  $S_N2$  reaction demonstrating the partially bonded hydroxide and bromide transition state leading to inversion of configuration at the carbon centre. (Diagram reproduced from Morrison and Boyd<sup>[2]</sup>.)

The Menshutkin reaction is used to describe the specific case between amines and bromoalkanes to form quaternary ammonium salts. The illustrative example of the formation of 1,6 - diquinuclidinium dibromide is shown below.



Scheme 3.1 The Menshutkin reaction showing the formation of 1,6-diquinuclidinium hexane dibromide.

Changing the base and  $\alpha,\omega$  - dibromoalkane appropriately can generate a multitude of possible organic templates as described throughout this thesis. It should be noted

however, that in the case of 1,4 - diazabicyclo[2.2.2]octane, DABCO, that the reaction mixture was initially in a 1:1 mole ratio between base and  $\alpha,\omega$  - dibromoalkane.

The actual experiments were performed such that the dibromoalkane and base in a 1:2 mole ratio were refluxed in an excess of ethanol at approximately 80°C for 72 hours. Once cool the excess ethanol was removed on a Buchi rotary evaporator and the resulting residue allowed to crystallise under refrigeration overnight.

Crystals were washed with acetone and cool ethyl acetate before being allowed to dry at room temperature in air. Characterisation was performed mainly using  $^{13}\text{C}$  NMR spectroscopy on a Varian 300 spectrometer. Additional characterisation such as melting point and microanalysis was carried out on templates of specific interest or in the event that the NMR was not conclusive evidence for the formation of the template. Microanalysis when used was performed on a Carlo Erba Elemental Analyser model 1106.

In the event of crystals not being produced, this was generally due to the hygroscopic nature of the organic molecule. This problem could be overcome by the addition of petroleum ether to crash out the template. This technique was used very rarely as apart from the characterisation there was little to no benefit in the use of the template and generally led to lower yields, typically 50-65% as opposed to 80-95%.

Once prepared and characterised the methylammonium salts were converted to the dihydroxide form using silver(I)oxide before being used as templates. This is important as the template is used during synthesis of microporous solids (and particularly magnesium aluminium phosphates, MAPOs) to increase the pH of the synthesis gel to between 6 and 8. Without converting the template to the hydroxide form, the MAPO synthesis gel would have a pH of only 2 and the formation of a microporous solid would be unlikely.

The template is mixed with a 100% excess of silver(I)oxide in water for 15 minutes. The beaker is covered in aluminium foil in attempt to reduce the level of light getting to the reaction mixture as silver halides are photosensitive. After 15 minutes the resulting

black slurry is filtered and washed with distilled water until the filtrate containing the template in the hydroxide form has a neutral pH indicating that all of the template has been washed through. The filtrate is then concentrated to approximately 5ml using a rotary evaporator. The template is now ready for use in the synthesis of microporous solids. The chemical equation describing the conversion process is:-



Figure 3.2 The conversion of dibromoalkanes with silver(I)oxide to the hydroxide form. This is an important step for the effective synthesis of microporous solids.

### 3.3.0 Results and Discussion

The templates used throughout this project have all been selected primarily for their physical properties, e.g. their size or shape. Additionally several templates such as; tripropylamine and tris-(2-aminoethyl)amine or, 1,4-diazabicyclo[2.2.2]octane and quinuclidine, have also been studied to examine the effects caused by changing the chemistry of the template. This chapter, is intended to explain the rationale behind the choice of these templates although their effect on the synthesis of microporous solids are not discussed here. The observed template effects are discussed in chapter four, which describes the synthesis of microporous solids. The main aim of this chapter therefore, is to describe the choice, size and shape of the organic template molecules themselves.

Due to the nature of this work, the results are presented in a summarised form and have been categorised into three broad areas depending on the type of template molecule described. The three template categories are:- (1) commercial, (2) systematic and (3) novel. The criterion for each of these categories is explained below.

(1) Commercial templates are those molecules that have been purchased commercially and used directly in the synthesis of microporous solids, without further modification. Most of these molecules have been studied previously for their

templating abilities and as such provide a useful reference to compare the results obtained here.

- (2) Systematic templates represent a category of molecules that have been synthesised in house to study the effect on the synthesis of microporous solids by systematically altering the size or shape of a template molecule. Some of these molecules have also been used before in the synthesis of microporous materials but not in such a rigorous systematic manner.
- (3) The further novel templates are the broadest category of molecules used in this project. These molecules were chosen to exploit specific trends observed in the previous two categories, namely increasing size. Most of these molecules have been synthesised in collaboration with other researchers. The use of phosphorous based and inorganic templates are also contained in this section.

## 3.3.1 Commercial Templates

All of the commercial templates used in this project are summarised below in table 3.1. With few exceptions, all of these chemicals were obtained from Aldrich and used without further purification.

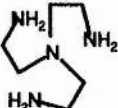
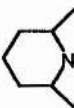
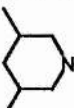
Template	Name	Appearance	Approx. Size (Å)	
			Length	Bulkiness
	Triethylamine	Clear Liquid	3.06	5.87
	Tripropylamine	Clear liquid	3.06	9.21
	Tris(2-aminoethyl)amine	Clear / yellow liquid	3.64	9.39
	Quinuclidine	White powder	3.63	2.50
	DABCO	White powder	2.54	2.50
	2,6-dimethylpiperidine	Clear liquid	4.96	11.96
	3,5-dimethylpiperidine (3,5dmp)	Clear liquid	4.85	6.79

Table 3.1 Summary list of the commercial templates used. All of the sizes listed are approximate and were generated from Hyperchem<sup>[3]</sup> so as to obtain the largest possible values. The molecular shapes represented here do not necessarily represent actual molecular conformations.

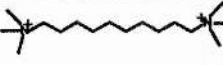
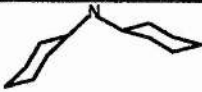
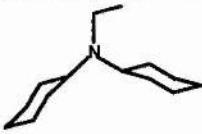
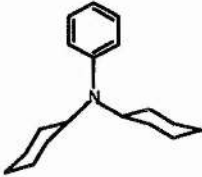
Template	Name	Appearance	Approx. Size (Å)	
			Length	Bulkiness
	Hexamethylene-tetramene	White powder	3.63	3.63
	Decamethonium Bromide	White powder	3.05	18.06
	Hexamethonium Bromide	White powder	3.05	13.04
	Dicyclohexylamine	clear liquid	6.70	6.69
	N:N'-Ethyl-dicyclohexylamine	clear liquid	8.39	5.48
	N:N'-Benzyl-dicyclohexylamine	clear liquid	8.31	7.99
	Sparteine	white powder	9.66	4.61

Table 3.1 (continued) List of commercial templates.

With the exception of the hexa- and decamethonium bromides which were ion exchanged for the aluminophosphate synthesis gels to ensure adequate pH during synthesis, all of these molecules were used without further modification. The graphical representations of these molecules, as shown above and in subsequent diagrams, are presented for ease of identification and do not necessarily accurately represent the true nature of these molecules. The lengths and widths of these molecules are also approximate and were generated using Hyperchem<sup>[3]</sup>, before geometry optimisation. These figures are given to indicate the magnitude of the size variations between different molecules as opposed to absolute values. The result of these templates on the synthesis of microporous solids are

described fully in section 4.3.1 of chapter four. To summarise, however, it is noted that the templates have a greater effect on the synthesis of the aluminophosphates than on the zeolites. Tripropylamine and tris-(2-aminoethyl)amine generate very different aluminophosphate materials despite being very similarly sized. This is believed to be caused by the chemical differences between the two molecules and this effect is also shown by the quinuclidine and 1,4-diazabicyclo[2.2.2]octane molecules.

### 3.3.2 Systematic Templates

Five different systematic series of templates have been prepared as described in the experimental section of this chapter. One of the main factors in the choice of the templates used, has been their ease of preparation since the templates are not in themselves the goal of this project. Four of the five series have been prepared essentially pure in yields typically in excess of 80%. The remaining series, based on 3,5-dimethylpiperidine, the only series to be based on amines as opposed to ammonium cations, was more difficult to synthesise. Table 3.2 lists the templates that have been varied in length systematically to investigate the effect on the synthesis of microporous solids, although again these results are presented in chapter four.

Molecule	Abbreviated Name	n, varied between of Series
	2,n,2	3 - 9
	3,n,3	3 - 8
	QuinCn	2 - 9
	DABCOc <sub>n</sub>	2 - 8
	3,5-dmpCn	3 - 8

Table 3.2 The Systematic Template homologous series. The positive charge is balanced in all cases by an appropriate number of bromide or hydroxide ions.

Each of the above template series provide an interesting study in themselves as each series systematically increases in length altering their templating abilities. This effect is shown in chapter four and demonstrated further in chapter seven which concentrates on the DABCO series in detail. Comparison between the different template series is also possible and each has been chosen carefully to allow this.

The triethylammonium series was chosen so that it could be directly compared with the quinuclidinium and the tripropylammonium series. The quinuclidine and triethylamine end members of the above series are very similarly sized and differ in the quinuclidine having an extra carbon so that there is a caged structure formed, as shown in the diagrams above. Consequently templates of the quinuclidinium series are slightly narrower but longer than respective templates of the triethylammonium series. Similarly the tripropylammonium series is bulkier than the triethylammonium series. Large

the tripropylammonium series is bulkier than the triethylammonium series. Large differences in the synthesis of microporous solids are observed when using these three different types of template (see chapter four). These differences are caused by the increasing bulkiness of the templates showing that altering the size and shape of a template molecule can have a great effect on the synthesis of microporous solids.

In a similar way the 3,5-dimethylpiperidine end-membered series was chosen to study the effect of increasing the bulkiness of the templates still further but in a controlled fashion (as with the quinuclidine). These templates are neutral tertiary amines and as such have different chemical and physical properties to the other, positively charged, ammonium based templates. These templates were also more difficult to synthesise than any of the other four template series and consequently, as described later, were not synthesised pure.

The DABCO series was chosen as a direct comparison to the quinuclidinium series and was of interest as the polymeric nature of this template in effect dictates the way in which the individual quinuclidinium templates are allowed to align in the synthesis gel. The polymeric templates are equivalent to individual quinuclidinium templates aligning head to tail in the synthesis gel. A comparison between the quinuclidinium and the DABCO series therefore may provide useful information as to how template packing affects the nature of the microporous solids synthesised.

### 3.3.3 The Triethylammonium Series

All of these templates were readily synthesised within 72 hours as described previously and characterised by  $^{13}\text{C}$  NMR spectroscopy. A small quantity of each template (typically around 20-30mg) was dissolved in  $\text{D}_2\text{O}$  and characterised on a Varian 300 MHz NMR spectrometer. Figure 3.3 shows a typical spectrum obtained for the 2,6,2 template molecule. The spectrum clearly shows only the 5 peaks expected from theory, after consideration of symmetry and subsequently the template can be considered to be pure. Other templates in this series were also determined as having been prepared

essentially pure as their respective NMR spectra showed no evidence of impurities being present.

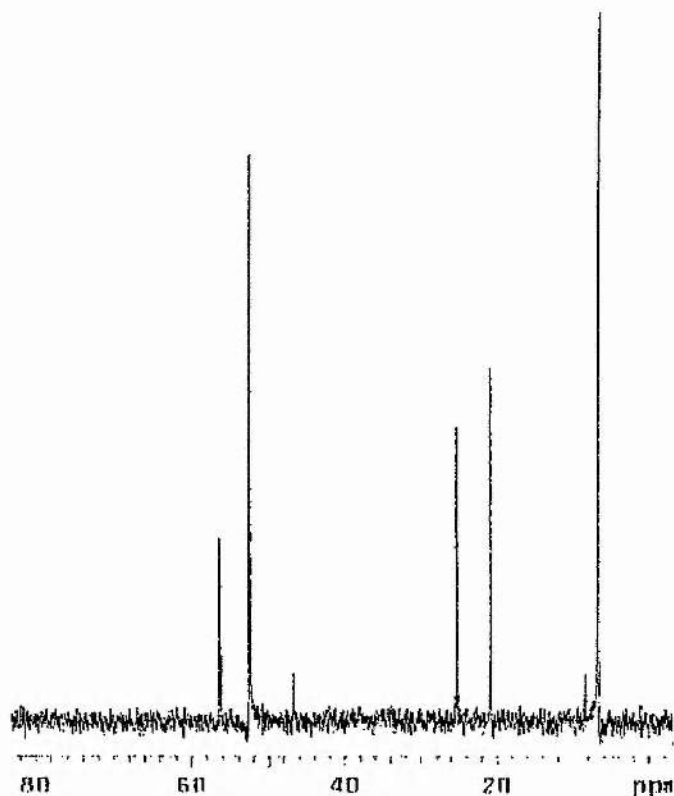


Figure 3.3 <sup>13</sup>C NMR spectrum of the 2,6,2 template molecule. The 5 peaks are as would be expected from theory after consideration of symmetry. This template and the others in this series were determined as being pure on the basis of their NMR spectra which showed no evidence of impurities being present.

Further characterisation has been performed on several members of this template series using microanalysis which confirms the purity of these molecules. The microanalysis was performed on a Carlo Erba Elemental Analyser model 1106. The results of the microanalysis is shown below and a summary of reaction yields of the triethylamine series are given in table 3.4.

In the course of this project the two main characterisation techniques used for the organic template were NMR spectroscopy and CHN microanalysis. In all cases for this

and the subsequent template series the NMR was the main technique due mainly to its sensitivity and reliability. The microanalysis technique has been used mainly as a support to the NMR. Microanalysis results can be affected by the presence of solvents or water and as many of the template molecules described here are hygroscopic, the data must be treated with caution. In the following tables the predicted values given for the relative percentages of carbon, hydrogen and nitrogen should be within 0.3% of the actual values obtained

Molecule	% C		% H		% N	
	Predicted	Actual	Predicted	Actual	Predicted	Actual
2,3,2	44.6	39.1	8.9	8.6	6.9	5.8
2,4,2	45.9	45.7	9.1	9.2	6.7	6.6
2,5,2	47.2	44.0	9.3	9.3	6.5	5.9
2,6,2	48.4	47.5	9.4	9.4	6.3	6.0
2,8,2	50.6	48.8	9.7	9.8	5.9	5.8

Table 3.3 Results of microanalysis performed on selected template molecules to verify their purity. The close agreement between the predicted and actual values of each template supports the NMR data showing that these compounds are pure. The 2,3,2 template may contain water).

Template	Appearance	Yield
2,3,2	White powder	92 %
2,4,2	White powder	90 %
2,5,2	White Powder	87 %
2,6,2	White powder	91 %
2,7,2	White powder	89 %
2,8,2	White powder	88 %
2,9,2	White powder	90 %

Table 3.4 Template reaction summary of the 2,n,2 series.

### 3.3.4 The Tripropylamine Series

The tripropylamine based template series has also been synthesised and characterised using the same methods as for the triethylamine based template series described above. One of the biggest differences between these templates, was that the tripropylamine based molecules formed mainly as oils rather than as powders. This is presumably due to the increased organic nature of these molecules making them more hygroscopic and less likely to crystallise. Attempts to “crash out” these templates into a solid form by adding the crude template oil to pet-ether or diethyl ether, were successful but resulted in low reaction yields and were not used frequently. Template purity was established by  $^{13}\text{C}$  NMR and consequently there was little need to crystallise the tripropylamine templates. A typical NMR spectrum from this series is shown below in figure 3.4.

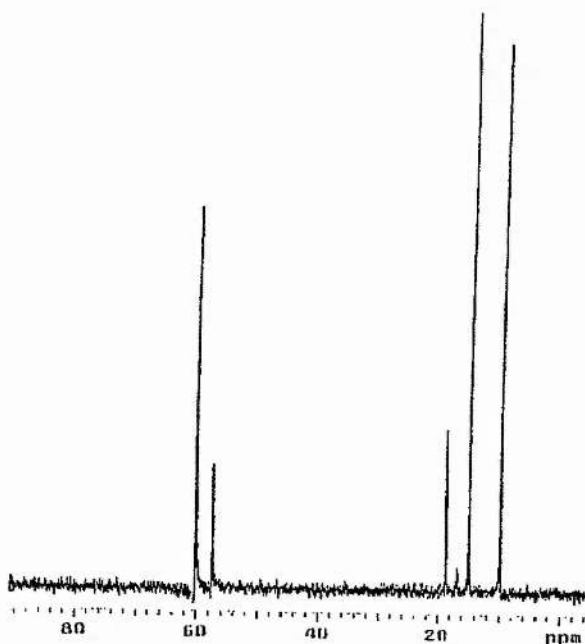


Figure 3.4  $^{13}\text{C}$  NMR spectrum of the 3,4,3 template showing only the theoretically predicted peaks indicating the purity of the template.

Microanalysis was performed on selected templates to confirm that the template molecules were synthesised correctly. A summary of reaction yields and overall

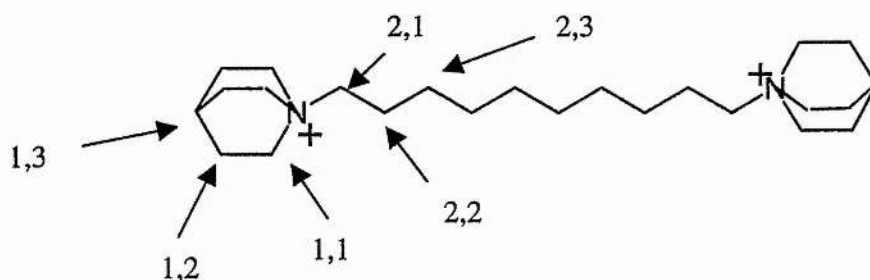
template lengths of the triethylamine series are given in table 3.5. Again, it is important to stress that all of these molecular lengths are approximate and are stated to demonstrate the systematic increase in the overall length of the templates.

Template	Appearance	Yield	Approximate length (Å)
3,3,3	White powder	92 %	11.46
3,4,3	Clear yellow liquid	90 %	12.85
3,5,3	Clear yellow liquid	87 %	13.94
3,6,3	Clear orange liquid	91 %	15.31
3,7,3	Clear orange liquid	89 %	16.43
3,8,3	Clear orange liquid	88 %	17.85

Table 3.5 Template summary showing the different molecular lengths of the 3,n,3 series.

### 3.3.5 The Quinuclidine Series

The quinuclidine based template series was also synthesised and characterised using the same methods as for the triethylamine based template series described above. The quinuclidine templates all formed as white powders with reaction yields typically in the range 87-97 %. A typical  $^{13}\text{C}$  NMR spectrum is shown below for the QuinC3 molecule. As is clearly apparent from the spectrum the pattern shows only the five predicted signals as shown in the figure below. This was also true of the other templates in this series and a  $^{13}\text{C}$  NMR peak summary of these molecules is given in table 3.6. The peaks are assigned as shown below:-



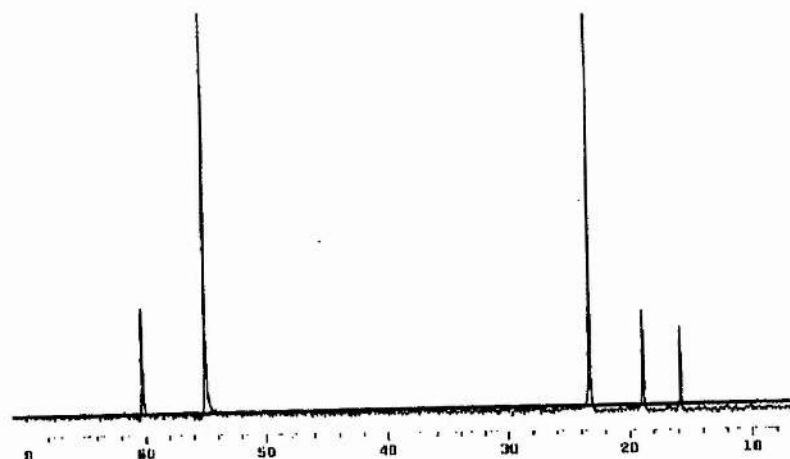


Figure 3.5  $^{13}\text{C}$  NMR spectrum of the QuinC3 sample again showing only the predicted peaks.

Molecule	Peak							
	1,1	1,2	1,3	2,1	2,2	2,3	2,4	2,5
QuinC10	54.62	25.68	19.16	64.43	23.42	25.68	28.12	28.31
QuinC9	54.62	25.64	19.00	64.43	21.40	25.65	28.04	28.18
QuinC8	54.63	25.61	19.08	64.44	21.41	23.39	27.96	
QuinC7	54.64	25.51	19.10	64.31	21.36	23.40	27.73	
QuinC6	54.62	25.31	21.34	64.05	23.33	25.31	31.51	
QuinC5	54.70	25.20	19.03	63.78	23.36	21.19		
QuinC4	53.48	22.02	17.64	61.87				
QuinC3	55.00	23.23	18.98	60.28	15.76			

Table 3.6  $^{13}\text{C}$  NMR peak summary for the QuinC<sub>n</sub> series to indicate the purity of these template molecules. Note the peak overlap between the 1,2 and the 2,1 carbon atoms of QuinC4 template which appears to have one peak too few.

Microanalysis was also undertaken on several of these template molecules, the results of which are shown below. A summary of reaction yields of the quinuclidinium series are given in table 3.8.

Molecule	% C		% H		% N	
	Predicted	Actual	Predicted	Actual	Predicted	Actual
QuinC3	48.1	46.6	7.5	6.8	6.6	6.2
QuinC4	49.3	46.0	7.8	7.7	6.4	5.9
QuinC6	51.5	48.5	8.2	8.4	6.0	5.6
QuinC7	52.3	49.3	8.4	8.7	5.8	5.5
QuinC9	54.3	51.3	8.7	9.1	5.5	5.1
QuinC10	55.0	54.4	8.9	9.0	5.3	5.3

Table 3.7 Results of microanalysis performed on selected template molecules to verify their purity. The close agreement between the predicted and actual values of each template shows that these compounds are pure.

Template	Appearance	Yield
QuinC3	White powder	97 %
QuinC4	White powder	95 %
QuinC5	White powder	92 %
QuinC6	White powder	93 %
QuinC7	White powder	90 %
QuinC8	White powder	91 %
QuinC9	White powder	87 %
QuinC10	White powder	85 %

Table 3.8 Template reaction summary for the diquinuclidinium templates.

### 3.3.6 The 1,4-diazabicyclo[2.2.2]octane (DABCO)-C<sub>n</sub> Series

The DABCO based template series was synthesised and characterised using the same methods as described above. The reaction ratios were altered however, so that the DABCO to  $\alpha,\omega$ -dibromoalkane ratio was one in order to permit the synthesis of polymeric cationic species. The ionene templates all formed as white powders with reaction yields typically in the range 67-82 %, interestingly the longer chained molecules tended to react quicker and produce larger yields than the shorter chained molecules ( $n < 5$ ). This may be due to a number of factors including solubility of the forming polymer in ethanol. A typical  $^{13}\text{C}$  NMR spectrum is shown below for the DABCO<sub>5</sub> molecule. As is clearly apparent from the spectrum the pattern shows the six predicted signals as well as two additional ones thought to be caused by the termination of the polymer. Further examination of the products of the reaction of DABCO with  $\alpha,\omega$ -dibromoalkanes containing 2, 3, 4, 5, 6, 7 and 8 (=n) methylene groups, (compounds denoted DABCO<sub>n</sub>) suggests that whereas no terminal C-Br or unreacted amine groups could be observed for n of 5 or above, indicating the condensation of very many DABCO units into the structure, for n = 4 oligomeric ions including on average around 10 DABCO units were synthesised. For n= 2 and 3, NMR indicates much shorter oligomers are present, containing just a few DABCO units.

Further characterisation using gel permeation chromatography was attempted but proved to be impractical owing to the polymers solubility in water as opposed to organic solvents. This will be explained more fully in chapter seven but an excellent description of gel permeation chromatography may be obtained from Cowie<sup>[4]</sup>.

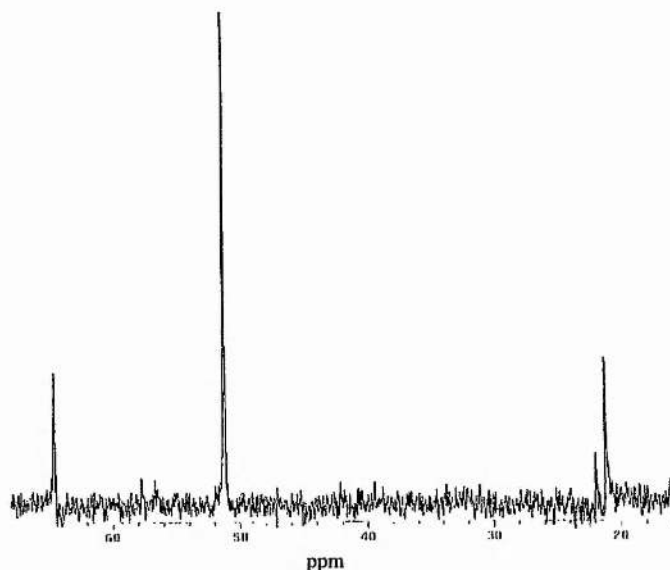


Figure 3.6 A typical  $^{13}\text{C}$  NMR spectrum of from the DABCO series. The above spectrum is for the DABCOC5 molecules.

Microanalysis was however performed and the results of which are shown below in table 3.9 a summary table of the reaction yields are also given.

Molecule	% C		% H		% N	
	Predicted	Actual	Predicted	Actual	Predicted	Actual
DabcoC2	32.0	28.3	5.3	4.75	9.3	7.77
DabcoC3	34.42	30.08	5.78	6.38	8.92	7.97
DabcoC4	36.6	31.42	8.4	6.26	8.5	7.10
DabcoC5	38.6	35.03	6.4	7.00	8.2	7.43
DabcoC6	40.47	36.12	6.79	6.91	7.87	6.89

Table 3.9 Results of microanalysis performed on selected template molecules to verify their purity.

Template	Appearance	Yield
DABCOC2	White powder	65 %
DABCOC3	White powder	70 %
DABCOC4	White powder	71 %
DABCOC5	White powder	74 %
DABCOC6	White powder	81 %
DABCOC7	White powder	73 %
DABCO8	White powder	70 %

Table 3.10 Template summary showing the reaction yields of the DABCO series. The yield was estimated by being based on the DABCO.

### 3.3.7 The 3,5-dimethylpiperidine Series

The final series examined in detail was based on the use of 3,5-dimethylpiperidine as the end group. These molecules required slightly more preparation than the previously described molecules as they required an additional step in their preparation to remove the additional hydrogen atom from the nitrogen. They are also synthesised with lower reaction yields. NMR spectroscopy and microanalysis however, both tend to indicate that these template molecules were not synthesised pure. Indeed the most reasonable explanation of the characterisation data is that there is a mixture of molecules comprising of the desired product and the half reacted product, i.e. 3,5-dimethylpiperidine having reacted at only the  $\alpha$ -end of the dibromoalkane and the desired product. A typical  $^{13}\text{C}$  NMR spectrum is shown below for the 3,5dmpC4 molecule. The microanalysis however, surprisingly showed a fairly close agreement between actual values and theoretical ones as shown in table 3.11. confirming the sensitivity of the NMR and why it has been used as the primary characterisation technique.

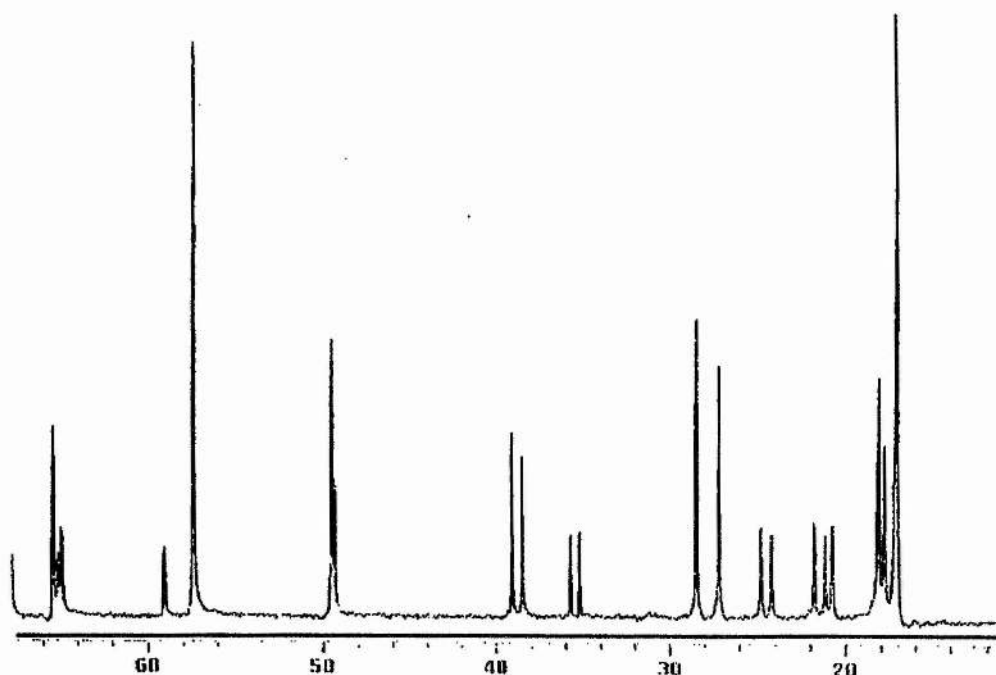


Figure 3.7 Part of the  $^{13}\text{C}$  NMR spectrum of 3,5dmpC4. The excessive number of peaks in this spectrum indicate that the template has not been prepared pure and is infact a mixture, possibly of mono and diquatarnary species.

Molecule	% C		% H		% N	
	Predicted	Actual	Predicted	Actual	Predicted	Actual
3,5dmpC3	47.60	49.39	8.40	9.33	6.60	7.17
3,5dmoC4	48.80	55.07	8.60	9.41	6.30	5.79
3,5dmpC5	58.60	56.44	8.10	9.21	5.70	5.50

Table 3.11 Results of microanalysis performed on selected template molecules.

Template	Appearance	Yield
3,5-dmpC3	White powder	48 %
3,5-dmpC4	White powder	45 %
3,5-dmpC5	White powder	52 %
3,5-dmpC6	White powder	61 %
3,5-dmpC7	White powder	51 %
3,5-dmpC8	White powder	40 %

Table 3.12 Template summary showing the different molecular lengths of the 3,5dmpC<sub>n</sub> series. The low reaction yields are an indication of the preparation difficulties associated with these templates.

### 3.3.8 Further Novel Templates

Novel templates, those molecules that have been chosen to emphasise or accentuate, trends already looked at by the other templates included in this section. Many of these molecules have been synthesised by myself or others and as such have been used and treated in a similar fashion to commercially available templates, i.e. without further purification or characterisation. All of the novel templates used in this project are summarised below in table 3.13.

Template	Abbreviated Name	Appearance
$\left( \left( n\text{Bu}_3\text{P}^+\text{CH}_2 \right)_2 \text{C}_6\text{H}_4 \right)_2 2\text{Br}^-$	RAA1	White powder
$\text{Ph}_3\text{P}^+\text{Pr}^-\text{I}^-$	RAA2	White powder
$\left( n\text{Bu}_3\text{P}^+\text{CH}_2 \right)_2 2\text{Br}^-$	RAA3	White powder
$\left( \text{H}_2\text{O} \right)_n \left( \text{CH}_2 \right)_n \text{Cl}^-$	Polymer	Clear liquid
$\left( \text{CH}_2 \right)_4$	4,4,4	Clear yellow oil
$\left( \text{CH}_2 \right)_6$	4,6,4	Clear yellow oil

Table 3.13 Summary list of the further novel templates used.

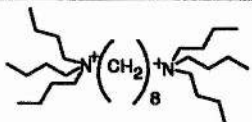
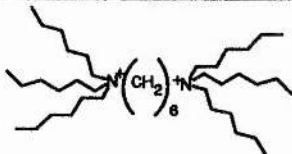
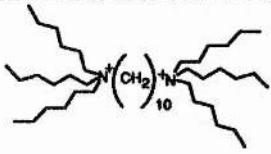
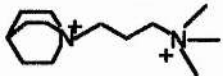
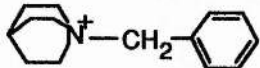
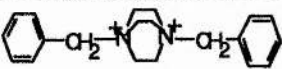
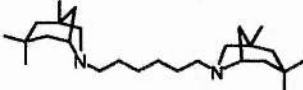
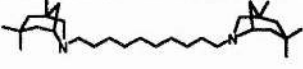
Template	Abbreviated Name	Appearance
	4,8,4	Clear orange oil
	6,6,6	Clear orange oil
	6,10,6	Clear orange oil
	Quin-TMAP	White powder
	DABCO-TMAP	White powder
	Quin-benzyl	White powder
	DABCO-benzyl	White powder
	VP1	White powder
	VP2	White powder

Table 3.1 (continued) List of 'further' novel templates.

All of these templates were used as shown above without further purification although they were ion exchanged to create the hydroxide form before being used in the synthesis

gels of the aluminophosphate systems. The 4,n,4 and 6,n,6 templates were used as oils and were not crystallised as their NMR spectra indicated that they were pure except for trace amounts of unreacted dibromoalkane and ethanol.

The novel quinuclidinium and DABCO templates were also synthesised and used without further purification as their NMR spectra also indicated that they were phase pure. These templates were synthesised using the same methods as before and were produced typically in yields in excess of 80%, as were the other quinuclidinium and DABCO templates described previously. The  $^{13}\text{C}$  NMR spectrum of Quin-TMAP is shown below. Again as with the 4,n,4 and the 6,n,6 templates the only appreciable impurity is that of ethanol.

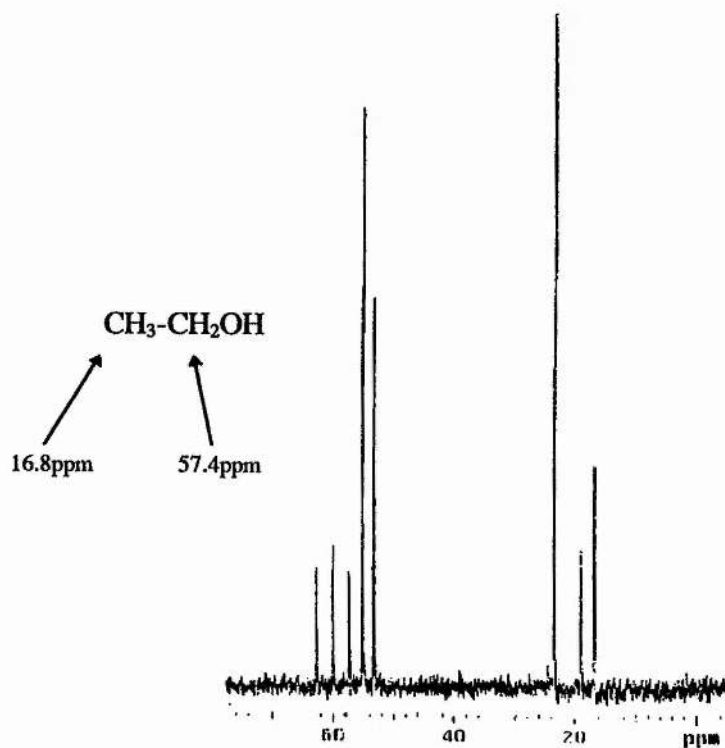


Figure 3.8 The  $^{13}\text{C}$  NMR spectrum of Quin-TMAP, the extra peaks at 16.8 and 57.4 ppm are due to the presence of ethanol as indicated.

### 3.4.0 References

- 1 S. Patai (Editor), *Chemistry of the Amino Group*, Interscience Publishers, John. Wiley & Sons, 1968
- 2 R.T. Morrison and R.N. Boyd, *Organic Chemistry (5<sup>th</sup> Edition)*, Allyn and Bacon Inc., 1987
- 3 Hyperchem, Version 4, Hypercube Inc.
- 4 J.M.G. Cowie, *Polymers: Chemistry and Physics of Modern Materials (2<sup>nd</sup> Edition)*, Blackie, 1991

## Chapter Four

### Template Study on Microporous Solids

#### 4.1.0 Introduction

Synthesising new microporous materials that can be used as heterogeneous catalysts has been the main aim of this project. The two most obvious ways in which this can be achieved are:-

- (1) to modify existing microporous solids. This can be achieved by incorporating different transition metals into the microporous framework structures. TS-1 for example is a titanosilicate material isostructural to ZSM-5 and used widely in epoxidation catalysis<sup>[1]</sup>. Alternatively the encapsulation of inorganic complexes can enhance the catalytic potentials of some microporous materials<sup>[2,3]</sup>, for example copper phthalocyanine complexes inside zeolite-Y. The modification of framework composition has been attempted in due course as part of the research described here. The encapsulation of inorganic complexes is described more fully in chapter eight.
- (2) to create new microporous materials. This is the main approach adopted in this project. The work has focused on the use of organic template molecules being added to zeolitic and aluminophosphate synthesis gels as a means to synthesising new microporous solids. The design and synthesis of these template molecules has already been discussed in chapter three. This chapter focuses on the application of the templates and the materials that they synthesise. In addition to known materials, five new materials have been synthesised in the course of this research, four of which are thought to be microporous. Two of these new materials have now had their structures revealed to become two of just one hundred and nine known distinct zeotypic topologies<sup>[4]</sup>. The catalytic potential of all of the new materials synthesised have not yet been fully investigated, but will form the basis of future research in this laboratory.

There are many synthetic targets that are still to be accomplished in the synthesis of microporous solids. Traditionally the synthesis of new microporous solids has been by Edisonian methods due to the complexity of the zeolite systems which makes them difficult to understand or control. The work contained in this thesis adopts a more rational approach to the synthesis of new materials. New methods for the synthesis of microporous solids, mainly aluminophosphates were also investigated in the course of this work.

#### 4.2.0 Experimental

The synthesis of zeolites during this project has been undertaken using three different methods, static, stirring and tumbling hydrothermal synthesis. In all three cases the initial preparation of the zeolitic gel before being placed into an autoclave has been very similar and is described here. The use of different synthesis gel compositions (including sources of silicon and aluminium), ageing, reaction temperatures and heating times have also been attempted to investigate the effect on the synthesis of zeolites. These variations are clearly marked in the text at the appropriate time and are not described here.

For the bulk of the zeolites synthesised during the course of this thesis a high silicon to aluminium ratio of 50:1 has been used to facilitate the synthesis of crystalline products in a short space of time. Zeolites were produced by hydrothermal synthesis from very basic gels (usually pH 12 to 14). These were prepared by the addition of hydrated aluminium oxide (pseudo-boehmite) ( $\text{Al}_2\text{O}_3 \cdot 3\text{H}_2\text{O}$  purchased from the Aldrich chemical company), 30 weight % colloidal silica, sodium oxide and the organic template to distilled water in the molar ratio of 1:101:20:9:5090. The gels were heated at 190 °C for 72 hours in stainless steel, 25ml or 40ml PTFE-lined autoclaves for static zeolite synthesis. Stirring experiments were performed using as a stainless steel 500ml Baskerville Stirring Autoclave and latterly a 50ml Parr PTFE-lined stirring autoclave.

The MAPOs were produced by hydrothermal synthesis from near neutral gels (usually pH 6 or 7). These were prepared by the addition of aluminium hydroxide hydrate ( $\text{Al}(\text{OH})_3 \cdot x\text{H}_2\text{O}$  purchased from the Aldrich chemical company), magnesium acetate

( $\text{Al}(\text{OH})_3 \cdot x\text{H}_2\text{O}$  purchased from the Aldrich chemical company), magnesium acetate tetrahydrate, orthophosphoric acid and the organic template (in its hydroxide form) to distilled water in the molar ratio of 0.9:0.1:1.0:0.4:40. The gels were heated at 190 °C for 48 hours in a stainless steel, 25ml PTFE-lined autoclave. Templates that were only capable of producing one positively charged ammonium ion, e.g. tripropylamine were added to the gel such that their mole ratio was 0.7 rather than 0.4. The synthesis of magnesium aluminophosphates by unconventional methods will be described later.

All of the microporous materials produced were characterised using x-ray powder diffraction using a STOE STADIP automated diffractometer. Further characterisation on selected materials were carried out by thermal analysis using a SDT 2960 analyser from TA Instruments, solid state MASNMR using a Bruker 500MSL spectrometer and scanning electron microscopy using a JEOL JSM-35CF microscope with an accelerating voltage of 10kV fitted with a LINK AN 10000 EDX system.

### 4.3.0 Results and Discussion

For simplicity the templates described in chapter three were presented in three broad categories: (1) commercial, (2) novel and (3) systematic templates. These categories are continued throughout this chapter although the zeolites and MAPOs that the templates generate are described simultaneously. Due to the nature of this work, many of the results are presented in a summarised form although several specific results are highlighted and discussed more fully, including the synthesis of five new materials.

General trends which appear over all three categories include the ease of preparation of MAPOs over zeolites. In all cases the MAPOs exhibit a broader range of products especially when studying the effect of systematic templates as in section (3) above. The MAPOs seem to be more susceptible to subtle template variations than the zeolites. This may in part be due to the high silica composition and harsh synthesis conditions employed in the production of zeolites in this project which are well suited to the synthesis of ZSM-5. In any event it should be noted that all of the results presented here

are repeatable, for unless otherwise stated at least two (in most cases three) of each preparation has been performed.

The reproducibility of experiments is vital when studying the effect of systematic template variations as microporous solids inherently have a wide range of parameters that can affect the final product. Every effort has therefore been taken to ensure that any variation in the microporous solids produced are associated with the template used rather than differences in the gel composition.

#### 4.3.1 Commercial Templates

Commercial templates have provided a convenient starting place to begin studying the effect of organic template molecules on inorganic microporous solids. In several cases the templates used had previously been reported in the literature, for example quinuclidine in the synthesis of MAPO-22<sup>[5]</sup> or decamethonium bromide in the synthesis of Nu-87<sup>[6]</sup> and as such provided standards by which to compare the results obtained. This facilitated the establishment of optimum synthesis conditions for both zeolites and MAPOs. It also immediately proved the need to repeat all experiments exactly (changing only the template used) as changing gel compositions or reaction times produced different results from those stated in the literature. Under the conditions used in this project for example, MAPO-16 is produced using quinuclidine rather than MAPO-22 (The production of MAPO-16 using quinuclidine is also cited in the literature<sup>[4]</sup>.)

Similarly the commercial templates were useful in proving the effect of subtle differences in the production of microporous solids. Tripropylamine when used as a template in the synthesis of a MAPO can produce MAPO-36 which is a known channel type structure<sup>[20]</sup>. Under the same reaction conditions but using tris(2-aminoethyl) amine, which is approximately the same size and shape as tripropylamine, produces a new cubic material, the structure solution of which has proven to be elusive.

A complete summary of the commercial templates used in this project and the materials that they synthesised are listed below in table 4.1.

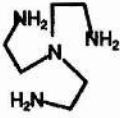
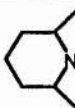
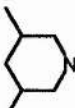
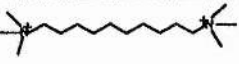
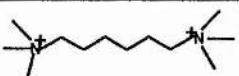
Template	Name	Zeolite produced	MAPO produced
	Triethylamine	ZSM-5	MAPO-5
	Tripropylamine	ZSM-5	MAPO-36
	Tris(2-aminoethyl)amine	ZSM-5	Unidentified New Phase
	Quinuclidine	ZSM-5	MAPO-16
	DABCO	ZSM-5	MAPO-5
	2,6-dimethylpiperidine	ZSM-5	MAPO-34 (chabazite)
	3,5-dimethylpiperidine (3,5dmp)	ZSM-5	MAPO-34 (chabazite)
	Hexamethylene- tetramine	—————	Aluminium ammonium phosphate
	Decamethonium Bromide	Nu-87	DAF-1
	Hexamethonium Bromide	EU-1	MAPO-17

Table 4.1 Summary of results obtained from the commercial templates used. The zeolite product in all cases is ZSM-5 suggesting this structure may be favoured under the reaction conditions used.

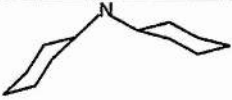
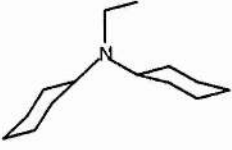
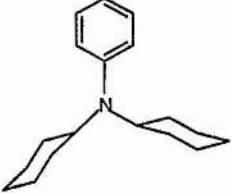
	Dicyclohexylamine	_____	MAPO-5
	N:N'-Ethyl-dicyclohexylamine	_____	MAPO-36
	N:N'-Benzyl-dicyclohexylamine	_____	MAPO-5
	Sparteine	_____	MAPO-5

Table 4.1 (continued) Summary of commercial templates.

### 4.3.2 Developing Optimum Zeolite Synthesis Conditions

Consideration of table 4.1 indicates a natural bias towards the synthesis of ZSM-5<sup>[7]</sup> under the zeolite synthesis conditions used in this project. ZSM-5 is an extremely stable channel type material used in the petrochemical industry for oil refining<sup>[8]</sup> and its production is not surprising. This natural bias towards ZSM-5 is however, unfortunate as it may conceal the more subtle effects of the template host interactions that may lead to the synthesis of new materials. Subsequently the gel chemistry and general synthesis of the zeolites have been varied in an attempt to crystallise zeolites other than ZSM-5.

Some of the most common variations, the silicon and aluminium source and their ratio, heating time and reaction temperature have been studied. The method by which a zeolite forms and the role its components and other synthesis parameters have on its formation is still uncertain. Consequently only a brief discussion of these results are indicated here, for a more detailed discussion of zeolite synthesis conditions, the reader is directed towards references [9-11].

A series of zeolites was synthesised using a variety of templates. The gel composition and hydrothermal synthesis conditions were systematically varied and the results are summarised in table 4.3.

Overall it was found in this work that low Si : Al ratios tended to take a long time to crystallise and usually produced less crystalline products. Silica sources other than colloidal silica also tended to generate less crystalline materials such that they were either amorphous or eventually became dense phases like quartz. Surprisingly the source of aluminium seemed less critical than the silica source, although Pseudo boehmite ( $\text{Al}_2\text{O}_3 \cdot 3\text{H}_2\text{O}$ ) was adopted as the standard as it appeared to be the most efficient source of framework aluminium.

S.I. Zones *et al*, were able to synthesise three new zeolitic materials, SSZ-13, -23 and -24 using N,N,N-trimethyl-1-adamantane from high silica gels<sup>[12]</sup>. They also concluded that high silica gels, with low Si :  $\text{HO}^-$  were the most suitable zeolite composition to obtain new zeolitic materials. Zones also noted that the formation of ZSM-5 and dense phases, like quartz, readily occurred at temperatures exceeding 150°C.

Variable Studied	Parameters of Test	Observed Effect
Silicon source	Cabosil (powder) Colloidal silica Soda-glass	Colloidal silica was able to crystallise more products than either of the other silica sources.
Aluminium source	Pseudo-boehmite Aluminium hydroxide Aluminium triisopropoxide Sodium aluminate	Each of the four sources of aluminium were able to generate crystalline products. Pseudo-boehmite was adopted as the standard source as it produced zeolites quicker than the others for a given gel composition.
Temperature	100 - 200°C	All zeolites described in this thesis required temperatures in excess of 160°C or else a reaction time of 14 days, which often resulted in the formation of quartz. High Si : Al ratios crystallised within 72 hours at 190°C, though these were biased towards ZSM-5.
Si : Al ratio	20-50 : 1	Low silica gels required long reaction times especially at lower temperatures and often failed to crystallise. Higher silica gels tended to crystallise quicker and more reliably.
Reaction time	2 days - 8 weeks	High silica gels crystallise within 3 days. 4 days and longer leads to the generation of ZSM-5 and quartz. Low silica gels require longer reaction times.

Table 4.2 Summary of zeolite synthesis conditions used in this project. Consideration of these results led to the adoption of the synthesis method described in the experimental section.

### 4.3.3 Synthesis of Aluminophosphates

Unlike the zeolites the aluminophosphates produced using the commercial templates demonstrate a range of products. This implies that the synthesis gels used are more sensitive to subtle template variations, which coupled with their ease of crystallisation (48 hours at 190°C) renders them ideal for template-host investigations.

Examples include the synthesis of MAPO-5 when using 1,4-diazabicyclo[2.2.2]octane (DABCO) but MAPO-16 when the template is changed to quinuclidine. As shown in table 4.1 these two template molecules are essentially the same size and shape and differ only by the DABCO molecule having a second nitrogen atom present.

MAPO-5 is also produced using dicyclohexylamine as the template. Changing this molecule to N:N'-ethyl dicyclohexylamine changes the aluminophosphate produced from MAPO-5 to MAPO-36. Again this apparently small change in template size is having a notable effect on the material produced. Both of the aluminophosphates are similar materials with unidimensional channels circumscribed by 12T atoms. This result is particularly interesting not because of the type of material produced but rather that the aluminophosphates are different. Since the templates are of a similar size one might expect similar, if not identical structures to be synthesised. Indeed increasing the size of the template still further to N:N'-benzylidicyclohexylamine results once more in the synthesis of MAPO-5.

### 4.3.4 New Synthesis Methods

The synthesis of zeolites and aluminophosphates has traditionally been achieved by the hydrothermal synthesis method already described, both in this chapter and in chapter one. High temperature and pressure methods which have also proven to be successful, are generally less suitable for the synthesis of aluminophosphates and are inherently more expensive, consequently they are now rarely used since the discovery of the hydrothermal method (discussed in chapter one). However, the synthesis of aluminophosphates, zeolites and microporous materials generally, often require the

addition of an organic additive or template to their synthesis gels. As larger and more elaborate organic templates are now being synthesised for the production of novel microporous materials often with an aim to develop large pore materials to be used for catalytic or adsorption purposes the need for a new synthesis technique to synthesise microporous solids is becoming a necessity. The problem arises because as organic molecules become larger they become hydrophobic in nature and consequently are insoluble in water i.e. they are not incorporated into the synthesis gel of the microporous solid.

The problems of incorporating large organic template molecules into aluminosilicate and aluminophosphate gels has been overcome by attempting two different synthetic strategies. The first, which is used by other researchers, was to use an organic solvent such as ethylene glycol instead of water. Morris and Weigel have recently published an excellent review on the use of organic solvents for the synthesis of molecular sieves<sup>[13]</sup>. The authors note that the use of a mineralising agent such as hydrofluoric acid is often required to obtain a highly crystalline zeolitic product. As this is a highly corrosive and dangerous material, the method used in this project was based on using a water / ethylene glycol mixed solvent, rather than incorporating hydrofluoric acid. A range of water / ethylene glycol mixtures were prepared and used in the synthesis of high silica / aluminium zeolites using large organic molecules as templates. Several concentrations were successful but a 10 % water / ethylene glycol ratio was determined as being the most successful in that highly crystalline zeolites were obtained after five to seven days at 160°C. Figure 4.1 below shows the diffraction pattern of a zeolite (ZSM-5) prepared under these conditions. Ethylene glycol was chosen as the organic solvent because it was miscible with water and still able to dissolve many organic compounds.

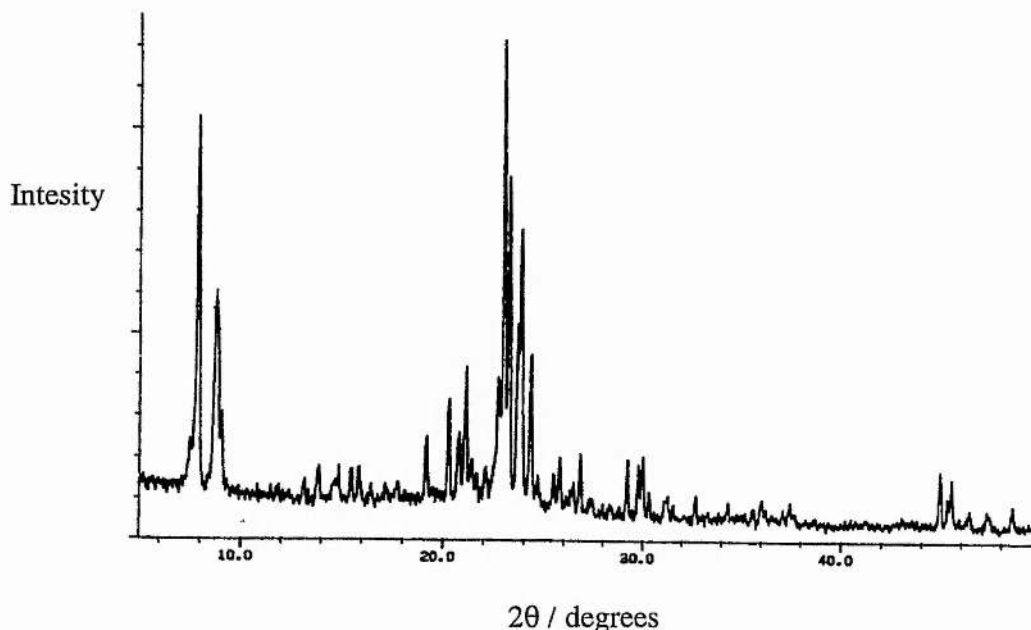
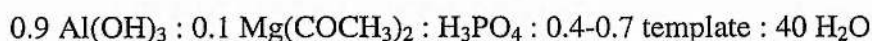


Figure 4.1 An x-ray diffractogram of ZSM-5 produced using a 10% water / ethylene glycol solvent mixture.

The second novel route for preparing microporous solids was developed for the aluminophosphates and utilised “reagent” quantities of solvent. The aluminophosphates synthesised during the course of this project typically had a gel composition of:



The phosphoric acid and template are both normally in the liquid phase and so it was decided to attempt to prepare a synthesis gel without using any other liquid or solvent than those already present. The  $\text{Al(OH)}_3$  and  $\text{Mg(COCH}_3)_2$  were added to an autoclave and mixed thoroughly before the organic template was added and again mixed thoroughly. Finally the acid was added, which resulted instantly in the formation of a gel which was then sealed in the autoclave and treated as in a normal aluminophosphate synthesis. The aluminophosphates that formed were the same as those generated by the analogous hydrothermal synthesis but were generally produced in lower yields (based on the final weight of crystallised product) to their hydrothermal counterparts. MAPO-36 and MAPO-5 were both produced from templates using this technique.

Finally another novel experiment looking into novel synthetic approaches for aluminophosphates was to attempt to synthesise a magnesium aluminophosphate whilst using no template. Using the synthesis composition outlined above but without the organic solvent did produce a partially crystalline product, the diffraction pattern of which is shown below in figure 4.2. This material is at present unidentified. A similar experiment for the zeolite resulted in the production of a dense phase.

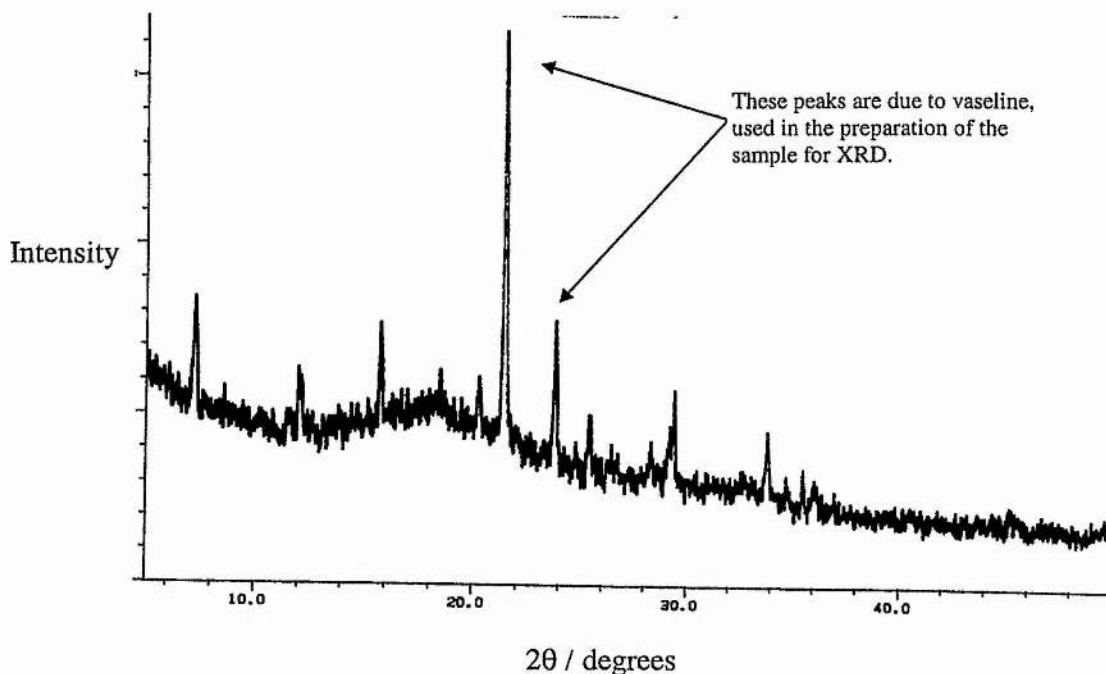


Figure 4.2 An magnesium aluminophosphate produced under normal hydrothermal conditions but without the use of an organic template.

#### 4.3.5 Characterisation of a New Phase

MAPO-36 was synthesised using tripropylamine as well as N:N' ethyldicyclohexylamine but not using tris(2-aminoethyl)amine, again proving the importance of the chemistry of the template. The MAPO prepared using tris-(2-aminoethyl)amine was found to be extremely crystalline as can be shown from the sharpness of the peaks produced in its diffraction pattern. The diffractogram which is shown below in figure 4.3 shows a typical cubic pattern with a maximum d-spacing of  $11.9483\text{\AA}$  at  $2\theta = 7.393^\circ$ .

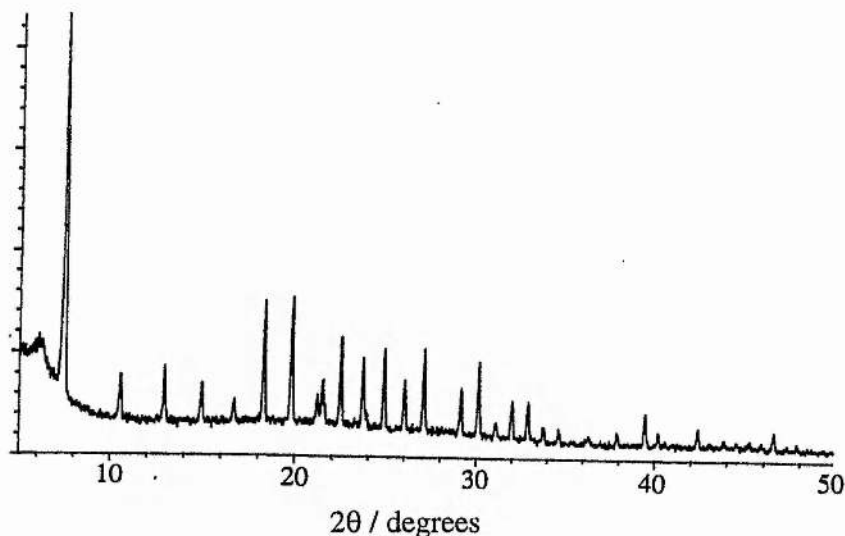


Figure 4.3 X-ray powder diffraction pattern of the MAPO produced using tris(2-aminoethyl)amine. Indexing using VISSER<sup>[14]</sup> indicates that the unit cell dimensions are likely to be body centered cubic material with,  $a = 16.5\text{\AA}$ .

As the pattern could not be identified from the JCPDS files<sup>[15]</sup> or the *Collection of Simulated XRD Patterns for Zeolites*<sup>[16]</sup> it identified the MAPO as being a new material. The pattern was indexed using VISSER<sup>[14]</sup> which confirmed that the sample was likely to be cubic, however, it was not able to help solve the structure. In order to gain a further insight into the material, a SAPO and  $\text{AlPO}_4$  were attempted with an appropriate variation in the gel chemistry, such that silicon was substituted for phosphorous. Unfortunately the SAPO failed to crystallise and the  $\text{AlPO}_4$  crystallised as  $\text{AlPO}_4\text{-5}$ . Additional preparations of the MAPO material were then synthesised with varying Mg : Al ratios and different concentrations of template. In all cases the same material as that shown above was prepared.

Calcination of the material results in loss of crystallinity. Solid state MASNMR obtained with the help of Mrs Barbara Gore at UMIST using a Bruker 500MSL spectrometer has provided further structural details.

From the  $^{13}\text{C}$  MASNMR spectrum it is apparent that the template molecule has been incorporated intact as it shows the two peaks as would be predicted. The  $^{27}\text{Al}$  spectrum indicates the presence of both tetrahedral and octahedral aluminium. Because of the octahedral species, this material is not suitable for Simulated Annealing experiments as the computer program (described more fully in chapter five) is designed to solve only tetrahedrally coordinated materials. Consequently more conventional methods of structure solution are necessary in this case. The  $^{31}\text{P}$  MASNMR shows a peak at -11ppm, which is downfield of that normally expected for P with four (Al) neighbours (usually at -27ppm).

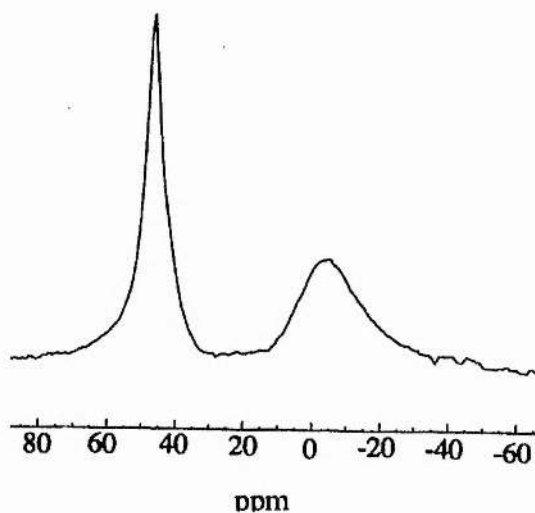


Figure 4.4  $^{27}\text{Al}$  MASNMR spectrum of the MAPO produced using Tris-(2-aminoethyl)amine. The spectrum indicates the presence of both tetrahedral and octahedral aluminium framework ions.

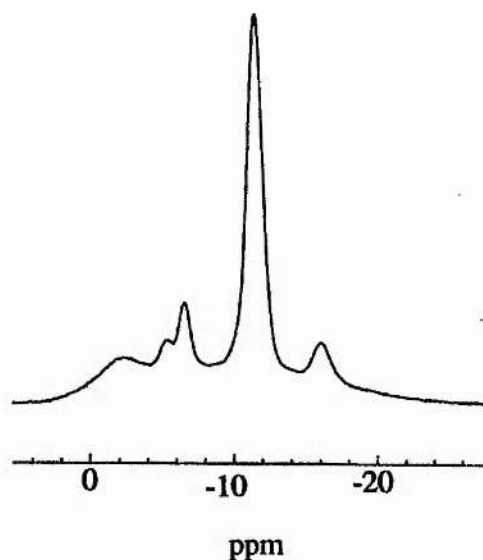


Figure 4.5  $^{31}\text{P}$  MASNMR spectrum of the MAPO produced using tris-(2-aminoethyl)amine. The main peak is offset from that usually expected from these materials (could be a HO- $\text{PO}_3$  group).

Scanning electron microscopy performed on the crystals using a JEOL JSM-35CF microscope revealed the crystals to be truncated tetrahedrons approximately 60  $\mu\text{m}$  in length. Single microcrystal x-ray diffraction was attempted at the Daresbury synchrotron source but insufficient data could be collected to permit structure solution.

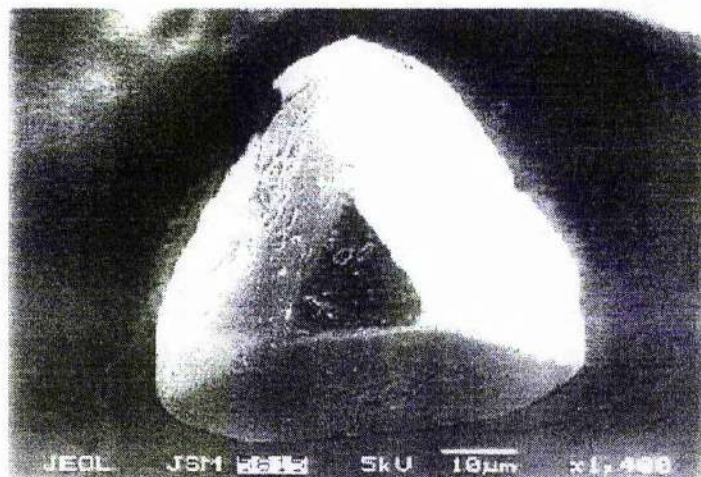


Figure 4.6 Scanning electron micrograph of the MAPO formed using tris-(2-aminoethyl)amine. Single microcrystal diffraction was not able to solve the MAPOs structure due to the absence of a sufficiently high quality crystal.

Further alterations to the gel chemistry has included the incorporation of cobalt and boron, in aluminophosphate based solids. The “CoAlPO” preparation resulted in the production of small purple crystals suitably large for conventional single crystal diffraction. On solving the crystal structure of this material it was identified as being isostructural with  $\text{Co}_3(\text{HPO}_4)_2(\text{OH})_2$ , the structure solution of which was reported by Pizarro *et al* in 1991<sup>[17]</sup>.

Incorporation of boron (using boric acid as the boron source) into the aluminophosphate synthesis gel such that the synthesis composition was a B : Al : P, ratio of 0.5 : 0.5 : 1.0 resulted in another new material. This material is trigonal in nature as distinct to cubic. The material shown below, crystallises as trigonal prisms similar in shape to MAPO-5 but having a different x-ray powder diffraction pattern (figure 4.8). The thermal analysis of this material indicates that the template has been incorporated into the structure as there is a total weight loss observed of 23.1% as shown in figure 4.9.

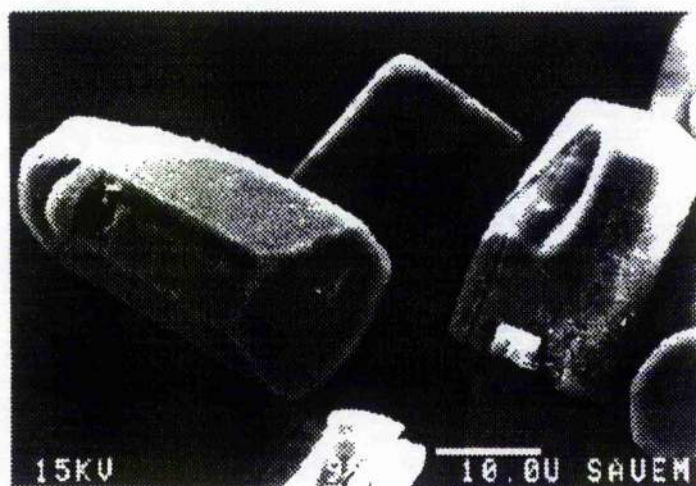


Figure 4.7 Scanning electron micrograph of the trigonal prismatic crystals formed using boron with the tris-(2-aminoethyl)amine template. (The above micrograph was taken using a sonicated sample.)

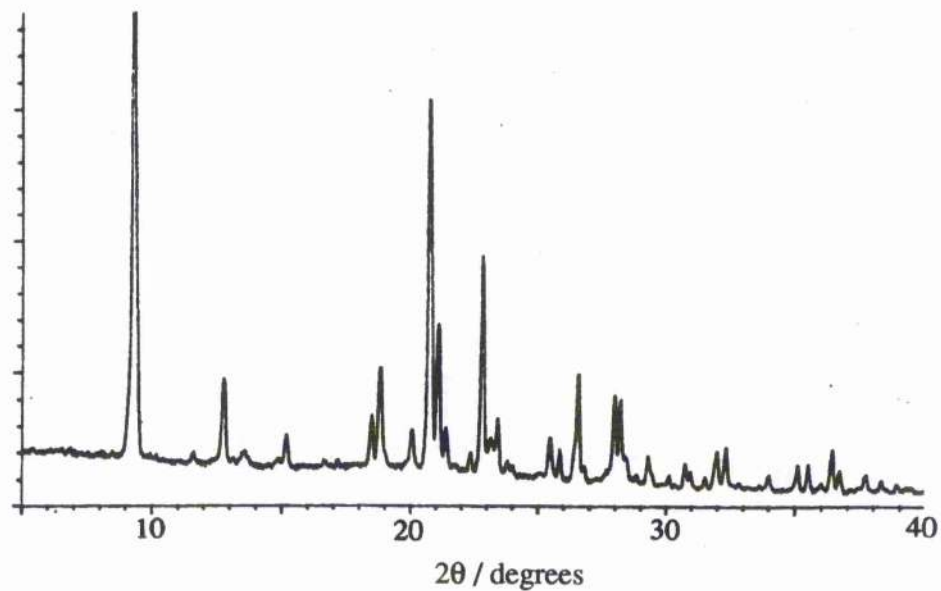


Figure 4.8 X-ray powder diffractogram of the BAiPO formed using tris-(2-aminoethyl)amine.

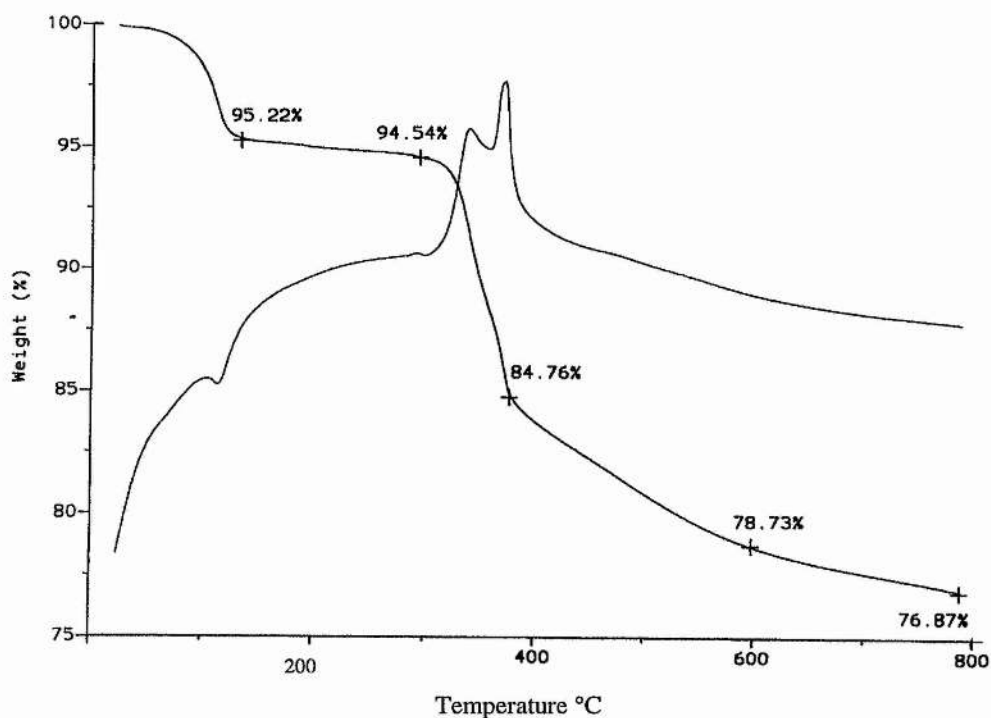


Figure 4.9 TGA/DTA isotherms of the boron aluminophosphate material produced using tris-(2-aminoethyl) amine.

Single microcrystal diffraction obtained in Grenoble using BM16 ID11<sup>[18, 19]</sup> indicates the structure to be trigonal. This data has only recently been obtained and is not of a suitably high standard to ensure a reliable structure solution. However, preliminary data analysis indicates a probable trigonal unit cell of;  $a = 14.4 \text{ \AA}$ ,  $c = 18.81 \text{ \AA}$  belonging to the  $P\bar{3}c1$  space group. Powder x-ray diffraction data was also obtained on this material at Grenoble using BM16. It is hoped that a combined single crystal and powder data refinement will help to elucidate the crystal structure of this material in the same way that the structure of SSZ-42 was obtained by Cambor *et al*<sup>[20]</sup>.

#### 4.3.6 Systematic Template Variation

The use of commercial templates, as described over the previous sections of this chapter, proved the importance of template chemistry and of reaction gel composition. They also indicated that the zeolite synthesis conditions used in this project were naturally biased towards the synthesis of ZSM-5. In an attempt to further investigate these template

properties and the importance of template size and shape, five systematic series of templates were synthesised.

There is known to be a close relationship between template size and shape and the materials that they synthesise<sup>[21, 22]</sup>. There are essentially two ways of systematically changing the size of a template<sup>[23]</sup>, namely changing its length,  $l$ , or its bulkiness,  $b$ , as indicated schematically below.

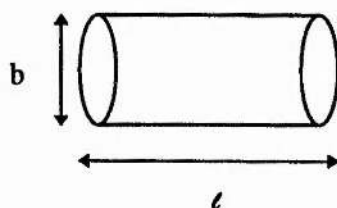


Figure 4.10 Schematic representation of a template showing the two directions by which it may be systematically changed in size.

To exploit this theory five systematic series of templates were synthesised. Each series is designed to meet the criterion discussed in chapter three and to vary both of the directions shown above. The five different series chosen to be studied in this project are shown below in table 4.3.

Template	Range of (n) value
	3-9
	3-9
	2-10
	2-10
	3-8

Table 4.3 Overview of the five different series studied in a systematic template study on the formation of microporous solids. The positive charges are counter balanced by bromide ions in all cases.

The use of triethylamine and tripropylamine end groups for the first two sequences were chosen as this would be a good way to investigate a direct change in 'bulkiness' as there was very little difference between these two series. Also a systematic study of these trimethylamine type templates has previously been undertaken<sup>[24]</sup> and this therefore acted as a reference series. Quinuclidine is a similar size and shape to triethylamine (as drawn above) but is much more constrained than triethylamine because of its additional apical carbon. It is interesting therefore to look at the effect that this subtle difference has on the outcome of the materials synthesised. The DABCO series was chosen to compare against the quinuclidine series. The second positive charge on the DABCO molecule though highly significant on its own, was thought to be secondary to the physical size and shape of these polymeric templates. DABCO templates should be able

in theory to synthesise the same materials as the quinuclidine templates if the microporous solids are channellar. (STA-1 which is a large pore three dimensional channel structure can be synthesised by both quinuclidinium and DABCO templates and as such adds support to this theory.) The 3,5-dimethylpiperidine templates were not thought to be pure but were used as they were to study the effect of increasing the bulkiness of the templates.

All of the templates were converted from their bromide form to the hydroxide form as described in section 3.2.0. The results of the MAPOs and zeolites synthesised using these templates are given in tables 4.4 - 4.8. All of the results presented here have been reproduced at least twice (more often three times) and all possible efforts were taken to ensure that the only appreciable difference between hydrothermal syntheses was the choice of template. In the event of an experiment not being carried out, a solid line denotes this, all other discrepancies are explained as appropriate. Trace impurities (below 5% of product) when present are not stated.

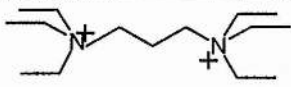
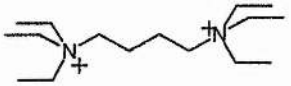
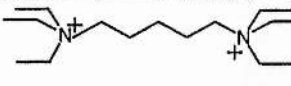
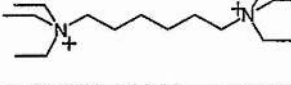
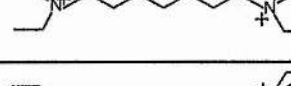
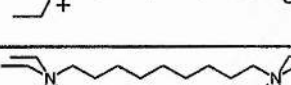
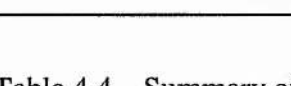
Template	Abbreviated Name	Zeolite Produced	MAPO Produced
	Triethylamine	ZSM-5	MAPO-5
	2,3,2	ZSM-5 + Quartz	MAPO-36
	2,4,2	ZSM-5 + Quartz	MAPO-5 / -56
	2,5,2	ZSM-5 + Quartz	MAPO-5
	2,6,2	ZSM-12	MAPO-5
	2,7,2	ZSM-5	MAPO-5
	2,8,2	ZSM-5	MAPO-5
	2,9,2	ZSM-5	MAPO-5/STA-1*

Table 4.4 Summary of Results for triethylamine series. Again there appears to be a natural trend towards ZSM-5 in the zeolites but the MAPOs show a range of products. \* The production of STA-1 was only witnessed once out of twelve preparations.

Once more there appears to be a natural tendency to synthesise ZSM-5 under the reaction conditions used as was true of the commercially obtained templates too. The formation of ZSM-12 is surprising as there were no appreciable differences between this and the other zeolite experiments except for the template used. There is a fair range of aluminophosphates synthesised by these templates. MAPO-5 is produced when there are five or more methylene groups present in the template chain which is not surprising as MAPO-5 is a stable large pore channel material which is well suited to the incorporation of these template molecules. When there are only four methylene units in the template

chain, however, MAPO-56 is also synthesised although this tends to co-crystallise with MAPO-5.

MAPO-56 is a porous material<sup>[7]</sup> and is crystallised using the quinuclidinium templates too when the chain length is also four methylene units long. As the two template molecules are of similar size this is not surprising and is in fact good evidence that there is a close connection between template size and microporous solid formed. Surprisingly however, STA-2 which is also synthesised readily and (almost) without fail using the QuinC4 template has not been synthesised using the 2,4,2-template. Similarly the formation of STA-1 using the 2,9,2-template has only been witnessed once despite repeated attempts to repeat this experiment.

The reason why the 2,3,2-template should form a large pore channel structure (MAPO-36) rather than a porous type material as might have been more expected is unknown. This is just one of the differences observed between this series and that of quinuclidine. Presumably the cage like nature of quinuclidine is responsible for the major differences between these two series. The end group carbons in the triethylamine templates are not constrained and are allowed to spread out covering a larger area than their analogous quinuclidine templates. As a result of this spreading out effect, the triethylamine molecules are more likely to generate larger pore materials than the quinuclidine templates and this effect is accentuated by the use of tripropylamine end groups.

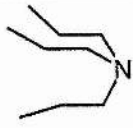
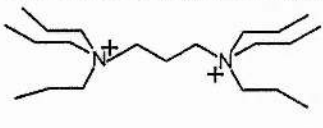
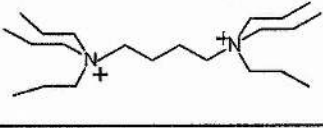
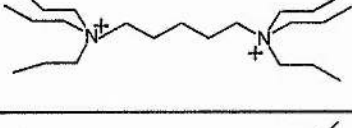
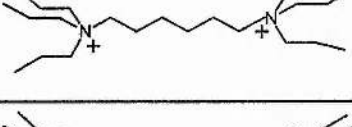
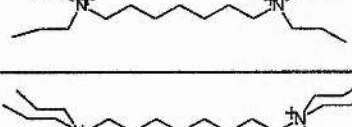
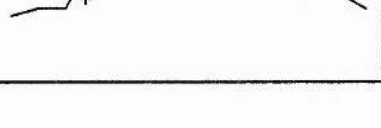
Template	Abbreviated Name	Zeolite Produced	MAPO Produced
	Tripropylamine	ZSM-5	MAPO-36
	3,3,3	ZSM-5	MAPO-5
	3,4,3	ZSM-5	MAPO-5
	3,5,3	ZSM-5	MAPO-5
	3,6,3	ZSM-5 / ZSM-12	MAPO-5
	3,7,3	_____	_____
	3,8,3	ZSM-5 / ZSM-12	MAPO-5

Table 4.5 Summary of Results for tripropylamine series. All of these products are large pore materials which is what would be expected as these are large template molecules.

The tripropylamine end groups are capable of spreading out over a comparatively large distance compared to the quinuclidine and triethylamine templates. This size increase is reflected by the synthesis of only large pore materials even at short interconnecting chain lengths. This is in sharp contrast to the quinuclidinium series which clearly differentiates between long and short chain lengths by the products they synthesise.

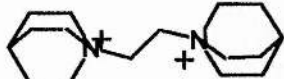
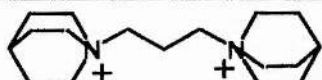
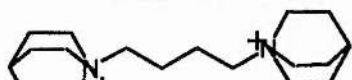
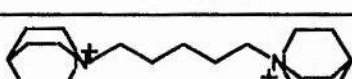
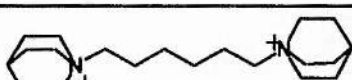
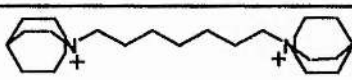
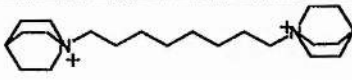
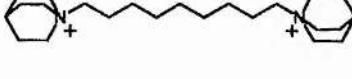
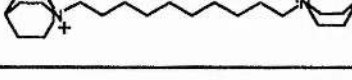
Template	Abbreviated Name	Zeolite Produced	MAPO Produced
	Quin	ZSM-5	MAPO-16
	QuinC2	—————	MAPO-5
	QuinC3	ZSM-5	MAPO-17
	QuinC4	Mordenite / ZSM-12	STA-2 / MAPO-56
	QuinC5	ZSM-5 + impurities	STA-2 / Layered phase
	QuinC6	EU-1	MAPO-36 / MAPO-5
	QuinC7	ZSM-5	MAPO-5 / STA-1
	QuinC8	—————	STA-1 / MAPO-5
	QuinC9	—————	MAPO-5 / STA-1
	QuinC10	—————	MAPO-5

Table 4.6 Summary of Results for the quinuclidine series. The synthesis of two new materials STA-1 and STA-2 has been achieved with this template series and their powder x-ray diffractograms are shown in figure 4.11.

Two new tetrahedrally coordinated aluminophosphate materials have been synthesised using these diquinuclidinium templates. STA-1<sup>[25]</sup> which forms with interconnecting chain lengths of 7, 8 or 9 methylene units was the first material identified. It is a three dimensional interconnecting channel structure having channels circumscribed by 12T-atoms. The structure was solved using single microcrystal diffraction on a crystal of the order of 30 x 30 x 30  $\mu\text{m}$  in size on beamline BM16 ID11 at the ESRF in Grenoble. Although the structure is not stable after template removal it does have the (joint) fourth lightest framework density currently known for aluminophosphates. A full description of this material and its structure solution is given in chapter five.

STA-2<sup>[26]</sup>, the second of these new materials is stable to template removal by calcination. It is formed when the length of the template is 4 or 5 methylene units long. When the chain length is 5, a second, as yet unidentified phase co-crystallises with the STA-2 phase. MAPO-56 can co-crystallise when the 4-methylene chain length is used but often the STA-2 in this case forms phase pure. The aluminosilicate analogue of MAPO-56, SSZ-16<sup>[27]</sup>, is also formed using the same templates as STA-2 but as yet no aluminosilicate analogue of STA-2 has been formed. Like STA-1, the structure of STA-2 was solved from microcrystal diffraction data collected at the ESRF in Grenoble on BM16 ID11. A full description of the structure, which has the most complicated 6-ring stacking sequence observed for these materials, is given in chapter 6.

The zeolite products synthesised using this series of templates were similar to those observed from the previous two series. The formation of mordenite which is also a large pore material for QuinC4 is different but could be attributed to the constrained template shape of these molecules over the relatively free end groups of the others.

The x-ray powder diffractograms of the aluminophosphates generated by this series is given below in figure 4.11.

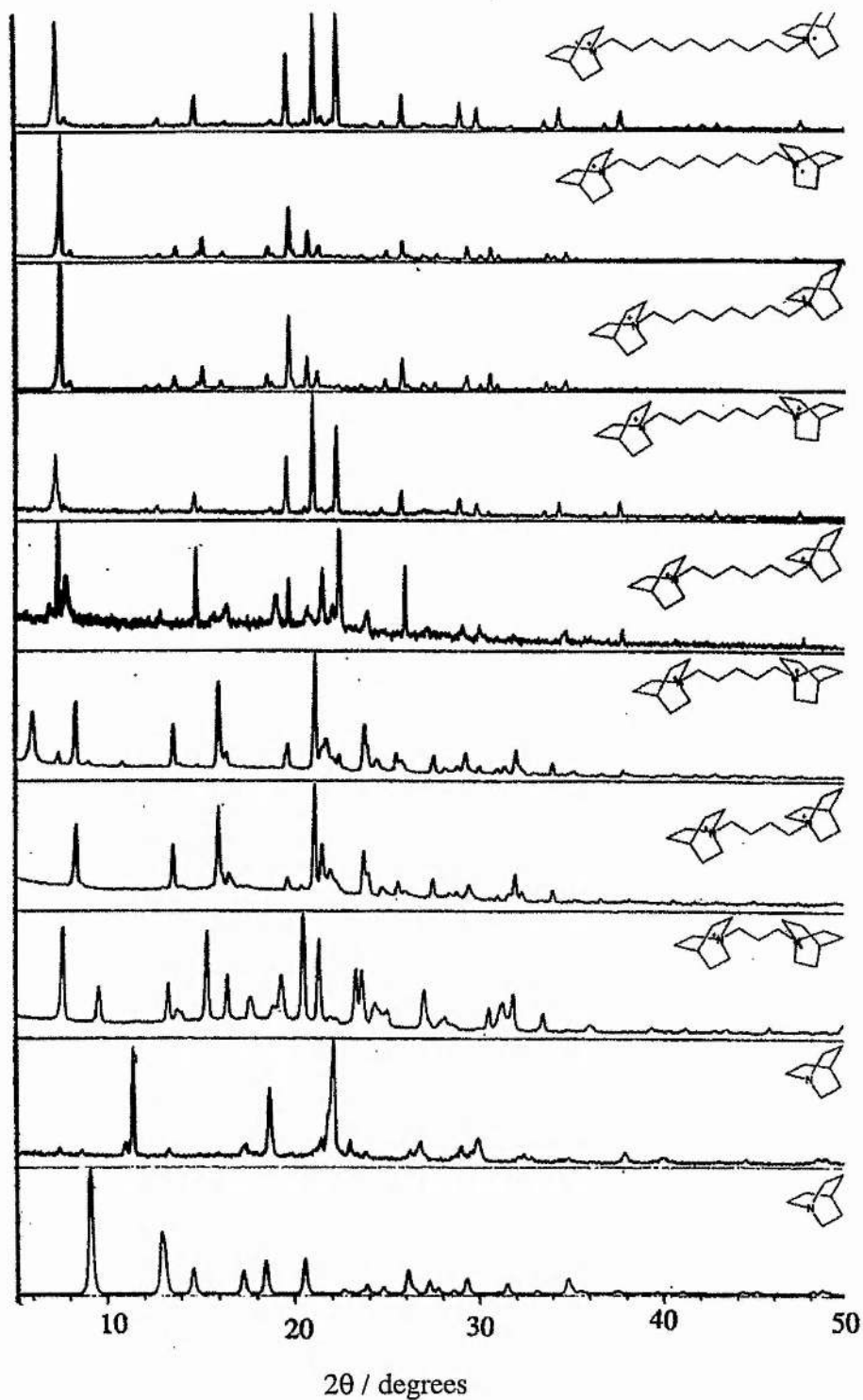


Figure 4.11 X-ray powder diffractograms of the aluminophosphates produced using the diquinuclidinium templates as indicated in the figure, the bottom pattern is of MAPO-22 as described in the literature. MAPO-5 produced using QuinC2 is omitted.

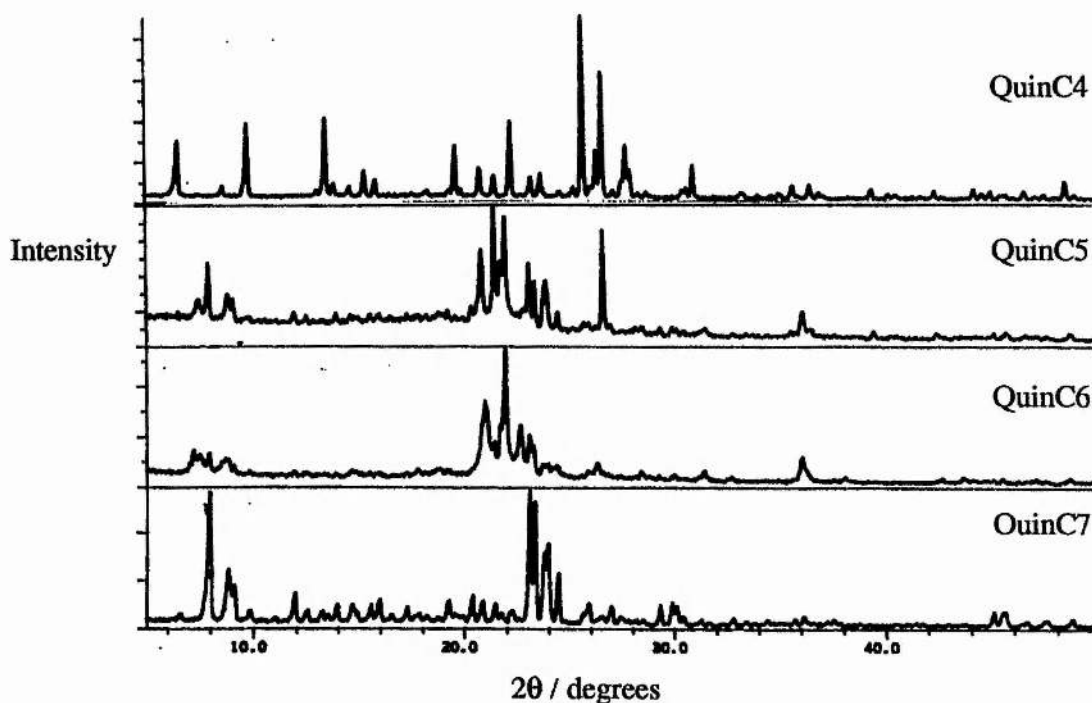


Figure 4.12 X-ray diffraction patterns of several of the zeolites produced using the diquinuclidinium templates. The templates responsible for each material is indicated in the figure. The formation of mordenite (top) by QuinC4 might be attributable to the constrained template shape of these molecules.

Many of these materials were characterised further to ensure that the template molecules were actually being incorporated into the framework structures. Carbon-13 MASNMR was able to confirm that the quinuclidinium template molecules were being encapsulated by the framework intact and the  $^{13}\text{C}$  MASNMR spectrum of the QuinC7 template is shown below for the ZSM-5 sample as shown above in figure 4.12. Evidence for the stability of the templates within the aluminophosphate materials is presented in chapters five and six. The TGA pattern obtained for the mordenite sample also shown above in figure 4.12 is shown in figure 4.14 to show the typical amount of template loading in these materials.

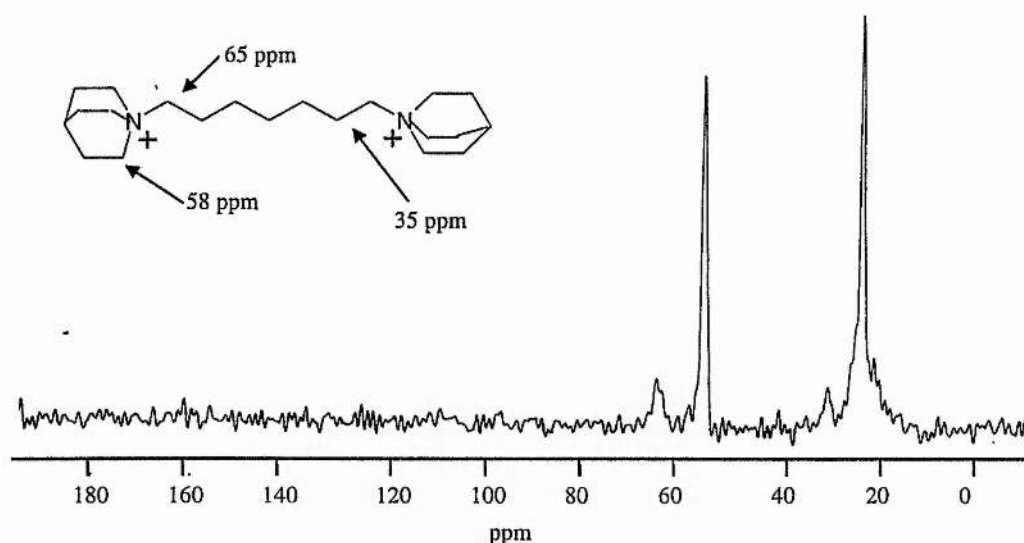


Figure 4.13  $^{13}\text{C}$  MASNMR of the QuinC7 molecule inside the ZSM-5 zeolite shown in figure 4.8. The peaks are formed by the carbon atoms indicated in the diagram with the other carbon atom resonances combining under the broad peak around 22 ppm. Peak overlap is often encountered in solid state NMR studies.

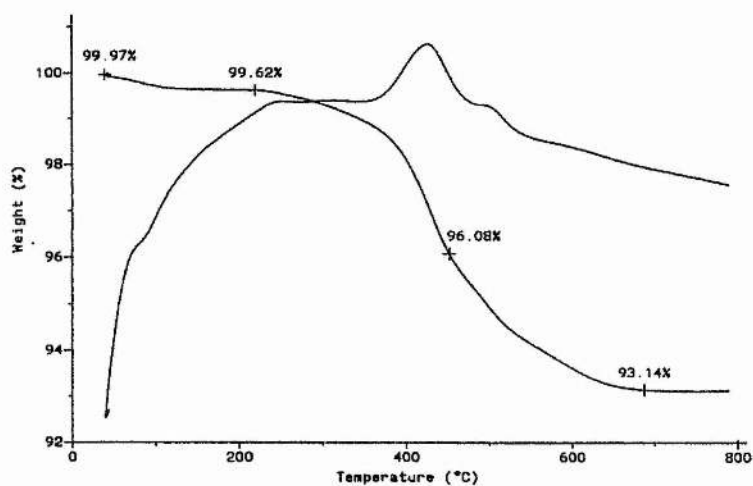


Figure 4.14 TGA/DTA patterns for mordenite produced using QuinC4. The weightloss pattern is typical for zeolites and confirms template incorporation.

In an attempt to further constrain the way in which the templates could generate microporous structures or fill channel type structures such as STA-1, polymeric equivalents of the quinuclidine series were prepared using DABCO. As stated before the effect of the increased positive charge though highly significant on its own was thought to be of secondary importance to the size and shape of the template molecules. Polymers of this kind have been synthesised by Rollman *et al*<sup>[28]</sup> and used in the synthesis of zeolites, but not aluminophosphates.

The observed results which are summarised below in table 4.7 are that the DABCO polymers with interconnecting chains of 4 or above tend to produce MAPO-31, which is a medium pore material. MAPO-5 can also form when the chain length is 4 and always when the chain length is 3 methylene units long. When the interconnecting chain length is reduced further to only 2 methylene units, another new material, STA-3 is produced.

Although MAPO-31 is the dominant material to form using these templates, only the DABCO6 templated material is very crystalline. All of the other materials show peak broadening due partly to decreased particle size and possibly due to crystallographic faulting caused by the incorporation of, "ill - fitting templates". These ideas are discussed fully in chapter seven where the use of computer modelling techniques have been used to account for the observed differences in the diffraction patterns as shown in figure 4.15.

As yet STA-3 has not been fully characterised and to date all attempts to synthesise crystals for single crystal x-ray analysis have proven unsuccessful. Similarly the x-ray powder pattern has not been indexed due to the lack of information that can be achieved from the observed peaks. Reproducing the experiment satisfactorily to produce sufficient quantities of phase pure STA-3 for MASNMR and thermal analysis has also proven to be difficult as the material tends to co-crystallise with MAPO-31 which is very difficult to separate from STA-3.

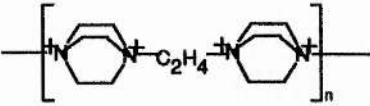
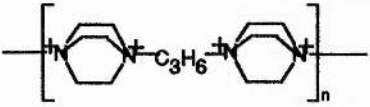
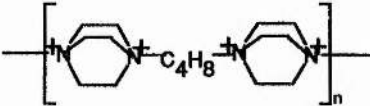
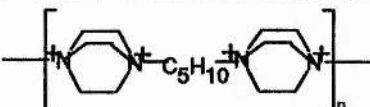
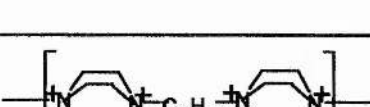
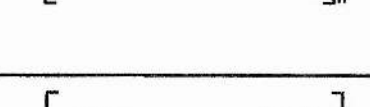
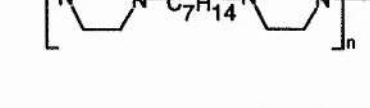
Template	Abbreviated Name	Zeolite Produced	MAPO Produced
	DABCO	ZSM-5	MAPO-5
	DABCOC2	—————	MAPO-31 / STA-3
	DABCOC3	ZSM-5	MAPO-5
	DABCOC4	ZSM-12	MAPO-31 / MAPO-5
	DABCOC5	ZSM-12	MAPO-31
	DABCOC6	ZSM-12	MAPO-31
	DABCOC7	ZSM-12	MAPO-31
	DABCOC8	ZSM-5 / ZSM-12	MAPO-31 / STA-1

Table 4.6 Summary of Results for the DABCO series. This table is slightly misleading as it does not account for the differences in crystallinity between the different MAPO-31 samples.

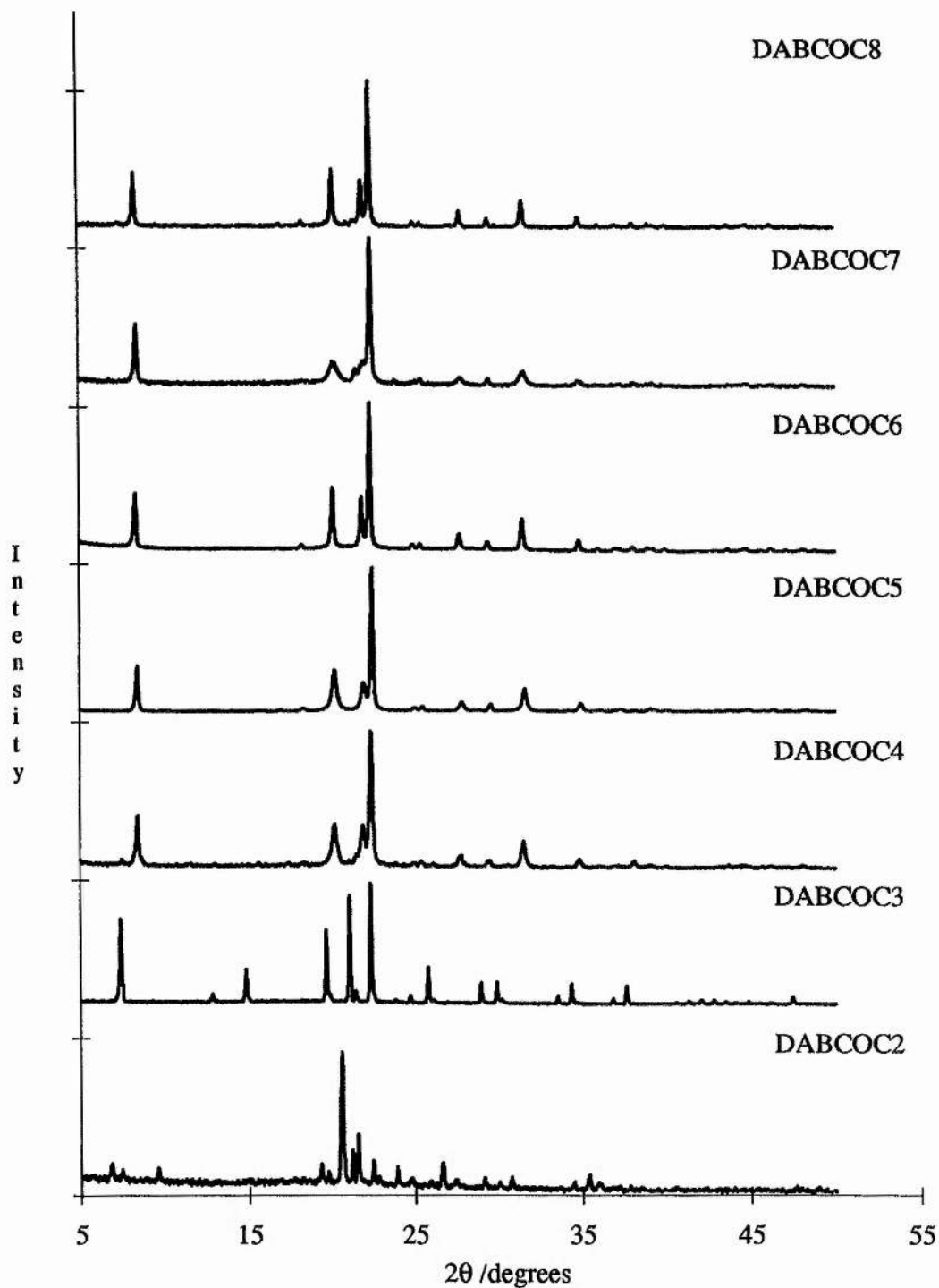


Figure 4.15 X-ray powder diffractograms showing the MAPOs produced using the DABCO polymeric templates. Notice that the DABCO6 template generates the most highly crystalline material.

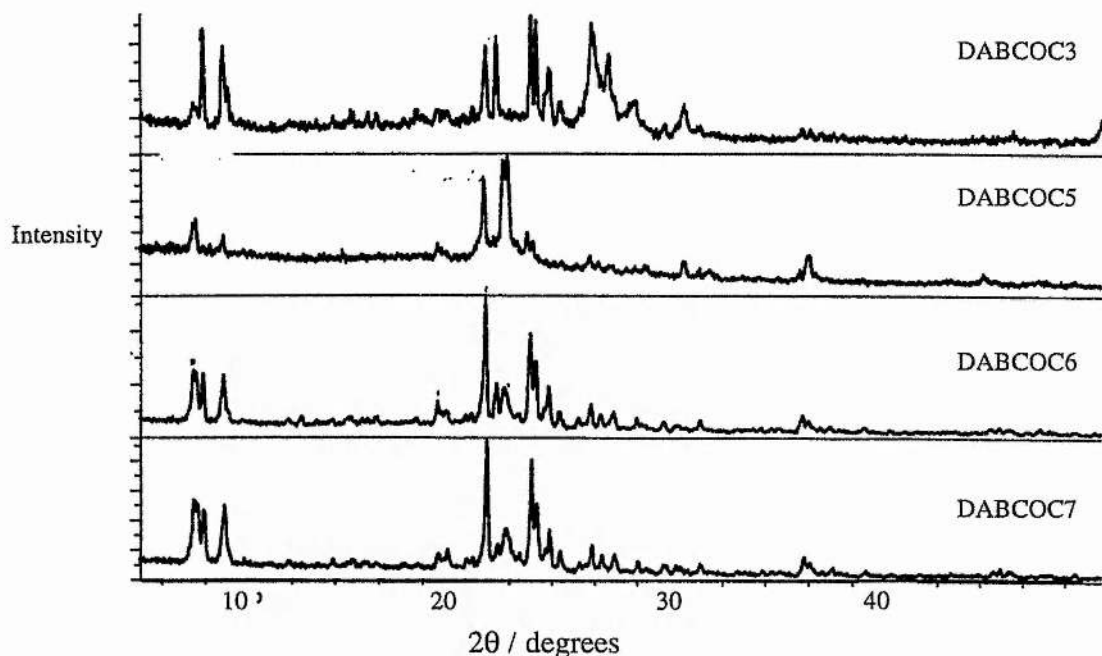


Figure 4.16 X-ray diffractograms of several of the zeolites synthesised using the templates indicated in the diagram.

The reasons why the smaller DABCOC3 template should generate the large pore MAPO-5 whilst the seemingly larger templates generate the medium pore, MAPO-31 are discussed fully in chapter seven. It is interesting to note however, that the aluminophosphates generated here are quite different to those generated using the analogous quinuclidine end-membered templates. There are two main reasons for these differences. Firstly, the DABCO templates are polymeric and as such act as the equivalent to the quinuclidinium templates aligning in a head to tail fashion. This is not necessarily the case in the synthesis gel and definitely not the case in the porous materials that the quinuclidinium templates generate e.g. MAPO-17 or MAPO-56. The enlarged polymeric DABCO templates therefore have a different way of packing in the synthesis gel and hence generate different materials, as would be predicted. The template packing argument does not account though, for the DABCO templates having the tendency to produce MAPO-31 whilst the quinuclidinium templates, MAPO-5. Again the smaller templates are generating the larger pore material, which is contrary to what would be predicted. The reason for this, the second reason why the DABCO polymers synthesise different aluminophosphates than their analogous quinuclidinium templates,

might be envisaged in terms of template mobility. A single quinuclidinium template will intuitively have a higher degree of freedom than a polymeric template. Even if the quinuclidinium template is unable to translate in the synthesis gel or in an aluminophosphate framework, it is still likely in most cases to be able to rotate. This rotation will give the quinuclidinium template an apparently larger volume than a static template of the same size. For example, consider an L-shaped molecule that can rotate around its axis the effect of spinning the molecule would produce an umbrella shaped molecule with a larger apparent volume than the L-shaped molecule if static. The polymeric DABCO templates do not have this same degree of freedom and consequently generate medium pore microporous solids.

Constraining the templates shape or size in any one direction is obviously important therefore in dictating the materials that they will generate. Having already constrained the length of the templates, it was decided to constrain the bulkiness of the templates, hopefully to generate materials other than MAPO-5. For this reason 3,5-dimethyl piperidine was chosen to be the end member of the final systematic series of templates studied. Unfortunately the synthesis of the phase pure templates proved to be more difficult, than the previous templates possibly because these are secondary as opposed to tertiary amines. The results of these synthesis are shown below in table 4.8.

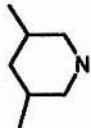
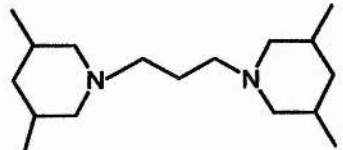
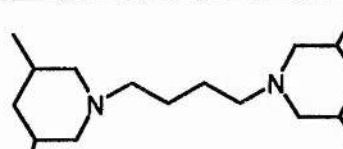
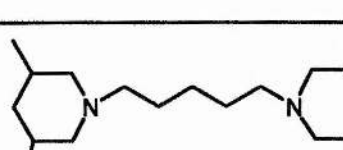
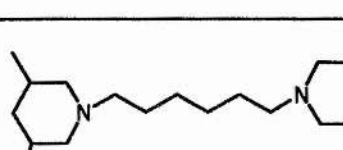
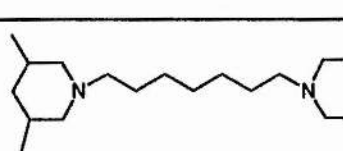
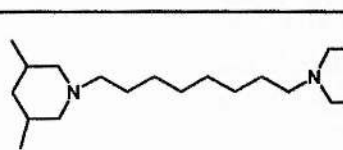
Template	Abbreviated Name	Zeolite Produced	MAPO Produced
	3,5dmp	ZSM-5 / quartz	MAPO-5 / MAPO-34
	3,5dmpC3	ZSM-12 / ZSM-5	Dense phase similar to quartz
	3,5dmpC4	ZSM-11* / ZSM-12	MAPO-5 / MAPO-34
	3,5dmpC5	ZSM-12 / ZSM-5	MAPO-31 / impurity phase
	3,5dmpC6	Amorphous	-----
	3,5dmpC7	-----	MAPO-5
	3,5dmpC8	-----	MAPO-5

Table 4.8 Summary of Results for the 3,5-dimethylpiperidine series. Increasing the size of the bulkiness of the template has generated predominantly large pore materials in both aluminophosphates and zeolite synthesis. \* ZSM-11 was observed only once.

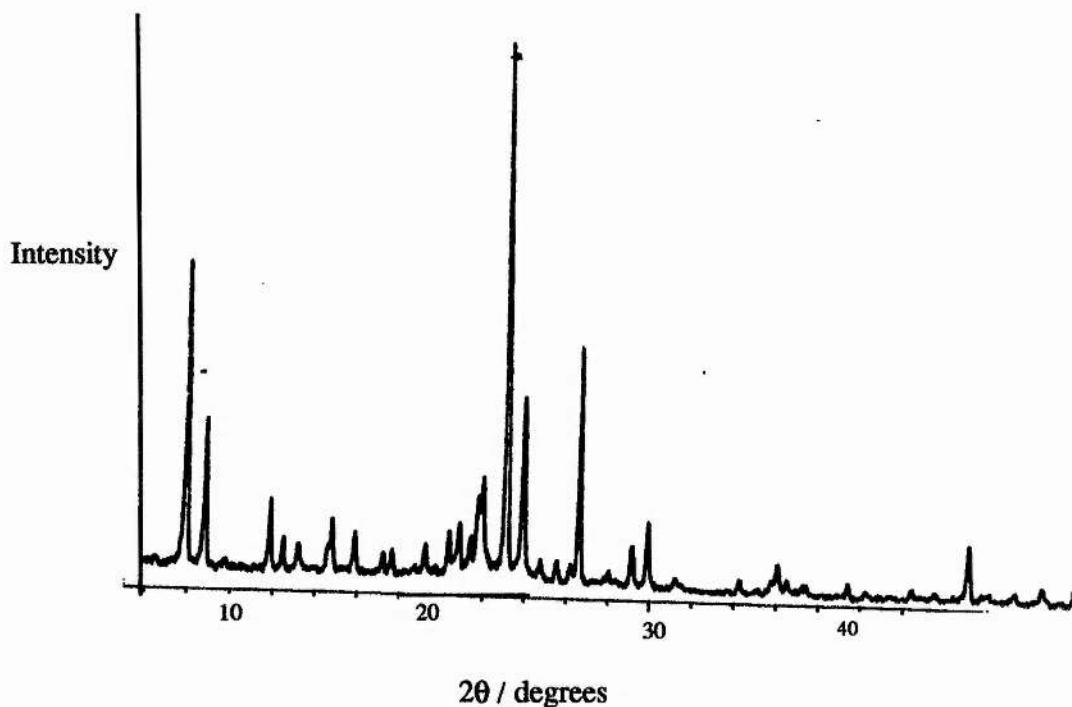


Figure 4.17 X-ray diffraction pattern of ZSM-11, produced using the 3,5-dmpC4 template as described above. This material was only formed once. The  $^{13}\text{C}$  MASNMR indicated that the template had remained intact during synthesis.

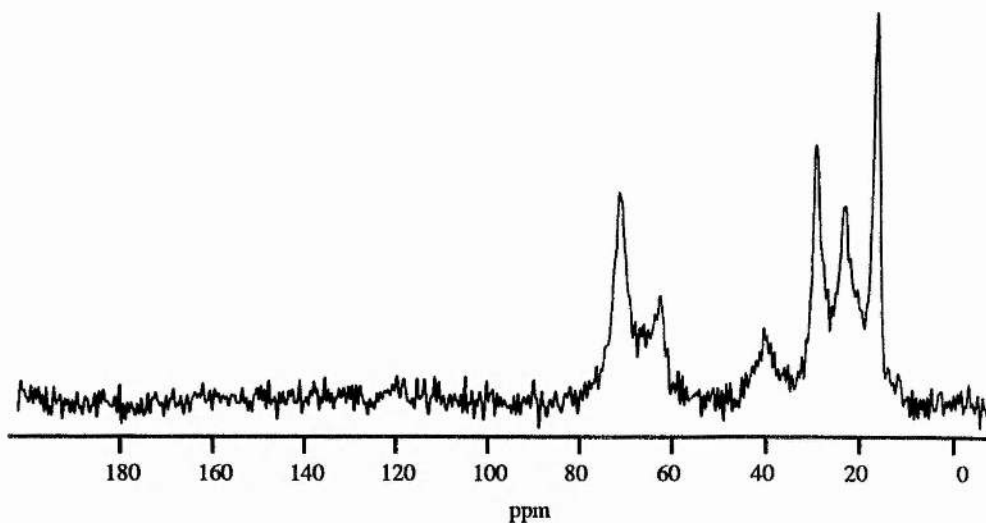


Figure 4.18 Carbon-13 MASNMR spectrum of the 3,5-dmpC4 template inside ZSM-11. The template is likely to have remained intact during this reaction but fragmented in other syntheses.

Increasing the size of the templates bulkiness has resulted in predominantly large pore materials being synthesised for both the aluminophosphate and the zeolite compositions, as was expected. However, the production of MAPO-31 and MAPO-34 in the aluminophosphate series was unexpected. As 3,5-dimethylpiperidine is known to crystallise MAPO-34 when used on its own, its synthesis here when the template (3,5dmpC4) should be significantly larger is surprising. It is possible that the template had a degree of unreacted 3,5-dimethylpiperidine associated with it or perhaps more likely a dibromobutane molecule which was only able to react at one side with the 3,5-dimethylpiperidine. All of these 3,5-dimethylpiperidine templates were difficult to synthesise and purify, so this is a probable explanation as to how MAPO-34 and similarly MAPO-31 could form. The lack of template purity could also account for the poor crystallinity observed with the zeolitic preparations.

Carbon-13 solid state MASNMR was performed on one zeolite from each series to ensure that the template was able to remain intact after crystallisation. Almost all of the spectra were as would be predicted from consideration of the appropriate solution NMR spectra, taking line broadening due to the solid state into account.

#### 4.3.7 Novel Templates

From use of the commercial and the systematically varying templates it is obvious that the size, shape and chemistry of the template, are all important in the synthesis of microporous solids. The novel templates that are described here, were all chosen to investigate one of these variables. For simplicity the results are presented so as to illustrate which property (size, shape or chemistry) is being investigated and as such are summarised in three tables (4.9 - 4.11).

Phosphorous is in the same group as nitrogen in the periodic table and is also capable of acquiring a positive charge. Subsequently with the aid of Dr. Alan Aitken of the organic chemistry department, several phosphorous based organic templates were synthesised and used as templates for the production of zeolites. The use of polymeric templates was shown to have interesting effects on the synthesis of aluminophosphates and to

further probe this area poly(diallyldimethylammonium chloride), low molecular weight, 20wt.% in water was used. Finally an inorganic complex prepared by Dr. Chris. Glidewell's group was used to investigate the change this would have on the synthesis of a zeolite. UTD-1<sup>[30]</sup>, the first 14-T atom containing zeolite was prepared using a cobalt complex and as such has generated considerable interest in the use of non-organic templates. The results obtained using these templates are summarised below in Table 4.9.

Template	Abbreviated Name	Zeolite Produced	MAPO Produced
$\left( \left( n\text{Bu}_3\text{P}^+\text{CH}_2 \right)_2 \text{C}_6\text{H}_4 \right)_2 2\text{Br}^-$	RAA1	Amorphous	_____
$\text{Ph}_3\text{P}^+\text{Pr}^-\text{I}^-$	RAA2	Amorphous	_____
$\left( n\text{Bu}_3\text{P}^+\text{CH}_2 \right)_2 2\text{Br}^-$	RAA3	ZSM-5 (using ethylene glycol)	_____
$\left( \text{H}_2\text{C} \text{---} \text{C} \text{---} \text{CH}_2 \right)_n \text{Cl}^-$	Polymer 1	Analcine	Failed to crystallise

Table 4.9 Summary of results for the novel templates chosen to change the chemistry of the template molecule.

All of the organic phosphorous compounds were difficult to dissolve in water and ethylene glycol was used to help the templates to be incorporated into the synthesis gels. Even then only one of the templates resulted in crystallising a zeolite. This would suggest that these templates may require additional variations to the gel chemistry before being used to their full potential. It was decided not to try and use these templates for the synthesis of aluminophosphates as their poor water solubility made them difficult to ion exchange to the hydroxide form necessary for aluminophosphate formation.

Analcime is very small pore material<sup>[7]</sup> and as such it is not possible that the polymeric template described above would be incorporated into the structure. Aluminophosphates attempted using this template failed to crystallise. Again ion exchange to produce the hydroxide form of the polymer was difficult and required the addition of sodium hydroxide to the synthesis gel to increase the pH to a satisfactory level. Although the addition of sodium hydroxide has had beneficial effects on the synthesis of aluminophosphates (e.g. STA-2), no crystalline product was synthesised using this polymeric template.

Overall the results obtained from radically changing the chemistry of the template molecules under investigation were disappointing and it was decided to return to more conventional templates for the remainder of the investigations. As template size was identified as being one of the most important factors in microporous solid formation large quaternary ammonium cations were synthesised. The results of these templates are listed below in table 4.10.

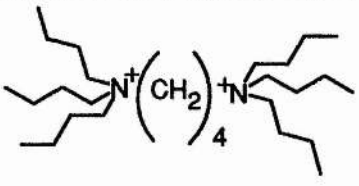
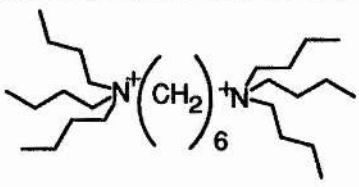
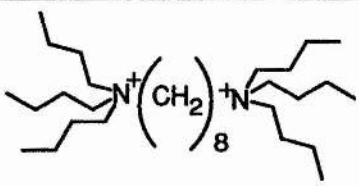
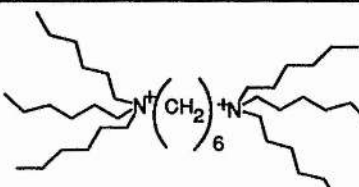
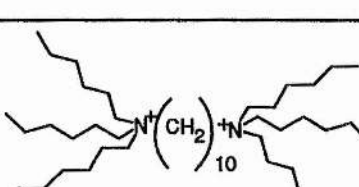
Template	Abbreviated Name	Zeolite Produced	MAPO Produced
	4,4,4	ZSM-5	MAPO-5
	4,6,4	ZSM-5	MAPO-5
	4,8,4	ZSM-5	MAPO-5
	6,6,6	ZSM-5	MAPO-5
	6,10,6	ZSM-5	MAPO-5

Table 4.10 Summary of results for the large diammonium cation templates.

All of these templates were only just water soluble and increasing their size would probably result in water insoluble organic molecules. As witnessed earlier the large tributyl - and trihexylammonium end groups like those of tripropylamine must spread over a large distance and hence synthesise only large pore materials. MAPO-5 and ZSM-5 are the only two materials observed when using such large templates. It is clear therefore, that when increasing the size of the template molecules, the size of the end

groups should be controlled so as to inhibit the automatic synthesis of either ZSM-5 or MAPO-5. That was the objective of the last set of novel templates, to increase the size of the template whilst controlling the size of the end group such as in the diquinuclidinium series described earlier. The results are summarised below in table 4.11.

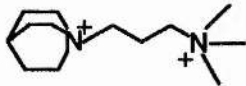
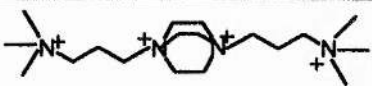
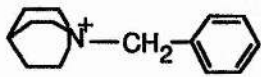
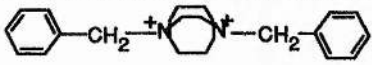
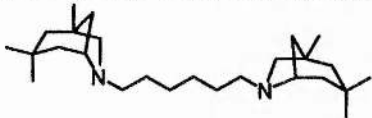
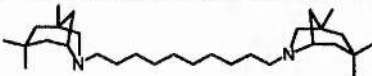
Template	Abbreviated Name	Zeolite Produced	MAPO Produced
	Quin-TMAp	ZSM-5	MAPO-17
	DABCO-TMAp	Amorphous	MAPO-34
	Quin-benzyl	ZSM-12	unidentified
	DABCO-benzyl	Amorphous	MAPO-5
	suggestions	ZSM-5	MAPO-5
	suggestions	ZSM-5	MAPO-5

Table 4.11 Summary of results for the large constrained templates. As predicted these show a wider variation of products, than the previous novel templates.

Again the constrained end groups of these templates allow them to generate more materials other than just MAPO-5, although ZSM-5 is still the only zeolitic phase formed. The last two templates, VP1 and VP2 were synthesised by Dr. Veronique Patinec.

The production of MAPO-17 by the Quin-TMAp template was expected as this is very similarly sized to the QuinC3 template which also forms the erionite structure. The production of MAPO-34 is interesting as this is a small pore type cage structure and the size of the template (DABCO-TMAp) would suggest the template to be distributed between cages intuitively preclude it from forming this material.

Computer modelling has still to be attempted to try and locate this template within the pores of MAPO-34, as has solid state MASNMR to confirm that the template has been incorporated intact.

#### 4.4.0 Conclusions

This work has shown the importance of template design on the synthesis of microporous solids particularly aluminophosphates. The aluminophosphates are susceptible to changes in the chemistry, size or shape of the templates used in their synthesis gels. There is also a close relationship between the size and shape of the template used and the structures that they can allow to crystallise from synthesis gels.

The careful use of template design used in this project has allowed the synthesis of five new materials, four of which are thought to be microporous. Two of the new materials have had their structure solved using single microcrystal diffraction at the ESRF in Grenoble.

The zeolite synthesis conditions used in this thesis are naturally orientated to the production of ZSM-5. Attempts to overcome this have not been successful. Recent advances in the production of zeolites from near neutral synthesis gels using hydrofluoric acid as a mineralising agent<sup>[20]</sup> have led to these conditions being adopted in this laboratory but at present they have not succeeded in the synthesis of new materials.

#### 4.5.0 References

- 1 R.A. Sheldon, *Current Opinion in Solid State & Materials Science*, 1996, **1**, 101
- 2 R. Raja and P. Ratnasamy, *Applied Catalysis A: General*, 1996, **143**, 145
- 3 S. Ernst, Y. Traa and U. Deeg, *Zeolites and Microporous Materials: State of the Art (1994)*, *Studies in Surface Science and Catalysis*, **84**, 925
- 4 IZA Web Site, <http://www.iza-sc.ethz.ch/IZA-SC/AtlasHome.html>
- 5 J.W. Richardson, *Naturwissenschaften*, 1989, **76**, 467
- 6 M.D. Shannon, J.L. Casci, P.A. Cox and S.J. Andrews, *Nature*, 1991, **353**, 417
- 7 W.M. Meier, D.H. Olson and Ch. Baerlocher, *Atlas of Zeolite Structure Types*, 4<sup>th</sup> Edition (revised), Elsevier, 1996
- 8 J.E. Naber, K.P. de Jong, W.H.J. Stork, H.P.C.E. Kuipers and M.F.M. Post, *Zeolites and Microporous Solids: State of the Art (1994)*, *Studies in Surface Science and Catalysis*, **84**, 2197
- 9 R. Szostak, *Handbook of Molecular Sieves*, Van Norstrand Reinhold, 1992
- 10 E.J.P. Feijen, J.A. Martens and P.A. Jacobs, *Zeolites and Microporous Materials: State of the Art (1994)*, *Studies in Surface Science and Catalysis*, **84**, 3
- 11 Alan Dyer, *An Introduction to Zeolite Molecular Sieves*, John Wiley & Sons, 1988
- 12 S.I. Zones, R.A. Van Norstrand, D.S. Santilli, D.M. Wilson, L. Yuen and L.D. Scampavia, *Zeolites: Facts, Figures, Future*, Elsevier Science Publishers, 1989, 299
- 13 R.E. Morris and S.J. Weigel, *Chemical Society Reviews*, 1997, **26(4)**, 309
- 14 J.W. Visser, *J. Appl. Cryst.*, 1969, **2**, 89
- 15 Powder Diffraction File - Inorganic Compounds, JCDPS International Centre for Diffraction Data, Philadelphia, 1984
- 16 M.M.J. Treacy, J.B. Higgins and R. von Ballmoos, *Collection of Simulated XRD Powder Patterns for Zeolites*, 3<sup>rd</sup> Edition (Revised), Elsevier, 1996

- 17 J.L. Pizarro, G. Villeneuve, P. Hagemuller and A. Le Bail, *J. Solid State Chem.*, 1991, **92**, 273
- 18 A. Kvik, M. Wulff, *Rev. Sci. Instr.*, 1992, **62**, 1073
- 19 M. Krumrey, A. Kvik, W. Schwegle, *Rev. Sci. Instr.*, 1994, **66**, 1715
- 20 M.A. Cambor, A. Corma and L.A. Villaescusa, *J. Chem. Soc. Chem. Commun.*, 1997, 749
- 21 R.E. Boyett, A.P. Stevens, M.G. Ford and P.A. Cox, *Zeolites*, 1996,
- 22 A. P. Stevens, *Ph.D. Thesis*, University of Portsmouth, 1996
- 23 Y. Nakagawa, *Studies in Surface Science and Catalysis*, 1995, **97**, 53
- 24 P.A. Wright, C. Sayag, F. Rey, D.W. Lewis, J.D. Gale, S.Natarajan and J.M. Thomas, *J. Chem. Soc., Faraday Trans.*, 1995, **91(19)**, 3537
- 25 G.W.Noble, P.A.Wright, P.Lightfoot, R.E.Morris, K.J.Hudson, Å.Kvik, H.Graafsma, *Angew. Chem. Int. Ed. Engl.*, 1997, **36**, 81
- 26 G.W. Noble, P.A. Wright and Å. Kvik, *J. Chem. Soc. Dalton Trans.*, 1997, **9**, 976
- 27 R.F. Lobo, S.I. Zones and R.C. Medrud, *Chem. Mater.*, 1996, **8**, 2409
- 28 D.H. Daniels, G.T. Kerr and L.D. Rollman, *J. Am. Chem. Soc.*, 1978, **100**, 3097
- 29 C.C. Freyhardt, M. Tsapatsis, R.F. Lobo, K.J. Balkus and M.E. Davis, *Nature*, 1996, 381, 295

## Chapter Five

### The Structure of STA-1

#### 5.1.0 Introduction

STA-1<sup>[1]</sup> was the first of the two new materials identified from the diquinuclidinium series of templates as described in chapter 4. STA-1 also became the first novel tetrahedrally coordinated microporous solid to have its structure solved by single microcrystal diffraction after *ab initio* methods based on simulated annealing using powder data proved unsuccessful. Although the structure was solved using single crystal diffraction the actual template location within the microporous framework was not located. Recent computer modelling performed in close collaboration with Dr. Paul Cox at the University of Portsmouth, however, has identified a possible location for the incorporated organic template. MASNMR and EDX has also been used to further characterise the solid.

#### 5.2.0 Experimental

STA-1 was produced by hydrothermal synthesis from near neutral gels (usually pH 6 or 7). These were prepared by the addition of aluminium hydroxide hydrate ( $\text{Al}(\text{OH})_3 \cdot x\text{H}_2\text{O}$  purchased from the Aldrich chemical company), magnesium acetate tetrahydrate, orthophosphoric acid and the C7-, C8- or C9-diquinuclidinium hydroxide to distilled water in the molar ratio of 0.9:0.1:1.0:0.4:40. The gels were heated at 190 °C for 48 hours in a stainless steel, 25ml PTFE-lined autoclave. The autoclaves were cleaned using hydrofluoric acid between successive preparations. The MAPOs were characterised using x-ray powder diffraction using a STOE STADIP automated diffractometer and analysed thermogravimetrically. The density of STA-1 was determined using a variable mixture of diiodomethane ( $3.325 \text{ gm}^{-3}$ ) and 1-bromobutane ( $1.276 \text{ gm}^{-3}$ ).  $^{31}\text{P}$ Phosphorus,  $^{27}\text{Al}$  and  $^{13}\text{C}$  MASNMR spectra were obtained using a Bruker 400 MSL spectrometer. Chemical analysis was performed by energy dispersive analysis of x-rays emitted in an electron microscope (EDX).

Single crystal diffraction data were collected on the Materials Science Beamline (ID-11, BL2) at the ESRF, Grenoble<sup>[2,3]</sup>. A crystal of approximate dimensions 30 x 30 x 30  $\mu\text{m}$  was glued to a fine glass fibre and mounted on the 3 circle fixed kappa Siemens diffractometer fitted with a Siemens SMART CCD detector and cooled to 200K. The wavelength was calibrated prior to the experiment as 0.484  $\text{\AA}$ . One thousand two hundred and fifty individual frames were collected at  $\omega$  intervals of 0.1°, with the detector covering  $8^\circ < 2\theta < 28^\circ$ , corresponding to a d-spacing range  $1.000 < d < 3.469 \text{\AA}$ . Normalisation and integration of the data were carried out using the Siemens SAINT software, giving refined lattice parameters of  $a = 13.620(4) \text{\AA}$ ,  $c = 21.649(5) \text{\AA}$  giving a cell volume and calculated density of  $4016 \text{\AA}^3$  and  $1.815 \text{gcm}^{-3}$  respectively for 411 contributing reflections. A total of 2097 reflections were processed, of which 954 were unique and 845 considered observed ( $I > 3\sigma(I)$ ).

### 5.3.0 Results and Discussion

STA-1 was first synthesised using QuinC9 (1,9-diquinuclidiniumnonane dihydroxide). Although this sample was essentially phase pure repeated synthesis attempts have only managed to produce either mixtures of STA-1 and MAPO-5 or solely MAPO-5<sup>[4,5]</sup>. Synthesis of STA-1 has now been achieved by using QuinC7, QuinC8, QuinC9, DABCOC8 (see chapter 7) and recently 1,2-diquinuclidinium ortho- benzyl hydroxide templates. MAPO-31<sup>[5,6]</sup> co-crystallises with STA-1 when the DABCOC8 polymeric template is used in the synthesis gel.

The QuinC7 template produces small microcrystals in the order of 30 x 30 x 30  $\mu\text{m}$  and consequently it was a sample produced using this template that was subsequently used in the structure determination at the ESRF. Figure 5.1 shows an example of one of these truncated square bipyramidal crystals which can easily be identified and differentiated from MAPO-5 crystals, which form as hexagonal prisms with a characteristic bar like morphology.

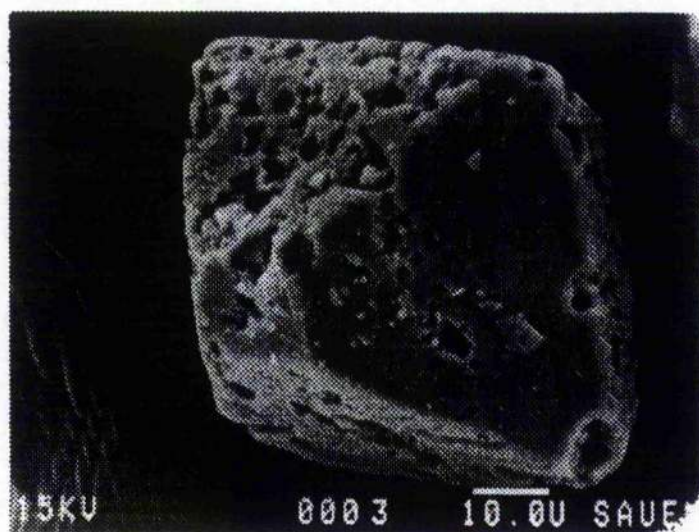


Figure 5.1 Scanning electron micrograph of STA-1 produced using the QuinC7 template. STA-1 can be easily differentiated even under optical microscopes from MAPO-5 due to its distinctive crystal morphology.

STA-1 forms as a white powder with similar morphologies when the Quin-C7, -C8 and -C9 templates are used but with very small crystallite sizes when the DABCOC8 template is used. The distinctive x-ray powder diffraction pattern of STA-1 as shown in figure 5.2 was responsible for the initial identification of STA-1 being a new microporous material since this pattern was not shown in the Collection of Simulated XRD Powder Patterns Zeolites<sup>[7]</sup>.

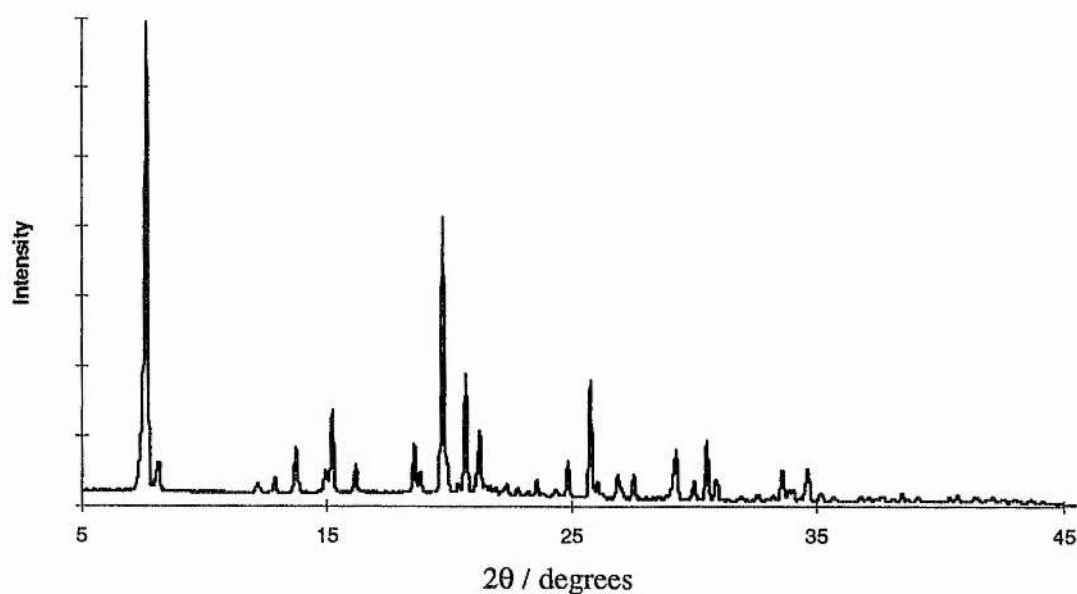


Figure 5.2 X-ray diffraction powder pattern for STA-1, shown here for the QuinC8 templated material. This pattern is unique to STA-1 and was responsible for its identification as a new material. (The above pattern was obtained from a sonicated sample.)

Indexing the above powder pattern, collected at room temperature on a STOE STADI/P powder diffractometer was achieved using VISSER<sup>[8]</sup>. This revealed STA-1 to be tetragonal with probable unit cell dimensions of:  $a = 13.810 \text{ \AA}$ ,  $c = 21.969 \text{ \AA}$ , with a symmetry close to body-centred but violated by weak reflections. Due to peak overlap at higher  $2\theta$  angles unambiguous space group identification was not possible although the choice was narrowed down to approximately ten possibilities.

Attempted syntheses of STA-1 in the purely aluminium and silicon aluminium phosphate form ( $\text{AlPO}_4$  and SAPO respectively) were unsuccessful. The reason why the  $\text{AlPO}_4$  and SAPO forms could not be synthesised is still unclear although this phenomenon is not unprecedented, DAF-1 for example<sup>[9]</sup> requires the presence of magnesium ions to crystallise and the effect of  $\text{Mg}^{2+}$  ion concentration on the synthesis of microporous solid frameworks was recently reported by Lewis *et al*<sup>[10]</sup>.

### 5.3.1 Establishing Framework Density

Phase pure STA-1 was obtained by means of a density separation utilising 1,1-diiodomethane and n-bromobutane. MAPO-5 has a density of  $2.1\text{gcm}^{-3}$  where as STA-1 was found to have a lower density of  $1.833(5)\text{gcm}^{-3}$ . Density separation was therefore possible as the two materials will float in the 1,1-diiodomethane / n-bromobutane mixture at different times as different densities are achieved. Careful monitoring of the crystal morphologies enabled the facile phase separation of STA-1 from MAPO-5. Enabling further detailed analysis on phase pure STA-1 to be obtained.

### 5.3.2 MASNMR Spectroscopy

Phase pure STA-1 was characterised by  $^{13}\text{C}$ ,  $^{27}\text{Al}$  and  $^{31}\text{P}$  MASNMR spectroscopy with the aid of Barbara Gore at UMIST using a Bruker 500MSL spectrometer. The  $^{13}\text{C}$  NMR spectrum of STA-1 shows that the QuinC8 template remains intact within the microporous solid. Although the resolution of the solid state sample is not as well defined as the spectrum obtained from solution NMR spectroscopy, there is a good agreement between the two spectra. Figure 5.3 below shows the spectra obtained for QuinC8 in the solid phase incorporated inside STA-1.

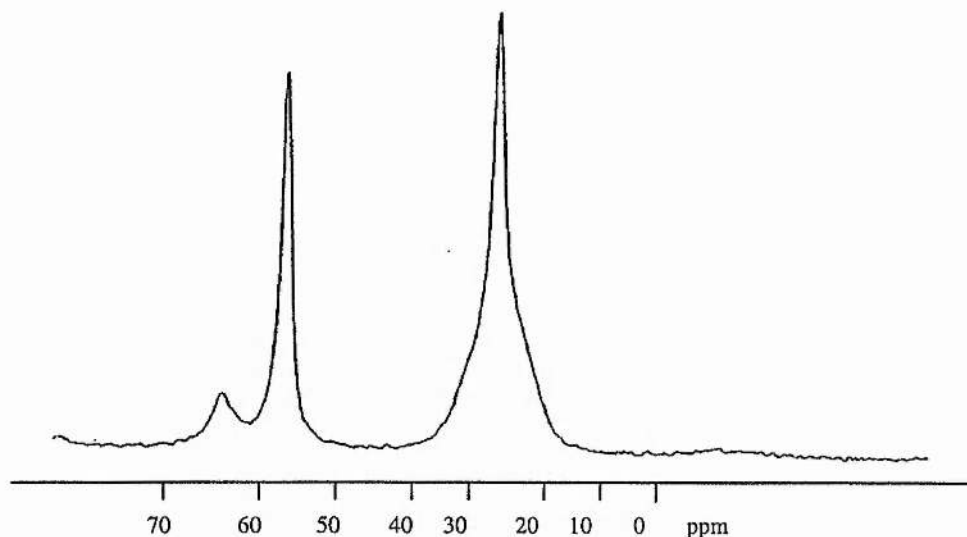


Figure 5.3  $^{13}\text{C}$  MASNMR spectrum of STA-1 solvent. The broad envelope of peaks between 10 and 30ppm (maximum at 24.5ppm) in the solid state is better resolved by solution NMR spectroscopy.

The  $^{27}\text{Al}$  and  $^{31}\text{P}$  MASNMR spectra were able to provide useful insights into the framework structure that were not obvious from x-ray powder diffraction. The single broad peak at approximately 39.3 ppm in the  $^{27}\text{Al}$  spectrum indicates that all of the aluminium atoms are tetrahedrally coordinated. This provides further proof that STA-1 is a tetrahedrally coordinated zeolitic type material as opposed to a layered type material and as such complies with one of the main requirements for Simulated Annealing. Further structural information was obtained from the  $^{31}\text{P}$  MASNMR spectrum which shows four possible peaks at  $\delta$  -27.2, -23.0, -19.3 and -15.3 ppm. This indicates that there are four distinct phosphorous environments within the crystal framework<sup>[11]</sup>. The different chemical shifts are likely to result from the different second nearest neighbour arrangements of the phosphorous. This information is not available from x-ray powder diffraction and is an example of the importance of using several techniques to fully characterise a new microporous solid.

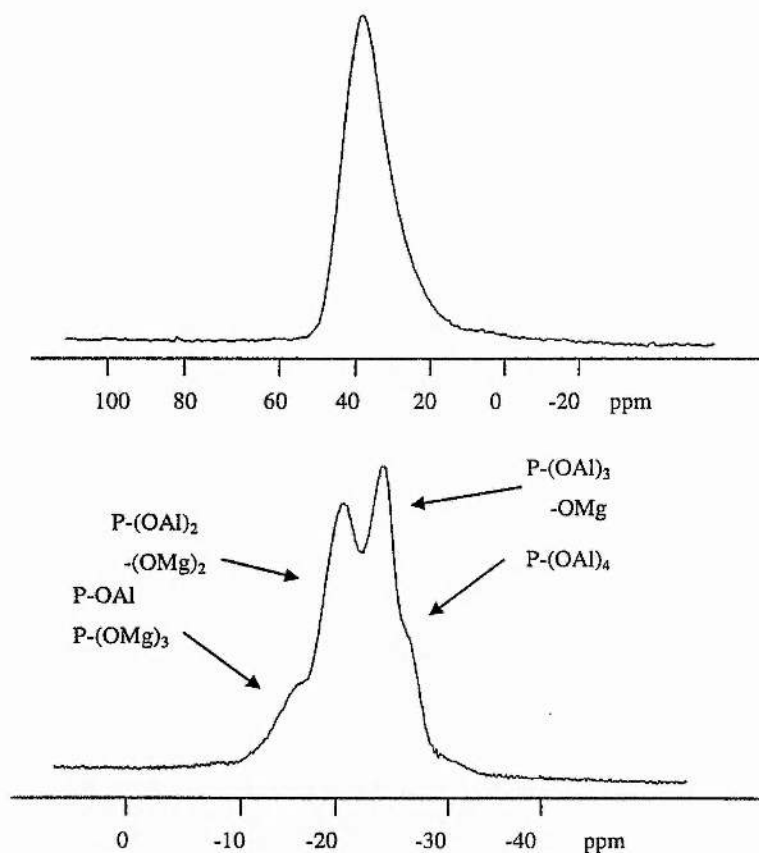


Figure 5.4 STA-1 MASNMR. (a)  $^{27}\text{Al}$  MASNMR spectrum of STA-1 showing the presence of only tetrahedral aluminium atoms, and (b)  $^{31}\text{P}$  MASNMR spectrum showing four peaks indicating four distinct phosphorous environments.

The requirements for Simulated Annealing (SA) were fully described in chapter two, but briefly the program requires that all atoms are tetrahedrally coordinated. It also requires an accurate estimate of the size of the unit cell, the total number of tetrahedral atoms, the number of crystallographically distinct T-atoms within the unit cell and the space group of the material. Once all of these parameters have been submitted the SA program can be used in an attempt to solve the crystal structure *ab initio*. Using VISSER to index x-ray powder diffraction data the size of the unit cell was known and the space group identified as being one of a possible ten systems. MASNMR spectroscopy was able to confirm that the material was tetrahedrally coordinated and as such would be suitable

for SA. The number of T-atoms in the unit cell was determined by TGA and density measurements.

### 5.3.3 Thermal Analysis

Thermal analysis was carried out at the Royal Institution, London. TGA showed that there was a 22.5 % weight loss over the range 16.7 - 600°C in flowing oxygen with a ramp rate of 10°C per minute. The pattern shows a gradual endothermic weight loss of 2.5 % up to approximately 350°C presumably due to water followed by a much sharper exothermic weight loss of 20.0 % between 400 and 500°C. This is due to the template being removed from within the framework. Unfortunately the framework is not stable once the template is removed and a massive loss of crystallinity is observed using x-ray powder diffraction. The loss of crystallinity was thought initially to be due to atmospheric water co-ordinating to the aluminium atoms in the framework creating octahedral sites rather than tetrahedral ones, leading to the collapse of the structure. However, repeated attempts to obtain a stable crystalline STA-1 sample after calcination followed by hexane absorption also proved futile. Consequently it is now thought that the lack of stability is due to the framework being supported by the incorporated template.

Density measurements on STA-1 and the TGA data as described above were used to determine the presence of 56T-atoms in the unit cell of STA-1. This is equivalent to 13.4 T atoms / 1000Å<sup>3</sup> which makes STA-1 only a little denser than that of the least dense aluminophosphate-based solids AlPO-50 (12.5 T/1000 Å<sup>3</sup>) and AlPO-37 (12.7) and less than both AlPO-46 (13.7) and VPI-5 (14.2)<sup>[12]</sup>. EDX and TGA of the sample indicate a composition Mg<sub>0.18</sub>Al<sub>0.82</sub>PO<sub>4</sub>.R<sub>0.094</sub>0.22H<sub>2</sub>O, where R represents the diquinuclidinium template.

### 5.3.4 Simulated Annealing<sup>[13]</sup>

Simulated Annealing is one possible way of circumventing the phase problem and of solving crystal structures from x-ray powder diffraction data.

SA is used to adjust an initially random arrangement of each type of atom within the unit cell so as to minimise the value of a figure of merit or energy function. The energy function is designed so as to produce solutions that are both chemically and physically feasible and concurrent with known experimental data. This process is described more fully in chapter two (section 2.3.2).

The SA program requires the chemical composition, dimensions and symmetry of the crystallographic unit cell as input. Almost all of these requirements were determined directly from experimental data. The size of the unit cell was determined from VISSER and the total number of T-atoms present in the unit cell was determined from density and TGA experiments. From NMR data it was possible to estimate the number of distinct T-atoms in the unit cell as being between 4 and 8. The space group was not unambiguously identified from the indexed powder data due to peak overlap at higher  $2\theta$  angles resulting in a loss of information on the systematic absences present. The space group was known to be tetragonal, and approximately ten space groups were identified.

The SA process can of course generate many possible zeolitic framework structures. The correct one is identified by comparison of the known and calculated diffraction patterns for each possible framework. As each framework will produce its own distinctive XRD pattern this provides a quick and easy method of identification.

Repeated attempts systematically changing the number of unique T-atoms in the unit cell from 4-8 and varying the space group still failed to produce a possible structure for STA-1. To ensure that the program was working properly, the parameters for SAPO-40<sup>[5,14]</sup> were set into the computer and the correct structure quickly identified. SAPO-40 was used as it was shown to have a unit cell ( $a = 22.045$ ,  $b = 13.699$  and  $c = 7.120\text{\AA}$ )

distinct T-atoms as opposed to SAPO-40 which has 4, was not capable of being solved using SA. STA-1 has eight crystallographically distinct T-atoms in its unit cell 4Aluminium and 4Phosphorous (but it should have been solved using 4 sites). SA was also unable to solve the known structure of ZSM-11.

Structure solution of STA-1 was not therefore achieved by *ab initio* techniques from powder diffraction data and an alternative method had to be found. Harding *et al*<sup>[16,17]</sup> recently reported the use of single microcrystal diffraction to solve the structures of known microporous solids, on crystals comparable in size to those available for STA-1.

### 5.3.5 Single Microcrystal Diffraction

Crystals of STA-1 prepared using the 1,7-diquinuclidiniumheptane template were therefore examined at the European Synchrotron Radiation Facility, Grenoble. The synchrotron ring is shown in figure 2.5. The crystal structure was solved from single crystal data collected on BL2 - ID11 which is maintained and operated by Åke Kvik and Heinz Graafsma. The help of Drs Russell Morris and Phil. Lightfoot is also gratefully acknowledged for their help in solving the crystal structure. Full details of the structure solution are given in the Experimental section of this chapter.



Figure 5.5 An ariel view of the ESRF in Grenoble, France. The synchrotron ring is clearly visible and has a circumference of 825 m.

The space group was identified as  $P\bar{4}n2$  from the systematic absences and intensity statistics. The framework structure was solved using SIR92 and refined using the teXsan suite<sup>[18]</sup> to final agreement factors  $R=0.059$ ,  $R_w = 0.076$ . The positions of the template molecules could not be determined from the single crystal data, presumably due to their disorder, and the simulated powder pattern calculated over the same d-spacing range as measured in the single crystal pattern closely matched that observed over the same range, although the intensities of reflections with higher d-spacings were very different, due to the presence of extra-framework scattering.

The atomic coordinates of STA-1 along with additional crystallographic information describing the intramolecular bond lengths and angles are given in tables 5.1 - 5.3 respectively.

Atom	x	y	z	B(eq)
P(1)	0.3905(2)	0.1197(2)	0.1332(1)	1.60(7)
P(2)	0.1100(2)	0.1207(2)	0.1892(1)	1.69(7)
P(3)	0.2094(2)	-0.1143(2)	0.0563(1)	1.70(7)
P(4)	0.2953(2)	0.7953	0.2500	1.73(5)
Al(1)	0.2022(3)	0.1119(3)	0.0597(1)	1.76(8)
Al(2)	0.1156(2)	-0.1114(3)	0.1885(1)	1.85(8)
Al(3)	0.3900(3)	-0.1082(3)	0.1346(1)	1.96(8)
Al(4)	0.2950(2)	0.2050	0.2500	1.57(5)
O(1)	0.3220(6)	0.1410(7)	0.0821(3)	3.0(2)
O(2)	0.3706(6)	0.1832(7)	0.1872(4)	3.3(2)
O(3)	0.3763(6)	0.0132(5)	0.1538(4)	2.4(2)
O(4)	0.4928(5)	0.1360(7)	0.1110(4)	2.5(2)
O(5)	0.1959(8)	-0.0099(5)	0.0369(4)	3.7(2)
O(6)	0.1260(6)	0.1403(6)	0.1220(3)	2.6(2)
O(7)	0.1812(6)	0.1848(6)	-0.0039(3)	3.1(2)
O(8)	0.1737(6)	0.1878(6)	0.2267(3)	2.5(2)
O(9)	0.1332(6)	0.0152(5)	0.2036(4)	2.5(2)
O(10)	0.3141(6)	-0.1304(7)	0.0715(4)	3.8(2)
O(11)	0.1439(6)	-0.1372(6)	0.1105(3)	2.9(2)
O(12)	0.0057(4)	0.1434(7)	0.2061(4)	2.5(2)
O(13)	0.1906(5)	-0.1879(7)	0.2353(3)	2.8(2)
O(14)	0.3577(6)	-0.1789(7)	0.1965(4)	4.0(2)

Table 5.1 The atomic coordinates of STA-1. Standard deviations are shown in brackets and the B(eq) value represents the isotropic temperature factor.

Atom - Atom	Distance (Å)	Atom - Atom	Distance (Å)
P(1) - O(1)	1.477(8)	Al(1) - O(1)	1.747(8)
P(1) - O(2)	1.478(8)	Al(1) - O(5)	1.731(7)
P(1) - O(3)	1.529(8)	Al(1) - O(6)	1.744(8)
P(1) - O(4)	1.490(7)	Al(1) - O(7)	1.721(7)
P(2) - O(6)	1.496(7)	Al(2) - O(9)	1.770(8)
P(2) - O(8)	1.497(7)	Al(2) - O(11)	1.767(8)
P(2) - O(9)	1.502(8)	Al(2) - O(12)	1.750(7)
P(2) - O(12)	1.499(7)	Al(2) - O(13)	1.775(8)
P(3) - O(5)	1.492(8)	Al(3) - O(3)	1.713(8)
P(3) - O(7)	1.494(7)	Al(3) - O(4)	1.717(7)
P(3) - O(10)	1.479(9)	Al(3) - O(10)	1.739(9)
P(3) - O(11)	1.506(8)	Al(3) - O(14)	1.708(8)
P(4) - O(13)	1.478(8)	Al(4) - O(2)	1.732(8)
P(4) - O(13)	1.478(8)	Al(4) - O(2)	1.732(8)
P(4) - O(14)	1.478(8)	Al(4) - O(8)	1.742(8)

Table 5.2 Intermolecular bond distances involving the non-hydrogen atoms. Estimated standard deviations in the least significant figure are given in parentheses.

Atoms	Angle (°)	Atoms	Angle(°)
O(1) - P(1) - O(2)	111.2(5)	O(1) - Al(1) - O(7)	104.2(4)
O(1) - P(1) - O(3)	109.0(5)	O(5) - Al(1) - O(6)	113.8(5)
O(1) - P(1) - O(4)	108.5(5)	O(5) - Al(1) - O(7)	108.4(4)
O(2) - P(1) - O(3)	107.6(5)	O(6) - Al(1) - O(7)	113.1(4)
O(2) - P(1) - O(4)	109.8(5)	O(9) - Al(2) - O(11)	109.9(4)
O(3) - P(1) - O(4)	110.7(5)	O(9) - Al(2) - O(12)	109.2(4)
O(6) - P(2) - O(8)	109.5(5)	O(9) - Al(2) - O(13)	112.8(4)
O(6) - P(2) - O(9)	110.0(5)	O(11) - Al(2) - O(12)	111.4(4)
O(6) - P(2) - O(12)	109.7(5)	O(11) - Al(2) - O(13)	107.7(4)
O(8) - P(2) - O(9)	110.5(5)	O(12) - Al(2) - O(13)	105.8(4)
O(8) - P(2) - O(12)	106.9(5)	O(3) - Al(3) - O(4)	112.7(5)
O(9) - P(2) - O(12)	110.2(5)	O(3) - Al(3) - O(10)	107.1(5)
O(5) - P(3) - O(7)	109.8(5)	O(3) - Al(3) - O(14)	109.0(5)
O(5) - P(3) - O(10)	108.8(6)	O(4) - Al(3) - O(10)	106.2(4)
O(5) - P(3) - O(11)	110.1(5)	O(4) - Al(3) - O(14)	110.4(5)
O(7) - P(3) - O(10)	107.1(5)	O(10) - Al(3) - O(14)	111.5(4)
O(7) - P(3) - O(11)	109.5(4)	O(2) - Al(4) - O(2)	114.4(6)
O(10) - P(3) - O(11)	111.5(5)	O(2) - Al(4) - O(8)	108.2(3)
O(13) - P(4) - O(13)	110.2(7)	O(2) - Al(4) - O(8)	108.0(4)
O(13) - P(4) - O(14)	110.4(4)	O(2) - Al(4) - O(8)	108.0(4)
O(13) - P(4) - O(14)	108.0(5)	O(2) - Al(4) - O(8)	108.2(3)
O(13) - P(4) - O(14)	108.0(5)	O(8) - Al(4) - O(8)	109.9(6)
O(13) - P(4) - O(14)	110.4(4)	P(1) - O(1) - Al(1)	138.8(5)
O(14) - P(4) - O(14)	109.9(8)	P(1) - O(2) - Al(4)	146.1(6)
O(1) - Al(1) - O(5)	110.0(5)	P(1) - O(3) - Al(3)	146.1(6)
O(1) - Al(1) - O(6)	106.9(4)	P(1) - O(4) - Al(3)	137.6(6)

Table 5.3 Intramolecular bond angles involving the non-hydrogen atoms.

Although the asymmetric unit of STA-1 consists of two 4-membered rings joined together by three vertices, with the other two remaining unjoined (Figure 5.6a), the framework may best be thought of as being made up of two different kinds of structural building units (Figure 5.6b and 5.6c), each possessing  $\bar{4}$  m symmetry, which are linked through a shared face, or four membered ring, as illustrated in figure 5.6d. The units depicted in Figure 5.6b may also be viewed as being obtained by the fusing together via shared edges of four sub-units containing 4-rings and 6-rings (Fig.5.6e) of the type that occur in chains in the recently observed aluminophosphate-based solids SAPO-40<sup>[14]</sup> and UiO-7<sup>[18]</sup>. The building units are arranged in a body-centred array, and it is the strict alternation of aluminium (and magnesium) with phosphorus in the tetrahedral cation sites that lowers the symmetry to primitive. The structure consists of large pore channels, bounded by 12-membered rings, that run parallel to both [100] and [010], but offset in z. A projection along [100] is shown in Figure 5.7. These channel systems are linked in the z-direction forming large cavities, so that connectivity is three dimensional, although the channel pathway in this direction is not straight.

GSAS has been used to perform a Rietveld analysis on the powder data obtained at room temperature on a STOE STADI/P laboratory diffractometer using the atomic coordinates obtained from the single crystal analysis and reasonable agreement was achieved. This process confirms that the single crystal solved at Grenoble was truly representative of the powder samples normally obtained for STA-1. The Rietveld refinement was carried out over the same data range as that used in the single crystal data analysis. Because the template molecules were not located (because of disorder) perfect agreement was not achieved. The fit was particularly poor at lower angles because the disordered template would have more effect on the diffractometer intensities here. The full x-ray powder pattern could not be refined as the atomic coordinates of the template molecules were not known.

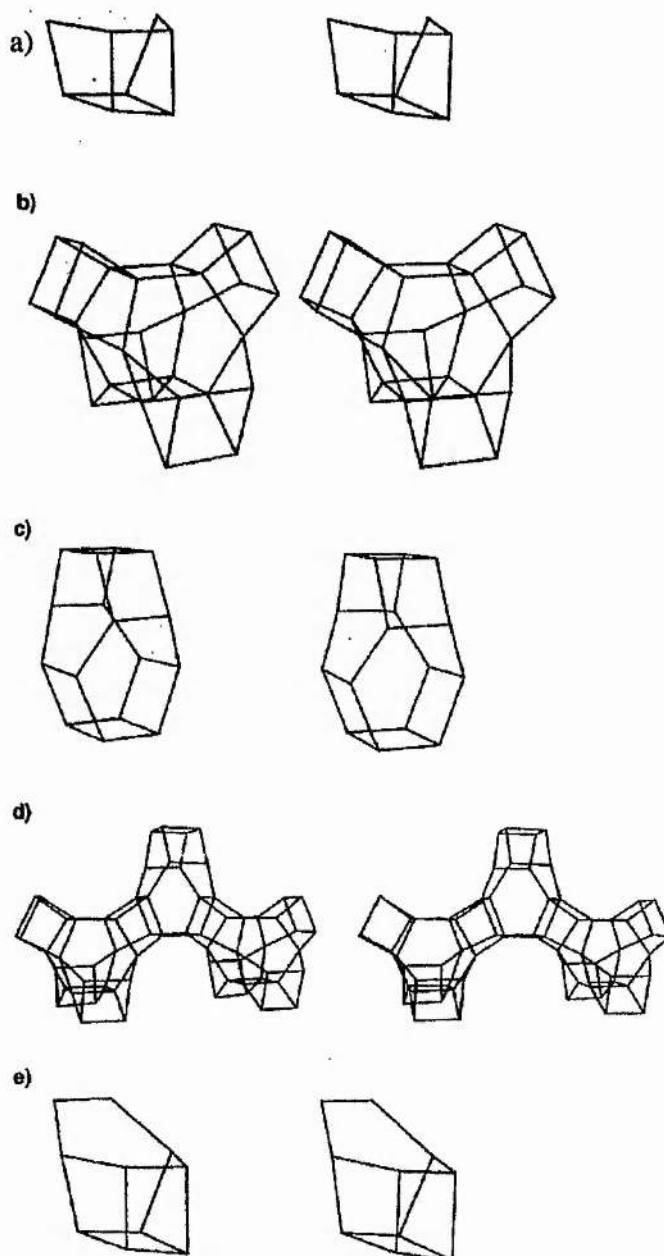


figure 5.6 Stereopairs of (a) the asymmetric unit and (b) and (c) the secondary building units within the STA-1 structure. The linkage of two units of type (b) to one of type (c) is indicated in (d), although in the structure four units would be joined via shared 4-rings to each of (b) and (c). The building unit (b) may also be thought of as being made up of four sub-units of type (e) fused together. For simplicity the oxygen atoms are omitted.

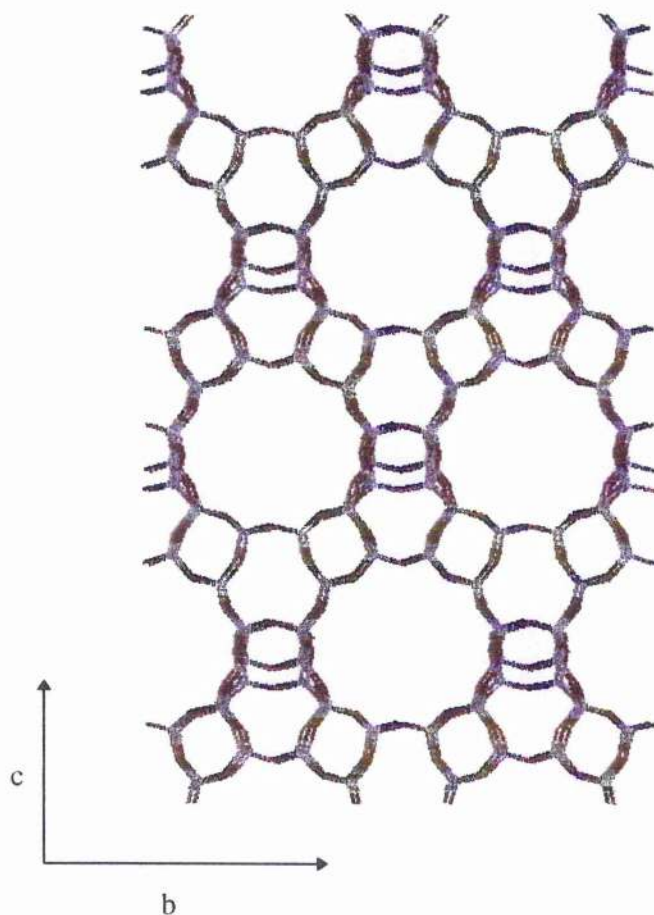


Figure 5.7 A projection of STA-1 along the  $[100]$  plane showing the 12 T-atom channel openings.

### 5.3.6 Template Docking into STA-1

Single crystal analysis although capable of solving the framework structure was not able to locate the location of the template molecules within the channels of STA-1, presumably due to molecular disorder.

Computational methods were therefore used to locate the possible location of the diquinuclidinium templates in the absence of available experimental techniques. Computer docking was performed using Biosym / MSI InsightII software utilising the docking program within the Catalysis Module. The program methodology was described briefly in chapter two, section 2.3.3, and is based on the CVFF potentials.

Both the QuinC8 template molecule and the STA-1 framework were created individually before the docking procedure was performed and at no time was the location of the template assumed. After an initial Monte Carlo energy minimisation of the template to generate the most likely molecular orientations, the template was refined using a simulated annealing approach. The QuinC8 template molecule was chosen despite the QuinC7 templated framework being the one solved because of a comparative study performed by Dr. Paul Cox using the DABCOC8 polymeric template (see chapter seven). Figure 5.8 shows a possible location of the QuinC8 template inside STA-1 as determined by computer docking calculations.

Ten possible docking positions were identified and further refined. The lowest energy template - host conformation was accepted as being the most likely one (figure 5.8). This showed the template to lie along the channels with the quinuclidinium end members in the channel intersections. This template position is also adopted by the DABCOC8 polymer as described more fully in chapter seven. Attempts to locate the position of the 1,2-diquinuclidinium ortho-benzyl template within the STA-1 framework have revealed interesting comparisons to the QuinC8 and DABCOC8 templates.

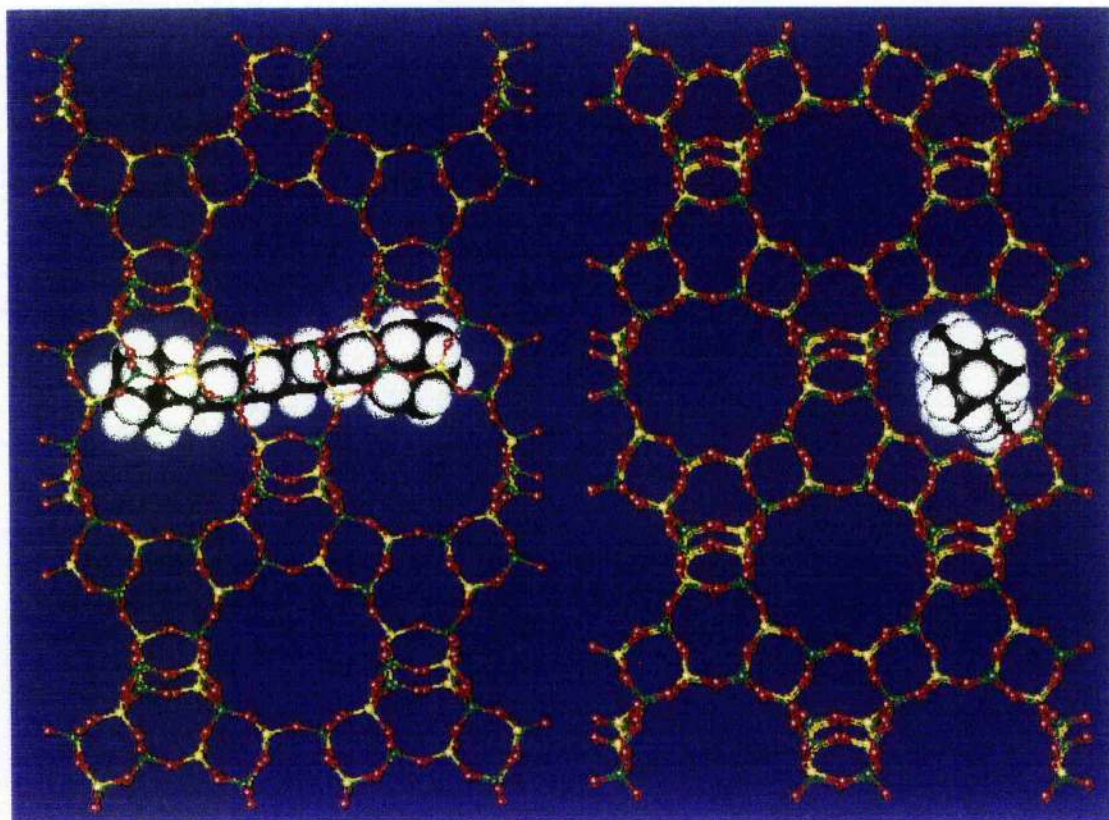


Figure 5.8 Template docking in STA-1. The QuinC8 molecule shown above is positioned such that the large quinuclidinium end groups lie between the framework intersections. The above diagram shows the framework along the [100] and [101] direction, for clarity.

The 1,2-diquinuclidinium ortho-benzyl template was also positioned at the channel intersections. Because this template is not long enough to stretch across two adjacent channel intersections like the QuinC8 template for example, there is a slight rotation in the *c*-direction such that the benzyl group is located centrally in the channel intersection and the quinuclidinium units fill the channels. This is the opposite situation to the more linearly shaped QuinC8 and DABCOC8 template molecules.

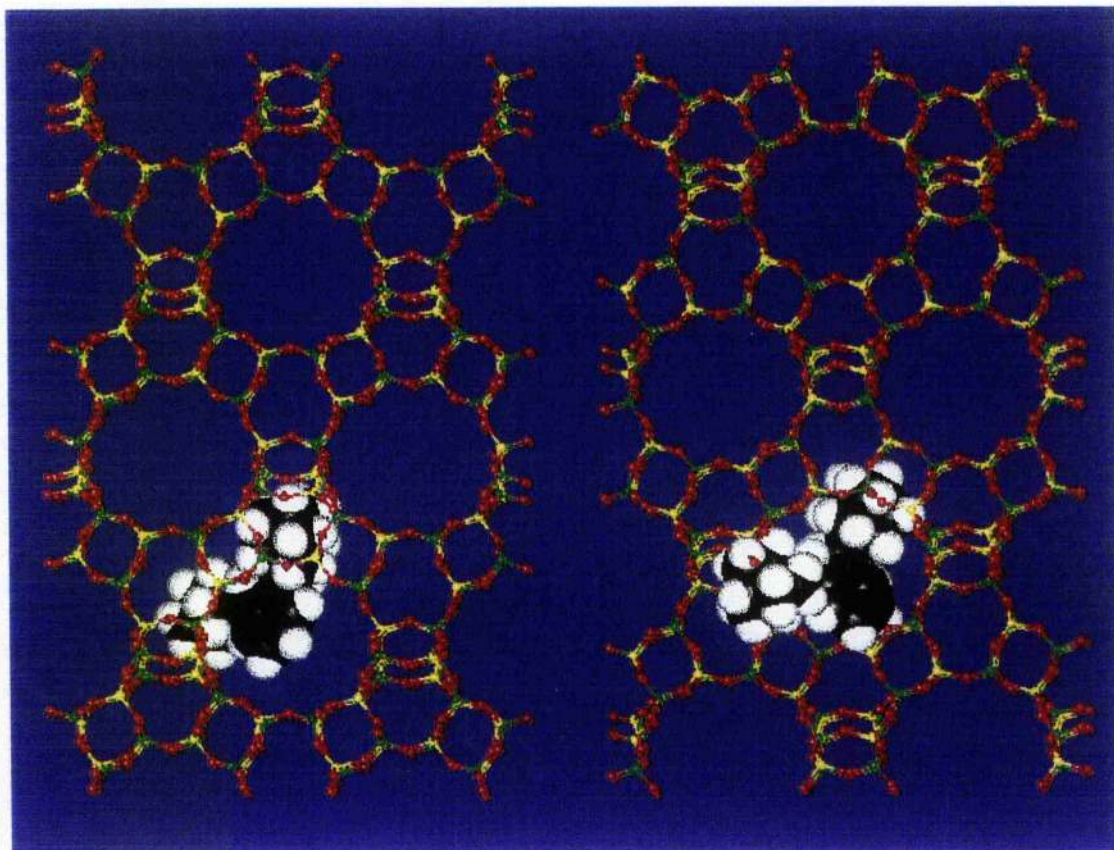


Figure 5.9 Template position of the 1,2-diquinuclidinium ortho-benzyl template within STA-1, again view along the [100] and the [010] directions. The template is again positioned along the interconnecting channels.

#### 5.4.0 Conclusions

The synthesis and structure solution of STA-1 underlines both the potential of rational template design for the preparation of novel microporous solids and also the power of modern synchrotron crystallographic facilities. The clear cut dependence of the crystallisation field of STA-1 on the length of the methylene chain linking the diquinuclidinium end groups suggests the template is able to find a very specific and energetically favourable site next to the framework. The exact location of the template molecule however, has still to be determined as this was not identified by the single crystal experiments or by computer modelling.

Computer modelling suggests several energetically similar template locations within STA-1 and in reality all of these may be adopted. If the template adopted more than one orientation the molecular disorder would lead to very little long range order and as such the template location would not be solvable by x-ray diffraction. This may explain why the template position was not found within the microporous framework even with the single microcrystal analysis, whilst other more ordered templates have been<sup>[19-21]</sup>.

This approach, by which a "supramolecular" template of desired shape can be built up by the reaction of readily available compounds, should be of wide applicability for the synthesis of microporous solids. The structure solution of STA-1 is, to our knowledge, the first of a completely novel tetrahedrally coordinated framework using microcrystal diffraction at a synchrotron source, although successful structure solution of families of structures closely related to those already solved by other methods has previously been achieved. King *et al*<sup>[22]</sup> solved the first microporous solid,  $\text{NH}_4[\text{Mo}_2\text{P}_2\text{O}_{10}]\cdot\text{H}_2\text{O}$  which has a void volume of approximately 12% as determined by water absorption isotherms. The structure which is isostructural with the natural mineral Leucophosphate,  $\text{K}[\text{Fe}_2(\text{OH})(\text{H}_2\text{O})(\text{PO}_4)_2]\cdot\text{H}_2\text{O}$ , has both octahedral and tetrahedrally coordinated anions. Prior to this structure the only structure solved using microcrystal diffraction at a synchrotron source was Eu-19<sup>[23]</sup> by Andrews and his co-workers in 1988. Since then, the power of this technique is such that microporous solids prepared only as crystals much smaller than those of STA-1 can readily be studied<sup>[24]</sup>.

### 5.5.0 References

1. G.W.Noble, P.A.Wright, P.Lightfoot, R.E.Morris, K.J.Hudson, Å.Kvick, H.Graafsma, *Angew. Chem. Int. Ed. Engl.*, 1997, **36**, 81.
2. A. Kvick, M. Wulff, *Rev. Sci. Instr.*, 1992, **62**, 1073
3. M. Krumrey, A. Kvick, W. Schwegle, *Rev. Sci. Instr.*, 1994, **66**, 1715
4. S.Qiu, W. Pang, H. Kessler and J.L. Guth, *Zeolites*, 1989, **9**, 440
5. W.M.Meier, D.H.Olson and Ch.Baerlocher, *Atlas of Zeolite Structure Types*, 4th Edtn (Revised), Elsevier, 1996
6. W.H. Baur, W. Joswig, D. Kassner, J. Kornatowski and G. Finger, *Acta. Cryst.*, 1994, **B50**, 290
7. M.M.J. Treacy, J.B. Higgins and R. von Ballmoos, *Collection of Simulated XRD Powder Patterns for Zeolites*, 3<sup>rd</sup> Edition (Revised), Elsevier, 1996
8. J.W. Visser, *J. Appl. Cryst.*, 1969, **2**, 89
9. P.A.Wright, C.Sayag, F.Rey, D.W.Lewis, J.D.Gale, S.Natarajan and J.M.Thomas, *J. Chem. Soc. Faraday Trans.* 1995, **91**, 3537
10. D.W. Lewis, C.R.A. Catlow and J.M. Thomas, *Chem. Mater.*, 1996, **8**, 1112
11. D.B. Akolekar and R.F. Howe, *J. Chem. Soc., Faraday Trans.*, 1997, **93**(17), 3263
12. M.E. Davis, C. Saldarriaga, C. Montes, J. Garces, C. Cowder, *Nature*, 1988, **331**, 698
13. Biosym Inc., Insight II, Version 2.0.0, *User Manual*, 1993
14. M. Estermann, L.B. McCusker and C. Baerlocher, *J. Appl. Cryst.*, 1992, **25**, 539
15. J.L. Schlenker, W.J. Rohrbaugh, P. Chu, E.W. Valyocsick and G.T. Kokotailo, *Zeolites*, 1985, **5**, 355
16. M. Helliwell, V. Kaucia, G.M.T. Cheetham, M.M. Harding, B.M. Kariuki and P.J. Rizhallah, *Acta Cryst.*, 1993, **49**, 413
17. G.M.T. Cheetham and M.M. Harding, *Zeolites*, 1996, **16**, 245
18. teXsan Single Crystal Analysis Software, version 1.6, 1993. Molecular Structure Corporation, The Woodlands, TX, USA, 77381
19. G. Sankar, J.K. Wyles, R.H. Jones, J.M. Thomas, C.R.A. Catlow, D.W. Lewis, W. Clegg, S.J. Coles and S.J. Teat, *Chem. Commun.*, 1998, 117

20. M.A. Cambor, A. Corma, P. Lightfoot, L.A. Villaescusa and P.A. Wright, *Angew. Chem. Int. Ed. Engl.*, 1997, **36(23)**, 2659
21. G.W. Noble, P.A. Wright and Å. Kvik, *J. Chem. Soc. Dalton Trans.*, 1997, **9**, 976
22. H.E. King, L.A. Mundi, K.G. Stronmaier and R.C. Haushalter, *J. Solid. State Chem.*, 1991, **92(1)**, 154
23. S.A. Andrews, M.Z. Papiz, R. McMeeking, A.J. Blake, B.M. Lowe, K.R. Franklin, J.R. Helliwell and M.M. Harding, *Acta Cryst. Section B*, 1988, **B44**, 73
24. M.J. Gray, J.D. Jasper, A.P. Wilkinson and J.C. Hanson, *Chem. Mater*, 1997, **9**, 976
25. A.P. Stevens, *Ph.D. Thesis*, The University of Portsmouth, 1996

## Chapter Six

### The Structural Chemistry of STA-2

#### 6.1.0 Abstract

The second new aluminium phosphate phase to be discovered using the diquinuclidinium templates described in chapter four has since been called STA-2 (St. Andrews-2)<sup>[1]</sup> and has been assigned the three lettered code SAT by the Zeolite Structure Commission. This material was synthesised from synthesis gels very similar to those of STA-1 but using the shorter quinC4 and quinC5 molecules as distinct to the quinC7 - C9 ones used for the synthesis of STA-1.

Unlike STA-1, STA-2 (SAT) is a stable porous material which retains its structure after template removal by calcination and shows potential as a heterogeneous catalyst. STA-2 has also been synthesised from a variety of compositions including the MAPO, pure AlPO<sub>4</sub>, SAPO and CoAlPO form, all of which may possess their own unique catalytic potentials. The structure was solved using single microcrystal x-ray diffraction at Grenoble with the help of Prof. Å. Kvick. The location of the template within the framework was determined directly from the diffraction data obtained and also from computer modelling.

#### 6.2.0 Experimental

Both the QuinC4 and the QuinC5 diquinuclidinium templates synthesised STA-2, the second new material produced by the quinuclidinium template series as discussed in chapter four. The experimental procedures for the template synthesis and MAPO synthesis conditions were described fully in chapters three and four respectively and will not be repeated here.

STA-2 originally formed as very fine crystals, and contained some poorly crystallised compounds. Attempts were therefore made to improve the crystallinity by altering the

gel chemistry of the MAPO synthesis gels. It was determined that increasing the mole ratio of the water from 40 to 333, resulted in phase pure, highly crystalline STA-2. The crystallinities of these materials were far superior to the samples produced via the normal synthesis conditions used throughout this thesis (see figure 6.1 below). The addition of sodium hydroxide to the MAPO synthesis gel (to determine the need for converting the template from the bromide to the hydroxide form) resulted in the production of crystals large enough for single microcrystal diffraction (also MAPO-56). The synthesis of the single crystals used in the determination of the STA2 structure is described more fully in section 6.3.3.

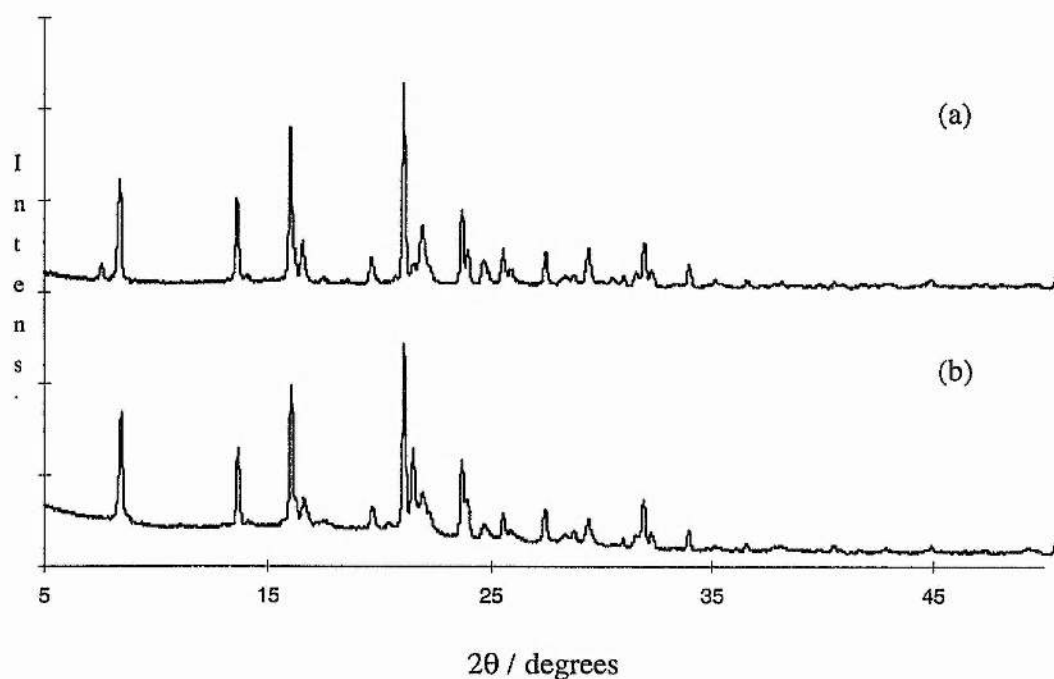


Figure 6.1 X-ray diffractograms of the (a) STA-2 sample produced using increased water and (b) an STA-2 sample produced by the standard method.

Characterisation of the as-prepared and calcined STA-2 was performed initially using x-ray powder diffraction using a STOE STADIP laboratory diffractometer using  $\text{Cu K}\alpha_1$  radiation with a primary monochromator. High resolution X-ray powder diffraction data were collected at room temperature in capillary mode on BM16 at the ESRF, Grenoble,

on a sample of the as-prepared MAPO-STA-2 powder. Thermogravimetric analysis (TGA) of the powder sample of STA-2 was performed using an SDT 2960 analyser from TA Instruments.  $^{13}\text{C}$  MASNMR spectra were obtained using a Bruker 400 MSL spectrometer. The  $^{13}\text{C}$  NMR of the template within STA-2 ( $\delta$  64.4, 56.4, 24.3 and 19.9 for the  $n = 4$  template) corresponded closely with that observed with higher resolution in  $\text{D}_2\text{O}$  solution ( $\delta$  63.19, 54.79, 23.30 and 18.98). The chemical analysis of microcrystals of STA-2 was performed by selected area energy dispersive analysis of X-rays in an electron microscope (EDX). To check the stability of STA-2 with respect to template removal, a sample was calcined at  $550^\circ\text{C}$  for 4 hours in flowing nitrogen and 8 hours in oxygen, the temperature having been raised to  $550^\circ\text{C}$  using a ramp rate of  $5^\circ\text{C}/\text{minute}$ , and the microporosity was measured volumetrically using nitrogen adsorption at liquid nitrogen temperature.

### 6.3.0 Results and Discussion

STA-2 was prepared from a gel of composition  $0.4 \text{ R}(\text{OH})_2 : 0.1 \text{ Mg}(\text{OAc})_2 : 0.9 \text{ Al}(\text{OH})_3 : \text{H}_3\text{PO}_4 : 40 \text{ H}_2\text{O}$ , when R represents the diquinuclidinium ion and the interconnecting chain of the template contained four and five methylene groups. The solid formed when the alkylammonium ion was used in its hydroxide form was indicated by SEM to consist of sub-micron particles with a poorly defined crystal shape, (figure 6.2) and laboratory X-ray powder diffraction (figure 6.3) revealed the presence of some amorphous material. Attempts to increase the magnesium content of the solid by raising the Mg/P ratio in the gel to 0.15 resulted in the co-crystallisation of MAPO-56, and the two solids could not be separated. Interestingly the aluminosilicate analogue of MAPO-56, SSZ-16<sup>[2]</sup> is also synthesised using the same diquinuclidinium templates as STA-2.

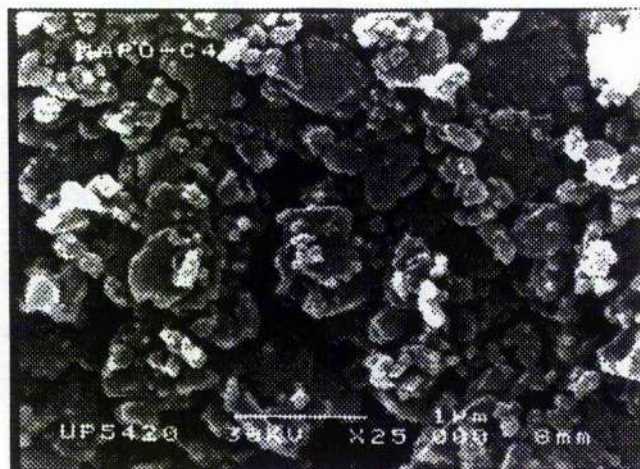


Figure 6.2 An SEM micrograph of STA-2 prepared with quinC4 in its hydroxide form. These sub micron particles are unsuitable even for microcrystal diffraction studies.

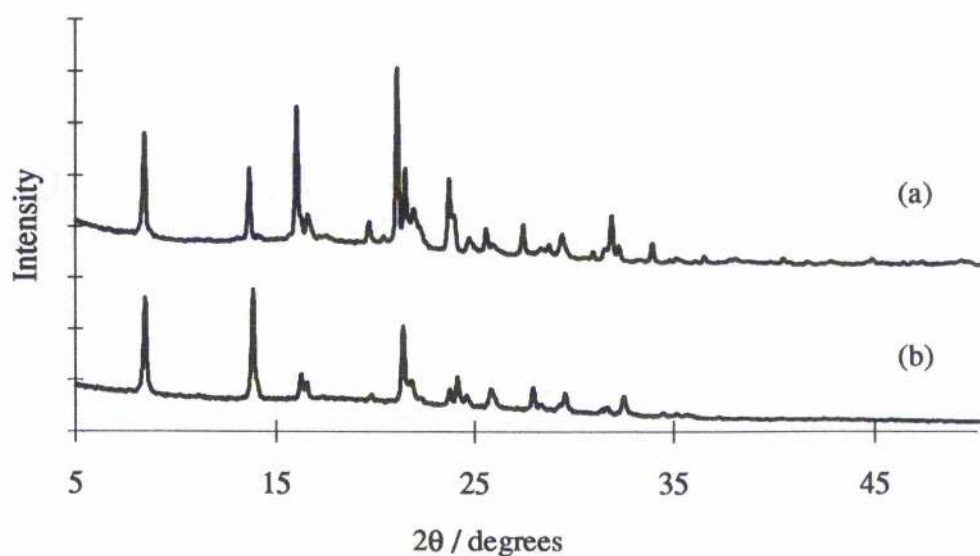


Figure 6.3 X-ray diffraction pattern of the (a) as prepared MAPO-STA-2 from a sample similar to that shown above in figure 6.2 and (b) a calcined sample showing the retention of the framework. The high level of background to signal intensity suggests that there may be some amorphous material present in this sample.

Attempts to index the STA-2 pattern using VISSER<sup>[3]</sup> were not successful possibly due to the presence of this amorphous material. Despite this pure STA-2 was also prepared as the aluminophosphate, the cobalt aluminophosphate and the silicoaluminophosphate by appropriate variation of the gel chemistry, since the framework was found to be stable even after template removal by calcination (figure 6.3b). The properties of these materials have still to be fully investigated. However, we were not able to solve the structure from the powder diffraction data.

### 6.3.1 Thermal Analysis and Adsorption

Thermogravimetric analysis gave one weight loss peak at 100°C, presumably due to water loss, of 7.0wt%, and a second, due to template removal, of 15.4wt%. Nitrogen adsorption<sup>[4,5]</sup> measurements on the calcined sample gave an isotherm mainly of Type I form, but also with some Type II characteristics, as shown in figure 6.6, presumably because the particle size was very small and the external surface area was not negligible. From 'monolayer' or pore filling coverage, a void volume of 0.095 cm<sup>3</sup>/g was calculated from a mass/mass uptake of 0.084 g/g at  $p/p^* = 0.1$ .

A Type I adsorption isotherm, is characterised as having an initially steep gradient rising swiftly onto an essentially horizontal plateau. This is caused by nitrogen being absorbed into the pores of the material until they are full, resulting in no more absorption and hence the flat plateau. This type of sorption is very common for microporous solids. Type II isotherms on the other hand are more common for aluminium oxide-type catalysts. This type of isotherm is identified as having a sharp gradient which becomes less steep as the adsorption continues and is caused by multilayer coverage of nitrogen on the surface (physisorption).

The type II adsorption characteristics may have been caused by the extremely small particle sizes present or perhaps the inclusion of some amorphous material, as the powder diffraction pattern also indicated a small amount of amorphous material may be present.

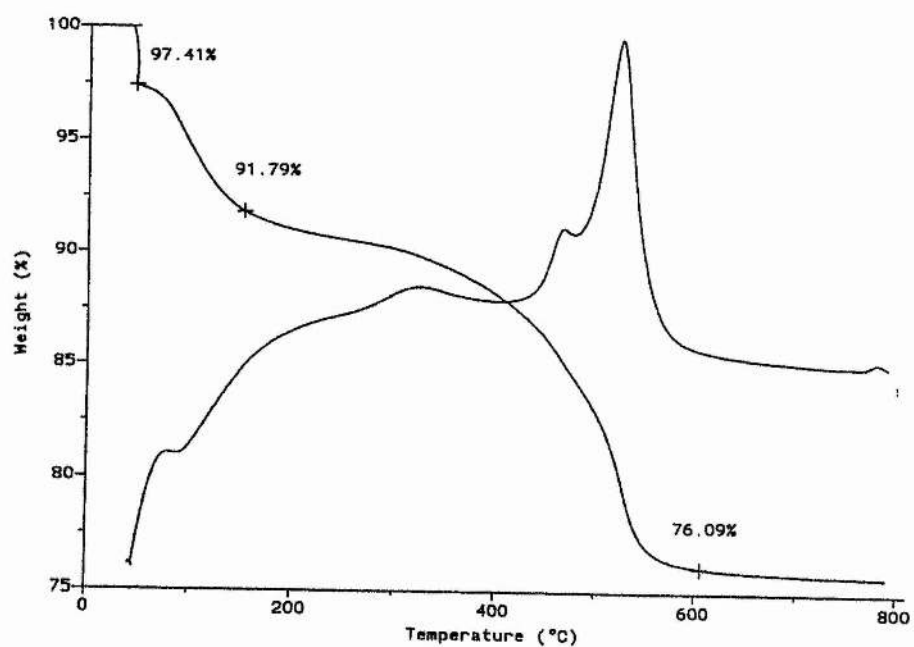


Figure 6.4 The TGA/DTA patterns for STA-2. The initial weight loss down to 97.41% is likely to have been caused by an experimental error rather than a genuine weight loss.

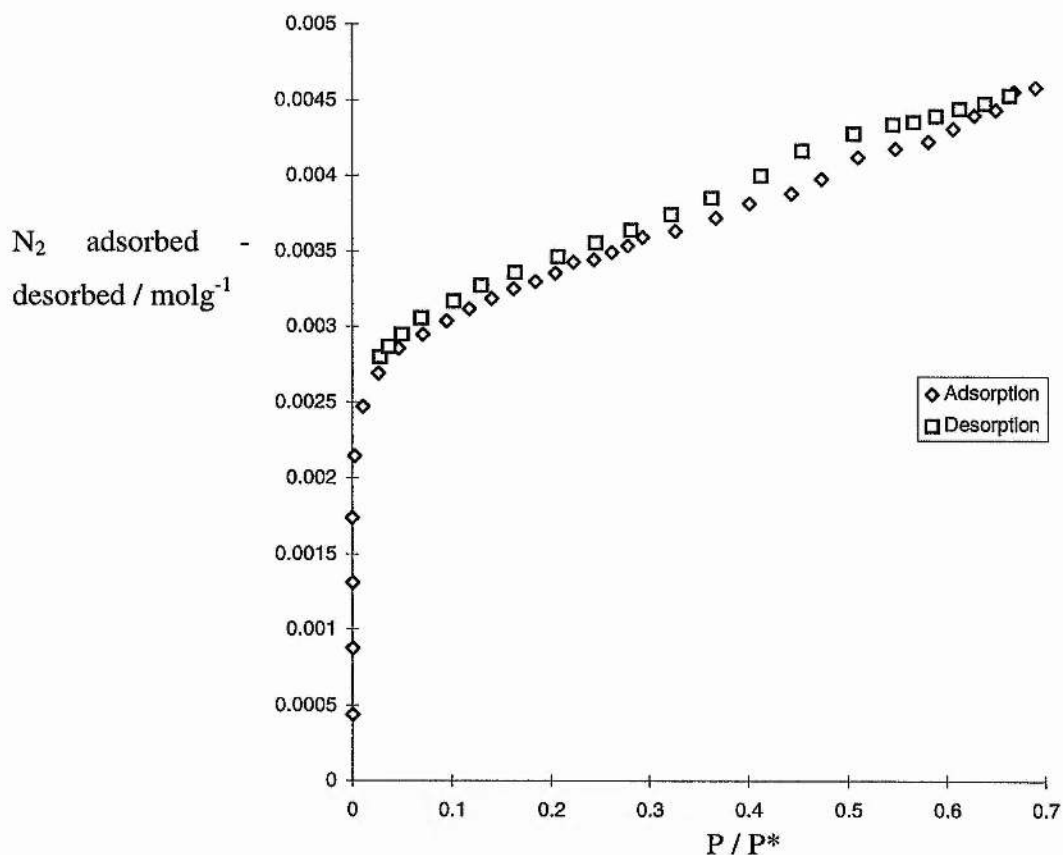


Figure 6.5 Adsorption isotherm for nitrogen on calcined STA-2 at 77K showing mainly Type I characteristics with a little Type II showing pore filling and possible particle size effects.

### 6.3.2 Solid State MASNMR<sup>[6,7]</sup>

Solid state <sup>13</sup>C MASNMR on the as-prepared MAPO-STA-2, showed that the organic template had been incorporated intact (figure 6.6) as might have been expected from previous experiments performed on STA-1. The solid state <sup>13</sup>C NMR spectrum is very well resolved and very similar to the spectrum obtained from the template in the solution state. The spectrum shows four resonances as opposed to the expected five in both the solution and solid state due to the position overlap of one of the chain carbons and the apical carbon of the quinuclidine.

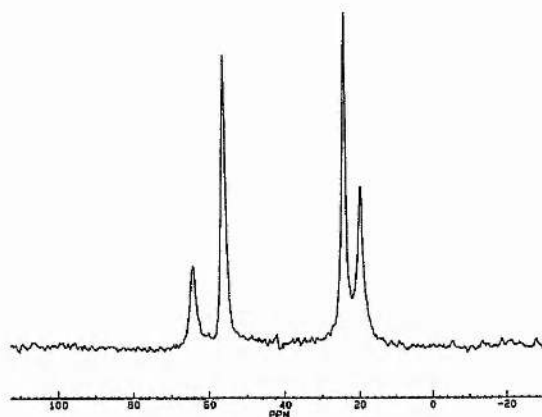


Figure 6.6  $^{13}\text{C}$  MASNMR spectrum of the as prepared MAPO-STA-2. The four peaks at  $\delta = 64.38, 56.44, 24.32$  and  $19.98\text{ppm}$  correspond extremely well to those obtained from solution NMR. This spectrum proves that the diquinuclidinium template is incorporated intact within the MAPO.

The  $^{31}\text{P}$  spectrum of calcined STA-2 (MAPO) shows two well defined phosphorous environments and a broad shoulder. If magnesium is in the sample (as EDX) suggests then it may have different environments, that are due to different numbers of magnesium in the second nearest neighbour sites.

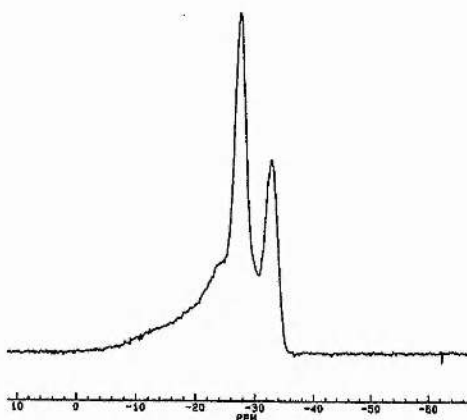


Figure 6.7  $^{31}\text{P}$  NMR spectra of calcined MAPO-STA-2. The spectrum shows three possible phosphorous environments.

The  $^{27}\text{Al}$  spectrum is, however, unexpected. The crystal structure of STA-2 from microcrystal diffraction shows tetrahedrally coordinated aluminium atoms however, the

spectrum obtained for the as prepared sample clearly exhibits three distinct aluminium environments. These environments have been attributed to tetrahedral sites and 5-coordinate aluminium sites. MASNMR was not in this case sufficiently sensitive to distinguish between the two crystallographic types of tetrahedral aluminium present in the sample, although the relevant peak at approximately 40ppm is broad and may conceal several peaks within it. The second 5-coordinate signal was initially thought to be due to water co-ordinating to framework aluminium as this peak was not present in spectra obtained from calcined samples.

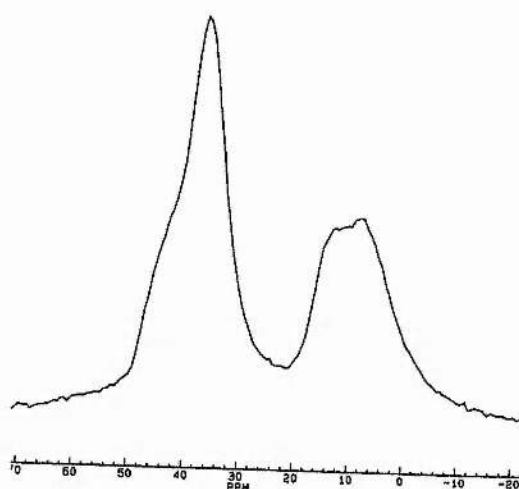


Figure 6.8  $^{27}\text{Al}$  MASNMR spectrum of MAPO-STA-2. This is an unexpected spectrum as the crystal structure of STA-2 shows only tetrahedral aluminium sites and as such should consist of only one peak at 40ppm. The second peak at 10ppm is due to 5-coordinate aluminium sites.

To test the assumption that the second peak in the aluminium NMR spectrum was due to water co-ordinating to framework aluminium, a sample of STA-2 was dried at 200°C in flowing (dry) nitrogen for eight hours before being loaded into a ceramic rotor and a new NMR spectrum obtained. This second NMR spectrum was identical to the first indicating that drying the MAPO had no appreciable effect on the aluminium framework. This means that weakly physically bound water molecules can not be

coordinating to the aluminium framework atoms as drying the MAPO would have removed them and the second 5-coordinate peak in the NMR spectrum.

If not due to water, the presence of hydroxide ions coordinating to the aluminium framework is the next most probable explanation for the second peak in the  $^{27}\text{Al}$  NMR spectrum. However, the  $^1\text{H}$  MASNMR shows two resonances one of which has a small shoulder indicating a third resonance. These three peaks (labelled in Hz) correspond approximately to  $\delta = 3.3, 2.3, 2.1$  ppm in a ratio of 8:10:1. These peaks can be attributed to the template protons as shown below. A hydroxyl proton for comparison would be expected to have a resonance of around 4 ppm and is not observed indicating that the spectrum is dominated by protons on the template molecules. The 8:10:1 ratio as opposed to the theoretical ratio distribution of 8:8:1 could be a consequence of the spectrum being obtained from the solid state and is therefore still consistent within experimental limits.

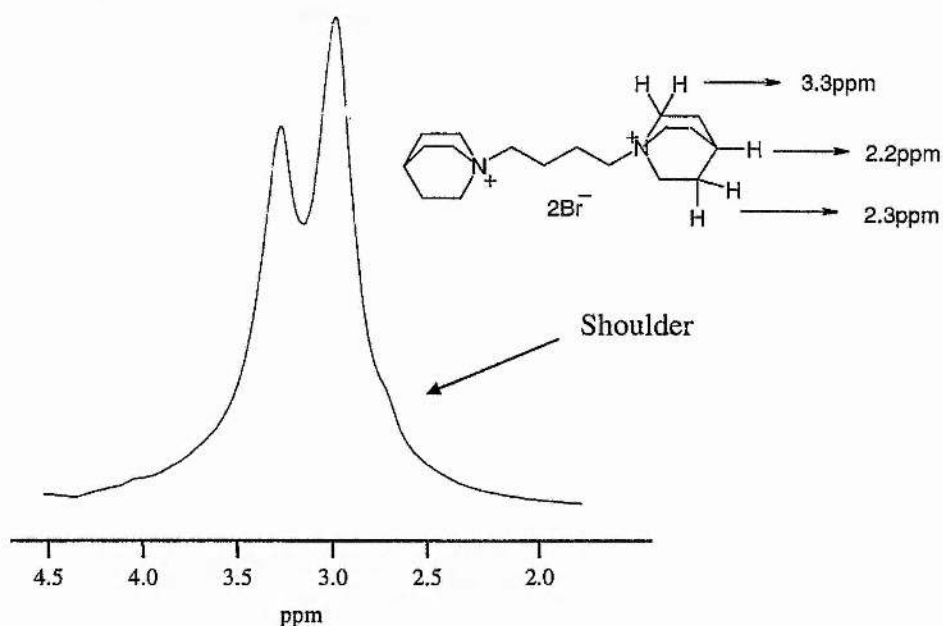


Figure 6.9 MASNMR  $^1\text{H}$  spectrum of 1,4-diquinuclidiniumbutane incorporated in STA-2. The three resonances are due to the template as indicated and not due to hydroxyl protons as was predicted. If symmetry is taken into account the overall proton ratio is 8:8:1 (the apical hydrogen).

All three NMR samples (as-prepared, dehydrated and calcined) were obtained from the same phase pure sample of STA-2, as determined from x-ray powder diffraction. The second 5-coordinate peak is therefore a genuine phenomenon and is not due to an impurity in the sample. The x-ray powder diffraction pattern of the sample used for NMR shows no evidence of impurities or other amorphous material present.

### 6.3.3 Synthesis of Single Crystals

As part of a program of synthesis to examine the effects of alkali cations on the synthesis of MAPOs (and thereby to determine the necessity of converting the alkyl ammonium bromide to the hydroxide form using silver oxide) a hydrothermal synthesis was performed using as-prepared tetramethylene-diquinuclidinium bromide and sodium hydroxide. The gel composition was adjusted so that the pH of the reaction gel was the same as that in the first set of experiments, performed in the absence of alkali cations. Under these conditions, the product was a mixture of phases, including rhombs and hexagonal plates, of dimensions of up to 50 $\mu$ m (figure 6.11). Powder diffraction indicated that the two crystal phases were MAPO-56 and STA-2. MAPO-56 crystallised as well-formed hexagonal plates whereas STA-2 crystallised as rhombs of sufficient size and quality for microcrystal diffraction and consequently a number of well-formed crystals of STA-2 were chosen for examination at the ESRF at Grenoble. Selected area EDX chemical analysis on the STA-2 crystals indicated a framework composition close to  $Mg_{0.15}Al_{0.85}PO_4$  in addition to traces of sodium. Assuming the template content to be similar to that measured on the powder samples, the as-prepared composition is likely to be  $Mg_{0.15}Al_{0.85}PO_4 \cdot 0.083R^{2+} \cdot 0.625H_2O$ , where the template charge is largely balanced by the negative charge on the framework.

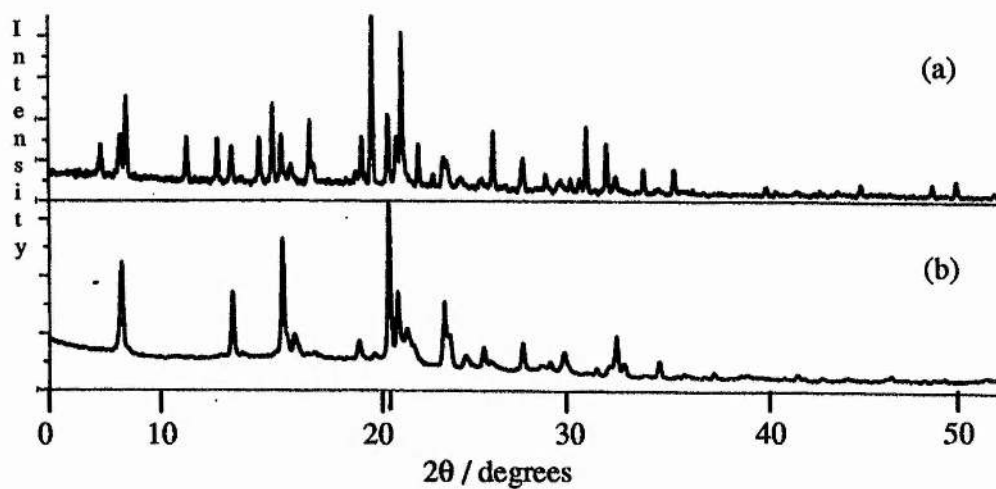


Figure 6.10 X-ray diffractograms of (a) the MAPO-56 / STA-2 mixture. The STA-2 peaks can be identified by comparison of the STA-2 diffractogram shown in (b).

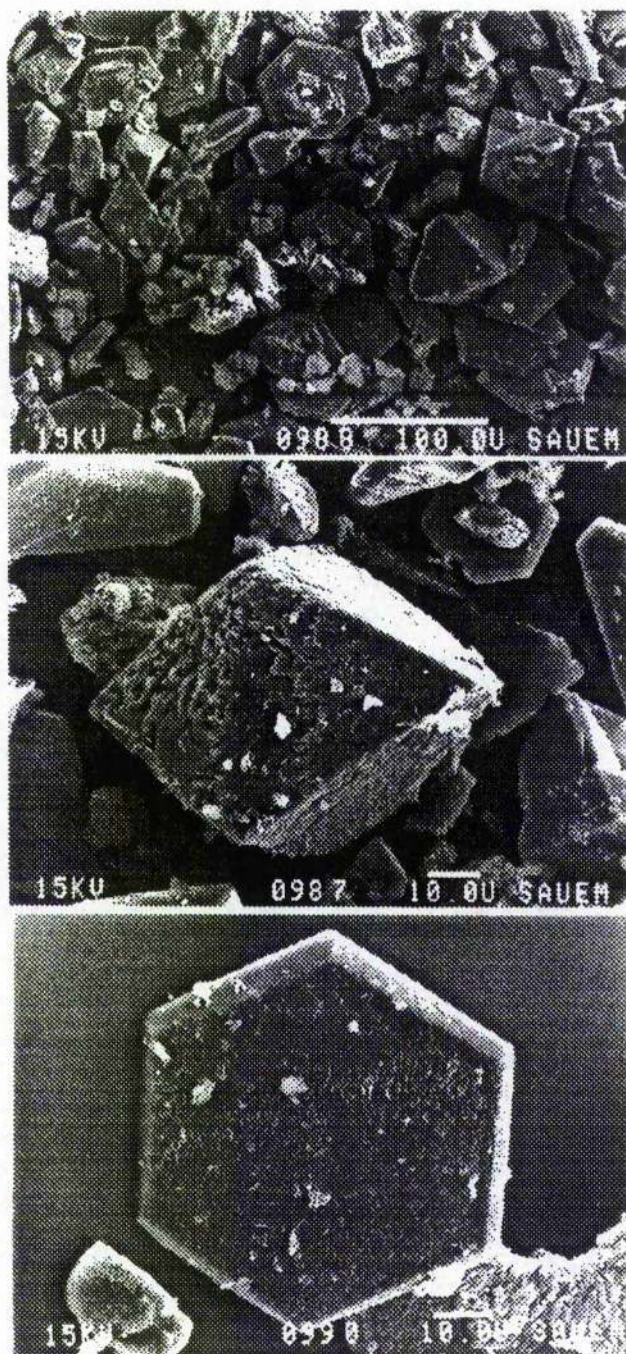


Figure 6.11 Scanning electron micrographs of the separated coarse fraction of a preparation performed using sodium hydroxide to control the pH of the starting gel. (Upper micrograph) Mixture of MAPO-56 and MAPO-STA-2. (Middle micrograph) A single microcrystal of STA-2. (Lower micrograph) a single crystal of MAPO-56.

### 6.3.4 Structure Solution

Microcrystal diffraction was carried out at Grenoble at a temperature of 200K in order to reduce the effects of thermal disorder of the included template. The as-prepared rather than the calcined sample was chosen for analysis because we were interested not only in the framework structure but also in the role the template molecules played in controlling the crystallisation. The structure was solved as detailed below.

Single crystal diffraction data were collected on the Materials Science Beamline (ID-11, BL2) at the ESRF, Grenoble<sup>[8,9]</sup> at 200K in order to limit the thermal motion of the template. A well-formed bipyrimidal crystal with edge lengths of 50  $\mu\text{m}$  was glued to a fine glass fibre and mounted on the 3 circle fixed kappa Siemens diffractometer fitted with a Siemens SMART CCD detector. The X-ray wavelength used was 0.512 $\text{\AA}$  obtained from a liquid nitrogen-cooled double crystal Si (111) monochromator. The wavelength was calibrated at an appropriate X-ray absorption edge. The crystal was cooled to 200K with an Oxford Cryostream nitrogen gas flow system and the data was collected using the Siemens SMART CCD system. 900 frames with an oscillation angle of 0.2 degrees were collected with an X-ray exposure time of 2 seconds per frame. The data was integrated and corrected with the Siemens software adapted for synchrotron use. The structure was solved using the direct methods programs in the SHELXTL program package[10]. The data statistics strongly indicated the trigonal space group  $R\bar{3}$  with an overall mean abs ( $E^*E-1$ ) value of 1.046; centric space groups have an expected value of 0.968 whereas non-centric space groups have a much lower value of 0.736. A total of 7925 reflections with a mean intensity/sigma (intensity) of 8.6 were obtained after integration. In the space group  $R\bar{3}$  these represented 4287 reflections and 3673 had intensities above three sigma. Symmetry averaging yielded 1993 reflections with an interconsistency index  $R(\text{int})$  of 0.077. The resolution limit was 0.78 $\text{\AA}$ . The indexing in the hexagonal cell resulted in a unit cell:  $a=b=12.726(2)$  and  $c=30.939(6)\text{\AA}$ .  $F(000) = 1635$ ,  $\mu = 0.19\text{mm}^{-1}$ .

The structure could be refined successfully in this space group to an R factor  $R(F) = 0.0757$  for 1593 reflections above four sigma and 0.0981 for all 1993 reflections.

The goodness of fit  $S=1.307$  and the total number of refined parameters was 142. The largest extra-residual in the final difference map was  $0.9 \text{ e}/\text{\AA}^3$ . No effort was made to locate the magnesium, which is expected on the basis of experience to substitute randomly for aluminium in the structure. All parameters were well-behaved with the exception of those of one of the chain C-atoms in the template molecule. The atom was treated as three-fold disordered with fixed coordinates obtained from the difference Fourier. The isotropic temperature factor was allowed to vary. The structure solution was also tried in the triclinic space groups  $P1$  and  $P\bar{1}$ , and although the refinement in  $P\bar{1}$  was successful ( $R(F) = 0.1061$  for 4287 reflections and 428 varied parameters, the standard deviations were twice those obtained in  $R\bar{3}$  and the apparent disorder in the central part of the template molecule was still retained. Hydrogen atom positions were generated using the teXsan suite of programs<sup>[11]</sup>. Attempts to refine them produced no significant improvement in  $R(F)$  so the geometric positions were retained.

The atomic coordinates are given in Table 6.1 and relevant framework and template interatomic distances given in Table 6.2. Strict ordering of aluminium and phosphorus in the tetrahedral cation sites is revealed by the bond lengths - the average Al-O distances are  $1.72\text{\AA}$  for Al(1) and  $1.73\text{\AA}$  for Al(2) and the average P-O distances are  $1.50\text{\AA}$  for P(1) and  $1.49\text{\AA}$  for P(2).

The framework structure (figures 6.12-6.15) can be viewed in terms of the building units and cavities that are arranged in columns parallel to the c-axis (6.13) (in the hexagonal setting of the rhombohedral cell), with adjacent columns offset by  $c/3$ . Two 'cancrinite' or  $\epsilon$ -cages, rotated by  $60^\circ$  with respect to each other, sandwich a double six-membered ring unit. Above and below this unit along  $c$  are cavities, approximately  $17\text{\AA}$  in length, that contain the template cations. For small molecules, access to 6 other cavities is possible through eight-membered rings. Each column, as described above, is adjacent to six others, which are identical and shifted by  $\pm c/3$ , alternatively, going round the original column.

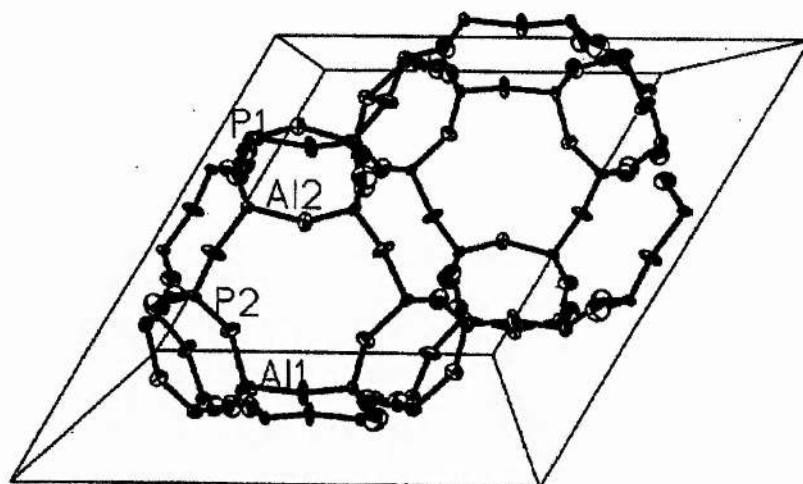


Figure 6.12 The unit cell. A singular column of STA-2 and a pair of joining columns.

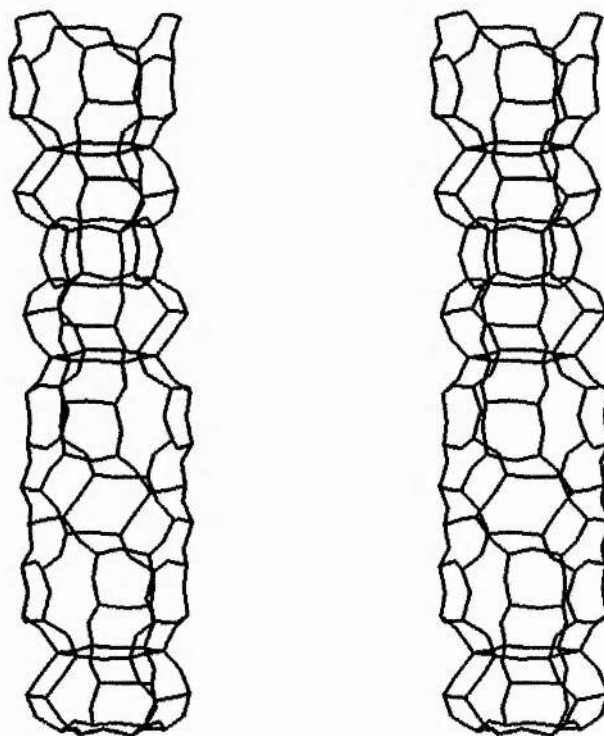


Figure 6.13 Stereoplot of one of the columns of the secondary building units of the STA-2 framework. The diagram clearly shows the large pore that encapsulates the organic template and the cancrinite cages.

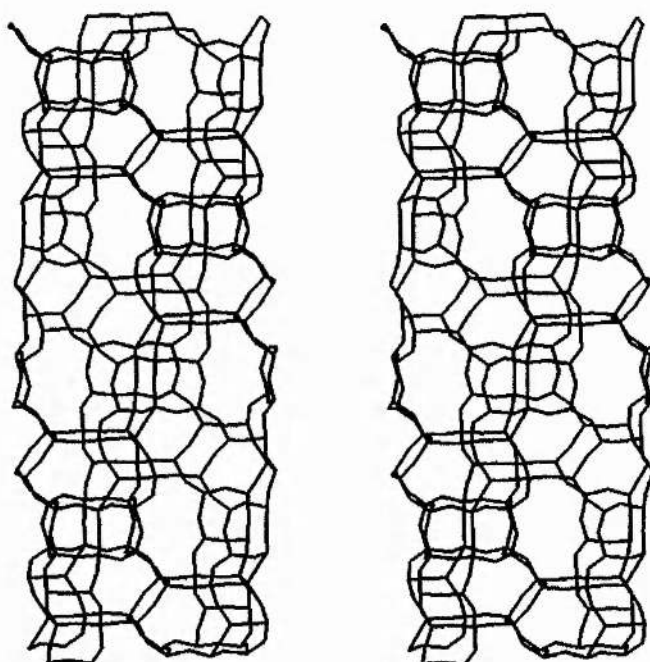


Figure 6.14 Stereoplot showing how the columns of secondary building units join as they run parallel to the *c*-axis.

The framework structure of STA-2 is one of the family of zeolitic structure types, of which there are now 14 known (Table 6.15) which are best considered as made up of flat 6-membered rings (the common description of rings made up of six tetrahedral cations and six oxygens) that are parallel to a hexagonal *ab* plane with lattice repeats of around 13Å. These 6-rings may have their centres at only one of the (0,0), (1/3,1/3) or (2/3,2/3) positions in the *ab* plane, and can link to other sets of 6-rings above and below them in the *c*-direction that may also have their centres at (0,0), (1/3,1/3) or (2/3,2/3), which can be denoted as the A, B and C positions. The structures that are produced are then conveniently described in terms of repeating stacking sequences; for example cancrinite has the sequence AB, chabazite the sequence AABBC and AlPO-56 the sequence AABBCBB. Using this nomenclature, the framework structure of STA-2 has the sequence AABABBCBCCAC, the most complex of any yet reported. The energy differences between the different polytypes are likely to be small, and even random stacking of double six-rings has been observed<sup>[12]</sup>. However, we see that very good crystals of MAPO-56 and STA-2 may be obtained, and this must be due to the templating action of the included organic cations. Bennett predicted the 6-ring sequence

observed in STA-2 in 1981 by a consideration of the crystallography of zeolite structures<sup>[13]</sup>.

The reason why such a complicated stacking sequence is produced in such a well-ordered way becomes clear when the experimentally-determined position of the diquinuclidinium cations is examined (figure 6.15).

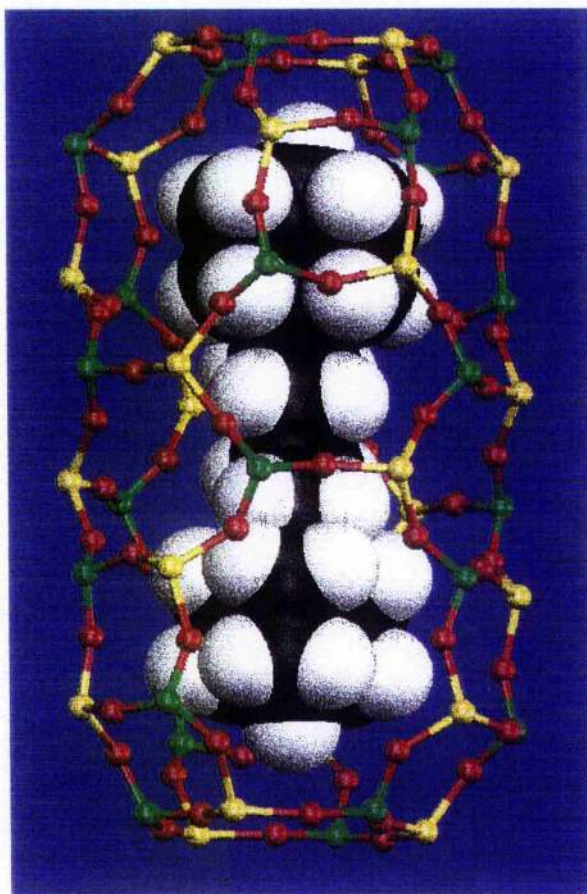


Figure 6.15 Shows the experimentally-determined position of the template within the large cavities in STA-2, with the template represented by a space filling model and the inorganic framework represented by a line drawing for clarity. H-atoms on the template have been placed geometrically and a single (trans) orientation has been taken for the methylene chain of the template, which is in fact disordered about the triad axis. Aluminium, phosphorous and oxygen atoms are shown as yellow, green and red respectively.

The position of the quinuclidinium fragments is particularly well described, although there is disorder in the positions of the atoms within the tetramethylene chain, as discussed in the experimental section and seen in the larger temperature factors and chemically inaccurate bond lengths C(4) - N(1) and C(4) - C(5), this is much smaller than usually observed for structures of this kind, and underlines the importance of the microcrystal technique, compared to the more usual powder diffraction method. The cations fit very closely in the large cavity within STA-2, and are stacked in a well ordered array throughout the structure. Both thermogravimetric analysis and crystallography indicate that each cavity is occupied by a template molecule. This is better demonstrated in figures 6.16 and 6.17 which show the systematic arrangement of templates as they align within the framework structure.

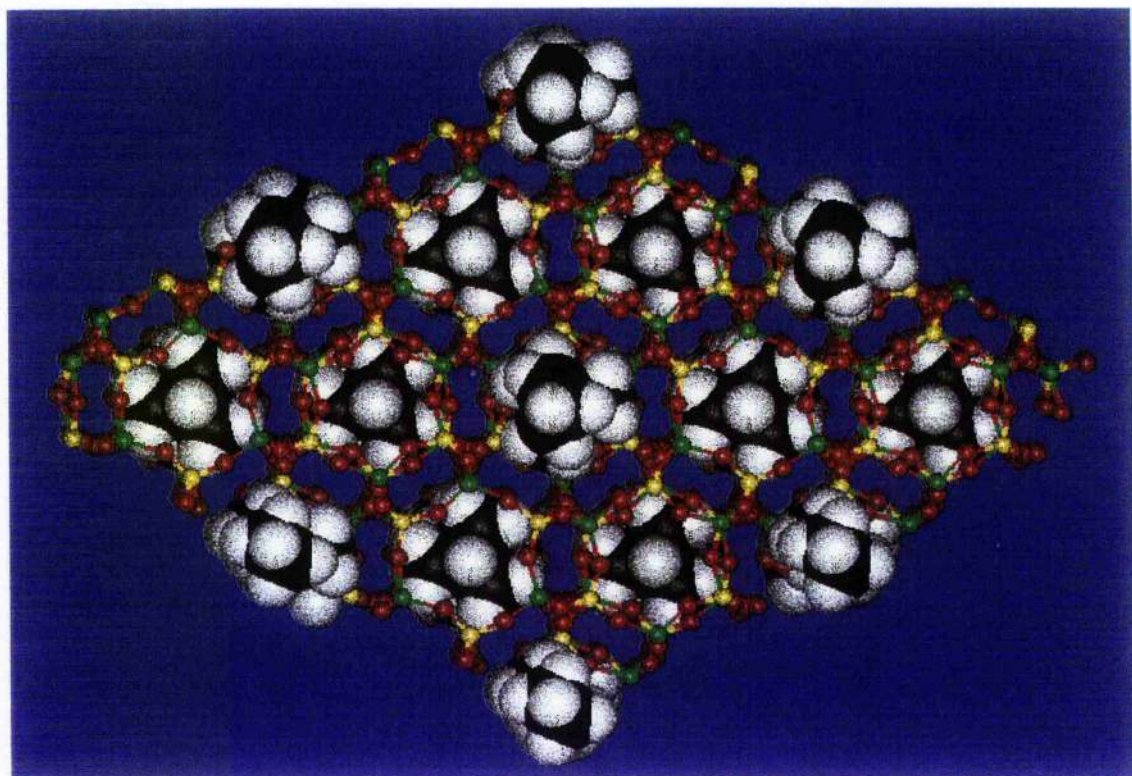


Figure 6.16 Template filling within STA-2 viewed along the c-axis. Showing that the template fills all pores in a systematic manner such that every large pore of STA-2 contains a template molecule.

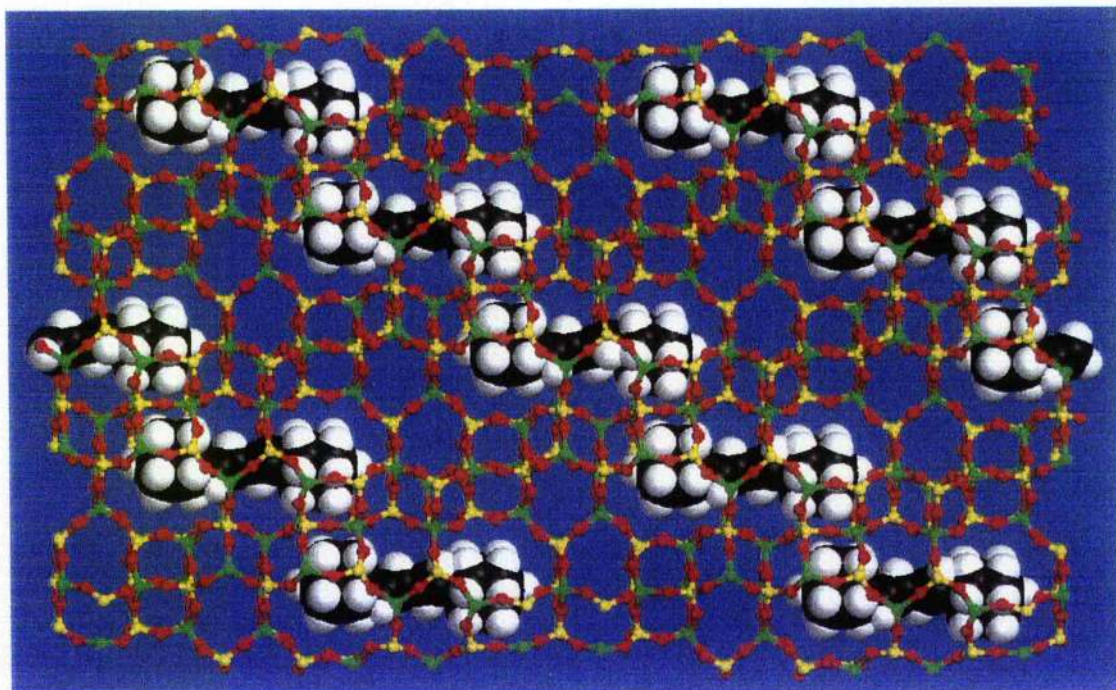


Figure 6.17 Framework shown looking down onto the  $[100]$  plane along the  $x$ -axis. For simplicity this diagram depicts one plane of template molecules and is equivalent to one horizontal layer of template molecules from the diagram above. The actual framework will contain templates above and below this plane offset by  $c/3$  on adjacent planes.

The reason that MAPO-56 co-crystallises with STA-2 under certain conditions becomes clear by considering the similarity in the cavity dimensions in the two solids. Although not identical, the dimensions of the cavity in the AFX structure type (figure 6.20) are very similar to those in STA-2 and very subtle effects must be responsible for determining which polytype will form. (It is of interest that SSZ-16, the aluminosilicate analogue to AFX, is templated by the same alkyl ammonium templates used for the magnesium aluminophosphates<sup>[2]</sup>.) Although STA-2 is prepared by the use of tetra- and pentamethylene diquinuclidinium ions it is interesting to note that with  $n=3$ , the stacking sequence giving the erionite structure type is favoured, presumably because the cation is more satisfactorily coordinated within the smaller erionite cages (figure 6.19). On the

other hand, with  $n=6$  the channel structure of the AFI<sup>[14]</sup> structure type is favoured, because the template is too long to fit in the cavities of STA-2.

From single crystal data, it has been possible to determine the exact template location and orientation within the cages of both STA-2 and MAPO-56. In both cases the template is oriented such that the carbons of the quinuclidine cages point in the direction of the 8T-atom window. This may account for the fact that SAT, AFX and ERI all have the same basic pore architecture since the quinuclidinium cation promotes the formation of this structure. Computer docking simulations based on these molecules have provided an excellent comparison between the theoretical and experimentally derived locations of templates within microporous solids. Figure 6.20 shows the diquinuclidinium template positions for ERI, AFX and SAT determined by computer docking. The quinuclidinium carbons are again pointing towards the 8T-atom cage windows. This confirms the accuracy of the computer modelling technique used (and explained) in chapter eight.

Atom	x	y	z	Ueq
Al(1)	0.75330(1)	0.75722(13)	0.29540(5)	0.01620(40)
Al(2)	0.57616(14)	0.90230(14)	0.21646(5)	0.02034(41)
P(1)	0.57783(12)	0.90432(12)	0.11444(5)	0.01842(37)
P(2)	0.75682(11)	0.00127(10)	0.29140(4)	0.01512(36)
O(1)	0.61376(11)	0.93930(10)	0.16168(4)	0.03460(40)
O(2)	0.53414(38)	0.75325(36)	0.22506(15)	0.03395(36)
O(3)	0.79283(38)	0.90717(36)	0.29395(17)	0.03778(12)
O(4)	0.46125(35)	0.92799(41)	0.23103(15)	0.03533(41)
O(5)	0.70143(39)	0.99588(39)	0.24720(15)	0.0354(10)
O(6)	0.86442(37)	0.12240(36)	0.29679(18)	0.0419(12)
O(7)	0.66892(44)	0.98312(45)	0.32674(16)	0.0455(13)
O(8)	0.65629(40)	0.00923(38)	0.08555(15)	0.03564(38)
N(1)	0.00000	0.00000	0.10248(42)	0.0688(53)
C(1)	0.00000	0.00000	0.18419(58)	0.0985(71)
C(2)	-0.0415(15)	0.0827(14)	0.1662(7)	0.1216(53)
C(3)	-0.0415(15)	0.0787(14)	0.1177(6)	0.1186(53)
C(4)	-0.0312	0.0351	0.0556	0.2155(12)
C(5)	0.00000	0.00000	0.02411(9)	0.188(17)
H(1)	0.0000	0.0000	0.2147	---
H(2)	0.1030	0.1631	0.1757	---
H(3)	-0.1222	0.0567	0.1762	---
H(4)	0.0090	0.1580	0.1069	---
H(5)	-0.1226	0.0498	0.1075	---
H(6)	0.0075	0.1208	0.0540	---
H(7)	-0.1164	0.0017	0.0540	---
H(8)	0.0851	0.0322	0.0249	---
H(9)	-0.0211	0.0263	-0.0015	---

Table 6.1 Atomic Coordinates for STA-2 at 200K. Hydrogen atom coordinates were generated by the teXsan suite<sup>[11]</sup>.

Bond	Distance (Å)	Bond	Distance (Å)
Al(1) - O(3)	1.714(4)	Al(2) - O(1)	1.760(5)
Al(1) - O(6)	1.687(4)	Al(2) - O(2)	1.715(4)
Al(1) - O(7)	1.731(5)	Al(2) - O(4)	1.711(4)
Al(1) - O(8)	1.751(5)	Al(2) - O(5)	1.722(5)
P(1) - O(1)	1.529(5)	P(2) - O(5)	1.524(5)
P(1) - O(2)	1.492(4)	P(2) - O(5)	1.524(5)
P(1) - O(4)	1.494(4)	P(2) - O(6)	1.473(4)
P(1) - O(8)	1.498(5)	P(2) - O(7)	1.497(5)
C(1) - C(2)	1.50(2)		
C(2) - C(3)	1.50(2)		
C(3) - N(1)	1.43(1)		
N(1) - C(4)	1.62(1)		
C(4) - C(5)	1.22(2)		
C(5) - C(5)	1.49(5)		

Table 6.2 Selected bond distances for STA-2, showing the standard deviations in parenthesis.

Atoms	Angle (°)	Atoms	Angle (°)
O(3) - Al(1) - O(6)	111.0(2)	O(1) - Al(2) - O(2)	109.8(2)
O(3) - Al(1) - O(7)	111.9(3)	O(1) - Al(2) - O(4)	110.3(2)
O(3) - Al(1) - O(8)	109.2(2)	O(1) - Al(2) - O(5)	108.2(2)
O(6) - Al(1) - O(7)	108.3(3)	O(2) - Al(2) - O(4)	110.3(2)
O(6) - Al(1) - O(8)	106.3(2)	O(2) - Al(2) - O(5)	110.4(2)
O(7) - Al(1) - O(8)	110.1(2)	O(4) - Al(2) - O(5)	107.8(2)
O(1) - P(1) - O(2)	109.7(3)	O(3) - P(2) - O(5)	109.5(3)
O(1) - P(1) - O(4)	110.1(3)	O(3) - P(2) - O(6)	109.8(3)
O(1) - P(1) - O(8)	110.0(3)	O(3) - P(2) - O(7)	110.2(3)
O(2) - P(1) - O(4)	108.6(3)	O(5) - P(2) - O(6)	108.4(3)
O(2) - P(1) - O(8)	110.1(3)	O(5) - P(2) - O(7)	110.8(3)
O(4) - P(1) - O(8)	108.3(3)	O(6) - P(2) - O(7)	108.1(3)

Table 6.3 Inorganic Framework Bond Angles.

Name	Layers in repeat	Sequence	a /Å	c /Å	Framework Density T /1000Å <sup>3</sup>
Cancrinite	2	AB	12.8	5.1	16.7
Offretite	3	AAB	13.3	7.6	15.5
Sodalite*	3	ABC	8.9	cubic	17.2
Gmelinite	4	AABB	13.8	10.0	14.6
Losod	4	ABAC	12.9	10.5	15.8
Chabazite*	6	AABBCC	13.2	15.1	14.6
EAB	6	ABBACC	13.3	15.2	15.4
Erionite*	6	AABAAC	13.3	15.1	15.6
Liottite	6	ABABAC	12.8	16.1	15.7
Afghanite	8	ABABACAC	12.8	21.4	15.9
AIPO-56	8	AABBCCBB	13.8	19.9	15.7
Levyne*	9	AABCCABBC	13.3	23.0	15.2
AIPO-52	12	AABBCCAACCBB	13.7	29.7	15.2
STA-2 <sup>#</sup>	12	ABAACACCBCBB	13.0	30.4	16.2

Table 6.4 6-Membered ring stacking polytypes.

\* Indicates both aluminosilicate and aluminophosphate analogues are known.

# Unit cell dimensions taken from GSAS data obtained at room temperature.

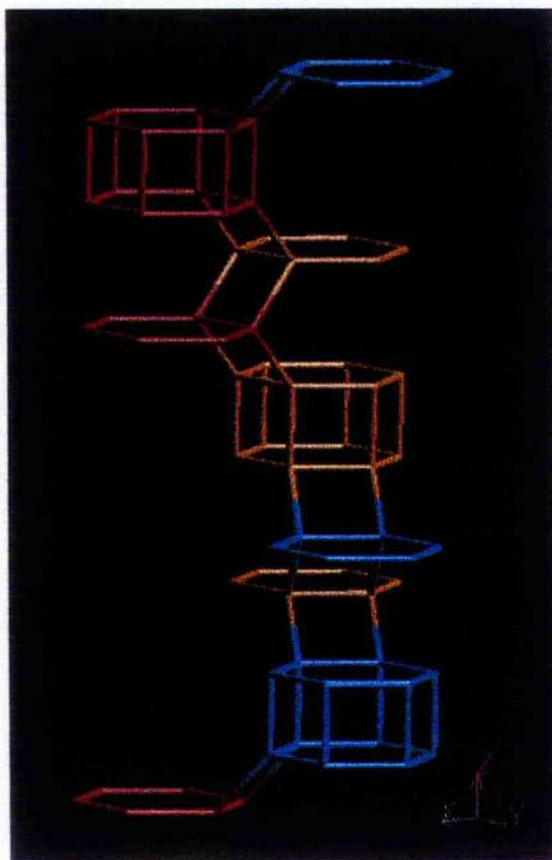


Figure 6.18 A graphic representation of the 6-ring sequence, where in this diagram A is red, B is blue and C is gold to give the ABBCBCCACAAB sequence. (Diagram taken from Atlas of Zeolite Structures<sup>[15]</sup>.)

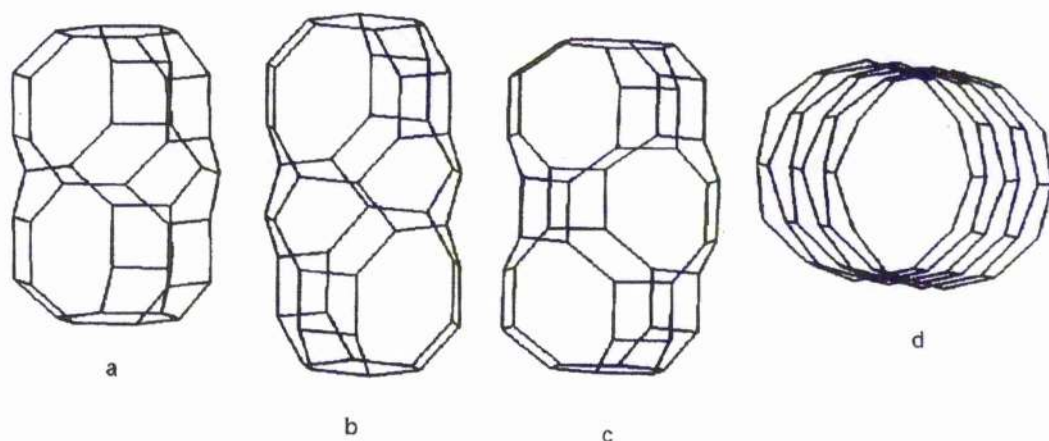


Figure 6.19 Line representations (oxygen atoms removed for clarity), to approximately the same scale, of cavities within the structure types of (a) AIPO-17, (b) STA-2 and (c) AIPO-56 which are produced using diquinuclidine templates, with linking methylene chains containing three and four CH<sub>2</sub> groups. (d) The channel structure of AIPO-5, which is prepared if longer methylene chains are present in templating molecules of the same kind, is also shown.

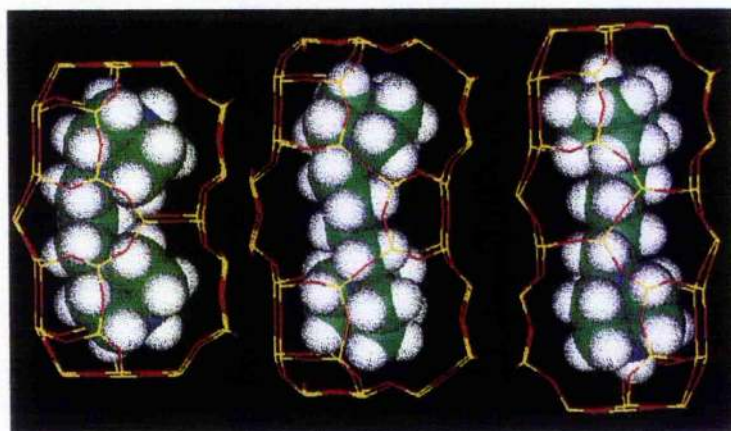


Figure 6.20 From left to right, the calculated position of the QuinC3 ion within the cage of the AIPO-17 (ERI) structure, the position of the QuinC4 ion within the STA-2 (SAT) structure and the position of the QuinC4 within the AIPO-56 (AFX) structure.

### 6.3.5 Rietveld Refinement<sup>[16]</sup> based on Structure Derived from Single Crystal Diffraction

To prove that the structure determined from the single crystal diffraction is essentially the same as that of the powder sample of STA-2 prepared without alkali cations the powder diffraction data collected at the ESRF were matched using the structural parameters determined by microcrystal diffraction, allowing the unit cell parameters and instrumental parameters (peak half-width, zero-point) to vary. The fit (figure 4,  $R_{wp} = 11.4\%$ ,  $R_p = 8.4\%$ , with unit cell parameters at room temperature of  $a=13.0121(7)\text{\AA}$  and  $c=30.406(2)\text{\AA}$ ) is sufficiently close to confirm it is the same phase, although further refinement is required to take into account the effects of particle size broadening and of additional structural disorder, and to determine the nature of the non-tetrahedral aluminium observed by NMR.

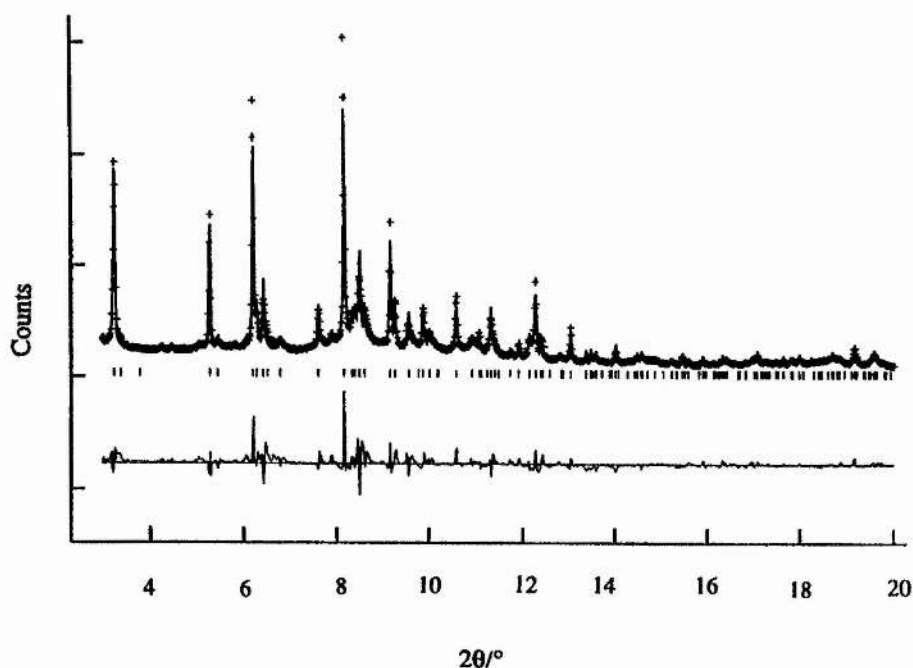


Figure 6.21 Fitted experimental X-ray powder diffraction profile,  $\lambda = 0.6004\text{\AA}$ , collected at station BM16, at the ESRF, Grenoble. ( $R_{wp}= 11.4\%$ ,  $R_p=8.4\%$ ).

### 6.3.6 Computer Modelling

Although the template location within STA-2 was determined experimentally by x-ray diffraction, computer modelling<sup>[17-19]</sup> was also used to identify its position within the MAPO. A combined experimental and computational approach was used, as much to verify the templates location as to confirm the strength of the computer modelling program itself. It was not possible to ascertain the template position for STA-1 for example by experimental methods, or for the polymeric templates described in chapter seven. It is important therefore to prove that the computer docking program used in this project is capable of determining the template location by purely computational methods for use in those microporous solids where experimental methods fail to elucidate the position of the organic template within.

Biosym-MSL Insight II software was used to dock the 1,4-diquinuclidiniumbutane molecule within STA-2 using a combined Monte Carlo / Simulated Annealing approach analogous to that used for STA-1, described previously in chapter five. The template molecule and framework were created separately and independently so that there was no connection between the two molecules prior to the start of the docking experiment.

The computer modelling experiment located the template in the same place as that observed experimentally. This not only confirms the location of the template within the large pores of STA-2 but also confirms the strength of the computer modelling technique used in chapters four, five and throughout chapter seven.

### 6.4.0 Conclusions

This study shows the sensitivity of crystal growth of microporous solids to precise conditions of the hydrothermal synthesis, and confirms that alkali cations do not prevent the formation of microporous aluminophosphates. Alkali cations can though, have a radical effect on the morphology of the phase produced as shown by comparison of figures 6.2 and 6.11 where the only significant difference in the synthesis conditions between the two was the addition of sodium hydroxide. In the absence of the

alkylammonium template, however, the alkali cations are not able in this case to synthesise microporous materials, although dense phase sodium aluminophosphates are formed.

The structure of STA-2 as obtained by microcrystal diffraction on a single crystal prepared in the presence of sodium does not show evidence of non-tetrahedral aluminium observed in NMR studies of STA-2 prepared in the absence of sodium. A possible explanation could be that the aluminium sites coordinate 4 or 5 oxygens in a disordered fashion, and x-ray diffraction observes only the weighted average structure, which is dominated by the tetrahedrally coordinated aluminiums. The close agreement of the powder diffraction pattern with that simulated using the structure obtained by single crystal diffraction strongly indicates both materials have the same framework structure, but further experiments are required to determine the exact location of the non-tetrahedral aluminium.

On the atomic scale, the work underlines the role templates play in determining complex periodic stacking arrangements, and how single microcrystal diffraction is a powerful tool not only to determine framework structures<sup>[1,20,21-23]</sup> but also to locate organic templates<sup>[24,25]</sup>. This should be of widespread applicability in experimental and computational studies aimed at the role and design of templates for the synthesis of targeted materials<sup>[26]</sup>. Specifically, STA-2 is a new small pore polytype of the series of structures formed by the stacking and linking of 6-membered rings (usually reported in terms of ABC type stacking).

### 6.5.0 References

- 1 G.W. Noble, P.A. Wright and Å. Kvik, *J. Chem. Soc. Dalton Trans.*, 1997, **9**, 976
- 2 R.F.Lobo, S.I.Zones, R.C.Medrud, *Chem. Mater.*, 1996, **8 (10)**, 2409
- 3 J.W. Visser, *J. Appl. Cryst.*, 1969, **2**, 89
- 4 R. Szostak, *Molecular Sieves, Principles of Synthesis and Identification*, van Norstrand Reinhold, 1989
- 5 British Zeolite Association, *3<sup>rd</sup> Euroworkshop on Zeolites*, Manchester, 1997

- 6 A.K. Cheetham and P. Day, *Solid State Chemistry Techniques*, Clarendon Press Oxford, 1983
- 7 R.A. Alberty and R.J. Silbey, *Physical Chemistry*, John Wiley & Sons, 1992
- 8 Å.Kvick, M.Wulff, *Rev.Sci.Instr.* 1992, **62**, 1073
- 9 M.Krumrey, Å.Kvick, W. Schwegle, *ibid*, 1994, **66**, 1715
- 10 G.M.Sheldrick, 1993, SHELX93, Program for the solution of crystal structures, University of Göttingen, Germany.
- 11 teXsan Single Crystal Analysis Software, version 1.6, 1993. Molecular Structure Corporation, The Woodlands, TX USA, 77381
- 12 R.Szostak and K.P.Lillerud, *J. Chem Soc Chem. Comm.*, 1994, **20**, 2357
- 13 J.V. Smith and J.M. Bennett, *Am. Mineral*, 1981, **66**, 777
- 14 W.M.Meier, D.H.Olson and Ch. Baerlocher. *Atlas of Zeolite Structure Types*, 4th Revised Edtn., Elsevier, 1996
- 15 International Zeolite Association, *Internet site*: <http://www.izc-sc.ethz.ch/IZA-SC/>
- 16 C. Giacovazzo (Editor), *Fundamentals of Crystallography*, Oxford University Press, 1995
- 17 Biosym / MSI Inc., Insight II, Version 3.0.0, *User Manual*, 1995
- 18 Biosym / MSI Inc., Catalysis, Version 4.0.0, *User Manual*, 1996
- 19 A.P. Stevens, *Ph.D. Thesis*, University of Portsmouth, 1996
- 20 G.W.Noble, P.A.Wright, P.Lightfoot, R.E.Morris, K.J.Hudson, Å.Kvick, H.Graafsma, *Angew. Chem. Int. Ed. Engl.*, 1997, **36**, 81.
- 21 M. Helliwell, V.Kaucic, G.M.T.Cheetham, M.M.Harding, B.M.Kariuki, P.J.Rizkallah, *Acta Cryst.B* 1993, **49**, 413
- 22 G.M.T. Cheetham, M.M.Harding, *Zeolites*, 1996, **16**, 245
- 23 M.J.Gray, J.D.Jasper, A.P.Wilkinson, J.C.Hanson, *Chem. Mater.*, 1997, **9**, 976
- 24 M.A.Cambor, M.Diaz-Cabanas, J.Perez-Pariente, S.J.Teate, W.Clegg, I.J.Shannon, P.Lightfoot, P.A.Wright and R.E.Morris, *Angew. Chem. Int. Ed.*, 1998, **37**, 2122
- 25 G. Sankar, J.K. Wyles, R.H. Jones, J.M. Thomas, C.R.A. Catlow, D.W. Lewis, W. Clegg, S.J. Coles and S.J. Teate, *Chem. Commun.*, 1998, 117
- 26 D.W.Lewis, D.J.Willock, C.R.A.Catlow, J.M.Thomas, G.J.Hutchings, *Nature*, 1996, **382**, 604

**Chapter Seven****Experimental and Computational Studies on Polymeric Templates****7.1.0 Introduction**

The use of cationic polymers and oligomers as structure-directing agents is of interest because their incorporation into growing microporous solids necessarily imparts pore space connectivity. Furthermore, periodicity inherent in the template itself can direct crystallisation towards products with periodicity related to the polymeric repeat. Rollman *et al.* found that 'ionene' polymers (1,4-diazabicyclo[2.2.2]octane (DABCO) units linked by methylene chains containing different numbers of carbon atoms) 'templated' fault-free gmelinite from aluminosilicate gels<sup>[1]</sup>. This project has utilised similar species, with varying numbers of methylene groups in the interconnecting chains, in the synthesis of magnesium aluminophosphates.

In order to understand the role of polymeric templates, they were directly compared to the diquinuclidinium cations linked by methylene chains that were described in chapter four using a similar range of numbers of carbons. Whereas polymeric species give the medium pore structure MAPO-31<sup>[2]</sup> of variable particle size, the diquinuclidinium templates give cage and channel structures bounded at their widest point by large pores. It was observed during the course of this study that MAPO-31 samples of varying crystallinity could be prepared using different polymers, and since MAPO-31 is known to be an active and moderately selective catalyst for butene isomerisation<sup>[3]</sup> this reaction was examined over a selection of these solids with different particle sizes.

Also of interest in the study of this series of templates was the synthesis of MAPO-5 when using the DABCOC3 polymer. This is interesting because at first glance it appears that the larger pore material is being synthesised using the smaller template species, since DABCOC4-DABCOC8 produce MAPO-31. Decreasing the size of the methylene chain further to two carbons (i.e. DABCOC2) results in the synthesis of a new magnesium aluminium framework structure which at present is still unsolved.

### 7.2.0 Experimental

All templates were synthesised by the reaction of DABCO with  $\alpha,\omega$ -dibromoalkanes in refluxing ethanol for up to 48 hours. The synthesis of the organic templates and the synthesis of the magnesium aluminophosphates are discussed in more detail in chapters three and four respectively. However, it was found that the larger chained templates ( $n \geq 5$ ) required considerably less time to form and readily precipitated out of the ethanol, although this may be attributable to solubility effects rather than reaction kinetics. Once precipitated the solids were washed with cold ethyl acetate and acetone to remove unreacted starting materials. The products were characterised by elemental analysis and  $^{13}\text{C}$  and  $^1\text{H}$  NMR.

The solution spectra of these templates showed that the templates were not all forming as polymers. The  $^{13}\text{C}$  NMR spectra for the DABCOC3 and the DABCOC4 templates showed a peak in their spectra at around 44.5ppm. This peak is from the three carbon atoms attached to a nitrogen atom in the DABCO unit and indicates the termination of the polymer. By measuring the relative intensity of this peak to that from carbons in the fully quarternised DABCO it is possible to estimate the overall length of the template molecule. DABCOC5 and the longer templates do not show this peak indicating that these are forming as polymers. Figure 7.1 below shows the solution  $^{13}\text{C}$  NMR spectra obtained from DABCOC3 and DABCOC5, the latter of which has been expanded to demonstrate the absence of the peak at 44.5ppm.

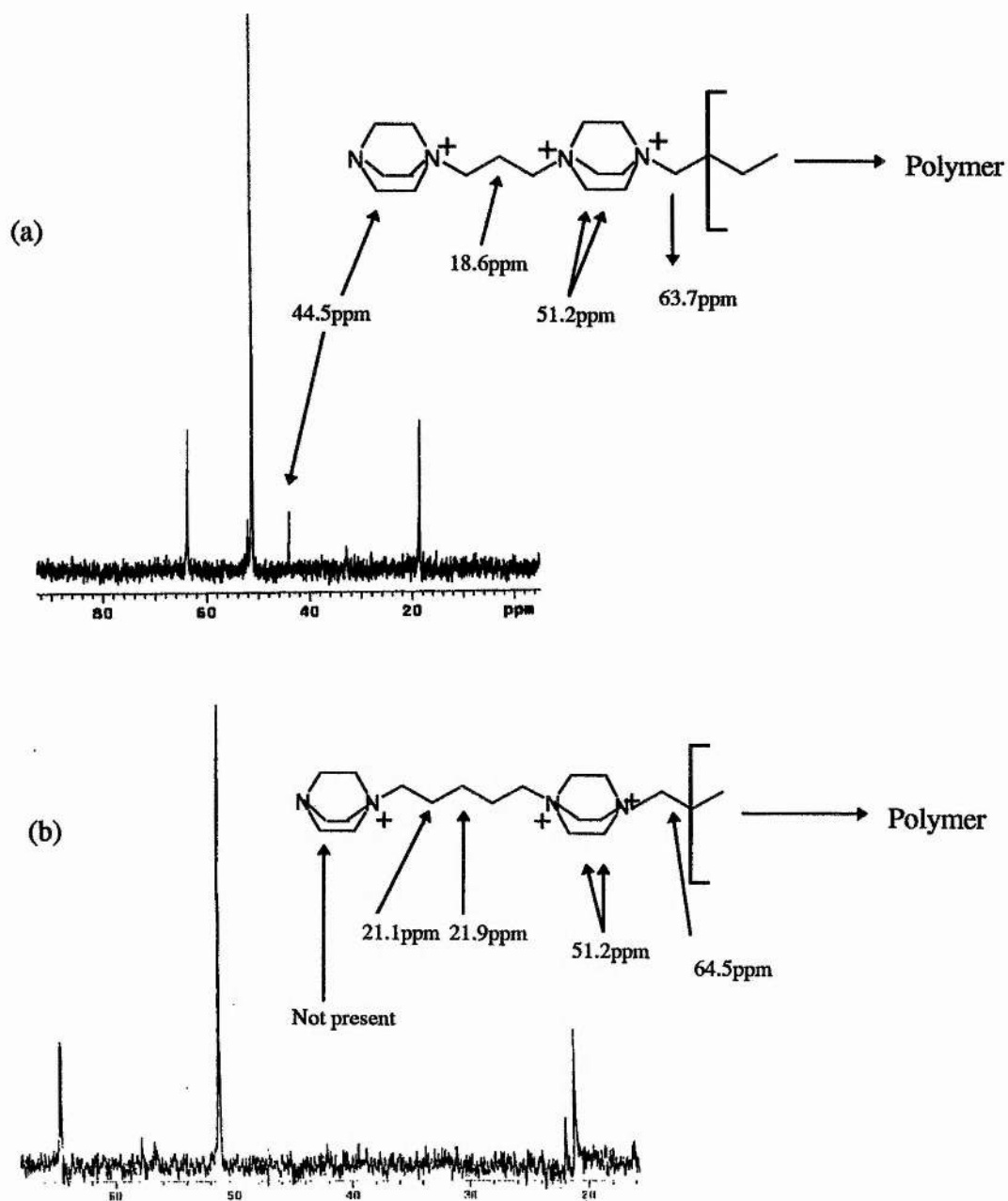


Figure 7.1 The  $^{13}\text{C}$  NMR spectra (solution) of (a) DABCOC3 and (b) DABCOC5 showing the absence of the resonance at 44.5ppm in the -C5 sample (caused by chain termination).

Hydrothermal syntheses of magnesium aluminophosphates were performed for 48 hours at 190°C using organic cations in the hydroxide form (as described in chapters three and four).

X-ray powder diffraction with monochromatic Cu  $K_{\alpha 1}$  radiation was performed using a STOE STADIP diffractometer and  $^{13}\text{C}$  MASNMR spectra of the products were collected by Dr. V. Patinec using a Bruker 500MHz NMR spectrometer.

Computer simulation of the fit of oligomeric units containing three DABCO units in the channel structures of the observed products was first performed by optimising the polymer chains outside the framework and then docking the polymers by eye. Subsequently, the energy of oligomeric units inside the pore structure was minimised using the CVFF forcefield within the program Discover<sup>[4]</sup> using a Silicon Graphics R8000 workstation. The framework structure was held fixed throughout the simulation. The author gratefully acknowledges the invaluable help of Dr. Paul Cox at the University of Portsmouth in performing these calculations.

It was found experimentally that changing the length of methylene chains within the polymeric templates results in a variation of particle sizes of the MAPO-31 product. In order to examine the effect of this on catalytic activity the skeletal isomerisation of butene over MAPO-31 samples prepared using DABCOC5, DABCOC6 and DABCOC7 templates was investigated. In the reactions 0.2g of pelletised sample was calcined at 550°C for 8 hours in oxygen to remove the template, and then contacted with a flow of but-1-ene (3 ml/min) in dry nitrogen (27 ml/min). The temperature was increased from 220°C to 380°C in 20°C steps and the product analysed using a gas sampling valve on a CE instruments GC8000 gas chromatograph fitted with a 25m long, 0.53mm diameter KCl /  $\text{Al}_2\text{O}_3$  PLOT column, which provided complete resolution of hydrocarbons containing up to five carbons.

**7.3.0 Results and Discussion**

The results of syntheses employing ionene (DABCO $C_n$ ) polymers and, for comparison, diquinuclidinium cations (Quin $C_n$ ), are given in Table 7.1. The ratio of MgO:Al<sub>2</sub>O<sub>3</sub>:P<sub>2</sub>O<sub>5</sub>: R(OH)<sub>2</sub>:H<sub>2</sub>O in the gel was initially kept at 0.1:0.45:0.5:0.4:40. Syntheses were also performed using DABCO and quinuclidine only as templates. These gave MAPO-5 and MAPO-16 respectively as products.

Number of carbons in methylene chain, n	MAPO produced with DABCO $C_n$	MAPO produced with Quin $C_n$
2	STA-3 (unknown)	MAPO-5
3	MAPO-5	MAPO-17
4	MAPO-31,-5	STA-2, MAPO-56*
5	MAPO-31	STA-2
6	MAPO-31	MAPO-5
7	MAPO-31	MAPO-5, STA-1
8	MAPO-31, some STA-1	STA-1, MAPO-5

Table 7.1 Magnesium aluminophosphate products of syntheses

As well as being used to identify the crystalline reaction products, x-ray diffraction reveals that some of the MAPO-31 samples exhibit considerable line broadening, especially for reflections of the type (hkl), where l is not zero as shown below.

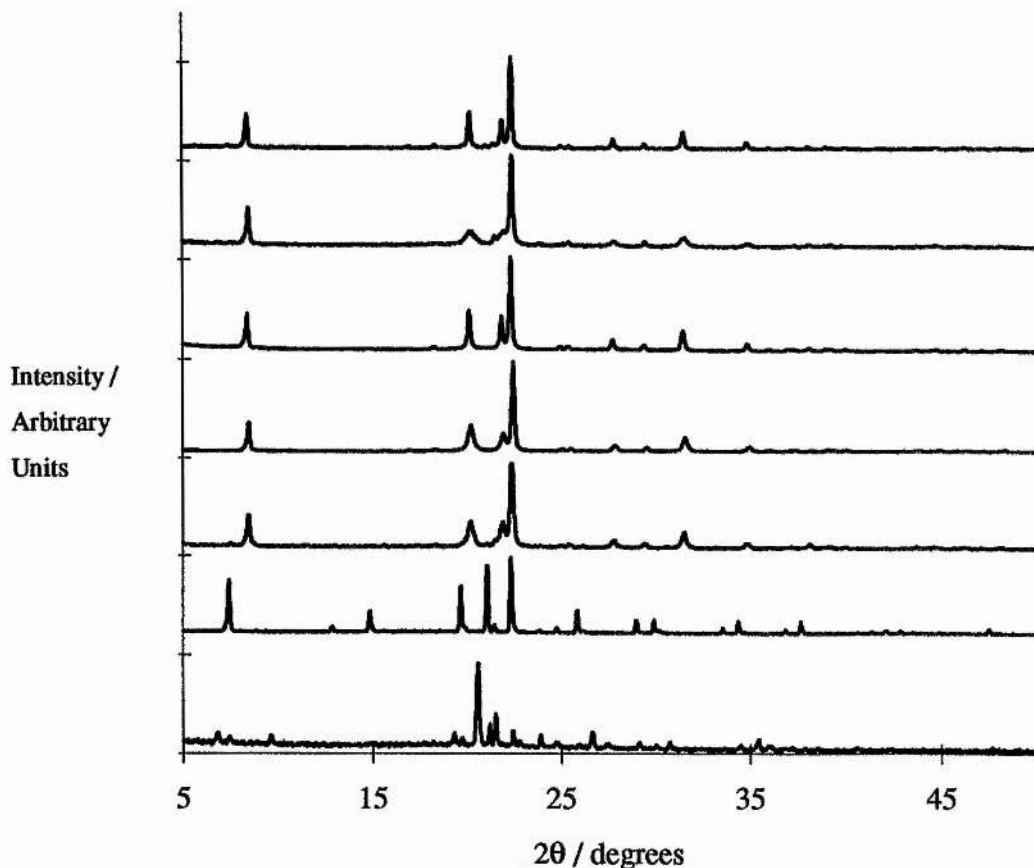


Figure 7.2 X-ray diffractograms of the MAPO samples prepared with (from the bottom) DABCO-C2, -C3, -C4 -C5, -C6, -C7 and -C8 templates.

Figure 7.1 is really to illustrate the range of products that are formed using the ionene compared to the diquinuclidinium templates (the corresponding diffractograms for the diquinuclidinium templates are shown in chapter four (figure 4.11)). For samples prepared with DABCO-C4, -C5 and especially -C7 ( $hkl$ ) reflections with  $l$  not zero are broadened, whereas for samples prepared with DABCO-C6 and DABCO-C8 they are narrower, and have similar linewidth to the ( $hk0$ ) reflections as illustrated below in figure 7.3. The line broadening is retained upon calcination (see figure 7.4).

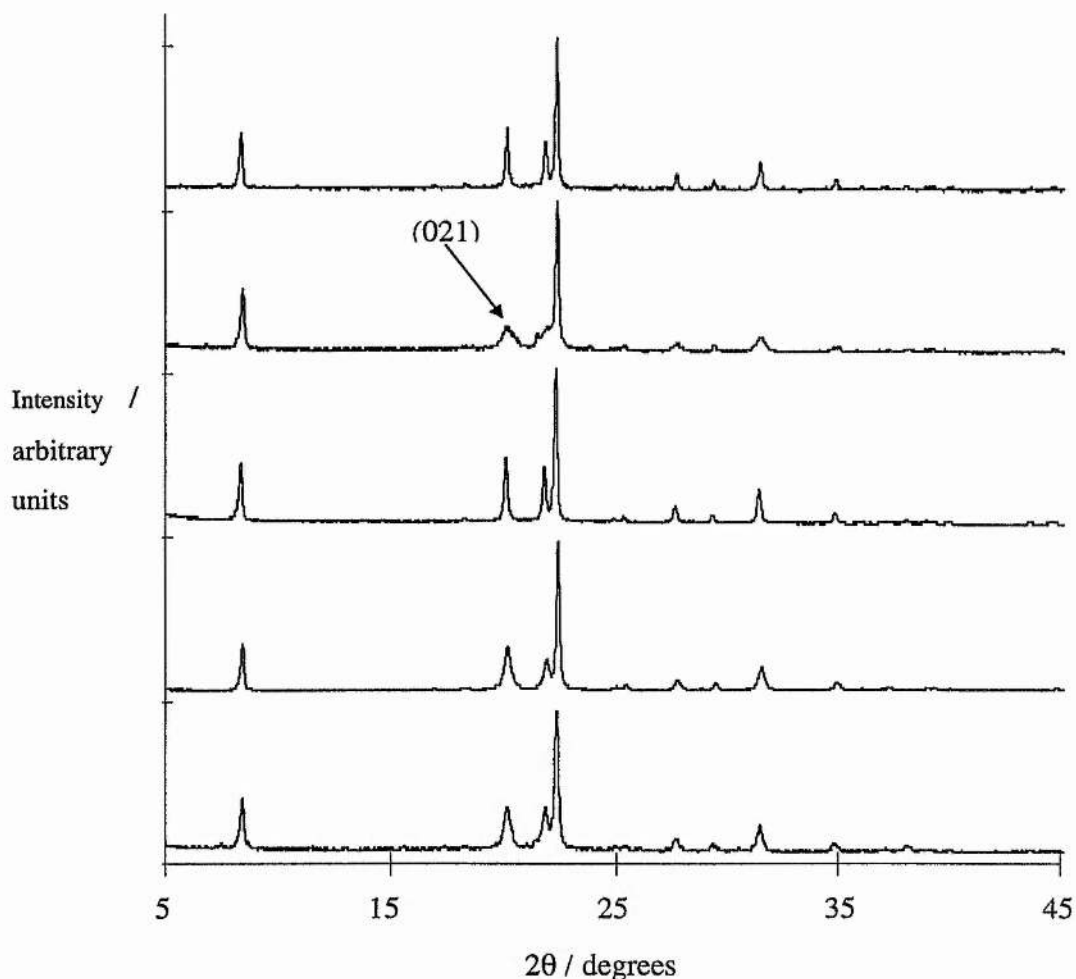


Figure 7.3 X-ray diffractograms of the MAPO-31 materials prepared by (from the bottom) DABCO-C4, -C5, -C6, -C7 and C-8 templates. The line broadening of the (021) peak, which is labelled for the  $n=7$  templated material is clearly visible for both the  $n=4, 5$  and  $7$  samples.

The cause of this line broadening must be reduced coherence length in the  $c$ -direction of the MAPO-31 structure. Optical light microscopy using a polarizing microscope showed that for  $n=6$  and  $8$ , small crystallites a few microns in all dimensions are present, whereas for  $n=4, 5$  and  $7$  no discrete crystallites are observed. For the DABCO-C7 sample shown in figure 7.3 above, application of the Scherrer formula<sup>[5]</sup> (using the peak

width of the (021) reflection and correcting for instrumental resolution) gives a coherence length of around 200Å in the *c* direction.

### 7.3.1 Scanning Electron Microscopy

To further investigate the particle size of the crystallites formed by the different ionene templates, scanning electron microscopy was performed using a JEOL JSM-35CF microscope. Selected area energy dispersive x-ray analysis (EDX) was also performed on these materials, revealing that all of the materials are essentially identical in terms of framework composition. This implies that the differences observed in the x-ray diffractograms between the different samples is probably due to either different crystallite sizes (which would cause peak broadening) or faulting of the MAPO-31 structure.

SEM analysis confirmed that the DABCOC6-MAPO forms have the largest crystallites and that the DABCO-C4, -C5 and -C7 templated materials do not have a definite crystal appearance. The particle size of MAPO samples prepared with C5, C6, C7 and C8 polymers decreases in the order C6, C8 > C5 > C7. These decreasing particle sizes correlate well with the extent of the observed line broadening in the materials' respective x-ray diffraction patterns.

It is important therefore to determine if the line broadening observed in the x-ray diffraction patterns of the MAPOs is caused by either (a) particle size effects or (b) structural faulting in the *c*-direction of the MAPO-31 structure. The different particle sizes confirmed by both scanning electron and optical microscopy means that particle size effects must be contributing to the observed line broadening in the x-ray diffractograms but what about framework distortions?

If the occluded templates are exerting stress on the framework of the MAPO-31 structure, it would be reasonable to assume that removing the template from the framework would relieve the stress and consequently permit the framework to adjust to a less energetic position. This in turn would alter the appearance of the observed x-ray

diffraction pattern. To test this theory a sample of the DABCOC5 templated sample was calcined at 550°C for 8 hours in flowing oxygen to ensure template removal. The x-ray diffractograms of this sample before and after calcination are shown below in figure 7.4. Due to similarity of these two diffractograms, it seems unlikely that structural distortion along the *c*-direction of the MAPO-31 samples is responsible for the line broadening observed in the x-ray diffractograms. This means that the line broadening is indeed caused by the different crystallite sizes observed earlier.

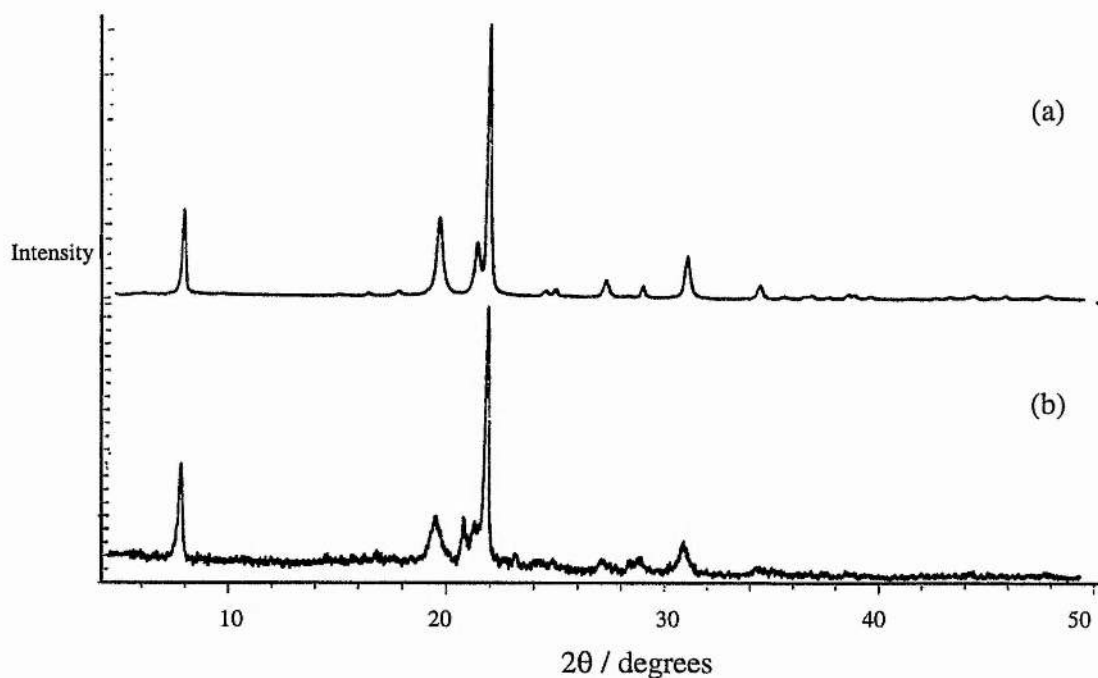


Figure 7.4 X-ray diffractograms of a DABCOC5 templated MAPO (a) before and (b) after calcination. The similarity between these two patterns prove that the observed line broadening observed for this template series is due to particle size effects.

### 7.3.2 Solid State MASNMR

All of the MAPOs were synthesised several times under exactly the same conditions as each other differing only in the nature of the DABCO<sub>n</sub> template added to the synthesis gel. Each time the same results were obtained, namely that the DABCO<sub>6</sub> templated MAPO was the most crystalline material, with the DABCO-C<sub>4</sub>, -C<sub>5</sub> and -C<sub>7</sub> templated materials exhibiting similarly broad peaks in their x-ray diffractograms as the ones illustrated previously. As the nature of the template was the only significant difference between syntheses, the template must be affecting the extent of the crystallisation of the MAPO-31 structure.

It is important therefore to determine the nature and amount of the organic species present inside of the MAPO-31 structures, consequently <sup>13</sup>C MASNMR and thermal analysis was carried out on selected samples.

Solid state <sup>13</sup>C MASNMR of selected MAPO's templated by diquinuclidinium ions shows that the cations remain intact during synthesis<sup>[6,7]</sup>. For the DABCO<sub>n</sub> templated species it is found that there is a small amount of fragmentation of the polymers, as shown by the appearance of a resonance at around 45 ppm corresponding to terminal tertiary amine species. Carbon-13 MASNMR spectra for the MAPO synthesised using DABCO<sub>3</sub> -C<sub>8</sub> (excluding the DABCO<sub>5</sub> sample) are shown below in figure 7.5. The intensity of this peak indicates average oligomeric chain lengths of around 4 DABCO units for the DABCO-C<sub>4</sub> polymers, with the chain length increasing for the entrapped DABCO-C<sub>7</sub> and DABCO-C<sub>8</sub> species (which have much smaller amounts of end-groups).

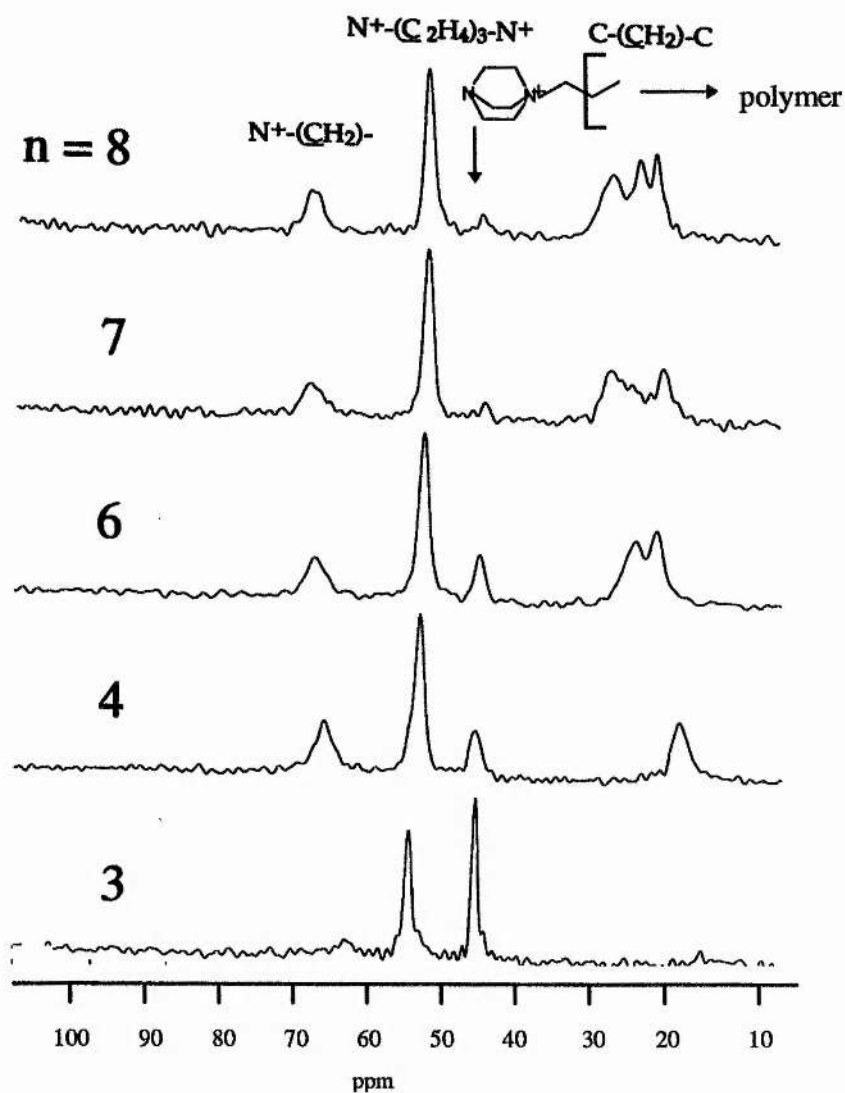


Figure 1.4  $^{13}\text{C}$  MASNMR spectra for the DABCO $_n$  templated MAPOs. The appearance of the peak at 45.5 ppm indicates that the polymer template is fragmenting within the MAPO as this is due to the carbon atoms indicated above. The other peaks are also as indicated in the diagram.

### 7.3.3 Thermal Analysis

Thermal gravimetric and differential thermal analysis were performed simultaneously on several of the MAPOs using a SDT 2960 analyser from TA Instruments. The MAPO-5

material containing the DABCOC3 template showed a gradual weight loss typical of these magnesium aluminophosphate materials and had a total weight loss of 14.37%. Water is likely to attribute approximately 2.52 % of this weight loss as this occurred below 200°C and under endothermic conditions which are usually associated with water desorbing from the microporous framework.

The MAPO-31 sample by comparison exhibits a slightly larger and steeper weight loss than the MAPO-5 sample. There is a similar weight loss due to water (2.65 %) but an increased weight loss can be attributed to the removal of the template (14.79%) giving an overall weight loss of 17.44%. Both samples were analysed under flowing air with a 5°C temperature increase per minute up to 800°C and their TGA isotherms are shown below in figure 7.6.

The formation of MAPO-5 by the apparently smaller DABCOC3 template therefore becomes more understandable since DABCO on its own is known to promote the formation of the MAPO-5 structure.

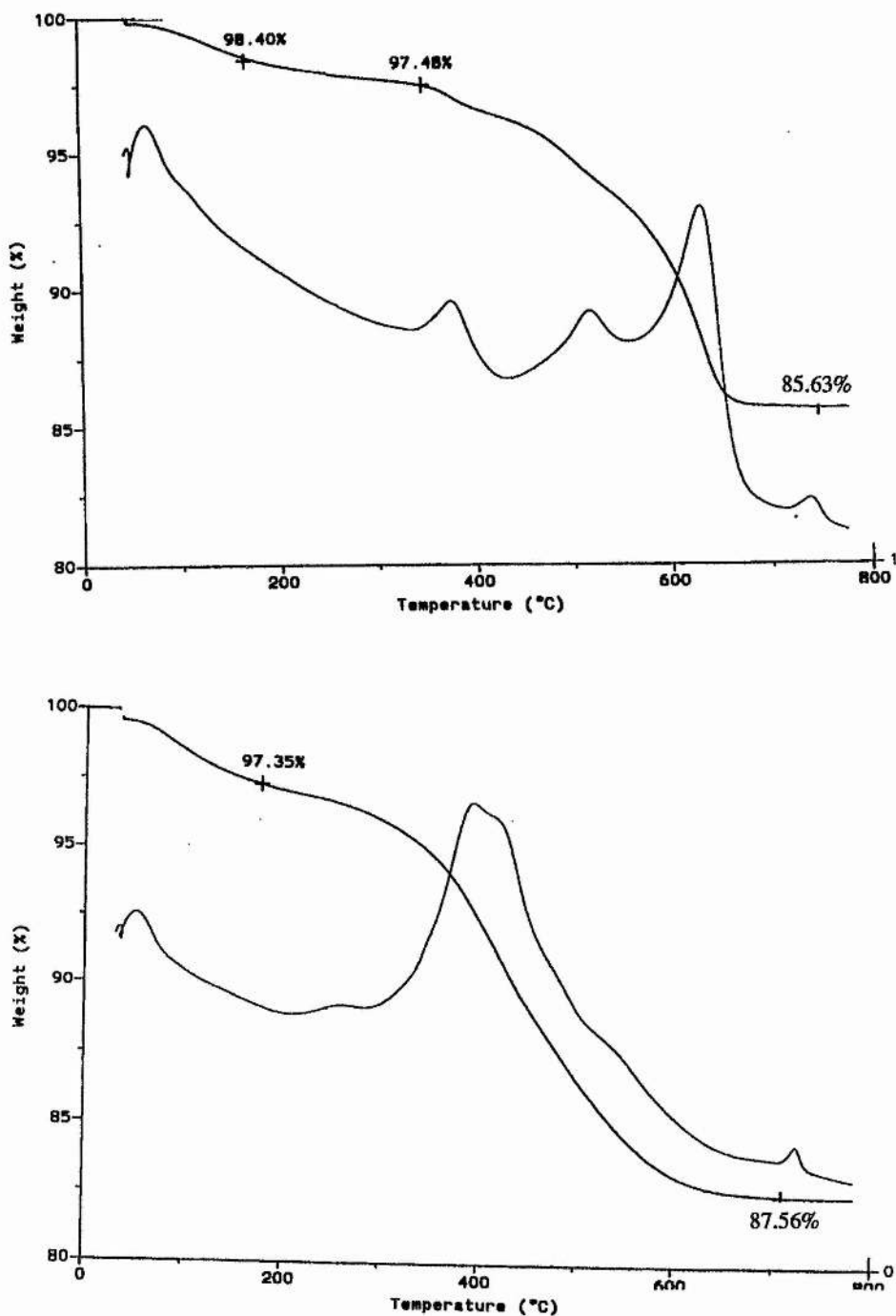


Figure 7.6 TGA/DTA profiles for the MAPOs templated by (top) DABCOC3 and (bottom) DABCOC5.

### 7.3.4 Computer Modelling

The use of polymeric templates DABCO $C_n$ , with  $n=4-8$ , results in the crystallisation of the medium pore MAPO-31, with variable crystallinity, as shown in figure 7.1. STA-1 co-crystallised in some preparations when the  $n=8$  polymer is used, however due to its small particle size separation of the STA-1 and MAPO-31 materials was not possible. A diffractogram showing the STA-1 / MAPO-31 mixture is shown below in figure 7.7.

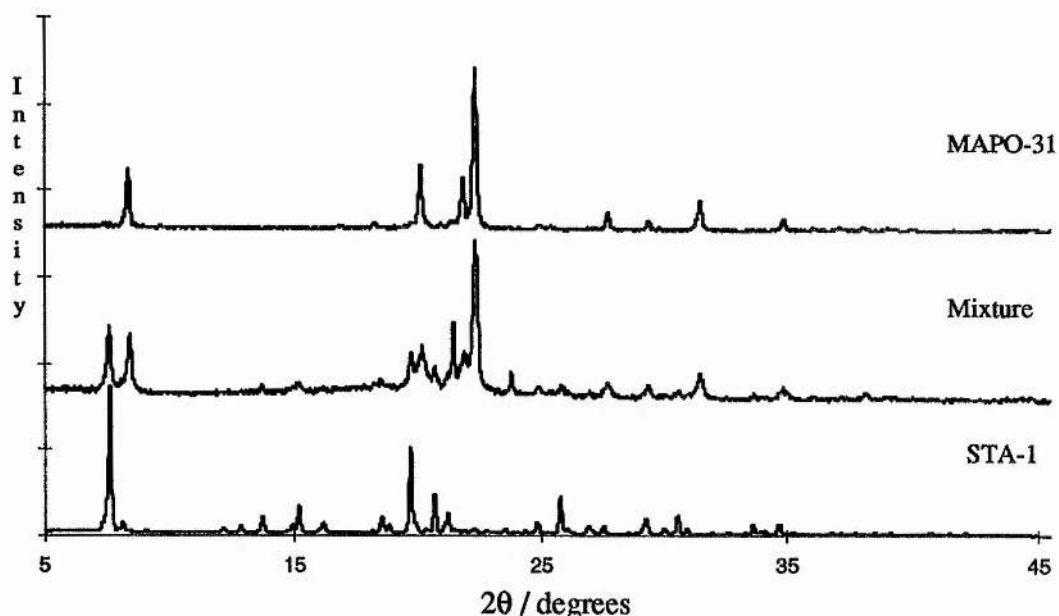


Figure 7.7 X-ray diffractogram showing the MAPO-31 / STA-1 mixture after using the DABCO8 template.

Using the  $n=3$  product, MAPO-5 is prepared phase pure and highly crystalline. It is of interest to know why MAPO-31 (pore diameter  $5.4\text{\AA}$ ) is favoured over MAPO-5 (pore diameter  $7.3\text{\AA}$ ) for the polymeric cations, whereas for the similarly-shaped diquinclidinium species preference is for the larger pore materials. Also, why do the  $n=6$  and  $8$  polymer templates give more crystalline MAPO-31 than the other polymers? It is also interesting that STA-1 can be templated by a polymeric cation.

To investigate these issues the non-Coulombic interactions of the polymeric templates with MgAPO-5, MgAPO-31 and STA-1 were investigated using computer modelling. Pore maps (framework van der Waals surfaces) of the AFI and ATO structures reveal that the AFI has approximately cylindrical large pore channels whose internal diameter oscillates so that adjacent wider portions are 4.24 Å apart whereas the medium pore channels of ATO can be viewed as a series of alternating and linked 'triangular' cavities, with each successive cavity 2.5Å apart and rotated by 60° with respect to each other.

Oligomers of the form DABCO-(CH<sub>2</sub>)<sub>n</sub>-DABCO-(CH<sub>2</sub>)<sub>n</sub>-DABCO were modelled outside the frameworks. Each DABCO unit is triangular in cross section viewed along the polymer chain, and the lowest energy configuration of successive DABCO units depends on whether the number of CH<sub>2</sub> groups linking them is even or uneven. When n is odd, successive DABCO units are aligned with their triangular cross sections in the same orientation, but when n is even, they are rotated by 60° with respect to each other. Fractions of the polymer chains can be compared to the ATO and AFI channels in terms of repeat length of DABCO units compared to repeat lengths between wider channel portions, and for ATO, relative orientation of the cross sectional triangles of the DABCO units and of the 'triangular cavities' of the pores. DABCO-C6 and -C8 units are found to match the repeat unit of the ATO structure closely, the orientations of each DABCO unit and triangular section of the ATO pore structure are the same, and the orientations of the DABCO units alternate in orientation. All of these factors favour crystallisation of highly ordered ATO. For n=4 the fits of repeat unit is not as close, and for n = 5 and 7 the DABCO units do not fit the triangular pore space closely on both sides of the channel.

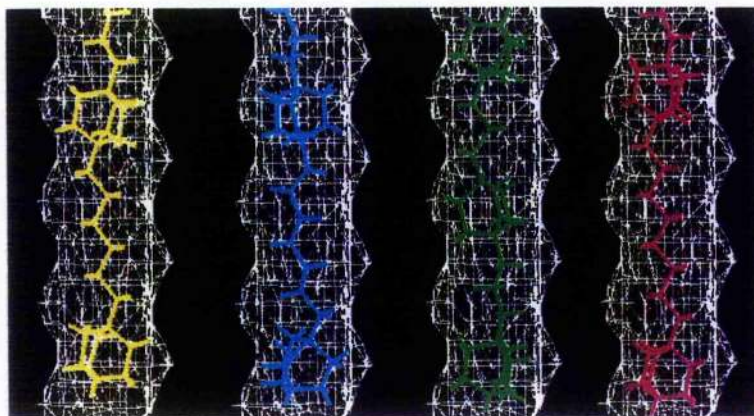


Figure 7.8 Energy minimised positions of selected oligomers within the ATO structure, From left to right, the DABCO-C6, -C7, -C3 and -C8 oligomers are shown in the pores.

To support this initial modelling, energy minimisation has been performed for oligomers with different methylene chain lengths. Only non-Coulombic interactions between the oligomeric units and the oxygen atoms are calculated. Although previous comparison with experimental data has shown that this approach gives good predictions for conformations within a single framework host, relative binding energies for a template molecule within different hosts are not expected to be so reliable. Selected results of our calculations of the oligomers within MAPO-31 are shown in figure 7.8. When considering the interactions of oligomers with the MAPO-31 structure, a significantly higher (less favourable) energy is calculated for the docking of the DABCO-C7 polymer compared to either the DABCO-C6 or DABCO-C8 polymers, as suggested previously by the docking configurations. For the  $n=6$  product, a fully periodic simulation has been carried out using a  $1 \times 1 \times 5$  supercell of the ATO structure and a portion of the polymer that is made up of 2 DABCO units and 2  $-(\text{CH}_2)_6-$  chains (The coordinates used are given in appendix 4). Including simulated atomic coordinates of the template in the ATO structure, taking statistical occupancy into account, a close fit to the experimental x-ray diffraction data is obtained (Figure 7.9). A combination of computer modelling and x-ray powder diffraction can therefore be used to propose models for the location of templates where diffraction techniques alone would not suffice.

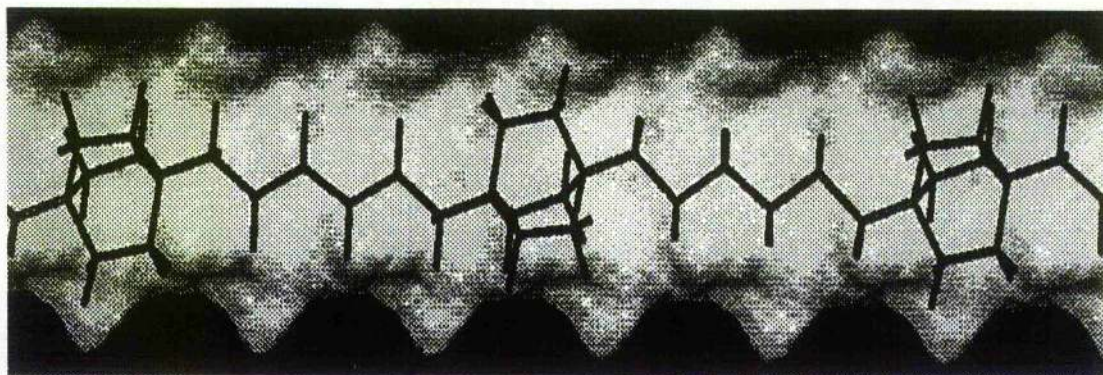


Figure 7.9(a) The DABCOC6 polymer within ATO, showing the close relationship between the periodicity of the oligomer and the MAPO-31 framework.

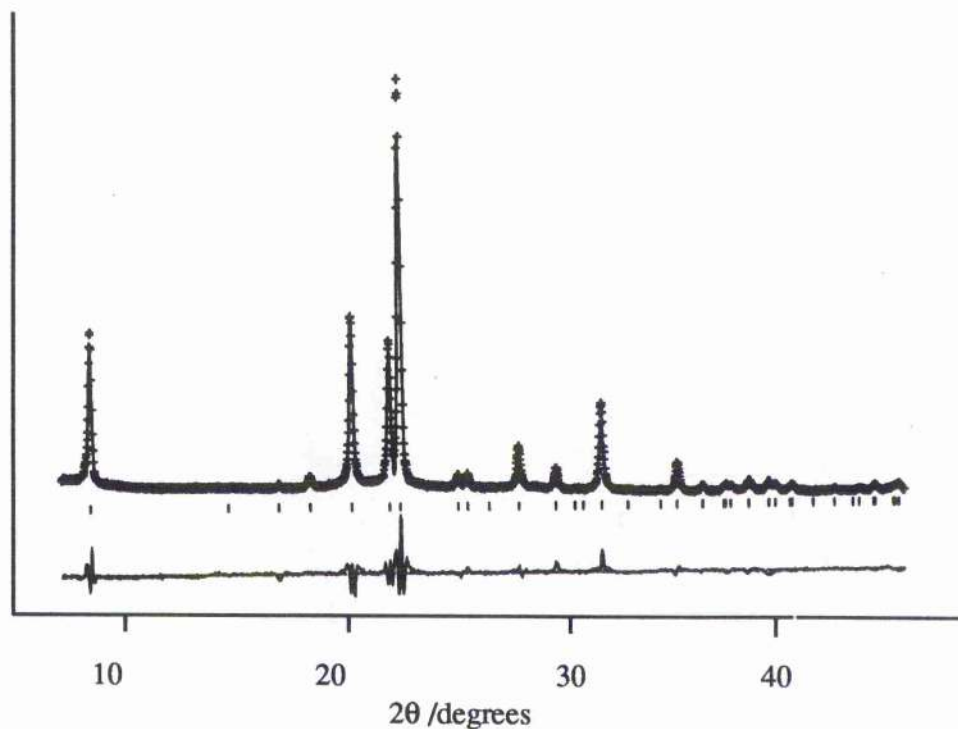


Figure 7.9(b) Profile fit and difference plot of X-ray data on MAPO-31 templated by DABCO-C6, ( $a=20.996(2)$ ,  $c=5.025(1)\text{\AA}$ ,  $R_{wp}=10.3\%$ )

When comparing calculated interaction energies of oligomers within the ATO and AFI structures, it is found that they are significantly less favourable for the ATO structure for

all values of  $n$ . Given the observation that all polymers give the ATO structure, this is unexpected, and underlines the difficulties of comparing calculations performed on different host solids. More sophisticated calculations that take into account lattice relaxation, Coulombic interactions, longer oligomeric units and even interaction with occluded water molecules will be required before binding energies for different frameworks can be compared directly.

### 7.3.5 Structure Blocking

Experimentally it was observed that the addition of DABCOC3 to a magnesium aluminophosphate synthesis gel promoted the formation of MAPO-5, probably due to the template fragmenting during synthesis. DABCOC6 by comparison appears to be more stable and promotes the MAPO-31 structure. The reasons for this were identified from the computer modelling studies carried out at Portsmouth showing that there was an almost ideal correlation between the alternating DABCO repeat unit and the MAPO-31 structure. In an attempt to determine how strong this interaction was and how efficiently the DABCOC6 polymeric template could synthesise MAPO-31, a series of mixed DABCOC3 / DABCOC6 polymers were synthesised by adding varying amounts of 1,3-dibromopropane and 1,6-dibromohexane together in the synthesis of the template. These mixed polymers were then converted to the hydroxide form as described earlier and used in the synthesis of magnesium aluminophosphates as before.

It was thought that increasing the amount of DABCOC3 to the resultant polymer should result in sharp an increase in the formation of MAPO-5, but this was not observed.

Relative amount of DABCOC3 (%)	Relative amount of DABCOC6 (%)	Phase formed
0	100	MAPO-31
5	95	MAPO-31
50	50	MAPO-31
75	25	MAPO-31
85	15	MAPO-5/MAPO-31
95	5	MAPO-5
100	0	MAPO-5

Table 7.2 Phase summary of the MAPOs produced using mixed polymeric templates.

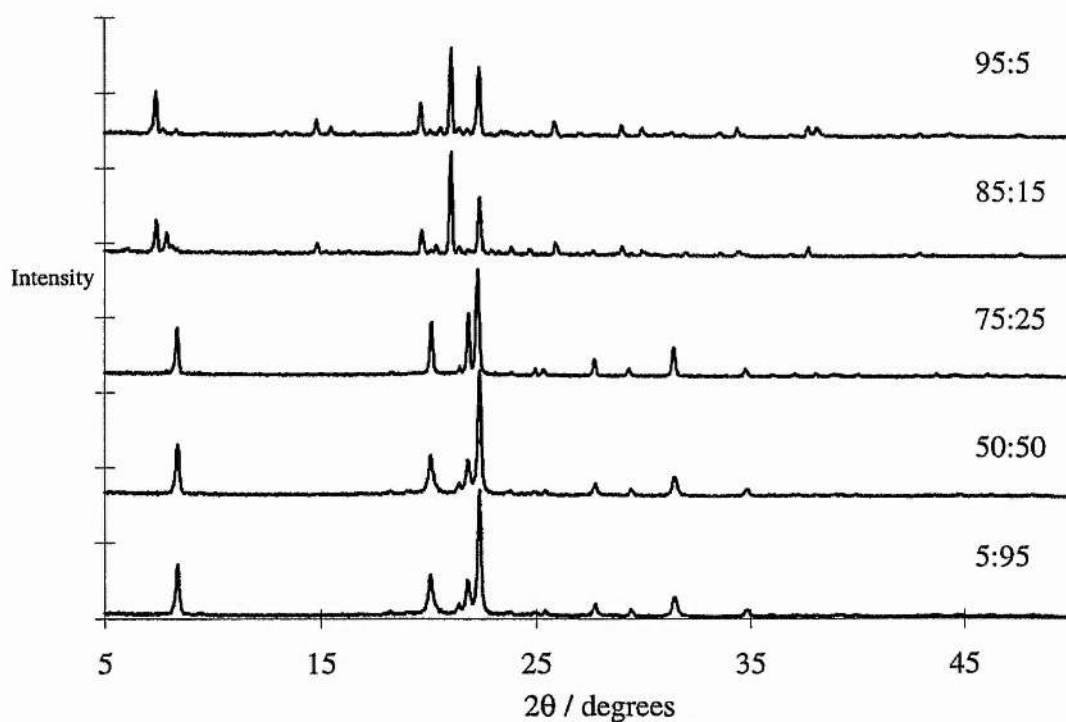


Figure 7.10 X-ray diffractograms of the MAPOs produced by the mixed polymeric templates. The numbers indicate the relative amount of DABCOC3 : DABCOC6 used in the synthesis of the template.

The incorporation of up to 85% DABCOC3 in the mixed polymeric template before the production of MAPO-5 is observed is surprising. The lack of mixed MAPO phases is also surprising (with the exception of the 85:15 mixture) as one would expect to see a mixture of MAPO-5 **and** MAPO-31 as the amount of DABCOC6 was increased, as opposed to MAPO-5 **or** MAPO-31. Jacobs *et al* whilst investigating the template effects of 15-crown-5 and 18-crown-6 on faujasite, witnessed a range of mixed compositions in their product as the amounts of each ether were varied<sup>[6]</sup>.

Two possible reasons for the selective behaviour observed in the synthesis of these MAPOs include possible fragmentation of the polymer and the relative strength of the DABCOC6 / MAPO-31 interaction compared to the DABCOC3 / MAPO-5 interaction. If the DABCOC6 templating influence was stronger than the DABCOC3 effect on the synthesis gel then MAPO-31 would crystallise preferentially to MAPO-5. Also the individual DABCOC3 polymer is known to fragment during the synthesis of magnesium aluminophosphates and if this were the case, short oligomers could probably be accommodated throughout the forming MAPO-31 structure, provided they were sufficiently interspersed with the DABCOC6 chains. This is likely to be the main reason why the relatively high concentrations of DABCOC3 in the mixed polymer are required to arrest the synthesis of MAPO-31 and promote the formation of MAPO-5 which could in turn accommodate DABCOC6 oligomers / polymers.

In the course of this research it has not been possible to unambiguously determine the exact composition and structure of the mixed templates before or after use as templates. The best way to study the organic templates either in solution or in the solid phase is by NMR spectroscopy. However, as many of the DABCOC3 and DABCOC6 peaks would overlap it would not be possible to determine the actual composition of the overall polymer. It is very probable that the polymers produced did not contain the same ratios as those intended i.e. a 50:50 DABCOC3 : DABCOC6 reaction mixture might not have produced a polymer containing a 50:50 ratio of 3- : 6-membered methylene chains. The relative rates of formation of the individual DABCOC6 polymers and DABCOC3 polymers suggest that DABCO reacts more quickly with 1,6-dibromohexane than with 1,3-dibromopropane and as such implies that the mixed polymer is likely to have a

series of 6-methylene chains interspersed with sections of 3-methylene units. This assumption is supported with the experimental observations outlined above.

Although not decisive, microanalysis was performed on the mixed polymers in an attempt to estimate the relative amounts of the incorporated 3- and 6-membered methylene chains. The results are listed in table 7.3 and the changing CHN compositions confirm that both 3- and 6-membered methylene chains have been incorporated into the mixed polymers. Gel permeation chromatography was considered as a means to determine the molecular weight of the polymers and hence give an accurate estimate of the length of the polymers. Unfortunately the water soluble nature of these polymers makes them unsuitable for this technique, as the water and similarly polar solvents can damage the column used in the process. The solubility of the polymers into more suitable solvents was not possible.

C3 : C6	% C		%H		%N	
	Predicted	Actual	Predicted	Actual	Predicted	Actual
100 : 0	34.42	30.08	5.78	6.38	8.92	7.97
95 : 5	34.72	30.77	5.80	5.77	8.87	7.78
75 : 25	35.93	31.67	6.03	6.19	8.66	7.53
50 : 50	37.45	35.52	6.29	6.02	8.40	7.20
25 : 75	38.96	35.17	6.54	6.54	8.13	7.18
0 : 100	40.47	36.12	6.79	6.91	7.87	6.89

Table 7.3 Microanalysis results for the mixed polymer templates. The table indicates that mixed polymers have been synthesised as their CHN values tend to lie between the two end member's values. The exact polymer composition can not, however, be determined.

### 7.3.6 Catalysis

MAPO-31 samples templated using DABCO-C5, DABCO-C6 and DABCO-C7, when converted into the acid form by calcination, showed similar product distributions in the reaction of butene. The solids all catalyse the skeletal isomerisation of but-1-ene as well as the more facile double bond isomerisation but they also catalyse the formation of hydrocarbons with 3 and 5 carbon atoms. The mechanism of this reaction has been discussed at length in the literature<sup>[7]</sup> - here we confine ourselves to noting that the rate of skeletal isomerisation of butene to 2-methylpropene, and the consequent approach towards an equilibrium distribution of butene isomers, is fastest for the most poorly crystalline DABCO-C7 templated solid and decreases for materials prepared using DABCO-C5 and DABCO-C6 (Figure 7.11)

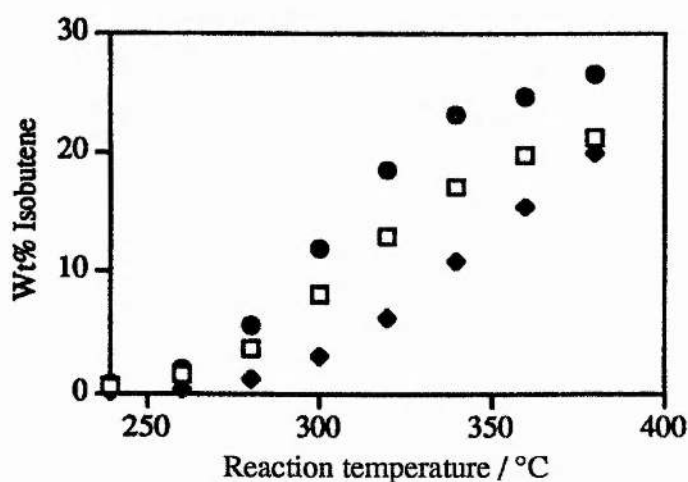


Figure 7.11 Weight% isobutene for isomerisation of but-1-ene (WHSV=2.5) over MgAPO-31 synthesised with DABCO-C5 (□) DABCO-C6 (■) and DABCO-C7 (●) templates (P.A. Wright *et al*<sup>[8]</sup>)

### 7.3.7 Synthesis of STA-3 using DABCOC2

As part of a series of syntheses the template effect of DABCO units joined by short 2-membered methylene chains were investigated. Unlike DABCO and DABCOC3 which both promote the formation of MAPO-5, DABCOC2 appears to favour the formation of

another material whose unidentified diffraction pattern indicates that this is a new microporous material.

The material is known to incorporate organic template molecules, as the MAPO turns from creamy yellow to black when heated briefly to 400°C under flowing air indicating the coking effect commonly observed during template removal. Insufficient quantities of the material have been obtained however to permit *in situ* examination of the template by  $^{13}\text{C}$  MASNMR. Similarly, due to the destructive nature of micro- and thermal analysis, these techniques have not been used on the material which shall now be called STA-3. The diffraction pattern of STA-3 is shown below with MAPO-5 and MAPO-31 for comparison.

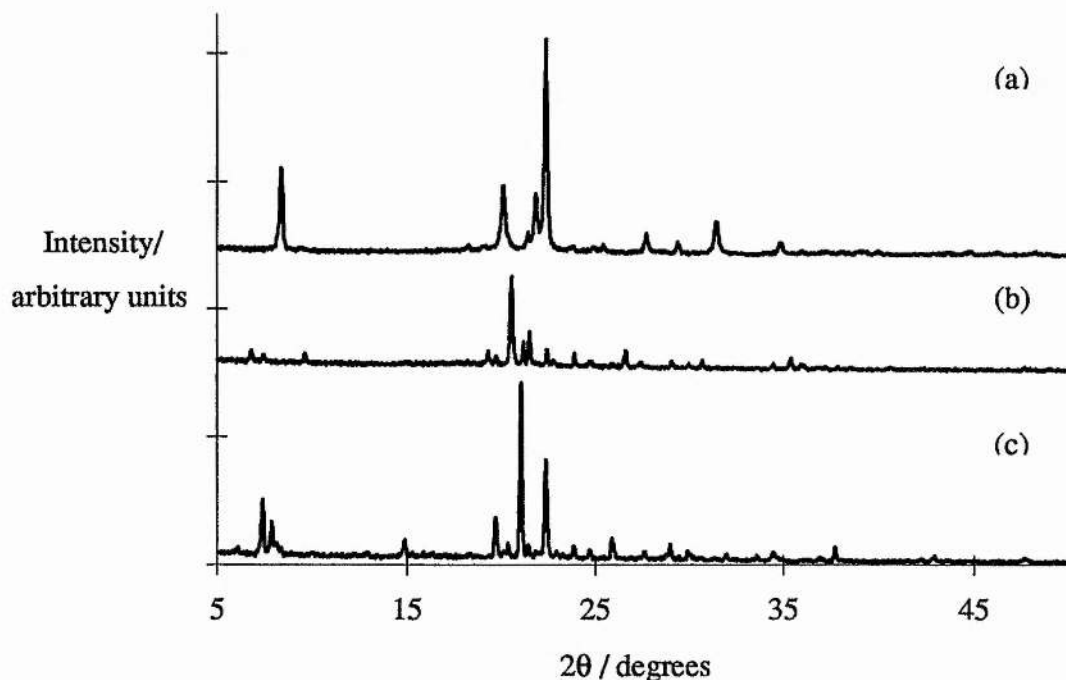


Figure 7.12 X-ray diffractograms of (a) MAPO-31 synthesised using DABCOC6, (b) STA-3 synthesised using DABCOC2 and (c) MAPO-5 synthesised using DABCOC3. The unique XRD pattern of the STA-3 material indicates that it is an unknown material.

STA-3 is readily synthesised using the same reaction conditions as those outlined in chapter four and has also been formed as a SAPO although not as an  $ALPO_4$ . Calcination of the material at  $500^\circ C$  for four hours in flowing oxygen results in no appreciable loss of framework crystallinity as determined by x-ray powder diffraction. The calcined sample as shown below actually has an improved x-ray powder diffractogram to the as-prepared sample since the peaks are narrower and more intense. Increased peak intensity is a common feature amongst microporous solids as the template is removed.

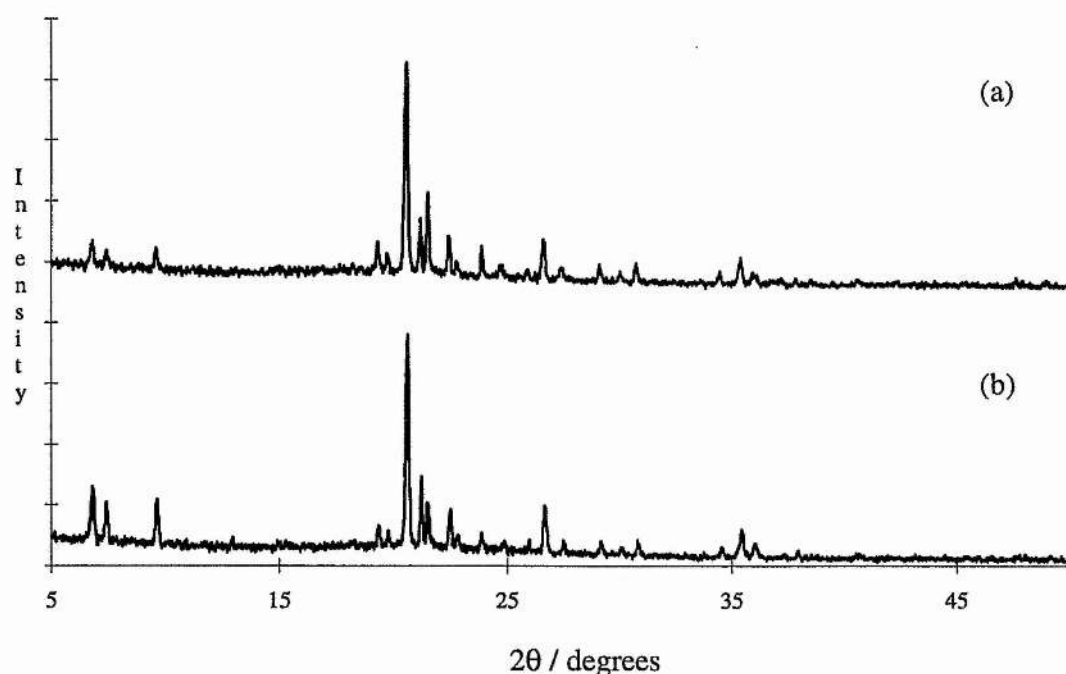


Figure 7.13 X-ray diffractograms of STA-3 (a) before and (b) after calcination at  $500^\circ C$  in flowing oxygen for six hours. The calcined sample exhibits improved crystallinity to the as-prepared sample.

Indexing the material has proved to be difficult and at present all attempts to index STA-3 using VISSER<sup>[11]</sup> have proven to be unsuccessful. The lack of known crystallographic information on STA-3, makes it extremely difficult to establish a model from which to begin structural solution or refinement programs. The similarity of the

STA-3 diffraction pattern and the fact that the material is produced by a similar (albeit smaller) template to MAPO-31, suggests that STA-3 and MAPO-31 could be related, structurally. STA-3 is therefore likely to have a medium pore channel type structure.

Scanning electron microscopy performed on the material reveals the crystallites to have no definite crystal morphology and consequently are unlikely to be of use in single microcrystal diffraction experiments such as those used to resolve the structures of STA-1 and STA-2 (see chapters five and six respectively). It is important therefore to improve the quality of the STA-3 crystallites in terms of size and morphology so that the structure solution of this material can be achieved. This was the motivation for beginning a series of experiments based on observations obtained from previous synthetic experiments as outlined in chapter four.

The reaction time, temperature of reaction, pH, water concentration and the addition of sodium cations were all investigated. It was determined that the synthesis of STA-3 was achieved between 1 and 3 days, with the optimal reaction time being 2 days. The optimal pH was determined to be 6 although preparations performed at pH6, 7, and 8 were all successful. Increasing the amount of water from 3 to 25ml was advantageous in the synthesis of STA-2 but not so for synthesis of STA-3 which favoured the more highly concentrated synthesis gels. Heating temperatures of 100, 160 and 190°C were all successful (though required different reaction times). A temperature of 190°C was used mainly in the course of this work since this maintained similar standards to the rest of the syntheses described in this thesis. 160°C may be more beneficial to the synthesis of STA-3 however as this produced a very highly crystalline material (but not phase pure). Finally, the addition of sodium cations in the form of sodium hydroxide (as used in the STA-2 preparations) was studied. No significant increase in crystal size was detected by visual inspection using an optical microscope.

#### **7.4.0 Conclusions**

The periodic distance between DABCO units in the oligomeric and polymeric templates described in this chapter have a major influence on the aluminophosphate products that

form. Unlike their diquinuclidinium analogues, the DABCO based templates form channel type structures irrespective of the length of the interconnecting methylene chain, and in doing so they have an influence on the particle size and consequently on the catalytic activity. It is found that the differences in particle size of MAPO-31 that result from using different polymeric / oligomeric species, and which result in the broadening of diffraction peaks, have an influence on the catalytic activity of the materials, once converted into the acid form, for the skeletal isomerisation of butene. The activity increases with decreasing particle size, and it is likely that this is due both to the lower average distance a reactant molecule must diffuse through the medium pore structure to the active sites in the pores and also to the lower susceptibility of smaller crystallites to deactivation by coking.

The discovery of another novel material is also of much interest as it can be readily synthesised in a variety of different compositions. The structure solution of this material although presently elusive may confirm the working hypothesis that the material is likely to have a small or medium pore channel type structure. The different framework compositions and the stable framework architecture of the material may make it ideal for solid acid catalysis similar to MAPO-31.

### 7.5.0 References

- 1 R.H.Daniels, G.T.Kerr and L.D.Rollman, *J.Am.Chem.Soc.*, 1978, **100**, 3097-3100
- 2 J.M.Bennett and R.M.Kirchner, *Zeolites*, 1992, **12**, 338
- 3 H.L.Zubowa, M.Richter, U.Roost, B.Parlitz, R.Fricke *Catal.Lett.*, 1993, **19**,67
- 4 Discover 3.1 program, MSI, San Diego, USA.
- 5 A.K. Cheetham and P. Day, *Solid State Chemistry Techniques*, Clarendon Press Oxford, 1993
- 6 E.J. Feijen, K.D. Vadder, M.H. Bosschaerts, J.L. Lievens, J.A. Martens, P.J. Grobet and P.A. Jacobs, *J. Am. Chem. Soc.*, 1994, **116**, 2950
- 7 A. Corma, *Chem.Rev.*, 1995, **95**, 559-614
- 8 R.E. Morris and P.A. Wright, *Chemistry and Industry*, 1998, 256

## Chapter Eight

### Encapsulation of Coordination Complexes

#### 8.1.0 Introduction

This thesis and the work described within it so far, has largely been concerned with the incorporation of organic molecules or templates within microporous solids in an attempt to produce new tailor made materials to act as catalysts. An alternative but related technique to produce better catalysts is to encapsulate organometallic or similar inorganic compounds within known microporous solids. By encapsulating homogeneous catalysts into the structure of heterogeneous catalysts new improved hybrid catalyst systems can be generated. A brief summary of the advantages and disadvantages of both homogeneous and heterogeneous catalysts is given below in table 8.1.

The main differences between the incorporation of templates into, and the encapsulation of inorganic complexes by zeolites; is that incorporation occurs during the synthesis of the zeolite whilst encapsulation usually occurs afterwards. The template method utilises the zeolitic framework as a purely heterogeneous catalyst, after template removal. In the encapsulated complex method, it is a combination of the zeolitic framework and the encapsulated complex itself that acts as the heterogenised homogeneous hybrid catalyst. These hybrid catalysts are designed to incorporate the high selectivity and mild reaction conditions of homogeneous systems whilst still maintaining the ease of separation of the catalyst from the reaction products, thus providing an efficient and reusable catalyst. Efficient reusable catalysts are both economical and environmentally friendly and as such are of both commercial and environmental interest.

The main similarity of the two techniques, incorporation of templates and encapsulation of inorganic complexes, is their characterisation. Both techniques require the characterisation of a molecule (either organic or inorganic) contained within another molecule (the zeolite). This is often a non-trivial task and has been overcome to an extent with the organic template molecules used in this project by the use of  $^{13}\text{C}$

MASNMR and the deliberately simple design of the organic molecules to be characterised. The use of MASNMR of inorganic molecules containing transition metals is not always possible however as they tend to be paramagnetic. The paramagnetic nuclei tend to have very rapid relaxation times which once Fourier transformed cause extremely broad lines in their spectra, resulting in very little useful information being obtained from any one spectrum. At present the best techniques to use for the characterisation of transition metal based complexes inside zeolites are infra-red (IR), ultra-violet (UV) or electron paramagnetic resonance spectroscopy (EPR). De Vos for example made wide use of both IR and UV in the characterisation of polyamide complexes absorbed into zeolite-Y<sup>[1]</sup>. The use of x-ray diffraction and other physical techniques e.g. nitrogen absorption to detect the decrease in pore volume associated with encapsulated molecules are also important but the spectroscopic methods are perhaps the most informative.

In this project the x-ray diffraction, TGA, UV and IR have been used to characterise encapsulated complexes inside zeolite-Y. Zeolite-X, Zeolite-Y (in both its cubic and hexagonal form) and Nu-87 have been prepared to act as zeolitic hosts for the encapsulation of complexes. Zeolite-X and cubic zeolite-Y are isostructural and differ only in their Si/Al ratios<sup>[2]</sup>, zeolite-Y having almost double the amount of silicon of Zeolite-X. A direct comparison of these two zeolites will demonstrate whether the zeolite acts only as a support or is involved in the catalytic process. Hexagonal zeolite-Y<sup>[2]</sup> possesses two distinct pores a large hyper-cage and a smaller hypo-cage and as such provides an interesting alternative framework to be studied as does Nu-87<sup>[2,3]</sup> which is a medium pore material.

At the onset of this Ph.D. project it was originally intended that both the synthesis of new materials by template design and the encapsulation of complexes within zeolites would be given equal weighting throughout the project. The rapid advances achieved in the synthesis of new materials by the template route however resulted in a change of emphasis in the aims and objectives of this project. The work described here is intended to demonstrate an alternative approach to the problem of synthesising new materials for catalysis.

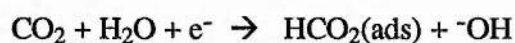
Type of Catalyst	Advantages	Disadvantages
Heterogeneous	Good thermal and mechanical stability.	Design and improvements limited due to lack of knowledge of active sites.
	High activity for a wide range of reactions.	Limited accessibility and therefore effectiveness of the catalytic components.
	Capacity to be used in packed or fluidised beds.	Severe and costly reaction conditions (i.e. high temperatures and pressures).
	Ease of separation.	
Homogeneous	Well studied and interpreted catalytic activity.	Separation problems - can be uneconomical.
	Reported catalytic activity under mild conditions.	Often require expensive metals (e.g. Pt, Pd, Rh, Ru).
	Efficient and reproducible use of metal atoms.	Potential environmental problems.
	Electronic and steric properties that can be varied and frequently controlled.	

Table 8.1 Homogeneous Vs Heterogeneous Catalysis<sup>[4]</sup>.

### 8.1.1 Coordination Complexes

The macrocycles considered throughout the course of this project include 3-methyl-1,3,5,8,12-pentaazacyclotetradecane, described later, Co-phthalocyanine and Mn-salen<sup>[5]</sup>. All three of these molecules are catalytically active.

3-methyl-1,3,5,8,12-pentaazacyclotetradecane and similar macrocycles can be used for the electrocatalytic reduction of CO<sub>2</sub><sup>[6,7]</sup> according to the equation :

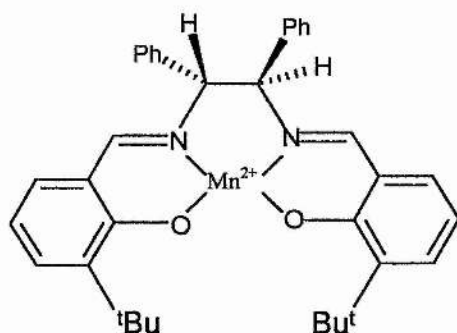


when using a bare mercury electrode in diethylformamide. Manganese complexes like the manganese salen complex shown below are used in the enantioselective epoxidation of unfunctionalised olefins<sup>[8,9]</sup>. This is an important goal in organic chemistry as it can lead to the synthesis of enantiomerically pure products.

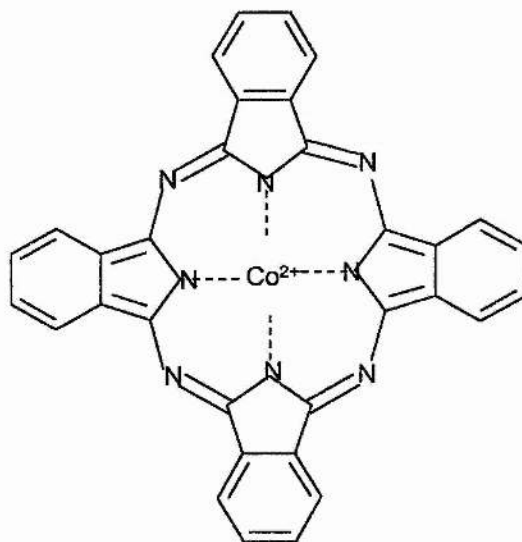
Metal phthalocyanine complexes are oxidative catalysts, the encapsulation of which in zeolites can improve their reaction yields and change their selectivity over the free complex<sup>[10]</sup>. There is some doubt over phthalocyanine complexes having a diameter of 13 Å being able to fit into the supercage of zeolite-Y (12 Å diameter). However, Paez-Mozo and co-workers<sup>[11]</sup> addressed this problem and concluded that phthalocyanine can fold slightly so as to fit into the zeolites pores. Their evidence for this was a lowering of pore volume and other data using XPS and HREM.

Although the encapsulation of phthalocyanines and salen macrocycles for catalysis are noble goals, the system most studied throughout this project is 3-methyl-1,3,5,8,12-pentaazacyclotetradecane. The aim is the *in situ* synthesis of the macrocycle in what would be, to the best of the author's knowledge, the first example of *in situ* synthesis of an azamacrocycle involving the reaction of two different molecules within the zeolite cavity and also the first example of the *in situ* synthesis of an azamacrocycle in solution as opposed to a dry zeolite.

De Vos and co-workers have recently published similar work<sup>[1]</sup>. The work involved the chelating of open or closed tetra- or pentadentate polyamines with transition metals inside the cavities of zeolite-Y. The amines were absorbed into the dry zeolites under vacuum before being characterised by the various techniques including IR and DRUV spectroscopies.



Manganese Salen



Cobalt Phthalocyanine

### 8.1.2 Encapsulation of Complexes

The encapsulation of a complex into a zeolite can be achieved by several methods: (1) by being physically adsorbed under vacuum, (2) whilst acting as a template during synthesis of the microporous solid and (3) by "ship-in-a-bottle" techniques, whereby the complex is formed *in situ*. Although all three methods have been attempted elsewhere, this project has largely been concerned with the incorporation of organic template molecules and the *in situ* synthesis of inorganic molecules within zeolites.

The encapsulation or incorporation of metal clusters, metal complexes and organometallics have already been achieved<sup>[12]</sup> and associated problems identified. These problems can include; the migration of metal ions to the external surface of the host to produce aggregation or leaching effects. Catalytic turnovers may be severely limited due to clogging of the pores requiring frequent regeneration operations which may damage the encapsulated complexes. Also there can be separation difficulties between the reactants, the products and the catalyst.

Despite these problems however, the potential advantages of producing a hybrid catalyst like those already described in section 8.1.0 continually drives this area of research.

As the size of the supercage is important this research has been based on medium and large pore materials for example Nu-87 and zeolite-Y. However only (cubic) zeolite-Y has been used in this project for the encapsulation of macrocycles.

The encapsulation of 3-methyl-1,3,5,8,12-pentaazacyclotetradecane as the complex for preliminary catalytic studies was chosen due to the availability of homogeneous analogues and departmental experience with such systems (Prof. R.W.Hay and J.A.Crayston). Compounds of this type are known to be of use in the electrocatalytic reduction of CO<sub>2</sub>.

## 8.2.0 Experimental

### 8.2.1 The Synthesis of 1,9-Diamino-3,7-diazanonane (2,3,2-tet.)

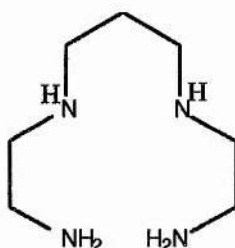


**Figure 8.1** 1,9-Diamino-3,7-diazanonane (2,3,2-tet.)

The procedure for this was taken (and adapted) to that found in references<sup>[13,14]</sup>. The composition for the 2,3,2-tet. was as shown below.

Substance	1,2-diaminoethane	1,3-dibromopropane	Potassium hydroxide
Mole ratio	0.500	0.040	0.125

The 1,2-diaminoethane was cooled to ice temperature in a 3-necked round bottomed flask before the 1,3-dibromopropane was added slowly with stirring. This mixture was then heated using an oil bath at 60°C for 3 hours. The liquid that formed was then transferred to a round bottom flask for use on a Buchi rotary evaporator. After concentrating the liquid to one third its original volume the oil was then returned to the 3 - necked round bottomed flask and the KOH was added.

Stirring as effectively as possible the flask was heated to 65°C in an oil bath for 6 hours. The resulting slurry was then washed with 100 ml of ether. The ether washings and the filtrate (containing the 2,3,2-tet.) were then concentrated to a viscous oil again using the Buchi and distilled under vacuum.

The product which appears as a clear oil distils at 138-148 °C at 2 torr. And is stored over sodium hydroxide under refrigeration.

The mechanism for this reaction is shown in scheme 8.1.

### 8.2.2 The Synthesis of 3-methyl-1,3,5,8,12-pentaazacyclotetradecane

The preparation of the azacyclam, 3-methyl-1,3,5,8,12-pentaazacyclotetradecane shown below, was achieved by a method based on the procedure described (in full) by De Blas *et al* <sup>[13]</sup>.

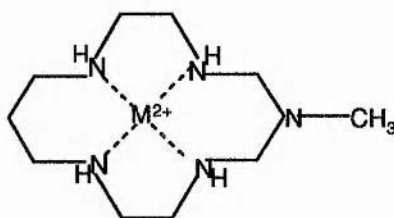


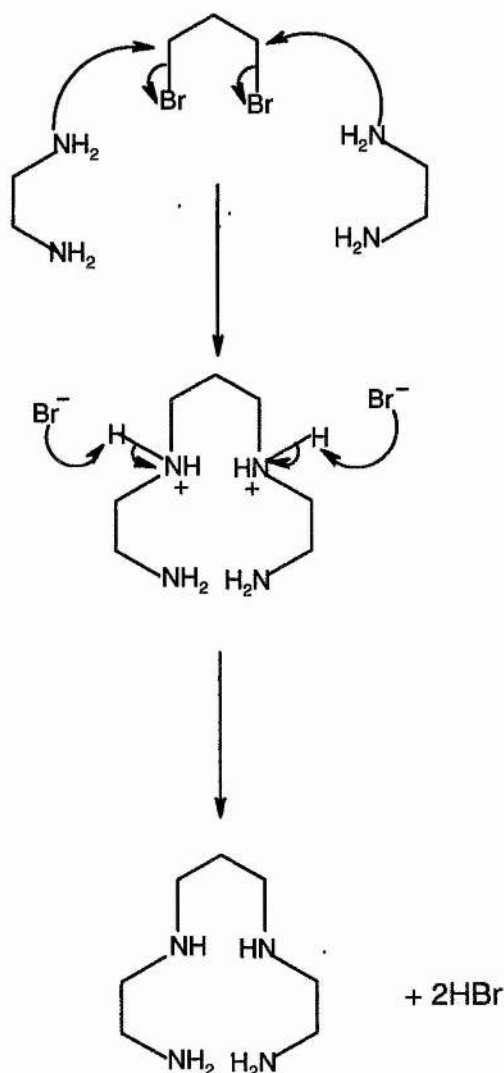
**Figure 8.1** 3-methyl-1,3,5,8,12-pentaazacyclotetradecane

A solution of  $\text{NiCl}_2 \cdot 6\text{H}_2\text{O}$  dissolved in 40 ml ethanol was placed in a round bottomed flask equipped with a reflux condenser, a thermometer and a dropping funnel. To this a 10 mmol solution of 1,9-diamino-3,7-diaazanonane (2,3,2-tet.) in 40 ml of ethanol was added dropwise with sufficient stirring. The 2,3,2-tet. had previously been prepared again by a method suggested by Andres De Blas <sup>[13,14]</sup>.

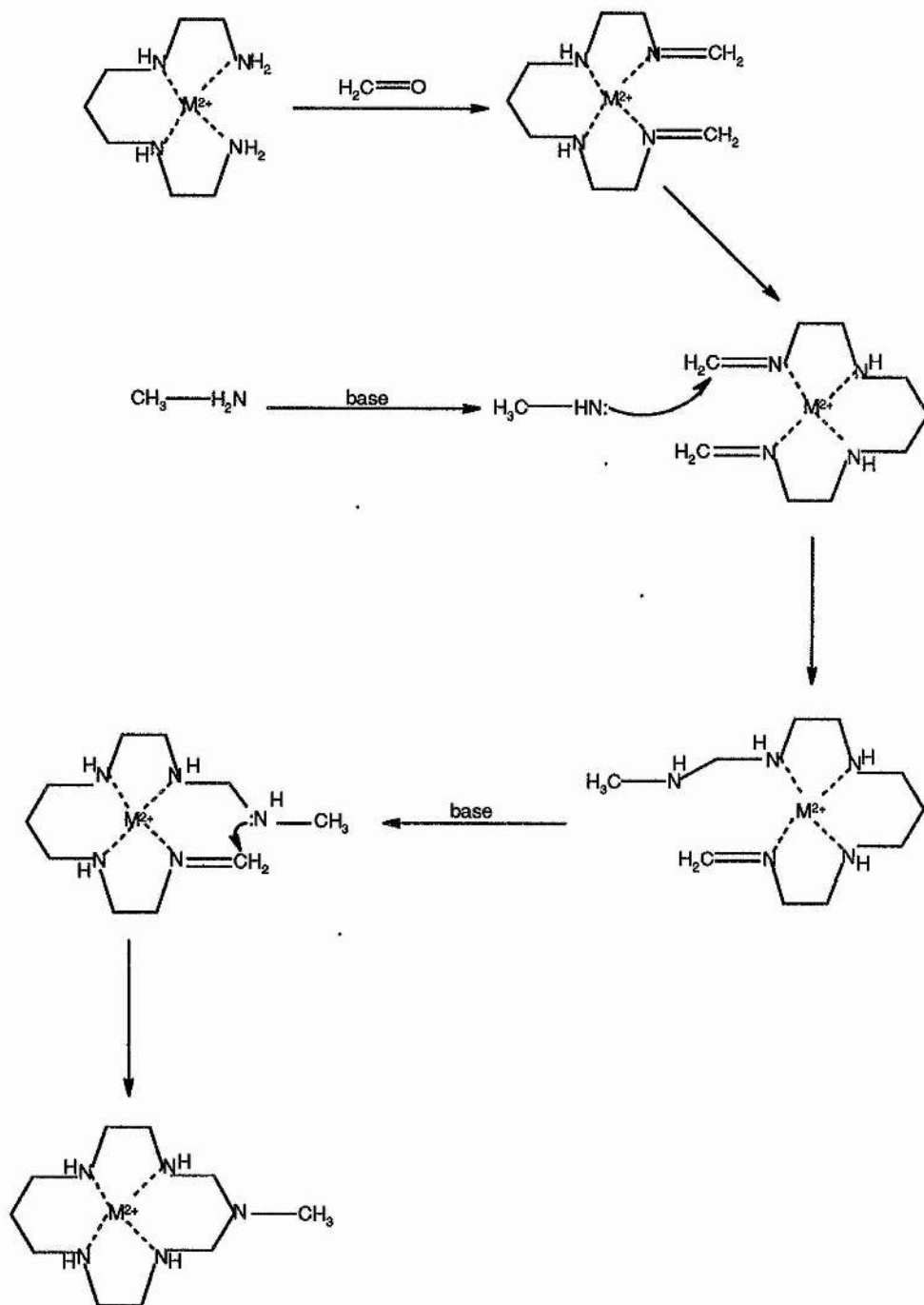
After warming to 50°C 10 mmol of methyl amine (aq. solution) was added dropwise again with stirring. Triethylamine was then added in one portion before 10 mmol of formaldehyde (40% aq. solution) was added in 4 portions over a period of 30 minutes. Heating and stirring was maintained for 7 days.

At the end of heating the reaction mixture was filtered to remove any metal hydroxide present and then the filtrate was concentrated using a Buchi rotary evaporator to favour crystallisation. After 3 days small needle-like crystals, pale violet in colour were obtained.

A proposed mechanism for this reaction is given in scheme 8.2.



Scheme 8.1 The mechanism of formation of 1,9-diamino-3,7-diazanonane (2,3,2-tet.)



Scheme 8.2 A proposed mechanism of formation for 3-methyl-1,3,5,8,12-pentaazacyclotetradecane.

### 8.2.3 Ion Exchange Between $\text{Na}^+$ and $\text{M}^{2+}$ in Zeolite-Y

Sodium form zeolite-Y (formula weight of 17116g) and the composition  $\text{Na}_{58}\text{Al}_{58}\text{SiO}_{134}\text{O}_{384}\cdot 240\text{H}_2\text{O}$  was obtained from Crossfield chemicals. Using this it was possible to calculate the number of moles of  $\text{Na}^+$  present in 2g of zeolite (i.e.  $6.777 \times 10^{-3}$ ). An equal amount of  $\text{M}^{2+}$  ions were then used to allow a 100% excess of  $\text{M}^{2+}$  ions so as to ensure a high degree of ion exchange.  $\text{MCl}_2 \cdot 6\text{H}_2\text{O}$  was used as the  $\text{M}^{2+}$  source. Exchange was monitored using atomic absorption and x-ray fluorescence.

The ion exchange procedure involved mixing the two chemicals together in 1litre of distilled water for 72 hours at room temperature. The resulting coloured powder was washed with water and allowed to dry at room temperature in air. Ni-zeolite-Y was green in colour, Cu-zeolite-Y, blue, Co-zeolite-Y, purple and Zn-zeolite-Y white.

### 8.2.4 The Encapsulation of 3-methyl-1,3,5,8,12-pentaazacyclotetradecane

Exactly the same process was used as described earlier in section 8.2.2 to make the macrocycle. The only difference being the metal source. In section 8.2.2 the metal source was  $\text{NiCl}_2 \cdot 6\text{H}_2\text{O}$  in this case the nickel source was Ni-zeolite-Y as prepared according to section 8.2.3 above (and similarly the appropriate M-zeolite-Y for the other macrocycles).

The only other notable change to the preparation of the free complex is that the final colour of the product is yellow (in the case of the macrocycle inside zeolite) but pale violet in the case of the free complex. The zinc encapsulated macrocycle was white in colour and the copper macrocycle one was purple. Neither the copper or the zinc free macrocycle were prepared indeed for geometrical reasons the free zinc macrocycle can not be prepared.

### 8.2.5 The Encapsulation of Cobalt Phthalocyanine

Following a procedure outlined by De Vos et al cobalt phthalocyanine was synthesised inside pre-exchanged cobalt zeolite-Y<sup>[10]</sup>. The zeolite was dried in a furnace at 200°C in flowing air. The purple powder was then transferred to a glass ampoule and dried further

at 150°C under vacuum at approximately  $2 \times 10^{-5}$  torr. A six fold excess of 1,2-dicyanobenzene was then added to the glass ampoule by relieving the vacuum momentarily. A graphic representation of the glass ampoule is shown in figure 8.3.

Once the dicyanobenzene was added the system was returned to a vacuum of  $2 \times 10^{-5}$  torr whilst heating the glass ampoule at 150°C for 2 hours. After this time had elapsed the ampoule was sealed, transferred to an autoclave for safety and heated at 200°C for 24 hours. On removal from the oven and after sufficient time to cool to room temperature the contents of the glass ampoule which were green in colour were removed and cleaned using soxhlet extraction methods. Acetone and ethanol were used sequentially for 48 hours each. The resultant zeolite was dark blue in colour. Characterisation was performed by x-ray powder diffraction and UV spectroscopy.

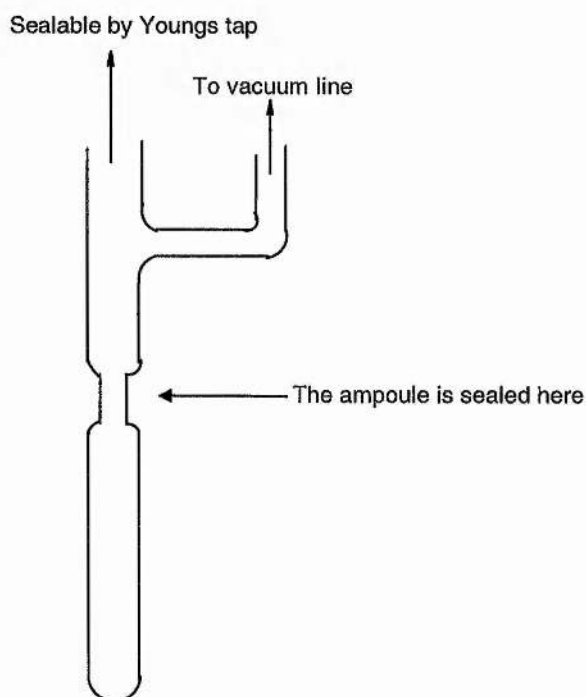


Figure 8.3 A graphic representation of the glass ampoule used in these experiments. The open tube is used to connect onto the vacuum line whilst the sample is put into the sealable stoppered part. The ampoule is sealed using an oxyacetylene torch at the thinner part.

### 8.3.0 Results and Discussion

The 1,9-diamino-3,7-diazanonane ligand required for the synthesis of the macrocycle was obtained in a 65 % yield and tested for purity using  $^{13}\text{C}$ NMR spectroscopy. The resulting spectrum is shown in figure 8.8 and shows pure 1,9-diamino-3,7-diazanonane. The peak values are in good agreement with those found in Aldrich<sup>[15]</sup>.

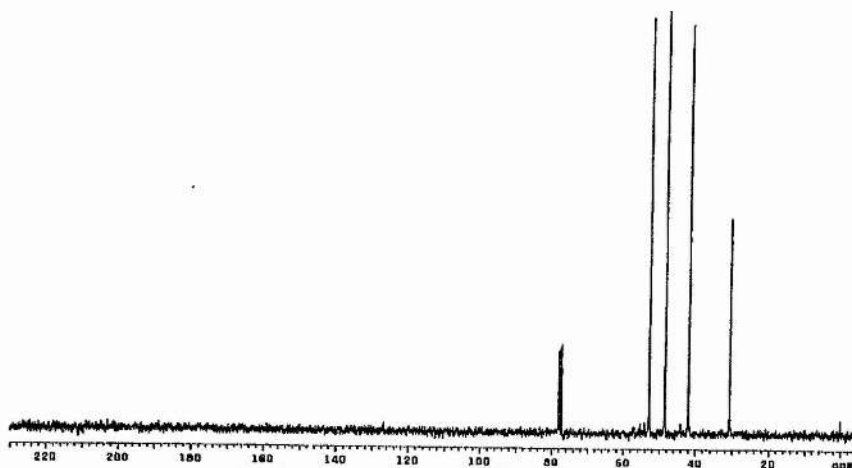


Figure 8.4 The  $^{13}\text{C}$  NMR spectrum of 1,9-diamino-3,7-diazanonane. The seven peaks are located at  $\delta$ 78.1, 77.7, 72.2, 52.8, 48.4, 41.9 and 30.6ppm, the first three of which are due to the solvent (deuterated chloroform).

The free 3-methyl-1,3,5,8,12-pentaazacyclotetradecane nickel complex formed pale violet needle-like crystals. These crystals were consistent with those found by De Blas the violet colour indicates that the nickel is actually in an octahedral environment rather than the expected square planar one. This is due to axial chloride ions coordinating with the metal to form an octahedral complex in the solid state. In solution however, the colour changes to yellow, which is more characteristic of square planar nickel and indeed UV-visible spectroscopy of the solution produces peaks at approximately 580nm and 280nm which are consistent with a nickel square planar complex. Indicating that it has in fact been formed. Because of the paramagnetic effects caused by the octahedral and square planar mixture of complexes, NMR spectroscopy can not be used in this case for characterisation.

However, the ion exchange between the  $\text{Na}^+$  and  $\text{Ni}^{2+}$  was tested by x-ray fluorescence (XRF) and found to be completely effective with an exchange of 2:1 in terms of charge. This implies that there are 8  $\text{Ni}^{2+}$  ions within the supercages of the zeolite. The 2:1 ion exchange between the  $\text{Na}^+$  and the  $\text{Ni}^{2+}$  proved that the zeolite would be a good  $\text{Ni}^{2+}$  source for the formation of the complex. Similar experiments were performed to make Zn-zeolite-Y and Cu-zeolite-Y so as to act as  $\text{Zn}^{2+}$  and  $\text{Cu}^{2+}$  sources respectively.

Using the Ni-zeolite-Y the synthesis was repeated and the resulting product was yellow. As the zeolite is naturally white the colour is likely to be due to the presence of the complex inside the zeolite. Since the product was washed repeatedly the complex must be inside the zeolite rather than on the surface. This theory is supported by thermal analysis which suggests that there is approximately a 14% loading i.e. 14% of the products weight is due to the complex, a further 14% is approximately due to water. A TGA and DTA profile is shown below in figure 8.5.

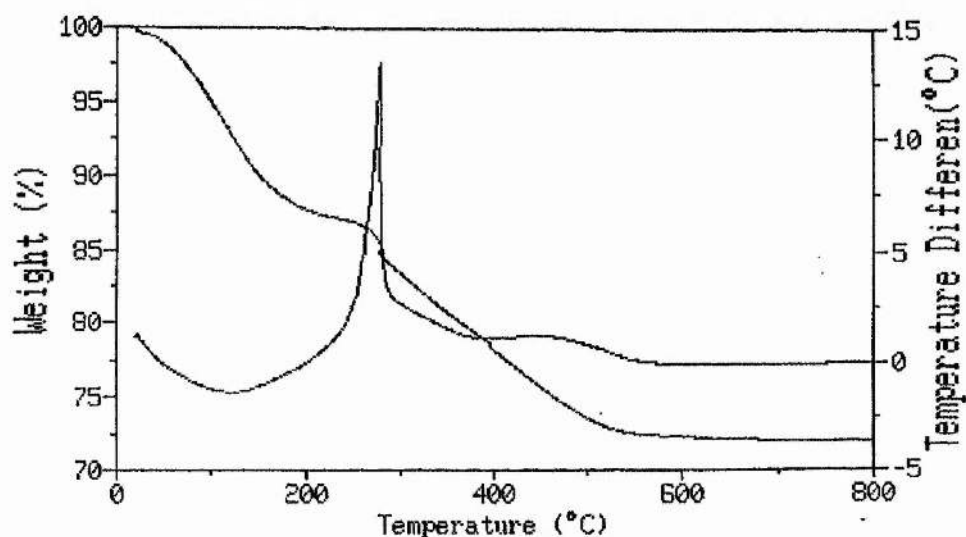


Figure 8.5 TGA and DTA profiles of the zeolite encapsulated complex. The TGA shows two gradual weight losses due to water loss and then loss of the complex itself. This is supported by the DTA pattern which shows a typical endotherm for the loss of water and a sharp exotherm for the removal of the complex.

X-ray diffraction data confirms that the zeolite framework is not appreciably affected by the incorporation or removal of the complex as shown in figure 8.6.

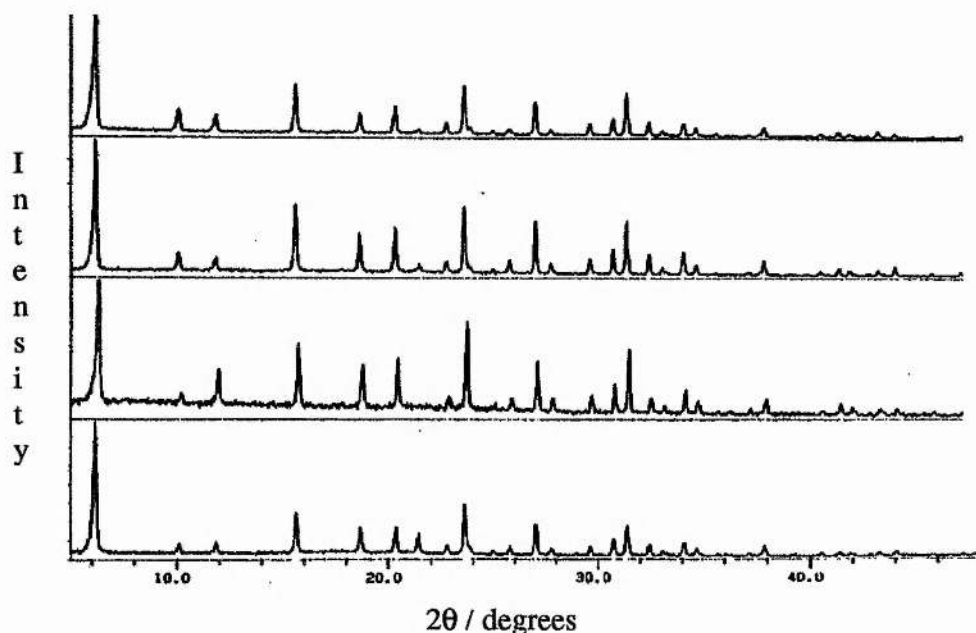


Figure 8.6 Diffractograms of (from the top) Zeolite-Y, Ni-zeolite-Y, Ni-zeolite-Y + complex and Ni-zeolite-Y + complex after calcination.

The UV spectrum of a pure sample of 3-methyl-1,3,5,8,12-pentaazacyclotetradecane (azacyclam) was obtained by dissolving a sample for analysis in water. This spectrum is shown in figure 8.7. The pattern has two characteristic peaks, one at approximately 450nm due to square planar nickel ions and the other at 650nm which is due to the presence of octahedral nickel ions. The relative intensities of the two peaks show that in solution almost all of the nickel ions are in the square planar conformation as predicted.

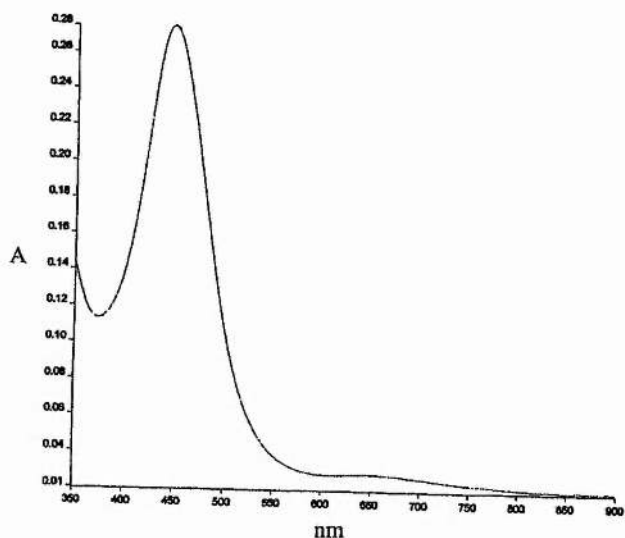


Figure 8.7 UV spectrum of 3-methyl-1,3,5,8,12-pentaazacyclotetradecane in water. Showing the two characteristic peaks of both square planar and octahedral nickel ions at 450nm and 650nm respectively.

The same spectrum should be obtained from the encapsulated material inside zeolite-Y in theory. However, in practice this will not be the case as the zeolite is not water soluble and so can not go into solution unlike the free azacyclam. To circumvent this problem a nujol paste of the zeolite encapsulated complex was prepared and a spectrum obtained. This is the main reason for the poor resolution exhibited by this spectrum although the peak at 450nm indicating that the nickel ions are square planar is still visible. To establish if this was merely an effect of the Ni-zeolite-Y in nujol as opposed to the encapsulated complex, a spectrum of the Ni-Zeolite and of untreated zeolite-Y were obtained and showed no evidence of this peak. Both of these spectra are shown below.

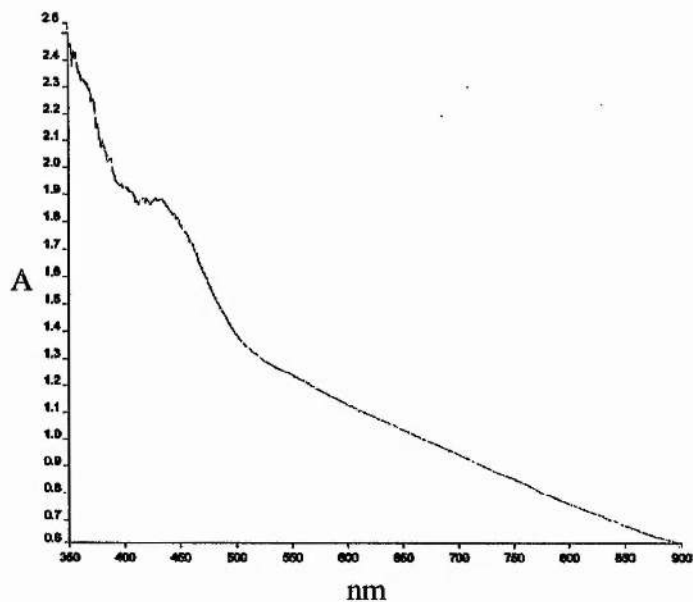


Figure 8.8 The UV spectrum of the encapsulated azacyclam in Ni-zeolite-Y prepared in nujol which is why the resolution of this spectrum is poor. The square planar peak at 450nm is still visible, however.

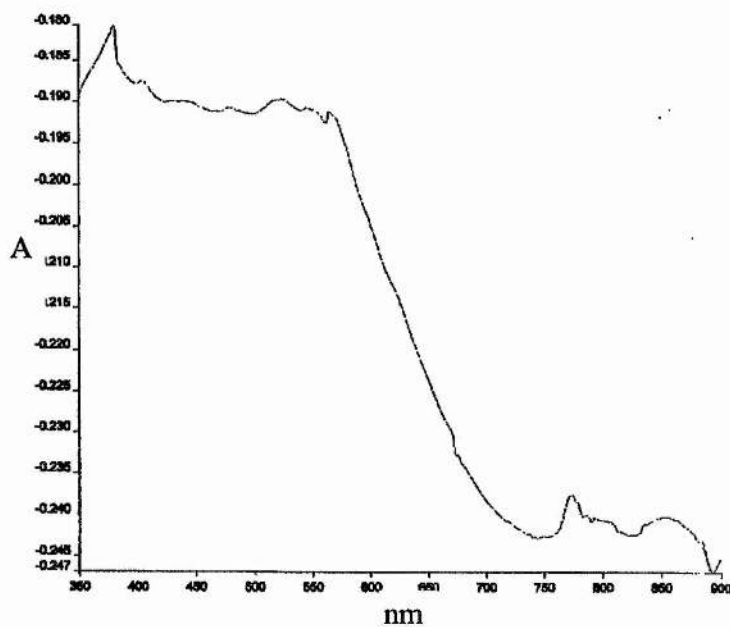


Figure 8.9 The UV spectrum of Ni-zeolite-Y in nujol, showing no evidence of any peaks due to nickel ions.

A full characterisation of the cobalt phthalocyanine complex (CoPc) inside zeolite-Y has not yet been undertaken. However, x-ray diffraction studies have shown that the zeolite structure is not been appreciably affected by the encapsulation of the CoPc. The colour of the zeolite changed from white to blue indicating the encapsulation of the cobalt complex. Encapsulation of CoPc is thought to have occurred as opposed to the CoPc molecule being attached to the external surface of the zeolite because of the extensive washing after being removed from the glass vial.

UV spectroscopy performed in the same way as that described for azacyclam previously shows the presence of a characteristic double peak around 650nm indicating the presence of cobalt phthalocyanine. This is believed to be inside the zeolite because of the colour change of the zeolite and the extensive washing under soxhlet extraction (using ethanol and acetone at 70°C for 4hours) which would have removed any phthalocyanine on the external surface of the zeolite.

#### 8.4.0 Conclusions

The successful synthesis of 3-methyl-1,3,5,8,12-pentaazacyclotetradecane and its probable encapsulation into zeolite-Y has been achieved. Similarly it would appear from characterisation experiments that cobalt phthalocyanine has also been encapsulated inside zeolite-Y, although by a different method. Neither of these of these compounds have been tested for their catalytic activity although zeolite-phthalocyanine complexes have previously been investigated.

#### 8.5.0 References

- 1 D. E. de Vos, D.L. Vanoppen, X.Y. Li, S. Libbrecht, Y. Bruynseraede, P.P. Knops-Gerrits and P.A. Jacobs, *Chem. Eur. J.*, 1995, **1**(2), 144
- 2 W.M.Meier, D.H.Olson and Ch.Baerlocher, *Atlas of Zeolite Structure Types*, 4th Edtn (Revised), Elsevier, 1996
- 3 M.D. Shannon, J.L. Casci, P.A.Cox and S.J. Andrews, *Nature*, 1991, **353**, 417
- 4 D.C. Bailey and S.H. Langer, *Chem. Rev.*, 1981, **81**, 109

- 5 W.Zhang, and E.N. Jacobson, *J. Org. Chem.*, 1991, **56**, 2296
- 6 C.I.Smith, J.A.Cryston and R.W.Hay, *J. Chem. Soc. Dalton trans.* 1993, 3267
- 7 F. Abba, G. De Santis, L. Fabbrizzi, M. Licchell, A.M.M. Lanfredi, P. Pallavicini, A.Poggi and F.Ugozzoli, *Inorg. Chem.*, 1994, **33**, 1366
- 8 P.P. Knops-Gerrits, D.E. De Vos, F. Thibault-Starzyk and P.A. Jacobs, *Nature*, 1994, **369**, 543
- 9 P.P. Knops-Gerrits, F. Thibault-Starzyk and P.A. Jacobs, *Zeolites and Microporous Materials: State of the Art (1994), Studies in Surface Science and Catalysis*, **84**, 1411
- 10 N. Herron, G.D. Stucky and C.A. Tolman, *J. Chem. Soc. Chem. Commun.*, 1986, 1524
- 11 E. Paez-Mozo, N. Gabriunas, F. Lucaccioni, D.D. Acosta, P.Patrono, A.L. Ginestra, P. Ruiz and B. Delmon, *J. Phys. Chem.*, 1993, **97**, 12819
- 12 G.A. Ozin and C.Gil, *Chem. Rev.*, 1989, **89**, 1749
- 13 A.De Blas et al, *J. Chem. Soc. Dalton Trans.*, 1993, 1411
- 14 E.K.Barefield, F.Wagner, A.W.Herlinger and A.R.Dahl, *Inorg. Synth.*, 1976, **16**, 222
- 15 Aldrich Library of  $^{13}\text{C}$  and  $^1\text{H}$  NMR Spectra

## Chapter Nine

### Conclusions and Future Work

#### 9.1.0 Introduction

The aim of this chapter is to summarise the conclusions that may be derived from the research described in this thesis. The chapter also attempts to suggest possible future work that may be undertaken to extend the research described in this thesis.

#### 9.2.0 Conclusions

This work has shown the importance of template design on the synthesis of microporous solids particularly aluminophosphates. The aluminophosphates are susceptible to changes in the chemistry, size or shape of the templates used in their synthesis gels. There is also a close relationship between the size and shape of the template used and the structures that they can allow to crystallise from synthesis gels.

The careful use of template design used in this project has allowed the synthesis of five new materials, four of which are thought to be microporous. Two of the new materials have had their structure revealed using single microcrystal diffraction at the ESRF in Grenoble.

The zeolite synthesis conditions used in this thesis are naturally orientated to the production of ZSM-5. Attempts to overcome this have not been successful. Recent advances in the production of zeolites from near neutral synthesis gels using hydrofluoric acid as a mineralising agent<sup>[1]</sup> have led to these conditions being adopted in this laboratory but at present they have not succeeded in the synthesis of new materials.

The synthesis and structure solution of STA-1 underlines both the potential of rational template design for the preparation of novel microporous solids and also the power of modern synchrotron crystallographic facilities. The clear cut dependence of the

crystallisation field of STA-1 on the length of the methylene chain linking the diquinuclidinium end groups suggests the template is able to find a very specific and energetically favourable site next to the framework. The exact location of the template molecule however, has still to be determined as this was not identified by the single crystal experiments or by computer modelling. Computer modelling suggests several energetically similar template locations within STA-1 and in reality all of these may be adopted. If the template adopted more than one orientation the molecular disorder would lead to very little long range order and as such the template location would not be solvable by x-ray diffraction. This may explain why the template position was not found within the microporous framework even with the single microcrystal analysis, whilst other more ordered templates have been<sup>[2-4]</sup>.

This approach, by which a "supramolecular" template of desired shape can be built up by the reaction of readily available compounds, should be of wide applicability for the synthesis of microporous solids. The structure solution of STA-1 is, to our knowledge, the first of a completely novel tetrahedrally coordinated framework using microcrystal diffraction at a synchrotron source, although successful structure solution of families of structures closely related to those already solved by other methods has previously been achieved. King *et al*<sup>[5]</sup> solved the first microporous solid,  $\text{NH}_4[\text{Mo}_2\text{P}_2\text{O}_{10}]\cdot\text{H}_2\text{O}$  which has a void volume of approximately 12% as determined by water adsorption isotherms. The structure which is isostructural with the natural mineral Leucophosphate,  $\text{K}[\text{Fe}_2(\text{OH})(\text{H}_2\text{O})(\text{PO}_4)_2]\cdot\text{H}_2\text{O}$ , has both octahedral and tetrahedrally coordinated cations. Prior to this structure the only structure solved using microcrystal diffraction at a synchrotron source was Eu-19<sup>[6]</sup> by S.A. Andrews and his co-workers in 1988. Since then, the power of this technique is such that microporous solids prepared only as crystals much smaller than those of STA-1 can readily be studied.

The study of STA-2 shows the sensitivity of crystal growth of microporous solids to precise conditions of the hydrothermal synthesis, and confirms that alkali cations do not prevent the formation of microporous aluminophosphates. Alkali cations can though, have a radical effect on the morphology of the phase produced as shown by comparison of figures 6.2 and 6.11 where the only significant difference in the synthesis conditions

between the two was the addition of sodium hydroxide. In the absence of the alkylammonium template, however, the alkali cations are not able in this case to synthesise microporous materials, although dense phase sodium aluminophosphates are formed.

On the atomic scale, the work underlines the role templates play in determining complex periodic stacking arrangements, and how single microcrystal diffraction is a powerful tool not only to determine framework structures<sup>[4,7-10]</sup> but also to locate organic templates<sup>[11-12]</sup>. This should be of widespread applicability in experimental and computational studies aimed at the role and design of templates for the synthesis of targeted materials<sup>[13]</sup>. Specifically, STA-2 is a new small pore polytype of the series of structures formed by the stacking and linking of 6-membered rings (usually reported in terms of ABC type stacking). The material is stable to the removal of the template whereupon it becomes a solid acid catalyst for such chemical conversions as the methanol-to-light olefins reaction.

Similarly the work using the DABCO polymeric / oligomeric templates has highlighted how sensitive the aluminophosphate system can be to subtle changes in the organic template. The systematic study of the DABCO series has shown that the template not only affects what aluminophosphate phase forms but also that it can have a direct influence on the size and morphology of the crystallites that form, influencing the catalytic performance of the material.

The DABCO<sub>2</sub> oligomers were also responsible for the production of another new aluminophosphate material, STA-3. The structure of this material has still to be determined but is likely to be a small to medium pore channel structure, possibly related to AlPO<sub>4</sub>-31.

The successful synthesis of 3-methyl-1,3,5,8,12-pentaazacyclotetradecane and its probable encapsulation into zeolite-Y has been achieved. Similarly it would appear from characterisation experiments that cobalt phthalocyanine has also been encapsulated inside zeolite-Y, although by a different method. Neither of these compounds have been tested

for their catalytic activity although zeolite-phthalocyanine complexes have previously been investigated.

One of the most striking conclusions derived from this work is the importance of the interdisciplinary approach to understanding the synthesis and achieving the characterisation of microporous solids. The use of diffraction techniques, spectroscopic techniques and computer modelling methods have all proven to be extremely important, for the advancement of this area of research.

Computer modelling allows an insight into microporous solids at the atomic level and facilitates our understanding of how, as in the case of the DABCO polymeric templates, the template can alter the physical properties of the aluminophosphate produced.

### 9.3.0 Further Work

The synthesis of new aluminosilicate materials has still to be achieved using the templates already synthesised during this project. Specifically an aluminosilicate form of STA-1 and STA-2 have still to be prepared. In the case of STA-1, an aluminosilicate form could be more stable to calcination and therefore render STA-1 more amenable to catalysis or adsorption applications. The use of synthesis conditions similar to those described by Cambor *et al*<sup>[1]</sup>, may be a way of achieving this.

The creation of additional new materials may be achieved again using the same templates by altering the chemistries of the synthesis gels of both the zeolite and the aluminophosphate type materials. Evidence for this is wide spread as the ability of one template to synthesise more than one microporous solid is abundant and has been aptly demonstrated with by the use of tris (2-aminoethyl)amine in this project.

The structure solution of both of the materials produced using tris (2-aminoethyl)amine has still to be achieved. The magnesium aluminophosphate is not thought to be microporous, however, the boron aluminophosphate is thought to be microporous and its structure solution is imminent after obtaining both powder and single crystal diffraction

new material produced using the DABCOC3 polymeric template is also an area for continued research.

Structure solution of these materials plus the use of computer modelling techniques will provide a deeper insight to the way in which these materials form and how the templates used dictate the structures formed. Utilising this knowledge will create the possibility of designing framework structures necessary for specific catalytic or adsorptive applications.

This must be the overall aim for this area of research and is still very much an area for continued intense research. In designing new framework structures the design and synthesis of new template molecules, organic or inorganic will be necessary. These molecules could then be exploited to create several new microporous solids. The synthesis of a chiral microporous solid has still to be achieved and is the goal of many research groups across the world. A better understanding of template design and template-host interactions might make this an achievable goal. Chiral aluminophosphates may be obtained by using specific or even biological templates for example enzymes. Enzymes encapsulated within mesoporous solids may also act as very good stereospecific catalysts that can combine the advantages of both homogeneous and heterogeneous catalysts, as was the aim of chapter eight.

STA-2 is still a subject for continued research. Future work In this area could be roughly divided into two groups, (1) synthesis / characterisation and (2) application.

(1) Although the synthesis of STA-2 is now well understood and can be repeated to produce a variety of different framework compositions of STA-2 (e.g. CoAlPO or AlPO<sub>4</sub>), the method of synthesis is still unclear. From consideration of structural diagrams such as figure 6.15, it is clear that the periodic array of template molecules is paramount to the synthesis of this material. It would be of interest therefore to determine if the templates arrange themselves in layers forcing the 'growing' aluminophosphate to encapsulate them as the crystal grows, or if the growing aluminophosphate is the directing force as to how the templates align themselves.

if the templates arrange themselves in layers forcing the 'growing' aluminophosphate to encapsulate them as the crystal grows, or if the growing aluminophosphate is the directing force as to how the templates align themselves.

There is much evidence in favour of the organic molecules being the directing force behind the size and shape of the developing aluminophosphate, as is apparent in figure 6.17. This diagram shows that  $\text{AlPO}_4\text{-17}$  (made with QuinC3),  $\text{AlPO}_4\text{-56}$  and STA-2 (both made with QuinC4 and QuinC5) all have pores that terminate in a 6-membered ring. Furthermore all three pores have trigonal symmetry along the axis of the pore such that there are three 8-membered rings separated by two 4-membered rings. From single crystal data obtained for STA-2 and from computer modelling experiments, it is clear that this generates an ideal pore size and shape to encapsulate quinuclidinium cations. Additionally, close examination of the  $\text{AlPO}_4\text{-17}$  pore and the STA-2 pore reveals that STA-2 is an extension of the  $\text{AlPO}_4\text{-17}$  pore made possible by the  $\bar{3}$  symmetry of STA-2 which allows the insertion of an additional three 6-rings. Further synthesis and characterisation work would be able to establish if this extension process could be continued to include the insertion of more 8-rings as akin to  $\text{AlPO}_4\text{-56}$ . Further characterisation studies could be attempted on samples of STA-2 synthesised using QuinC5 which showed evidence of an as yet unidentified phase. This may be concealing the identity of another new microporous phase. Also the aluminosilicate analogue of STA-2, like STA-1 has still to be synthesised as this may have interesting catalytic properties. The synthesis of a zeolite form of STA-2 would hopefully be achieved with low silicon or from HF mineralised gels, as the synthesis conditions used in this project is more likely to produce ZSM-11 or ZSM-5.

The question as to how the template controls the aluminophosphate phase that forms could hopefully be resolved using Atomic Force Microscopy (AFM). AFM would be useful in studying the surface of the aluminophosphates and may reveal the stacking sequences of the template molecules. These techniques would hopefully be able to locate possible template positions on the surface of the crystals. Single microcrystal diffraction experiments to investigate *in situ* template location with aluminophosphates are being

(2) The catalytic properties of STA-2 have not been fully investigated. The wealth of structural compositions that can be synthesised make this a particularly attractive material to characterise especially if an aluminosilicate analogue can be synthesised. Absorptive properties of STA-2 could also be investigated.

#### 9.4.0 References

- 1 M.A. Cambor, A. Corma and L.A. Villaescusa, *J. Chem. Soc. Chem. Commun.*, 1997, 749
- 2 G. Sankar, J.K. Wyles, R.H. Jones, J.M. Thomas, C.R.A. Catlow, D.W. Lewis, W. Clegg, S.J. Coles and S.J. Teat, *J. Chem. Soc. Chem. Commun.*, 1998, 117
- 3 M.A. Cambor, A. Corma, P. Lightfoot, L.A. Villaescusa and P.A. Wright, *Angew. Chem. Int. Ed. Engl.*, 1997, **36**(23), 2659
- 4 G.W. Noble, P.A. Wright and Å. Kvik, *J. Chem. Soc. Dalton Trans.*, 1997, **9**, 976
- 5 H.E. King, L.A. Mundi, K.G. Stronmaier and R.C. Haushalter, *J. Solid. State Chem.*, 1991, **92**(1), 154
- 6 S.A. Andrews, M.Z. Papiz, R. McMeeking, A.J. Blake, B.M. Lowe, K.R. Franklin, J.R. Helliwell and M.M. Harding, *Acta Cryst. Section B*, 1988, **B44**, 73
- 7 M.J. Gray, J.D. Jasper, A.P. Wilkinson and J.C. Hanson, *Chem. Mater.*, 1997, **9**, 976
- 8 G.W. Noble, P.A. Wright, P. Lightfoot, R.E. Morris, K.J. Hudson, Å. Kvik, H. Graafsma, *Angew. Chem. Int. Ed. Engl.*, 1997, **36**, 81
- 9 M. Helliwell, V. Kaucic, G.M.T. Cheetham, M.M. Harding, B.M. Kariuki, P.J. Rizkallah, *Acta Cryst. B* 1993, **49**, 413
- 10 G.M.T. Cheetham, M.M. Harding, *Zeolites*, 1996, **16**, 245
- 11 M.J. Gray, J.D. Jasper, A.P. Wilkinson, J.C. Hanson, *Chem. Mater.*, 1997, **9**, 976
- 12 P. Lightfoot, R.E. Morris, P.A. Wright, *et al*, *Structure solution of SSZ-23*, in press
- 13 G. Sankar, J.K. Wyles, R.H. Jones, J.M. Thomas, C.R.A. Catlow, D.W. Lewis, W. Clegg, S.J. Coles and S.J. Teat, *J. Chem. Soc. Chem. Commun.*, 1998, 117

**Characterisation Techniques**

XRD	X-ray diffraction
NMR	Nuclear magnetic Resonance spectroscopy
MASNMR	Magic angle spinning NMR spectroscopy
MQ-MASNMR	Multiple quantum MASNMR spectroscopy
TGA	Thermal Gravimetric Analysis
DTA	Differential thermal analysis
CHN	Microanalysis
XRF	X-ray Fluorescence
SEM	Scanning electron microscopy
EDX	Energy dispersive x-ray analysis
IR	Infra-red spectroscopy

**Inorganic**

$\text{Mg}(\text{COCH}_3)_2 \cdot 4\text{H}_2\text{O}$	Magnesium acetate tetrahydrate
$\text{Al}(\text{OH})_3 \cdot x\text{H}_2\text{O}$	Aluminium hydroxide hydrate
$\text{H}_3\text{PO}_4$	Phosphoric acid
$\text{SiO}_2$	Silica
$\text{Co}(\text{COCH}_3)_2$	Cobalt acetate
HF	Hydrofluoric acid

**Organic**

Quin	Quinuclidine
QuinCn	1,n-diquinuclidinium alkane
Quin-TMAp	1-quinuclidinium, 3-trimethylammonium propane
Quin-benzyl	benzylquinuclidinium bromide
Dabco or DABCO	1,4-diazabicyclo[2.2.2]octane
DABCOc <sub>n</sub>	Polymer with dabco and n-membered methylene chains

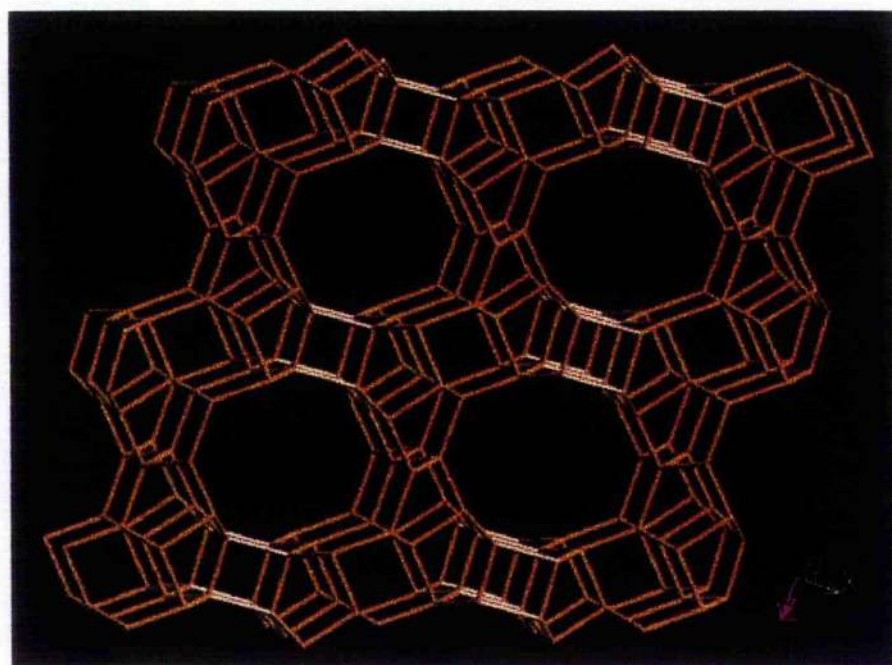
DABCO-TMAp	DABCO with two $\omega$ -trimethylammonium propanes attached
DABCO-benzyl	DibenzylDABCO
3,5-dmp	3,5-dimethylpiperidine
3,5-dmpCn	1,n-(3,5-dimethylpiperidinium) alkane
2,n,2	1,n-triethylammonium propane alkane
3,n,3	1,n-tripropylammonium butane alkane
4,n,4	4,n-tributylammonium pentane alkane
6,n,6	1,n-trihexylammonium alkane
Cn	n-membered methylene chain

## Aim

The purpose of this section is to give details of several of the well known materials that have been repeatedly synthesised during this project.

## Zeolites

### ZSM-12



#### Structure Details

Space Group:  $C 1 2/c 1$  (No. 15)

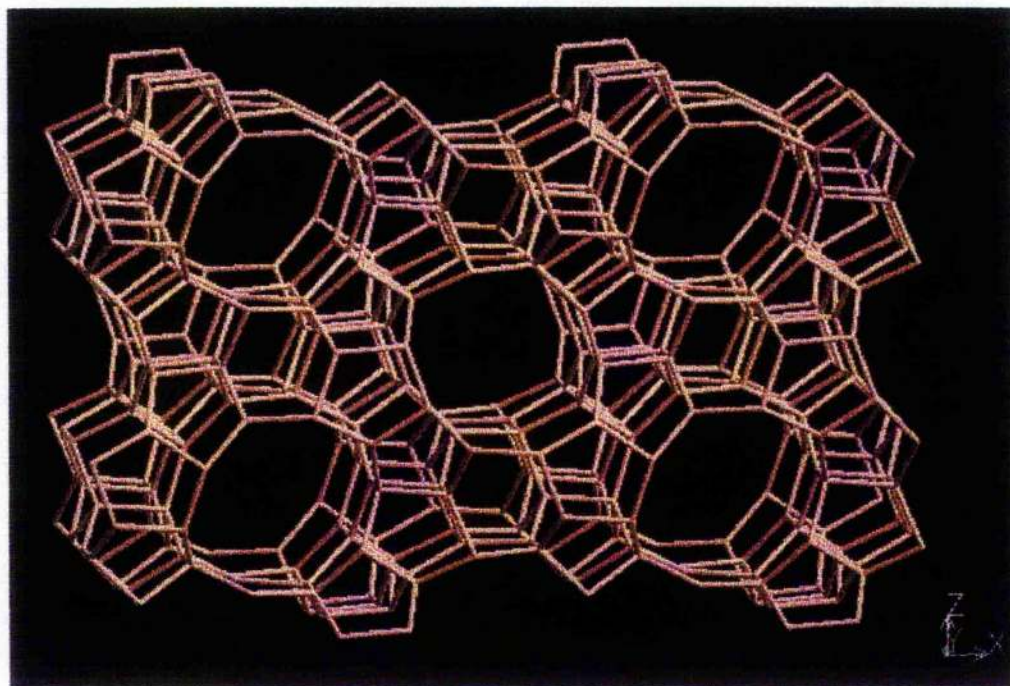
Unit Cell:  $a = 24.8633$ ,  $b = 5.01238$ ,  $c = 24.3275 \text{ \AA}$ ,  $\alpha = \gamma = 90^\circ$ ,  $\beta = 107.722^\circ$

Determined by: X-ray Rietveld refinement,  $R_{exp} = 0.058$ ,  $R_{wp} = 0.181$ ,  $RI = 0.069$

## Atomic Coordinates:

Atom	x	y	z
Si1	0.4402	0.5319	0.4129
Si2	0.0678	-0.0708	0.4589
Si3	0.3754	0.0320	0.3609
Si4	0.1338	0.4218	0.4484
Si5	0.2836	0.0822	0.4275
Si6	0.2139	0.5853	0.3832
Si7	0.2869	0.0100	0.2463
O1	0.4280	0.5053	0.4730
O2	0.5034	0.4725	0.4225
O3	0.4245	0.8220	0.3872
O4	0.3301	-0.0045	0.3956
O5	0.0841	-0.3624	0.4513
O6	0.3452	-0.0218	0.2972
O7	0.2504	0.2441	0.2629
O8	0.2602	0.3716	0.4078
O9	0.1554	0.5101	0.3911
O10	0.1853	0.4480	0.5026
O11	0.2997	0.0905	0.1886
O12	0.3995	0.3370	0.3702
O13	0.1069	0.1372	0.4394
O14	0.2343	0.8828	0.4093

## ZSM-5 (MFI)



## Structure Details

Space Group: P 1 21/n 1 (No. 14)

Unit Cell:  $a = 19.879$ ,  $b = 20.107$ ,  $c = 13.369$  Å,  $\alpha = \gamma = 90^\circ$ ,  $\beta = 90.67^\circ$

Determined by: X-ray single crystal refinement,  $R_w = 0.045$

## Atomic Coordinates:

Atom	x	y	z	B <sub>iso</sub>	Occ
Si1	0.0555	0.4206	-0.3199	0.26	1.00
Si2	0.0309	0.3137	-0.1636	0.29	1.00
Si3	0.0625	0.2796	0.0535	0.29	1.00
Si4	0.0623	0.1240	0.0367	0.29	1.00
Si5	0.0280	0.0768	-0.1580	0.26	1.00
Si6	0.0558	0.1956	-0.3133	0.26	1.00
Si7	-0.1715	0.4254	-0.3193	0.29	1.00

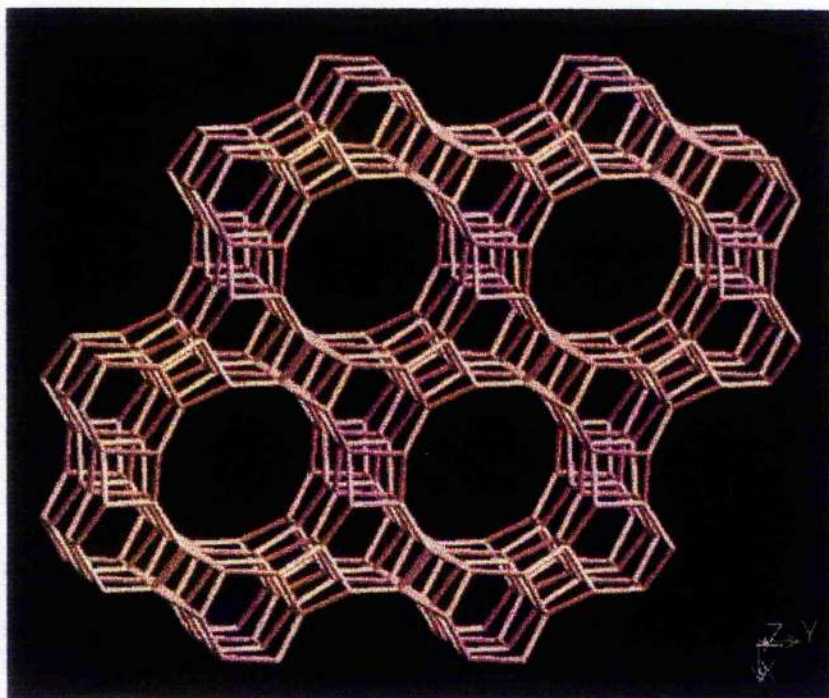
Si8	-0.1265	0.3123	-0.1739	0.29	1.00
Si9	-0.1759	0.2732	0.0360	0.26	1.00
Si10	-0.1763	0.1190	0.0344	0.29	1.00
Si11	-0.1294	0.0716	-0.1752	0.29	1.00
Si12	-0.1653	0.1908	-0.3141	0.29	1.00
Si13	0.4430	0.4284	-0.3346	0.26	1.00
Si14	0.4731	0.3124	-0.1881	0.29	1.00
Si15	0.4389	0.2770	0.0294	0.29	1.00
Si16	0.4356	0.1216	0.0338	0.29	1.00
Si17	0.4732	0.0710	-0.1784	0.26	1.00
Si18	0.4378	0.1874	-0.3174	0.29	1.00
Si19	0.6720	0.4239	-0.3142	0.26	1.00
Si20	0.6313	0.3128	-0.1684	0.32	1.00
Si21	0.6689	0.2731	0.0461	0.29	1.00
Si22	0.6701	0.1187	0.0387	0.29	1.00
Si23	0.6308	0.0727	-0.1776	0.32	1.00
Si24	0.6807	0.1945	-0.2979	0.26	1.00
O1	0.0588	0.3779	-0.2194	0.79	1.00
O2	0.0662	0.3106	-0.0564	0.63	1.00
O3	0.0472	0.2018	0.0465	0.92	1.00
O4	0.0671	0.1032	-0.0784	0.63	1.00
O5	0.0443	0.1230	-0.2693	0.66	1.00
O6	0.0477	0.2483	-0.2248	0.89	1.00
O7	-0.1533	0.3769	-0.2289	0.89	1.00
O8	-0.1669	0.3050	-0.0725	0.79	1.00
O9	-0.1558	0.1960	0.0316	0.76	1.00
O10	-0.1689	0.0885	-0.0753	0.89	1.00
O11	-0.1511	0.1208	-0.2630	0.87	1.00
O12	-0.1376	0.2483	-0.2424	0.95	1.00
O13	-0.0485	0.3189	-0.1490	1.03	1.00
O14	-0.0509	0.0781	-0.1529	0.74	1.00
O15	0.1253	0.4145	-0.3771	0.82	1.00

O16	-0.0041	0.3923	-0.3892	0.87	1.00
O17	-0.1340	0.4022	-0.4186	0.71	1.00
O18	0.1298	0.2003	-0.3583	0.63	1.00
O19	0.0026	0.2099	-0.4008	0.82	1.00
O20	-0.1275	0.1948	-0.4188	0.68	1.00
O21	0.0515	0.0032	-0.2041	0.58	1.00
O22	-0.1475	-0.0023	-0.2098	0.68	1.00
O23	-0.2501	0.4239	-0.3413	0.82	1.00
O24	-0.2435	0.1987	-0.3356	0.68	1.00
O25	-0.2525	0.2822	0.0676	0.61	1.00
O26	-0.2526	0.1101	0.0697	0.53	1.00
O27	0.4503	0.3799	-0.2408	0.92	1.00
O28	0.4480	0.3143	-0.0754	0.68	1.00
O29	0.4318	0.1991	0.0094	0.82	1.00
O30	0.4478	0.0812	-0.0669	0.84	1.00
O31	0.4351	0.1206	-0.2527	0.63	1.00
O32	0.4401	0.2505	-0.2451	0.79	1.00
O33	0.6590	0.3797	-0.2169	0.74	1.00
O34	0.6459	0.3148	-0.0508	0.58	1.00
O35	0.6513	0.1961	0.0270	0.68	1.00
O36	0.6559	0.0822	-0.0653	0.92	1.00
O37	0.6678	0.1232	-0.2504	0.92	1.00
O38	0.6694	0.2497	-0.2144	0.84	1.00
O39	0.5530	0.3054	-0.1913	1.05	1.00
O40	0.5519	0.0851	-0.1834	0.84	1.00
O41	0.3714	0.4186	-0.3885	0.89	1.00
O42	0.5015	0.4154	-0.4135	0.76	1.00
O43	0.6320	0.3938	-0.4087	0.74	1.00
O44	0.3711	0.1900	-0.3847	0.66	1.00
O45	0.5032	0.1862	-0.3863	0.74	1.00
O46	0.6326	0.2074	-0.3914	0.92	1.00
O47	0.4576	-0.0039	-0.2104	0.66	1.00

O48      0.6481    -0.0013    -0.2120    0.71      1.00

### Aluminophosphates

#### MAPO-5 (AFI)



Space Group:    P 6 c c (No. 184)

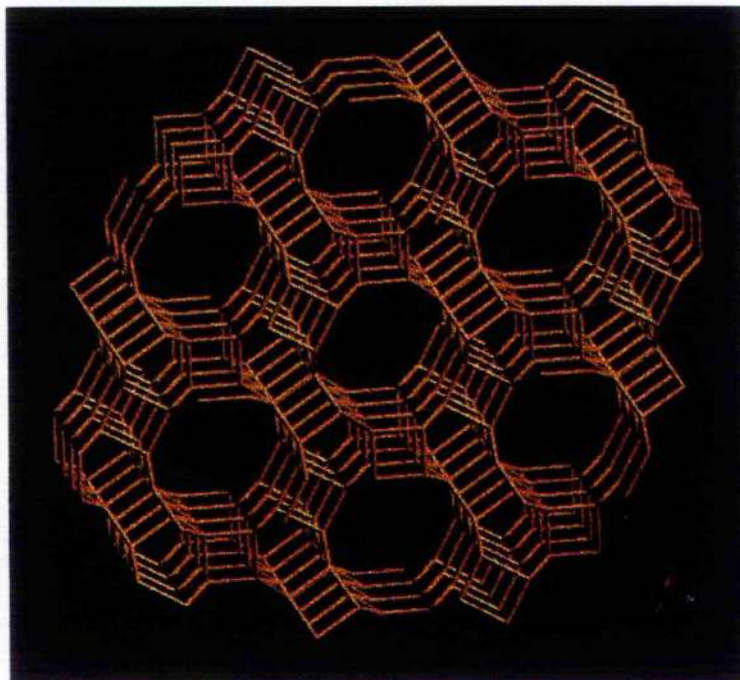
Unit Cell:      a = 13.74, b = 13.74, c = 8.474 Å,  $\alpha = \beta = 90^\circ$ ,  $\gamma = 120^\circ$

Determined by: X-ray single crystal refinement,  $R_w = 0.042$

## Atomic Coordinates:

Atom	x	y	z	B_iso	Occ
P1	0.4529	0.3281	0.0530	2.25	1.00
Al1	0.4571	0.3382	0.4250	1.89	1.00
O1	0.4214	0.2090	0.0080	4.18	1.00
O2	0.4550	0.3299	0.2510	5.33	1.00
O3	0.3658	0.3597	0.0040	4.11	1.00
O4	0.5742	0.4175	0.0070	5.03	1.00
C1	0.1040	0.0410	0.6660	3.95	0.17
C2	0.1250	0.9790	0.7500	3.95	0.17
C3	0.1040	0.9790	0.4160	3.95	0.17
C4	0.0000	0.8950	0.5000	3.95	0.17
C5	0.0410	0.8950	0.3590	3.95	0.17
C6	0.0820	0.9570	0.2210	3.95	0.17
N1	0.0000	0.0000	0.5430	3.95	0.50
F1	0.5000	0.5000	0.3170	3.95	0.17

## MAPO-31 (ATO)



Space Group:  $R\bar{3}H$  (No. 148) Hexagonal Setting

Unit Cell:  $a = 20.839$ ,  $b = 20.839$ ,  $c = 5.041 \text{ \AA}$ ,  $\alpha = \beta = 90^\circ$ ,  $\gamma = 120^\circ$

Determined by: X-ray single crystal refinement,  $R_wF = 0.018$ ,  $RF = 0.051$

## Atomic Coordinates:

Atom	x	y	z	B <sub>iso</sub>	Occ
Al	0.6174	0.0846	0.0381	1.89	0.98
P	0.4713	0.0877	0.1138	1.31	0.93
O1	0.5513	0.1071	0.1317	3.00	1.00
O2	0.4239	0.0089	0.0133	3.32	1.00
O3	0.4459	0.0953	0.3880	3.32	1.00
O4	0.4647	0.1406	0.9208	3.32	1.00
C1	0.0460	0.0130	0.1110	15.79	0.46
C2	0.0640	0.0290	0.3880	15.79	0.25
C3	0.0000	0.0000	0.3000	15.79	0.33

## Additional information on STA-2.

Empirical formula (asymmetric unit)	$\text{Mg}_{0.3}\text{Al}_{1.7}\text{P}_2\text{O}_8 \cdot 0.167\text{C}_{18}\text{H}_{34}\text{N}_2^{2+} \cdot x\text{H}_2\text{O}$
Temperature	200 K
Diffractometer geometry	3 circle fixed kappa Siemens diffractometer, fitted with a Siemens SMART CCD detector detector CCD area detector
Wavelength	0.512 Å
Crystal system	$R\bar{3}$ (hexagonal setting)
Unit cell dimensions	a = 12.726(2) Å c = 30.939(6) Å
Unit cell volume	4339.3 (1.3) Å <sup>3</sup>
Z	18
Density (calcd - using TGA data)	2.15 g/cm <sup>3</sup>
Density (measured)	2.05(5) g/cm <sup>3</sup>
Crystal size	0.05 x 0.05 x 0.05 mm <sup>3</sup>
Reflections collected	7925
Independent reflections	1993
F(000)	1635
$\mu$ 0.19 mm <sup>-1</sup>	
Resolution limit	0.78 Å
Refined parameters	142
Goodness-of-fit	S=1.307
R(F)	0.0757 for 1593 reflections > 4 ? 0.0981 for all 1993 reflections
Largest diff. peaks in Fourier	0.9 e/Å <sup>3</sup> , -0.55e/Å <sup>3</sup>

The atomic positions used in the MAPO-31 / DABCOC6 docking experiment described in section 7.3.4 using atomic coordinates derived from computational studies are as follows:

Atom	Mult.	Frac.	x	y	z	U <sub>iso</sub>
P1	18	1.0000	0.4703	0.0891	0.1206	3.0
Al1	18	1.0000	0.6162	0.0821	0.0609	3.0
O1	18	1.0000	0.5510	0.1085	0.1267	2.5
O2	18	1.0000	0.4252	0.0095	0.0293	2.5
O3	18	1.0000	0.4480	0.1023	0.3873	2.5
O4	18	1.0000	0.4690	0.1360	-0.1130	2.5
C1	18	0.0371	0.6511	0.2978	0.6586	2.5
C2	18	0.0371	0.6798	0.3505	0.9135	2.5
C3	18	0.0371	0.6557	0.3103	0.1980	2.5
N1	18	0.0371	0.6608	0.3203	0.3571	2.5
C4	18	0.0371	0.7353	0.3413	0.2370	2.5
C5	18	0.0371	0.6496	0.3845	0.2902	2.5
C6	18	0.0371	0.6425	0.3918	0.9745	2.5
N2	18	0.0371	0.6676	0.3468	0.8067	2.5
C7	18	0.0371	0.7416	0.3624	0.9249	2.5
C8	18	0.0371	0.6142	0.2666	0.8737	2.5
C9	18	0.0371	0.6043	0.2553	0.1895	2.5
N3	18	0.0371	0.6657	0.3199	0.8600	2.5
C10	18	0.0371	0.6908	0.2749	0.6921	2.5
C12	18	0.0371	0.7290	0.4113	0.7930	2.5
C11	18	0.0371	0.7191	0.4001	0.4772	2.5
N4	18	0.0371	0.6725	0.3464	0.3095	2.5
C13	18	0.0371	0.6838	0.2821	0.3765	2.5
C14	18	0.0371	0.5981	0.3254	0.4279	2.5
C15	18	0.0371	0.5917	0.3042	0.7418	2.5
C16	18	0.0371	0.6776	0.3564	0.4687	2.5
C17	18	0.0371	0.6536	0.3161	0.7532	2.5

C18	18	0.0371	0.6822	0.3688	0.0081	2.5
C19	18	0.0371	0.6654	0.3124	0.6990	2.5
C20	18	0.0371	0.6620	0.3452	0.4140	2.5
C21	18	0.0371	0.6633	0.2997	0.1611	2.5
C22	18	0.0371	0.6700	0.3670	0.5055	2.5
C23	18	0.0371	0.6713	0.3215	0.2527	2.5
C24	18	0.0371	0.6680	0.3542	0.9675	2.5